

Cranfield University

Emma Louise Worthington

**Piezoelectric Energy Harvesting: Enhancing
Power Output by Device Optimisation and Circuit
Techniques**

School of Applied Sciences

PhD Thesis

Academic years: 2006-2010

Supervisors: Dr. Meiling Zhu and Dr. Paul Kirby

31st March 2010

Cranfield University

School of Applied Sciences
Microsystems and Nanotechnology Centre
Department of Materials

PhD Thesis

Academic Years 2006-2010

Emma Louise Worthington

**Piezoelectric Energy Harvesting: Enhancing
Power Output by Device Optimisation and Circuit
Techniques**

Supervised by Dr. Meiling Zhu and Dr. Paul Kirby

30th August 2010

This dissertation is submitted in partial fulfilment of the requirements for the degree of
Doctor of Philosophy

©Cranfield University, 2010. All rights reserved. No part of this publication may be
reproduced without the written permission of the copyright holder.

ABSTRACT

Energy harvesting; that is, harvesting small amounts of energy from environmental sources such as solar, air flow or vibrations using small-scale ($\approx 1\text{cm}^3$) devices, offers the prospect of powering portable electronic devices such as GPS receivers and mobile phones, and sensing devices used in remote applications: wireless sensor nodes, without the use of batteries. Numerous studies have shown that power densities of energy harvesting devices can be hundreds of μW ; however the literature also reveals that power requirements of many electronic devices are in the mW range. Therefore, a key challenge for the successful deployment of energy harvesting technology remains, in many cases, the provision of adequate power. This thesis aims to address this challenge by investigating two methods of enhancing the power output of a piezoelectric-based vibration energy harvesting device.

The thesis starts with a survey of the power requirements of a range of electronic devices and systems. It then moves to a review of the various energy harvesting technologies available for harvesting from the different types of energy source, including: solar, air flow, thermal, pressure variations, radio frequency radiation and mechanical. For each energy source, the most commonly employed mechanism for energy conversion is detailed, relative advantages and disadvantages are outlined, and power output levels that have been achieved through experiment are reported. A comparison is then made between power levels harvested, and power requirements of electronic devices and systems. Following this, the piezoelectric concept is introduced, both in historical and technological contexts, and a review of the history and state-of-the-art in power enhancement of piezoelectric generators is given, which includes both power

enhancement through advances in the design of the generator and power enhancement through use of the harvesting circuitry.

The thesis then moves to studying two methods of enhancing the power output of a piezoelectric-based vibration energy harvesting device. The first method concerns the harvesting device itself. Through initial investigation, the power output of a prototype device, fabricated from a commonly available piezoelectric buzzer, was ascertained using a simple test setup built around the 'sweep in' function of a function generator; the result was $8.18\mu\text{W}$. The prototype device was built without any guidance on how the geometric dimensions of it might affect its power output. Therefore, to achieve a higher power output, it was considered that a modelling approach might be useful. However, it was considered that the model should not simply predict outputs of the device (e.g. power or voltage) when provided with dimensions and material characteristics, rather, the model should be used with an optimisation algorithm to provide the device design itself; i.e. the model should be designed for use with a computer-based optimisation algorithm, such that the output of the optimisation process is a list of values for the device dimensions that together constitute a design that has been optimised for maximum power output. To this aim, an analytical model has been developed. The model results in an expression for the power output of the device that, because it has within its arguments all of the dimensional parameters of the device, can be used with a computer-based optimisation algorithm to optimise the geometrical parameters of the device. An example of how the model can be used is given using the complex conjugate optimisation algorithm provided by Mathcad 2000 Professional software, and a design for a device optimised for maximum power output given a volume constraint of 1cm^3 was obtained. The optimised device was then fabricated and tested using an improved test setup based on National

Instruments hardware and software, and the maximum power achieved from the optimised harvesting device, under vibration acceleration amplitude of $\pm 0.23g$, was $370.37\mu W$, which occurred with a $325k\Omega$ resistive load. A voltage amplitude of $15.52V$ was measured at this maximum power level, and the resonant frequency of the device with a $325k\Omega$ load was $87Hz$.

The second method investigated concerns the harvesting circuitry. Initial investigations were performed using the prototype harvesting device and two bridge rectifier circuits: one using silicon rectifier diodes and the other using schottky-type diodes. It was found that although schottky-type diodes have a lower forward bias voltage, their higher reverse current meant that more energy was harvested using the silicon rectifier diodes ($13.5\mu J$ in comparison with $7.6\mu J$). Since the bridge rectifier is the circuit that is most usually used as an interface to energy harvesting devices, the operation of it was also analysed via circuit simulation, and two main mechanisms that inhibit power transfer from the harvesting device to load were observed: 1) power is lost due to the internal impedance of the generator, 2) during steady-state operation, the generator spends much of its time in the open-circuit condition. The latter mechanism occurs because under steady-state conditions the smoothing capacitor is already charged, and therefore the diodes don't conduct until the voltage output of the harvesting device reaches the capacitor voltage plus the forward bias voltage of one of the diodes in the rectifier. Following this, a new harvesting circuit concept was proposed. The new concept comprises: a Synchronised Switch Harvesting on Inductor (SSHI) functional block, which boosts the output voltage of the piezoelectric generator; a 'storage' functional block, in which charge is collected per half-cycle of the piezoelectric generator output and then dumped into a large storage capacitor; and a 'DC-DC converter' block, which uses the reservoir of charge in the

storage block to power a buck-boost DC-DC converter, which in turn can provide regulated DC power to an end application system. The new concept holds several advantages over the traditional bridge rectifier, which are: 1) the concept takes advantage of the increase in the voltage output of the harvesting device that results from using the SSHI technique; 2) the concept can harvest during the whole of each AC cycle, unlike the bridge rectifier circuit; 3) the concept inherently converts from AC to DC, by the accumulation of charge in two storage capacitors (one collecting positive charge and one collecting negative charge) which are then connected together in series to form an energy reservoir with a positive terminal and a negative terminal. This negates the need for four rectifier diodes and allows for the connection of a buck-boost DC-DC converter; and 4) through impedance matching to the piezoelectric generator, maximum power transfer can occur at all times. In addition, because the concept adopts the philosophy of storing charge over time such that an energy reservoir is built up (from which the application system can then be powered), higher power applications can be powered than would be possible by using a ‘continuous powered’ approach, such as the bridge rectifier. The concept also uses pre-existing maxima and minima detection circuitry (since it is already required for the SSHI technique) therefore a minimum of extra components needs to be added, and the concept is simple: if built into a full energy harvesting system, the controlling microprocessor only needs to fulfil a few functions and can operate with a very low clock rate, and therefore it can be very low power and a small size. A prototype circuit that can implement the concept was designed and built, using a mixture of discrete and integrated components, and the performance of the concept was assessed through two different approaches: (1) an experimental approach was adopted to compare it with a bridge rectifier circuit in terms of the amount of energy that could be harvested into storage capacitance (2) a simulation approach was adopted in order to compare it with

another technique reported in the literature in terms of maximum average power output over time. Through the experimental approach, it was found that the new concept harvested 247% more energy into storage capacitance than the bridge rectifier circuit in a similar length of time and for the same input vibration conditions. Through the simulation approach, it was found that the maximum average power output of the piezoelectric harvesting device when the new concept was used was nearly eleven times more than when the technique reported in the literature was used.

Both the analytical model and new harvesting circuit concept developed in this thesis provide methods by which the power output of a piezoelectric-based vibration harvester can be enhanced: by using the model, the power output of the optimised device was an improvement by a factor of 45 over the power output of the prototype device, and through use of the new circuit concept, 247% more energy can be harvested into storage capacitance than if the bridge rectifier circuit is used. The simulations also show that the new concept enhances the power output of the harvesting device, by as much as eleven times that achieved through the use of another technique given in the literature. An enhanced level of output power means that a greater number of potential applications can be realised, and this study goes some way towards closing the gap that exists between the power requirements of electronic devices and systems, and the amount of power that can be harvested by piezoelectric conversion of vibration energy.

Page intentionally blank

ACKNOWLEDGEMENTS

My thanks go to all those people who have helped me through my academic years at Cranfield. To my supervisor Meiling Zhu, for taking me on as her first PhD student; for her careful guidance, technical help, and for sharing with me her experience and expertise in mechanical engineering; I feel that together we have made a valiant and successful foray into the field of energy harvesting. To all the other people of buildings 70 and 50, technical staff and students alike, thank you for sharing with me many things: advice, support, screwdrivers, various pieces of hardware, friendship, laughs, and interesting conversations. To the people with whom I shared lunchtime badminton sessions and the odd circuit-training experience, thank you for the company – I enjoyed our games very much. Thank you also to David Pitts, of the Cranfield School of Health, who provided me with a much needed sounding board at the times when I felt bereft in the absence of electronic expertise, and for also providing me with spare electronic components when I needed them.

I would also like to thank both Shad Roundy, and Elie Lefevre, both of whom found the time to respond very rapidly to email queries from a new PhD student grappling with the complexities of trying to find her way around the field of energy harvesting.

To my old colleagues working in Stevenage: During the 4½ years I spent with you I learnt many engineering skills that have stood me in good stead during my time at Cranfield. In particular I would like to thank Roger Orr, for spending so much time with me showing me the values of a methodical approach and paying attention to detail, and in addition Dennis Rapley, Kim Cole, Keith Pollard, Peter Roberts and Tony Kaye for the

many times they each helped me to learn and gain new skills, and for the wisdom they often passed on.

To my brother, Martyn, thanks for the belief that you have in my abilities - despite the distance we have always shared a good bond. To my parents, in your wisdom you let me choose my own path in life - I thank you for that and for the continued love and support that you have always given me.

Last but by no means least, I would like to thank Christopher Roberts, who is not only an excellent professional electronics design engineer, whose brains I like to pick, but who also gave me much emotional support during my PhD. Thank you for checking that I ate properly, took time out when I needed to, and maintained a sense of perspective. Thank you also for all the encouragement and your belief, when mine was waning, that I would eventually finish this thesis!

CONTENTS

List of Figures.....	viii
List of Tables.....	xx
Nomenclature.....	xxiii
Acronyms & Abbreviations.....	xxiii
Variables.....	xxvi
Constants.....	xxx
CHAPTER 1: INTRODUCTION	1
1.1 Motivation.....	3
1.2 Research Context.....	9
1.3 Scope.....	11
1.4 Aims and Objectives of the Research.....	16
1.5 Contribution.....	18
1.5.1 Optimisation of the Geometric Dimensions of the Harvesting Device.....	18
1.5.2 A Proposed Novel Harvesting Circuit Concept.....	19
1.6 Methodology.....	23
1.7 Thesis Structure.....	24
CHAPTER 2: LITERATURE REVIEW	26
2.1 Overview of Power Requirements of Electronic Devices and Systems.....	27
2.2 Overview of Energy Harvesting Technologies by Energy Source, with a focus on power generation capability.....	29
2.2.1 Solar.....	29
2.2.2 Air Flow.....	33
2.2.3 Thermal.....	39

2.2.4	Pressure Variations.....	44
2.2.5	Radio Frequency Radiation.....	45
2.2.6	Mechanical: Vibrations and Human Movement	50
2.2.6.1	Electromagnetic Conversion	52
2.2.6.2	Electrostatic Conversion.....	58
2.2.6.3	Piezoelectric Conversion	64
2.3	Justification for Focussing on Piezoelectric Conversion of Vibration Energy	68
2.4	Justification for Focussing on Power Enhancement.....	72
2.4.1	Other Potential Avenues of Exploration	73
2.4.1.1	Geometric Variations of Piezoelectric Harvesters.....	73
2.4.1.2	Wearable and Implantable Piezoelectric Harvesters	76
2.4.1.3	Tuned or Wideband Piezoelectric Harvesters	79
2.4.1.4	Durability of Piezoelectric Harvesters.....	81
2.4.2	Justification for Focussing on Power Enhancement	81
2.5	Overview of Piezoelectricity	83
2.5.1	A Brief History of Piezoelectricity	83
2.5.2	Basic Description of the Piezoelectric Effect.....	88
2.6	History and State-of-the-Art in Power Enhancement of Piezoelectric Generators.....	94
2.6.1	Power Enhancement through Design of the Harvesting Device	95
2.6.1.1	Geometric Advancements.....	95
2.6.1.1.1	Triangular-shaped Cantilevers.....	96
2.6.1.1.2	Geometric Variations of the Proof Mass	98
2.6.1.2	Mathematical Optimisation	101

2.6.1.3	Studies Providing Design Guidelines	103
2.6.2	Power Enhancement through use of the Harvesting Circuitry	106
2.6.2.1	Impedance Adaptation	106
2.6.2.2	Synchronised Techniques	108
2.6.2.2.1	Synchronised Switch Harvesting on Inductor (SSHI)	108
2.6.2.2.2	Synchronous Electric Charge Extraction (SECE)	113
2.7	Conclusions of the Literature Review	115
 CHAPTER 3: DEVELOPMENT OF THE ANALYTICAL MODEL, OPTIMISATION, AND TEST OF THE PIEZOELECTRIC GENERATOR.....		117
3.1	Description of the Design	118
3.2	Initial Investigations	121
3.2.1	Prototype Device Fabrication	122
3.2.2	Prototype Test Setup	124
3.2.3	Testing the Prototype Device	129
3.3	Conclusions of the Initial Investigations	135
3.4	Analytical Modelling	138
3.4.1	Background	138
3.4.1.1	Source Vibrations	140
3.4.1.2	Transducer (Energy Harvesting Device)	142
3.4.1.3	Harvesting circuitry	147
3.4.1.4	Conclusions of the background to the analytical modelling	149
3.4.2	Development of an Analytical Model for Optimisation of the Geometric Parameters of the Harvesting Device	152
3.4.2.1	Modelling Approach	152

3.4.2.2	Determination of $W_d(L_b)$ for Equation (15).....	158
	Determination of k for Equation (20).....	160
3.4.2.3	Determination of ζ for Equation (20).....	162
3.4.2.4	Determination of EI for Equation (21).....	163
3.4.2.5	Determination of $f(x)$ for Equation (15).....	164
3.4.2.6	Determination of Equation (14) for σ_1	165
3.4.2.7	Determination of the Electrical Outputs.....	168
3.5	Device Optimisation.....	171
3.5.1	Vibration Characteristics of the Intended Application Environment.....	173
3.5.2	Space-envelope Constraints.....	173
3.5.3	Material Characteristics.....	174
3.5.4	Optimisation Software.....	175
3.5.5	Optimisation Results.....	183
3.6	Fabrication of the Optimised Design.....	187
3.7	Testing of the Optimised Design.....	188
3.7.1	Improved Test Setup and Equipment.....	188
3.7.2	Testing Procedure.....	201
3.8	Test Results for the Optimised Design.....	203
3.9	Conclusions.....	207
CHAPTER 4: DESIGN AND TEST OF THE NEW HARVESTING CIRCUIT CONCEPT.....		210
4.1	Initial Investigations.....	211
4.1.1	Design of Two Bridge Rectifier Circuits.....	215
4.1.2	Bridge Rectifier Circuit Test Setup.....	216

4.1.3	Testing the Bridge Rectifier Circuits	217
4.2	Conclusions of the Initial Investigations	233
4.3	A Proposed New Harvesting Circuit Concept.....	237
4.3.1	Background	237
4.3.2	The New Concept.....	238
4.3.3	Advantages of the New Concept.....	252
4.4	Implementation of the Concept (Electronic Circuit Design).....	253
4.4.1	Design of the Main Generator Block	255
4.4.2	Design of the SSHI Block	256
4.4.3	Design of the Storage Block	261
4.5	Construction of the Circuit	265
4.6	Testing of the Circuit.....	266
4.6.1.1	Test Setup for the SSHI Tests.....	267
4.6.1.2	Testing Procedure for the SSHI Tests	268
4.6.1.3	Test Setup for the Complete Harvesting Circuit Concept Tests.....	273
4.6.1.4	Testing Procedure for the Complete Harvesting Circuit Concept Tests	275
4.7	Test Results	277
4.7.1	SSHI Test Results and Discussion	277
4.7.2	Complete Harvesting Circuit Concept Test Results and Discussion	287
4.8	Simulation of the Concept: Analysing Average Power Output for the Purpose of Comparison with Other Circuit Techniques.....	293
4.8.1	Introduction	293
4.8.2	Description of the Simulations.....	294

4.8.3	Simulation Results	308
4.8.3.1	Simulation to determine the theoretical maximum average power output of the piezoelectric harvesting device	308
4.8.3.2	Simulation to determine the maximum average power output of the harvesting device when the technique proposed by Ottman et al.	309
4.8.3.3	Simulation to determine the maximum average power output of the harvesting device when using the concept proposed in this thesis.	310
4.9	Conclusions	322
 CHAPTER 5: CONCLUSIONS, DISCUSSION & RECOMMENDATIONS FOR FUTURE WORK.....		333
5.1	Review of Aims and Objectives	335
5.2	Conclusions of the Harvesting Device Optimisation	336
5.3	Conclusions of the Proposed New Harvesting Circuit Concept.....	339
5.4	Discussions	347
5.4.1	Implications of the work	347
5.4.2	Recommendations for Future Work.....	348
5.4.2.1	Regarding the Optimisation of the Harvesting Device Performed in this Thesis.....	348
5.4.2.2	Regarding the Harvesting Circuit Concept Developed in this Thesis	351
5.4.2.3	Further Work regarding areas other than Power Enhancement.....	355
5.4.3	The Future and Toward MEMS Harvesting Devices.....	356

References	359
Appendices	373
Appendix A: Circuit Schematic for the Accelerometer	373
Appendix B: Properties of the materials used in construction of the optimised piezoelectric vibration energy harvesting device of Chapter 3	374
Appendix C: Mathcad file used for optimisation of the piezoelectric vibration energy harvesting device	375
Appendix D: Circuit schematic for the custom-built load board	377
Appendix E: User Interface of LabVIEW SignalExpress, showing the configuration of each step used in the program developed in this thesis	378
Appendix F: Monostable Multivibrator Calculations for the Circuit that Implements the SSHI Function (calculated using Mathcad)	383
Appendix G: Monostable Multivibrator Calculations for the Circuit that Implements the New Charge Storage Concept.....	384
Appendix H: Power budget for the circuit built to implements the proposed harvesting concept	385
Appendix I: Simulation circuit used to obtain power consumption of darlington driver output plus optocoupler MOSFET relay	386
Appendix J: Simulation circuit used to obtain power consumption of darlington driver output plus optocoupler phototransistor output	387
Related Publications and Posts.....	388
CV	390

LIST OF FIGURES

Figure 1-1 A basic block diagram of an energy harvesting system.	11
Figure 1-2 A lumped element equivalent electrical circuit of the input vibrations and piezoelectric transducer.	12
Figure 2-1 Power requirements of a range of modern electronic devices and systems (sources specified individually).	28
Figure 2-2 (a) Crankshaft design of a ‘Small scale windmill’ [40] (b) Camshaft design of an air-powered electric energy generator [32]	35
Figure 2-3 A piezoelectric bimorph in a von Kármán’s vortex street [34]	36
Figure 2-4 Working principle of a thermocouple [45]	40
Figure 2-5 Machine cross-section of the compressed-air-to-electric power generator used in [54].	45
Figure 2-6 Electric and magnetic field components of an electromagnetic wave.....	46
Figure 2-7 (a) ‘Moving magnet’ electromagnetic vibration energy harvester design given in [62] (b) Implementation of design [62]	52
Figure 2-8 ‘Moving coil’ electromagnetic vibration energy harvester design given in [63]	53
Figure 2-9 (a) A spring-mass system (b) Side view schematic of the electromagnetic vibration energy harvester presented in [65]	53
Figure 2-10 Working principle of an electrostatic vibration energy harvester [68].	59
Figure 2-11 Three types of electrostatic converter (a) in-plane, overlap varying type (b) in-plane gap closing type (c) out-of-plane gap closing type [80].	59
Figure 2-12 Schematic of a constant charge electrostatic vibration energy harvester [81]	60

Figure 2-13 (a) The direct and (b) the indirect piezoelectric effects. The broken lines indicate the original dimensions [90].	64
Figure 2-14 Power requirements of a range of electronic devices and systems, maximum output powers recorded for the different energy sources, and average power densities of meso-scale generators harvesting from the different energy sources.	70
Figure 2-15 A rectangular piezoelectric bimorph cantilever.....	73
Figure 2-16 Schematics of the different configurations of piezoelectric energy harvesting device developed to date (a) a triangular cantilever [92] (b) a pre-stressed bender [98] (c) a bi-stable device [99] (d) a cymbal harvester [91] (e) a circular (disc) harvester [100] [101] (f) a spiral shaped harvester [102].	74
Figure 2-17 Six methods of achieving wideband or tunable piezoelectric vibration energy harvesters.	80
Figure 2-18 A unit cell of a simple cubic lattice	88
Figure 2-19 (a) Cubic unit cell geometry (b) crystallographic axes.....	89
Figure 2-20 Categorisation of crystals belonging to the seven lattice systems	90
Figure 2-21 Weiss domain patterns in a tetragonal PLZT 12/40/60 ceramic [126].	91
Figure 2-22 Weiss domains in the poling process of a piezoelectric ceramic (a) before poling (b) during poling, (c) showing remanent polarisation after poling	92
Figure 2-23 Orthogonal axes system used to describe the properties of piezoelectric materials [127].	93
Figure 2-24 FEM analysis of a rectangular piezoelectric cantilever. The red areas denote areas of high stress [99].	96
Figure 2-25 Schematic of a cantilever-based piezoelectric generator showing potentially wasted volume.	98
Figure 2-26 Rectangular piezoelectric cantilever beam with U-shaped mass [128].	99

Figure 2-27 Cross section of a rectangular piezoelectric beam with a curved L-shaped mass [129].	100
Figure 2-28 The curved L-shaped beam utilises more of the otherwise wasted volume than does the flat L-shaped beam [129].....	100
Figure 2-29 Photograph of the rectangular piezoelectric cantilever with L-shaped mass [129].	101
Figure 2-30 Cross section of a fully electroded clamped circular unimorph plate [100].	105
Figure 2-31 Cross section of the piezoelectric layer of the ‘regrouped electrode’ version of the clamped circular unimorph plate [100].	105
Figure 2-32 Deflection and stress of the clamped circular unimorph plate [100].....	105
Figure 2-33 Adaptive energy harvesting circuit given in [93].	107
Figure 2-34 Required circuit components, and resultant voltage waveform, for the SSHI technique [1].	108
Figure 2-35 Method of measuring the effect of the SSHI technique for the AC case (a) circuit for measuring the power output of the generator without the use of SSHI (b) circuit for measuring the power output of the generator with the use of SSHI.....	111
Figure 2-36 Method of measuring the effect of the SSHI technique for the DC case (a) circuit for measuring the power output of the generator without the use of SSHI (b) circuit for measuring the power output of the generator with the use of SSHI.....	112
Figure 2-37 Circuit that performed SECE in [134].	113
Figure 2-38 Theoretical cycles of the piezoelectric voltage as a function of the displacement (1) impedance adaptation technique (2) SECE technique [134].	114
Figure 3-1 A piezoelectric vibration energy harvester configured as a cantilever beam	118

Figure 3-2 Schematics of differently arranged piezoelectric cantilever-based vibration energy harvesting devices (a) a unimorph (b) a bimorph poled for parallel (c) a bimorph poled for series (d) a multilayer bimorph poled for parallel.....	120
Figure 3-3 A buzzer transducer	122
Figure 3-4 First prototype vibration energy harvesting device in aluminium holder..	124
Figure 3-5 First shaker & aluminium fixture.	125
Figure 3-6 Location of accelerometer relative to location of beam.	126
Figure 3-7 First developed test system.	127
Figure 3-8 Oscilloscope trace of use of the ‘sweep in’ input of the function generator to obtain a frequency sweep from 0Hz to 200Hz.	128
Figure 3-9 Transfer function of the voltage-controlled oscillator	129
Figure 3-10 Oscilloscope trace showing the responses of the shaker plus aluminium fixture and the prototype harvesting device.	129
Figure 3-11 Oscilloscope trace showing the output of the linear voltage ramp generator and response of the shaker plus aluminium fixture.	130
Figure 3-12 Peak voltage and average power output of the prototype harvesting device.	131
Figure 3-13 A piezoelectric generator represented as an AC voltage source in series with its own internal impedance.....	132
Figure 3-14 Ratio of internal impedance value to external load resistor value versus external load resistor value.....	133
Figure 3-15 Graph showing trends of the voltages generated across and powers dissipated by both the fixed-value internal impedance of a piezoelectric generator and the varying-value external load resistance.....	134

Figure 3-16 Possible block diagrams for basic energy harvesting systems; (a) requiring power conditioning only (b) requiring both power conditioning and power management.	139
Figure 3-17 Different vibration types.....	141
Figure 3-18 Equivalent electric circuit of a piezoelectric generator with base excitation [137].	142
Figure 3-19 Schematic of the harvesting device showing the notation of the dimensional parameters used in derivation of the model.	153
Figure 3-20 Representative circuit of the harvesting device, where: C_p is the capacitance of each piezoelectric layer.	154
Figure 3-21 Cantilever with an end mass represented as a spring-mass system.	158
Figure 3-22 Force analysis for a cantilever with an end mass.....	161
Figure 3-23 Method of finding the area moment of inertia for a composite beam.	164
Figure 3-24 Strain distribution in a curved beam.....	167
Figure 3-25 Origin of equation (54) for the value of the mass, m	176
Figure 3-26 Schematic of the optimised device (all dimensions are in mm).	183
Figure 3-27 Simulated values of the power and voltage outputs of the optimised device.	184
Figure 3-28 Photo of the optimised vibration energy harvester.	188
Figure 3-29 First automated test system.....	189
Figure 3-30 (a) Photo of the final experimental test setup (b) schematic of the final experimental test setup.	195
Figure 3-31 Photo of the custom-built load board.....	198

Figure 3-32 V20 electrodynamic shaker and fixture with no energy harvesting device installed.....	200
Figure 3-33 Response of V20 electrodynamic shaker plus fixture from 50Hz to 500Hz	200
Figure 3-34 Measured output voltage of the optimised device versus vibration acceleration amplitude (frequency of vibration = 60Hz)	202
Figure 3-35 Measured output voltage of the optimised device with different load resistor values (constant acceleration of $\pm 0.23g$)	204
Figure 3-36 Measured output voltage and power of the optimised device versus load resistor value.....	205
Figure 4-1 (a) Traditional bridge rectifier circuit and (b) synchronous rectifier circuit.	212
Figure 4-2 Graph showing the current versus voltage curves of a diode and a MOSFET operating in the ohmic region.....	213
Figure 4-3 Circuit incorporating the two bridge rectifiers.	215
Figure 4-4 Test setup used for testing the bridge rectifier circuits.....	216
Figure 4-5 Charging curve of the $1\mu F$ capacitor using the bridge rectifier with silicon rectifier diodes.....	218
Figure 4-6 Charging curve of the $1\mu F$ capacitor using the bridge rectifier with schottky diodes.....	218
Figure 4-7 Measured voltage amplitude across, and calculated power dissipated by, different value load resistors for two different types of rectifier circuit: one with silicon rectifier diodes, the other with schottky diodes.....	220
Figure 4-8 (a) Bridge rectifier circuit built in Switchercad (b) Simulated waveforms in Switchercad.	222

Figure 4-9 First cycle of the simulated waveforms.	223
Figure 4-10 Circuit during the positive half-cycle of the piezoelectric generator output voltage.	224
Figure 4-11 (a) Simplified circuit of the positive half-cycle showing calculated voltages across components (b) Simulated voltage waveforms for the circuit of Figure 4-10 showing simulated voltages across components.	225
Figure 4-12 Circuit during the negative half-cycle of the piezoelectric generator output voltage.	228
Figure 4-13 (a) Simplified circuit of the negative half-cycle showing calculated voltage drops across components (b) Simulated voltage waveforms showing simulated voltage drops across components.	228
Figure 4-14 Simulated waveforms of the bridge rectifier circuit; (a) with a piezoelectric generator that has 200Ω source impedance (b) with a piezoelectric generator that has 50Ω source impedance.	229
Figure 4-15 Operation of the circuit showing times (shaded) when no power is transferred from the piezoelectric harvesting device to the smoothing capacitor and load resistor.	231
Figure 4-16 Piezoelectric vibration energy harvesting device connected directly to a load capacitor.....	238
Figure 4-17 (a) Charge pump circuit for collecting positive generated charge in one storage medium and negative generated charge in another storage medium (b) Hypothesised voltage waveforms for the circuit showing charge accumulation in both storage mediums.....	240
Figure 4-18 Comparison of the voltage output waveforms of the piezoelectric generator in the normal case and in the SSHI case.....	242
Figure 4-19 Circuit that can be formed to supply a DC-DC converter.	243

Figure 4-20 A comparison between the charging and discharging profiles for a battery and a supercapacitor for similar charge [148].	245
Figure 4-21 Schematic of the final form of the proposed harvesting circuit (showing current flow in the positive half-cycle of the piezoelectric generator AC voltage output).	246
Figure 4-22 Schematic of the proposed harvesting circuit showing current flow in the negative half-cycle of the piezoelectric generator AC voltage output.	247
Figure 4-23 Hypothesised voltage waveforms for the proposed harvesting circuit, showing charge accumulation in both supercapacitors.	247
Figure 4-24 Circuit formed by the series connection of two charged supercapacitors, to supply a buck-boost DC-DC converter.	248
Figure 4-25 Block diagram of the proposed harvesting circuit and envisaged power management circuitry.	251
Figure 4-26 Circuit schematic of the electronic circuit designed to implement the proposed new harvesting circuit concept.	254
Figure 4-27 Circuit diagram designed to implement the SSHI technique (greyed-out parts are irrelevant).	258
Figure 4-28 Circuit diagram designed to implement the charge transfer function (greyed-out parts are irrelevant).	262
Figure 4-29 Photo of the built prototype harvesting circuit.	266
Figure 4-30 Test equipment setup for SSHI tests.	267
Figure 4-31 (a) Waveform after initial adjustment; i.e. after following steps 1-4 outlined above (b) Photo of the SSHI waveform achieved after further ‘fine tuning’ adjustments (channel 1 shows the SSHI waveform. Channel 2 shows the pulse that controls the length of time the inductor is switched into the circuit for).	272

Figure 4-32 Test equipment setup for charge storage tests.	274
Figure 4-33 Measured output voltage of the piezoelectric vibration energy harvesting device with and without the SSHI technique (frequency = 60Hz; acceleration = $\pm 0.23g$).	277
Figure 4-34 Oscilloscope traces showing the voltage output of the optimised harvesting device when connected to a series of different load resistor values.	279
Figure 4-35 SSHI circuit with resistive load, built in Switchercad.	280
Figure 4-36 Simulated waveforms showing the voltage output of the optimised harvesting device when connected to a series of different load resistor values.	281
Figure 4-37 Phasor diagrams for a CR series circuit (a) the voltage phasor diagram (b) the impedance phasor diagram.	282
Figure 4-38 Relationship between the ratio X_C/R and the phase angle between V_{src} and V_R	283
Figure 4-39 (a) SSHI circuit with capacitive load, built in Switchercad (b) Simulated waveform showing the voltage output of the optimised harvesting device with a matched capacitive load.	286
Figure 4-40 Voltage amplitude of piezoelectric generator and voltage obtained on the $220\mu F$ capacitor for both the bridge rectifier circuit and the proposed harvesting circuit (vibration of $\pm 0.125g$ at 60Hz).	287
Figure 4-41 Voltage amplitude of piezoelectric generator and voltage obtained on the $220\mu F$ capacitor for both the bridge rectifier circuit and the proposed harvesting circuit (vibration of $\pm 0.095g$ at 60Hz).	289
Figure 4-42 Voltage amplitude of piezoelectric generator and voltage obtained on the $220\mu F$ capacitor for the bridge rectifier circuit under different acceleration conditions (frequency of vibration = 60Hz).	291

Figure 4-43 Voltage amplitude of piezoelectric generator and voltage obtained on the 220 μ F capacitor for the proposed harvesting circuit under different acceleration conditions (frequency of vibration = 60Hz).	291
Figure 4-44 Voltage amplitude of piezoelectric generator, voltage obtained on the 220 μ F capacitor collecting positive charge, and voltage on the 220 μ F capacitor collecting negative charge for the proposed harvesting circuit (vibration of $\pm 0.125g$ at 60Hz).	292
Figure 4-45 Simulation circuit, built in Switchercad for the purpose of ascertaining the theoretical maximum average power output of a piezoelectric harvesting device.	295
Figure 4-46 (a) Adaptive energy harvesting circuit given in [93] (b) Steady-state battery current as a function of DC-DC converter duty cycle [93].	296
Figure 4-47 Circuit simulation for the technique proposed by Ottman et al: (a) Circuit used to obtain the peak open-circuit voltage output of the generator (b) Circuit used to ascertain the load resistor value which results in maximum power output, the power dissipation in the load, and the power extracted from the harvesting device.	297
Figure 4-48 Circuit diagram of Figure 4-26 through Figure 4-28, showing those parts of the circuit which are referenced to the main circuit 0V (which in turn is connected to ground), and those parts of the circuit that are floating.	299
Figure 4-49 Circuit schematic of the proposed harvesting concept, built in Switchercad for simulation purposes.	301
Figure 4-50 Simulation of the proposed harvesting circuit concept, showing the SSHI waveform only.	304
Figure 4-51 Circuit schematic of the proposed harvesting concept including an additional set of reservoir capacitors, built in Switchercad for simulation purposes. ...	306
Figure 4-52 Simulated average power dissipated by the load resistor for the circuit of Figure 4-45 (page 295).	308

Figure 4-53 Simulated curves for the average power dissipated by the load resistor, average power output of the harvesting device, voltage amplitude of V_{rect} , and $\frac{1}{2}$ the open-circuit voltage of the harvesting device for the technique proposed by Ottman et al.	309
Figure 4-54 (a) Simulated voltages across the reservoir capacitors $SC1$ and $SC2$ (b) Simulated instantaneous power dissipated by the load resistor (c) Simulated SSHI waveform; all for the circuit concept proposed in this thesis.	311
Figure 4-55 Simulated voltages across the bucket capacitors $C1$ and $C2$, and simulated SSHI waveform, for the circuit concept proposed in this thesis.	313
Figure 4-56 Simulated curves for the average power dissipated by the load resistor and average power output of the harvesting device, for the harvesting circuit concept proposed in this thesis.	314
Figure 4-57 Simulated curves for the average power dissipated by the load resistor for the harvesting circuit concept proposed in this thesis.	315
Figure 4-58 A theory representation of a charged capacitor being discharged through a load resistor, which is a situation akin to the charge/discharge simulation of the concept proposed in this thesis.	315
Figure 4-59 Simulated average power output of the harvesting device, and simulated total power dissipation in the complete circuit (components plus load) for the harvesting circuit concept proposed in this thesis.	318
Figure 4-60 A comparison of average power dissipated in the load resistor, and average power output of the harvesting device, for all three simulation circuits.	319
Figure 4-61 A schematic of the experimental system used by Ottman et al [93] (this author's interpretation).	327
Figure 5-1 Simulated effect of different beam lengths on the power output of the optimised harvesting device.	350

Figure 5-2 Simulated effect of different mass densities on the power output of the optimised harvesting device.	350
Figure 5-3 A DC-DC buck converter developed by linear technologies for providing power from a vibrating piezoelectric bimorph [151].....	357

LIST OF TABLES

Table 1-1 List of potential environmental energy sources	4
Table 2-1 Power output levels of meso-scale solar energy harvesters	32
Table 2-2 Advantages and disadvantages of solar energy harvesting	32
Table 2-3 Power output levels of small-scale air flow energy harvesters	37
Table 2-4 Advantages and disadvantages of air flow energy harvesters.....	38
Table 2-5 Power output levels of small-scale thermal energy harvesters	42
Table 2-6 Advantages and disadvantages of thermal energy harvesters	43
Table 2-7 Power output levels of small-scale RF energy harvesters.....	48
Table 2-8 Advantages and disadvantages of RF energy harvesters	49
Table 2-9 Advantages and disadvantages of vibration and human motion energy harvesters	51
Table 2-10 A comparison of the advantages and disadvantages of the three main vibration conversion methods.....	51
Table 2-11 Power output levels of meso-scale electromagnetic vibration energy harvesters	55
Table 2-12 Power output levels of meso-scale electrostatic vibration energy harvesters	62
Table 2-13 Power output levels of meso-scale piezoelectric vibration energy harvesters	66
Table 2-14 Summary of piezoelectric harvesting device shapes and their purpose.....	75
Table 2-15 Summary of work performed to date on shoe-based piezoelectric harvesters	77

Table 2-16 Elasto-piezo-dielectric constitutive equations [122].....	94
Table 3-1 List of substitutions into the objective function: equation (53), in Mathcad 2000 professional.....	178
Table 3-2 Input variables for the optimisation problem.....	179
Table 3-3 Output variables of the optimisation problem.....	181
Table 3-4 Constraints of the optimisation problem.....	181
Table 3-5 Dimensions of the optimised vibration energy harvester.....	183
Table 3-6 Results from a sensitivity analysis where the length of the beam, L_b , is constrained to 6.433mm but the resonant frequency remains constrained at 120Hz and the device volume constrained within 1cm^3	185
Table 3-7 Results from a sensitivity analysis where the length of the mass, L_m , is constrained to 11.7mm but the resonant frequency remains constrained at 120Hz and the device volume constrained within 1cm^3	186
Table 3-8 The effect of different fixtures on the frequency response of the shaker plus fixture.....	192
Table 3-9 A sample of the data recorded when performing shaker plus fixture response tests using the first automated test setup.....	193
Table 3-10 Comparison of experimental results from the optimised device with simulated results from modelling of the optimised device and experimental results from the prototype device.....	205
Table 4-1 Comparison of measured voltages and the calculated energies and powers obtained using the two bridge rectifier circuits.....	219
Table 4-2 Simulated power dissipation of the various circuit components of Figure 4-51 with different load resistor values.....	317

Table 5-1 A comparison of maximum average output powers achieved, and power consumptions of circuits, for the circuit concept proposed in this thesis and the circuit technique proposed by Ottman et al [93] [150].	344
Table 5-2 Micro-power vibration energy harvesting device power outputs when connected directly to a resistive load.	358

NOMENCLATURE

Acronyms & Abbreviations

AC	Alternating Current
ADC	Analogue-to-Digital Converter
AM 1.5G	Air Mass 1.5 Global illumination
BaTiO ₃	Barium Titanate
BCD	Bipolar-CMOS-DMOS technology
CFPG	Coulomb Force Parametric Generator
CLCC	Ceramic Leadless Chip Carrier
CMOS	Complementary Metal-Oxide-Semiconductor
CR	Capacitive-Resistive electrical network
CSV	Comma Separated Values
DAC	Digital-to-Analogue Converter
DC	Direct Current
DMOS	Double-diffused Metal-Oxide-Semiconductor
EIRP	Equivalent Isotropically Radiated Power
ESR	Equivalent Series Resistance
FEM	Finite Element Method
FPGA	Field-Programmable Gate Array
GaAs	Gallium Arsenide
GPS	Global Positioning System
HDL	Hardware Description Language
IC	Integrated Circuit

ID	Identification
IEEE	Institute of Electrical and Electronics Engineers
IO	Input/Output
ISO	International Organisation for Standardisation
JPEG	Joint Photographic Experts Group
LC	Inductive-Capacitive electrical network
MEMS	MicroElectroMechanicalSystems
MIT	Massachusetts Institute of Technology
MOSFET	Metal Oxide Semiconductor Field Effect Transistor
MP3	MPEG-1 Audio layer 3 (a digital audio compression format)
MPEG	Moving Picture Experts Group
NI	National Instruments
PC	Personal Computer
PDA	Personal Digital Assistant
PE-PP	Polyethylene- Polypropylene
PK	Peak
PK-PK	Peak-to-Peak
PLZT	Lanthanum-doped Lead Zirconate Titanate
PSI	Piezo Systems Inc
PVDF	Polyvinylidene Fluoride
PZT	Lead Zirconate Titanate
RF	Radio Frequency
RFID	Radio Frequency IDentification
RMS	Root Mean Square

SDOF	Single Degree Of Freedom
SECE	Synchronous Electric Charge Extraction
SHM	Simple Harmonic Motion
SI	Système International d'unités (International Systems of units)
SiGe	Silicon-Germanium
SSHI	Synchronised Switch Harvesting on Inductor
TCL	Tool Command Language
TKR	Total Knee Replacement
TMG	Thermo-Mechanical Generator
UHF	Ultra High Frequency
USB	Universal Serial Bus
UWB	Ultra Wide Band
WISP	Wireless Integrated Sensing Platform

Variables

α_{pn}	Seebeck coefficient between materials p and n ; used in Figure 2-4, page 40
a	Acceleration of the driving vibrations. Also the radius of the circular piezoelectric harvesting device detailed in [100]; used in Figure 2-31, page 105
A	Area of one plate of a capacitor (as in equation (2), page 58), or one electrode on the cantilever (as in equation (52), page 171). Also represents an ammeter if placed in a circle, as per Figure 2-13 on page 64
b	Width of the cantilever
b_m	Width of the mass
B	Magnetic field
c	Damping coefficient
C	Capacitance
C_p	The capacitance of one of the piezoelectric layers of the cantilever
C_{stor}	Storage capacitance; used in Figure 2-12, page 60
C_v	Variable capacitance; used in Figure 2-12, page 60
d	Distance
d_{31}	Piezoelectric charge coefficient (induced charge density displacement in direction “3” per unit stress applied in direction “1” or induced strain in direction “1” per unit electric field applied in direction “3”)
D	Charge density displacement (also sometimes called polarisation or dielectric displacement)
D_3	Charge density displacement in the “3” direction
ε	Strain (synonymous with S)
ε_1	Strain in the “1” direction
ε_r	Relative permittivity
ε_p^σ	Absolute permittivity of the piezoelectric material under constant stress conditions
E	Electric field

E_3	Electric field in the “3” direction
E_p	Young’s modulus of the piezoelectric ceramic material used in construction of the cantilever
E_s	Young’s modulus of the material that constitutes the centre layer of the cantilever; i.e. the ‘substrate’ layer
f	Frequency
$f(x)$	A normalised shape function that satisfies the boundary conditions of the cantilever
F	Force
g_{ij}	Piezoelectric voltage coefficient
h_{av}	Height from the position of the neutral axis to the position of half the height of the upper piezoelectric layer of the cantilever; as per Figure 3-19, page 153
h_{lp}	Height of the lower piezoelectric layer of the cantilever
h_m	Height of the mass
h_n	Height from the bottom of the cantilever to the position of the neutral axis, as per Figure 3-23 (page 164) and Figure 3-24 (page 167)
h_p	Height of one of the piezoelectric layers of the cantilever
h_p	Position of the top of the cantilever; used in equation (38), page 167
h_s	Height of the centre (i.e. substrate or ‘shim’) layer of the cantilever
h_{up}	Height of the upper piezoelectric layer of the cantilever
I	Area moment of inertia
I_p	Current output of a piezoelectric energy harvesting device
I_R	Current flowing through a resistor
I_s	Reverse bias saturation current of a diode
k	Spring constant
k_{31}	Piezoelectric electromechanical coupling coefficient (field developed in direction “3” per unit stress applied in direction “1” or induced strain in direction “1” per unit charge density applied in direction “3”)
k_{33}	Piezoelectric electromechanical coupling coefficient (field developed in

direction “3” per unit stress applied in direction “3” **or** induced strain in direction “3” per unit charge density applied in direction “3”)

L	Inductance
L_b	Length of the cantilever
L_m	Length of the mass
m	Mass value
M	Bending moment
M_{int}	Internal bending moment
n	Radius of the inner region of the circular piezoelectric harvesting device detailed in [100]; used in Figure 2-31, page 105
N	Reaction force
N_{int}	Internal force acting on the cantilever; used in Figure 3-22, page 161
P	Polarisation
$P_{ave_in_R}$	The average power dissipated by a load resistance
θ	Relative phase displacement between the movement of the mass and movement of the host structure (the host structure is the structure on which the energy harvesting device is mounted)
Q	Charge
Q_3	Charge in the “3” direction
ρ_m	Density of the mass material
ρ_p	Density of the piezoelectric ceramic material
ρ_s	Density of the material that constitutes the centre layer of the cantilever; i.e. the substrate or ‘shim’ layer
R	Resistance
R_{Dson}	The resistance between the drain and source terminals of a MOSFET when in its on state
R_L	Value of load resistance
R_{opt}	Optimal load resistor value

σ	Stress (synonymous with T)
σ_1	Stress in the “1” direction
s_{ij}	Piezoelectric elastic compliance coefficient
S	Strain (synonymous with ε)
t	Time
T	Stress (synonymous with σ)
T_{amb}	Ambient absolute temperature
T_{CJ}	Temperature of the hot junction of a thermopile-based thermal energy harvester; used in equation (1), page 41
T_{HJ}	Temperature of the hot junction of a thermopile-based thermal energy harvester; used in equation (1), page 41
V	Voltage. Also represents a voltmeter if placed in a circle, as per Figure 3-13 on page 132
V_3	Voltage in the “3” direction
V_{DC}	DC voltage
V_{int}	Voltage across the internal impedance of an electrical source
V_L	Voltage across a load resistor
V_{oc}	Open-circuit voltage
V_{piezo}	Voltage between the ground reference of a bridge rectifier circuit and one terminal of a voltage source representing the piezoelectric energy harvesting device; as per Figure 4-8, page 222
V_{pk}	Peak voltage value of an AC voltage waveform (synonymous with the amplitude of an AC voltage waveform)
V_{pk-pk}	Peak-to-peak voltage value of an AC voltage waveform
V_R	Voltage across a resistance
V_{RMS}	RMS voltage
V_{src}	A voltage source
Ω	Ohms: the SI unit of electrical impedance and electrical resistance

w_1	Deformation of the end of a cantilever that has no end mass
w_2	Deformation of the end of a cantilever that has an end mass
ω_n	Natural frequency of the cantilever (also called the resonant frequency of the cantilever)
$W_d(L_b)$	Out-of-plane displacement at the end of the cantilever
$w_d(x, t)$	Out-of-plane deflection of the neutral axis at any distance x along the length of the cantilever
W_s	Deflection at the end of a static cantilever
$w_s(x)$	Deflection at any distance, x , along the length of a static cantilever
x	Any point along the length of the cantilever
X_c	Capacitive reactance
y	Any vertical distance from the neutral axis of the cantilever
\ddot{y}	Acceleration of the harvesting device (resulting from the input vibration)
Y	Amplitude of host structure motion (the host structure is the structure on which the energy harvesting device is mounted)
ζ	Damping ratio (ratio between actual damping and critical damping)
Z_{int}	Internal impedance of an electrical source
Z_L	Value of load impedance
Z_t	Total impedance of a circuit external to an electrical source (i.e. not including Z_{int})

Constants

Symbol	Name	Value
ε	Charge carried by an electron	$1.602177 \times 10^{-19} \text{C}$
ε_0	Permittivity of free space	$8.854 \times 10^{-12} \text{C}^2/\text{N} \cdot \text{m}^2$
k_B	Boltzmann's constant	$1.38066 \times 10^{-23} \text{J/K}$

CHAPTER 1: INTRODUCTION

Energy harvesting relates to the practice of scavenging small amounts of energy from ambient environmental sources (e.g. wind, water, heat, vibration) in order to power either some small, low power electronic system directly, or to charge an electrical storage reservoir (usually a rechargeable battery or capacitor) that can be used to power a higher power application at time intervals. Much of what has been learnt about energy harvesting has been learnt in the last fifteen years or so, and it is enough to fuel the promise that many electronic systems can have built-in energy harvesting functionality in the future. However, at present the low amounts of power that can be delivered from energy harvesting devices is proving a barrier to adoption of the technology. Device optimisation is one way in which the power density of a harvesting device can be significantly improved. Another way in which the power output can be enhanced is through the use of the ‘harvesting circuitry’; i.e. the circuitry that is usually connected to the output of the harvesting device to condition and/or manage the electrical power output. In this thesis, both of these avenues are explored.

In regard to device optimisation, an analytical model of a piezoelectric cantilever-based vibration energy harvesting device is developed whose resulting expression for the power output of the device can be used as an objective function in a computer-based optimisation algorithm. The required inputs to the optimisation problem are the target resonant frequency for the device and constraints for the volume of the device. The output is a design (i.e. the dimensions) for a device that is geometrically optimised for maximum power output. In this thesis, the developed model is used in conjunction with a conjugate gradient optimisation algorithm, provided by Mathcad 2000 Professional software (Parametric Technology Corporation/Mathsoft, MA, USA). The resulting

harvesting device design was found, through experiment, to be capable of producing a maximum power output of $370.37\mu\text{W}$ for a volume of 1cm^3 and a resonant frequency of 87Hz . This achieved power level is amongst the highest of power densities reported in the literature to date.

In regard to the harvesting circuitry, this thesis also proposes a novel harvesting circuit concept for the purpose of obtaining an enhanced power output. The suggested circuit is based on a combination of a charge pump-type circuit and the Synchronised Switch Harvesting on Inductor (SSHI) technique, which is a technique that is known to increase the power output of piezoelectric energy harvesters by as much as 900% [1]. By combining these two functions in the manner that has been conceived in this thesis, the functions become mutually conducive to the aim of enhancing the power output of a piezoelectric generator. Aside from taking advantage of the voltage boosting effect the SSHI technique is known for, the particular implementation of the technique adopted in this thesis also enables a charge pump-type circuit to collect charge during the whole of each AC cycle of the piezoelectric generator output, rather than for just part of it as occurs with the commonly-used bridge rectifier circuit. Therefore, in the new harvesting circuit concept suggested in this thesis, at least two mechanisms are in place for enhancing the power output of a piezoelectric vibration energy harvester. In addition, consideration has been given to allow conditioning of the harvested power such that a regulated DC supply, which is the preferred format for most electronic device and systems, might be obtained. The result is a circuit that is capable of producing over three times the amount of DC power than the standard bridge rectifier circuit for the same input vibration conditions, with additional provision for easy formatting of the power to form a regulated supply.

This first chapter of the thesis presents the motivation for carrying out the research, describes the context in which the research fits, specifies the aims and objectives, and presents the contribution of the research. The chapter ends by presenting an overview of the methodology used and describing the rest of the thesis structure.

1.1 Motivation

Harvesting energy from the environment is not new. Windmills and water wheels have been around for centuries, and active research has been carried out on them for as long. John Smeaton (born in 1724) carried out scientific research on waterwheels, and by experiment found out that the overshot wheel (powered from water falling on the wheel from above) is two times more efficient than the undershot wheel (where the wheel is rotated by water flowing underneath). The above example is, of course, an example of large-scale energy harvesting. More recently there has been a lot of attention on small (meso or micro) scale energy harvesting, where obtaining a few milliwatts of power from one of a wide range of environmental sources (see Table 1-1 on the following page), using small-scale devices (e.g. μm to cm package sizes) is the goal.

Table 1-1 List of potential environmental energy sources

Mechanical	Air flow
<p>Vibration:</p> <ul style="list-style-type: none"> Car engine compartment, Trains, Ships, Helicopters, Bicycle, Aircraft wings, Bridges, Kerbsides, Floors (offices, train stations, nightclubs), Speakers, Window panes, Walls, Household appliances (fridges, washing machines, microwave ovens), Pumps, Motors, Compressors, Chillers, Conveyors. <p>Rotation:</p> <ul style="list-style-type: none"> Pedals, Wheels. <p>Others mechanical sources:</p> <ul style="list-style-type: none"> Acoustic, Shock absorbers, Vehicle braking, Blood pressure, Chest expansion from breathing, Vehicles passing over/by energy harvesting devices, Walking or running (i.e. footfall), Bending of the joints (e.g. knee or arm), Typing, Pressing switches, 	<ul style="list-style-type: none"> Wind, Air conditioning ducts, Convection, Ventilation ducts, On moving vehicles. <hr/> <p style="text-align: center;">Fluid flow</p> <hr/> <ul style="list-style-type: none"> Water supply/waste pipes, Ocean currents, Rivers, Blood flow. <hr/> <p style="text-align: center;">Thermal</p> <hr/> <ul style="list-style-type: none"> Domestic radiators, Human skin, Vehicle exhausts, Thermal solar. <hr/> <p style="text-align: center;">Electromagnetic Fields</p> <hr/> <ul style="list-style-type: none"> Solar (outdoor), Indoor lighting, Radio frequency, Cell phones, High tension power line emissions, Microwaves, Infrared, Gamma radiation from decaying materials. <hr/> <p style="text-align: center;">Others</p> <hr/> <ul style="list-style-type: none"> Alpha & Beta particles.

Currently, the research literature demonstrates small-scale devices capable of harvesting levels of power that vary from nanowatts to a few milliwatts, depending on the energy source type (solar/wind etc), method of conversion, and device size. The motivation for developing these small-scale devices for harvesting these small amounts of energy from the environment stems from several sources:

1) Portable consumer and industrial products are increasingly integrating more functions (e.g. mobile phones that have the capability to access the internet), and although there have been advances in low-power electronics, this increase in capability leads to greater demands on the battery powering the device.

Consequently the battery remains as representing a large percentage of system size and weight. It also represents the last major maintenance problem for many for portable devices, as it regularly requires re-charging. Most people have suffered frustration when a battery in a much-needed appliance: a mobile phone, global positioning system (GPS) receiver or personal digital assistant (PDA), has run out at the most inconvenient moment. In addition, as the effort to increase battery energy density continues, there may be growing safety concerns, as one report comments: “Using new materials and chemistries, batteries are approaching explosives in terms of energy density” [2]. Harvesting energy from the environment can alleviate these problems, by extending the life of a battery so that it either needs to be charged less frequently, or can be replaced by a smaller battery.

2) There is currently a strong drive toward ubiquitous sensing. In the future it is envisaged that tiny, ubiquitous sensor nodes will be embedded in the environment around us, communicating between themselves and controlling our environment for us without us being aware of them. Three recent quotes sum-up this view:

Bill Gates, 2003 [3]:

“As people find more ways to incorporate these inexpensive, flexible and customisable devices into their lives, the computers themselves will gradually ‘disappear’ into the fabric of our lives”.

Gene Frantz, Texas Instruments Principal Fellow, 2006 [4]:

“You can almost say that we are on the path to the vanishing product – where the product will be so small and insignificant in size, but so significant in capability, that we really don’t know where we have it; we just know we have it”.

Kris Pister, founder of Dust Networks Inc, 2006 [5]:

“About a decade ago, it seemed clear to me that there was a technological path to integrating sensing, computation, communications and power into a millimetre-scale package. All of the technology drivers were going in the right direction, following Moore’s Law-type exponentials down to zero size, power and cost. I coined the term ‘smart dust’ to describe where all of that was headed”.

For this vision to become reality, these thousands of tiny computational sensor nodes will need a power supply. Replacing batteries in this number of devices is prohibitive in terms of costs, manpower, and time, and hardwiring them to mains power supplies is prohibitive for the same reasons. Harvesting energy from ambient environmental sources has the potential to provide an indefinite supply of power.

3) Still pertaining to sensing technology, wireless sensors are being used in increasingly remote locations, e.g. on wild animals (Zebranet [6]), on pipelines in Alaska [7], and under-sea. Such sensors allow researchers to gather information, or can allow engineers to remotely assess information about the health of structures such as pipelines or machines. For example, wireless sensors that transmit vibration

information of rotating motors can give an indication of which parts are nearing failure, allowing repairs to be undertaken as and when needed rather than on a regular time-slot basis, thus saving costs and time. Continually replacing batteries in remote sensors can either be difficult and expensive, or simply impossible.

4) Another kind of remote environment, though not in the same literal sense as being far away, is the inside of the human body. Energy harvesting could feasibly be seen as an enabler for the development of implantable medical devices. Implantable medical devices already exist that are run from batteries which can be recharged using RF energy. If energy harvesting could be employed to harvest energy from the temperature gradients, vibrations or movements that exist naturally in humans, re-charging would be either unnecessary or reduced. The benefits of self-powered medical devices are significant: currently most battery powered medical implants have battery lifetimes of 7 to 10 years, after which the patient is subjected to more potentially risky invasive surgery; this could be avoided. In addition there are potential monetary savings to be made: one estimate for the cost of a replacement cardiac pacemaker is £10,000 [8], which could be saved many times over and used elsewhere.

Each of the four aforementioned arguments; i.e.: energy harvesting for portable electronics (mentioned in 1); for wireless sensor nodes (the ‘ubiquitous’ case mentioned in 2 and the ‘remote’ case discussed in 3), and for medical devices (mentioned in 4) provides a compelling case for harvesting energy in small amounts from the environment, but of the application areas identified, it is the possibility of ubiquitous and remotely-placed wireless sensor nodes that is currently capturing the imagination of the research community. This is likely due to the wide application potential of this

technology. In industrial sectors such sensors could provide feedback for automated processes and predict worn parts of machinery before machinery failure. In both industry and domestic domains they have the capability to sense and record the use of utilities (e.g. gas, water and electricity), thus providing information that leads to a more intelligent use of world energy resources. One estimate, which pertains to the United States only, suggests that the equivalent of 35 million metric tonnes of carbon emissions per annum could be saved with improved building automation [9]. In contributing to the every day life of citizens, sensor nodes will enable the tailoring of an environment to suit the individuals in it. For safety, sensor nodes could be integrated into children's shoes and clothing, so that parents receive an alarm when their children wander from the local vicinity. Medical body sensor networks could monitor blood pressure or glucose levels, so that appropriate action can be taken to halt patient deterioration.

The last thing to mention in relation to the motivation for harvesting energy from the environment is a key contributing factor that makes everything detailed so far appear feasible: the vast reduction in the power consumption of modern electronics. Low-power design is an area that has been seeing strong growth for some years. Power management techniques such as shutting parts of the system down when not in use, slowing clock rates down, and dynamically altering the operating voltage of electronic components are now commonly in use. Technology is also becoming available that consumes less power, e.g. low-power CMOS and processors that have core voltages of 1V or below, and with advances in MicroElectroMechanicalSystems (MEMS) fabrication processes, a wide variety of low-power microelectromechanical devices will also become available. As more products become available that consume less power, harvesting energy from environmental sources becomes more feasible as a source, and it

is really this closing gap between the power required and the power that can be achieved that is currently forming a pivotal point in the advent of energy harvesting.

1.2 Research Context

This thesis is set in the domain of what might be termed ‘meso-scale’ energy harvesting devices for powering small low-power electronic devices or systems, such as wireless sensor nodes or MEMS devices. It is difficult to find a definitive description of what constitutes a ‘macro’, ‘meso’, or ‘micro’ scale energy harvesting device in the literature available. Indeed, comparison of energy harvesting devices on many fronts: power output, size or efficiency has been proven difficult so far because of the wide variation in device types, structures and conversion mechanisms. This author therefore feels it necessary to elaborate on her understanding of what constitutes a meso-scale device so that the reader may fully understand the context which is referred to throughout the thesis. ‘Meso’ comes from ancient Greek, and means ‘middle’ or ‘intermediate’, and as such, ‘meso’ applied to energy harvesting devices can be interpreted as those that are not large-scale, such as solar panels seen on the roofs of houses for example, nor are micro-scale, such as those with μm -size dimensions that require MEMS fabrication processes (e.g. multi-depositions of material layers, micromachining, or etching) in their construction. In broad terms, the term ‘meso’ here is used to describe a device that is no more than a few cm^3 in volume (or a few cm^2 in area), that has dimensions in the mm-cm range, and that can be built largely without resorting to MEMS processing techniques. Of course, this is a somewhat loose definition, of which some energy harvesting devices may cross the boundaries, but it was felt necessary to attempt to clarify this in order to put some bounds on the scope of this work. This done, we can now turn our attention to the energy source and conversion mechanism considered:

Of the many ambient environmental sources of energy available, vibrations are the concern of this thesis. This is chiefly because vibrations are one of the most prevalent sources of energy that can be found environmentally (see Table 1-1 on page 4, where vibrations can be seen to represent much of the ‘mechanical’ category of energy source). There are three main mechanisms by which vibrations can be converted into electrical energy: electromagnetic, electrostatic and piezoelectric. It is piezoelectric conversion that is utilized here, chiefly because the use of piezoelectricity allows for a generator that is completely self-contained; i.e. it does not require any external supporting accrements. In addition, piezoelectric converters have a minimum of moving parts, and are capable of generating power with voltage levels that can be easily conditioned (e.g. converted to DC or boosted). Electrostatic converters usually require an external voltage source to accomplish energy conversion, and electromagnetic converters, in addition to producing power at voltage levels that are very low (e.g. a few hundred mV up to around 2V) and that are consequently difficult to convert using conventional electronic devices, also tend to require carefully manufactured micro-scale moving parts.

The decision to focus on enhancing the power output of piezoelectric energy harvesting devices arises largely from the fact that there still exists a significant gap between the amounts of power required by many (currently battery-powered) electronic devices, and the amount of power that can be harvested by using meso-scale energy harvesters. Also, taking a broader view, it could be argued that continuing to push the boundaries of achievable power output is effort that is never wasted, since electrical power is one of the most useful of all resources, and the more power available ‘for free’, the more potential applications can be realised. The decision to focus on device optimisation

originally stemmed from this author's belief that there is a need for a method of determining the maximum power level that can be obtained from a space-envelope (volume) that an energy harvesting device may utilise in an application. By understanding what the maximum power can be for the space envelope under consideration, the system designer is greatly aided when he/she constructs a 'power budget' for a proposed application system, and thus ultimately assessing system feasibility becomes easier. The decision to develop circuitry whose primary function is to boost the output power of the generator but, at the same time, must condition and manage the power, comes from this author's view that although recently, a number of circuit techniques have been reported in the literature that prove an ability to increase the power output of the harvesting device, not many are also capable of conditioning the power into a useable format. The power is simply not useful for many applications unless it is in the form of a regulated DC supply.

1.3 Scope

It can be considered that there are three main blocks to a typical, complete, energy harvesting system: the harvesting device (energy transducer), the harvesting circuitry and the end application system:



Figure 1-1 A basic block diagram of an energy harvesting system.

In the literature, there are some works that concentrate on all three blocks of the system, so that a full system is realised and analysed at project conclusion. More often than not however, works in the literature focus only on one block: typically either on some

aspect of the transducer device or on some aspect of the harvesting circuitry. This thesis aims to consider the first two blocks of the system, while the third block, the end application, will not be considered. The reason for this is simply that this author's interest lies predominantly in the harvesting circuitry part of the system, but obviously, one cannot design, build and test some harvesting circuitry unless there is an energy harvesting device with which to use it. The project therefore 'evolved' such that both aspects of the system (transducer plus circuitry), by necessity were considered, whereas the end application was not, because consideration of all three system blocks was deemed too ambitious.

In taking a view of the energy transducer block, one way to examine a piezoelectric-based vibration energy harvesting device, such as is the topic of this thesis, is to represent it with a lumped element equivalent electrical circuit, as shown below:

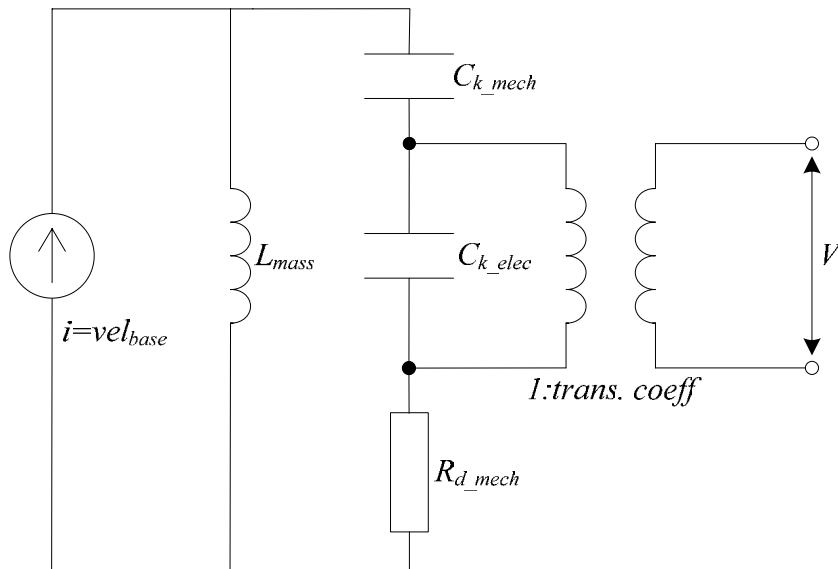


Figure 1-2 A lumped element equivalent electrical circuit of the input vibrations and piezoelectric transducer.

This model includes a vibrational input to the system, in the form of a current source, and representation of the piezoelectric mechanical resonant system, in the form of the other lumped electrical elements: L_{mass} is analogous to the mass; the two capacitors: C_{k_mech} and C_{k_elec} represent the structural stiffness, though while C_{k_mech} remains at a constant value C_{k_elec} can change depending on the electrical load applied at the output terminals; R_{d_mech} is an element that represents mechanical damping; V is the voltage output and the ideal transformer with the ratio $1:trans. coeff$ represents electromechanical coupling. If the lumped element equivalent electric circuit parameters are known, this type of model can be used for design and analysis purposes when conducting studies into the energy harvesting system as a whole. However, the electrical output described by the model is simply ‘measured’ as a voltage at the output of the represented mechanical resonant system, whereas the scope of this thesis, as mentioned above, also includes the harvesting circuitry. This type of model therefore has some use in terms of describing the behaviour of the transducer part of the system in response to the input vibrations, but it does not include harvesting circuitry functions such as voltage rectification and regulation. It therefore ‘stops’ at the interface between the energy transducer block and harvesting circuitry block of Figure 1-2.

In terms of the vibration input, the current source is analogous to the velocity of the motion of the base structure to which the piezoelectric energy harvesting device is attached, which is why it is placed in parallel with the inductor, which represents the mass, and series capacitor-resistor network, which represents the structural stiffness and mechanical damping of the device. Several significant system-level features of a piezoelectric vibration energy harvesting device can be usefully represented by this model, including the effect of piezoelectric backward coupling (i.e. coupling ‘back’

from the electrical domain to the mechanical domain), impedance matching and energy stored in the piezoelectric ceramic.

In recent years, it has been noted by several research groups that the resonance frequencies of a piezoelectric harvesting device will shift in response to a variation in load impedance value. In the literature, a load impedance is actually often represented by a load resistance; i.e. a simple load resistor that is connected directly to the output terminals of the device. The reasons for doing this will be discussed in section 3.4.1.3 (beginning on page 147), but put simply, it is a convenient method of characterising the output of the generator. It has been noted [135] [138] [139] [140] that as the value of the load resistor is increased from a low value to a high value (i.e. in the direction of zero to infinity), the modal frequencies of the device shift upwards. The lumped element equivalent electrical circuit of Figure 1-2 can model this resonance frequency shift through the following mechanism:

- A load resistor is placed across the electrical output terminals.
- As the value of the load resistor is increased, C_{k_elec} moves from a short-circuit to an open-circuit condition. The total capacitance in the system then decreases, and the resonant frequency of the C-R and L parallel circuit increases.

Another significant behaviour in regard to a piezoelectric-based vibration energy harvester is that of impedance matching. Conventional circuit theory suggests that maximum power transfer from source to load occurs when their impedances are matched, making it conducive to aim for this condition. In regard to piezoelectric harvesting devices, the source impedance is often taken, when calculating theoretical values, to be the reactance of the self-capacitance of the device. The self-capacitance arises due to the construction of the device: a piezoelectric device is usually constructed

from one or more layers of piezoceramic material (which is also a dielectric), which are ‘sandwiched’ between electrode layers; that is, the piezoelectric layers have electrode material plated or patterned on their top and bottom surfaces in order to enable a path of electrical conduction. In Figure 1-2, C_{k_elec} represents the self-capacitance of the piezoelectric device, and its reactance depends on the physical dimensions of the device (not represented in the figure), the relative permittivity of the piezoceramic material (also not represented in the figure), and the frequency of the vibrations (represented by i), as per equations (51) and (52) described later in this thesis (page 170). Although the transformer in Figure 1-2 is used to represent coupling between the mechanical and electrical domains, it might also be construed as an impedance matching transformer, which enables an impedance match between the load applied at the electrical output terminals and the electrical impedance of the harvesting device (i.e. reactance of C_{k_elec}).

Given that the piezoelectric harvesting device has some self-capacitance, it inherently also will always contain some charge as long as the harvesting device is in a dynamic state. This ‘residual’ charge represents energy that is retained within the piezoelectric ceramic, and thus it cannot be used to power an external load. This is represented in Figure 1-2 as the energy stored within C_{k_elec} , as per the equation for energy stored in a capacitor: $\frac{1}{2} \cdot C \cdot V^2$.

A vibration energy harvesting system is a complex dynamic system, incorporating source vibrations, transducer, harvesting circuitry and end application. The lumped element equivalent circuit of Figure 1-2 is useful for giving an overview of part of the system, in terms of the fact that it includes the source vibrations and features of the piezoelectric transducer itself, e.g. mechanical resonance, energy stored within the piezoelectric ceramic, impedance matching and shift in resonant frequency with change

in load resistor value. However, it does not include useful harvesting circuit functions such as voltage rectification or regulation, or an electrical storage medium. In addition, it assumes ideal components (there are no parasitic elements to the components that represent the elements); the transformer is ideal, and dielectric losses are not accounted for. Also, dimensional and material parameters are not considered, so that the elements are given values which are calculated without regard to the physical properties of the device.

The scope of this thesis is base excited vibration energy harvesting, and the model of Figure 1-2 is applicable to this. It is not applicable for direct force or ‘impact’ type energy harvesting systems, e.g. those that are shoe-based. For those systems, the energy input can be much higher because the device can often be larger, the displacement of the device further and the force applied greater. In addition, the energy input can potentially be more predictable, since it is often determined by human motion. Moreover, it is unlikely that direct force or impact type harvesters will work at resonance, whereas base excited vibration-based devices are actively designed towards working at resonance. In this thesis, the work carried out by this author is with consideration to a base excited vibration energy harvesting system.

1.4 Aims and Objectives of the Research

Aims:

The main aim of this research is to enhance the power output of a piezoelectric vibration energy harvesting device, by two means: computationally optimising the geometric parameters of the generator such that the best use is made of the volume the device may utilise in an application, thereby resulting in an increase in the ‘power density’ (W/cm^3)

of the device, and: through use of the ‘harvesting circuitry’; i.e. the circuitry that is usually connected to the harvesting device to condition and/or manage the electrical power output. However, since an enhanced level of output power is not useful for most applications unless it is converted into a regulated DC supply, this research also aims to condition the enhanced electrical power.

Objectives (towards optimising the harvesting device):

- 1) Develop an analytical model of the piezoelectric generator that has the capacity to be used for two distinct purposes, described as follows:
 - a) In order to optimise the geometric dimensions of the generator such that the power is maximised for a volume dictated by the application environment, the model must produce an expression for the power output of the generator that can be used as an objective function with a computer-based optimisation algorithm,
 - b) In order to enable the design and development of the harvesting circuitry, the model must be capable of predicting other electrical outputs of the device (in addition to power), namely: voltage and source impedance.
- 2) Use the model with a computer-based optimisation algorithm to obtain dimensions for a device that is optimised for maximum power output, given volume constraints and a target resonant frequency.
- 3) Design and build a suitable test setup.
- 4) Fabricate and test the optimised design.

Objectives (towards the development of a novel harvesting circuit concept):

- 1) The bridge rectifier circuit is the most commonly used interface circuit for energy harvesting devices for the purpose of converting AC to DC in order to make the power more useable. However, a bridge rectifier does not result in a *regulated* DC supply. Therefore, as a starting point, the first objective is to analyse in detail the operation of the standard bridge rectifier circuit, in order to find an area in which power efficiencies can be gained, while also considering the need to include voltage regulation.
- 2) Develop a novel, improved concept for the harvesting circuitry based on the findings from objective (1) immediately above,
- 3) Perform the electronic design for a circuit that will implement the concept developed in objective (2) immediately above,
- 4) Build and test the circuit and compare the performance of the new concept with that of the standard bridge rectifier circuit.

1.5 Contribution

This thesis investigates two possible methods of enhancing the power output of a piezoelectric cantilever-based vibration energy harvesting device. The first is based on a geometric optimisation of the piezoelectric generator itself. The second relates to the harvesting circuitry; i.e. the circuitry that is usually connected to the generator output to condition and/or manage the electrical power.

1.5.1 Optimisation of the Geometric Dimensions of the Harvesting Device

In regard to the piezoelectric vibration energy harvesting device, an analytical model has been constructed that considers the effect each geometric parameter has on the power output of the device. By relating each dimension of the device to the power output, the model results in an expression for the power output whose arguments include every dimension of the piezoelectric generator. The advantage of this is that the expression can be used as an objective function in a computer-based optimisation algorithm to provide a design (i.e. the dimensions) for a harvesting device that is optimised for maximum power output subject to some volume constraint and some target resonant frequency. In the work presented in this thesis, the developed expression was used as an objective function of an optimisation problem with constraints typical of those expected in a practical situation. The result was an optimised device, with a volume of 1cm^3 , which produced a maximum power output of $370.37\mu\text{W}$ at a resonant frequency of 87Hz . This amount of power represents one of the highest power densities published to date, and is state-of-the art in terms of the power output achieved for a 1cm^3 volume device.

1.5.2 A Proposed Novel Harvesting Circuit Concept

The operation and performance of a bridge rectifier circuit has been analysed both through experiment, and through circuit simulation using Switchercad (Linear Technology, Milpitas, CA, USA) software. As a result of this analysis, shortfalls of the bridge rectifier circuit were identified; mainly that during steady-state conditions the piezoelectric generator spends much of its time in the open-circuit condition, where there is no power transfer from generator to load. In addition, the output of a bridge rectifier, although DC, is not *regulated* DC, which is the preferred format of supply for most electronic devices and systems in use at the current time. Through an initiative to

try and overcome these shortfalls, a new harvesting circuit concept is proposed that combines a charge-pump type circuit, whereby charge is collected per half-cycle of the piezoelectric generator output and then dumped into a larger storage capacitor, with the Synchronised Switch Harvesting on Inductor (SSHI) technique that has been reported in literature [1]. The new concept contributes several advantages over the bridge rectifier circuit; these being:

- 1) The ability to power higher power applications, because the new concept adopts the philosophy of storing charge over time such that an energy reservoir is built up (from which the application system can then be powered), rather than powering the application by a 'continuous powered approach' i.e. one in which the application system is powered immediately from a harvesting device (albeit with some power conditioning) such that no electrical storage medium is used and more immediate use of the power output from the harvester is made.
- 2) Power enhancement because energy is collected during the whole of each AC cycle of the piezoelectric generator voltage output waveform, rather than for just part of it as occurs with the bridge rectifier circuit,
- 3) Power enhancement through the use of the SSHI technique,
- 4) Power enhancement through impedance matching to the internal impedance of the piezoelectric generator,
- 5) Power enhancement through the use of two diodes in the AC-DC conversion process, rather than four as occurs with the bridge rectifier circuit.

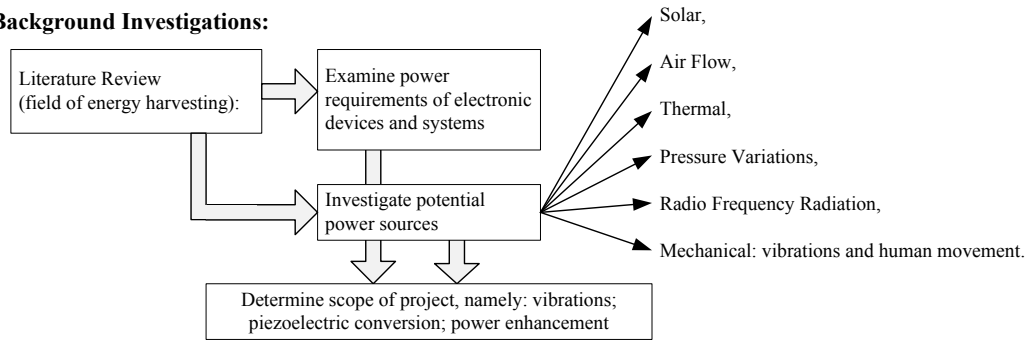
- 6) Provision for the use of a DC-DC buck-boost converter. Since DC-DC converters operate by pulse-width modulation of their input power, the current loading profile they present to their supply is uneven. The new concept enables charge to be collected in two storage reservoirs, which can then be used to supply a DC-DC converter of the user's choice.

In the work presented in this thesis, a circuit has been built that can implement the new harvesting circuit concept, and the performance of the concept is assessed in two ways: (1) it is compared, through experiment, to the performance of the standard bridge rectifier circuit in regard to how much energy can be stored in a large reservoir capacitance (i.e. with no electrical load using the power). In this case, the most notable result is that, for a vibration acceleration amplitude of $\pm 0.125g$, a total of 2mJ of energy was harvested in two 220 μ F storage capacitors, in comparison with 0.577mJ of energy harvested into one 220 μ F storage capacitor using the bridge rectifier circuit. The second method of assessing the performance of the concept is: (2) it is compared, through simulation, with two other circuits for the purpose of comparing average power output over time (instead of energy harvested into storage capacitance as per the experimental comparison with the bridge rectifier circuit). The two other circuits were: a) one in which a variable value load resistor was directly connected across the output terminals of the harvesting device, used as a method of determining the 'theoretical maximum' average power output (see Figure 4-45 on page 295), and b) one that implements the technique proposed by Ottman et al [93] (see Figure 4-46 on page 296). It was shown that for the same input conditions, the maximum average power output of the piezoelectric harvesting device when the new concept was used was nearly eleven times more than when the technique proposed by Ottman et al [93] was used (i.e. an increase

from $222.01\mu\text{W}$ to 2.44mW), and was nearly eight times more than the theoretical maximum average; i.e. from $315.26\mu\text{W}$ (theoretical maximum), to 2.44mW . The new concept is capable of obtaining more power from the harvesting device than the ‘theoretical maximum’, which was ascertained by the circuit in which a load resistor was directly connected across the output terminals of the device, because the new concept takes advantage of the SSHI technique, which boosts the output voltage of the device.

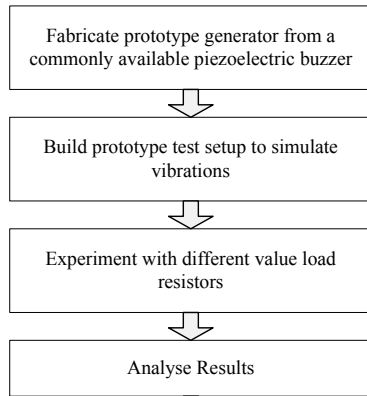
1.6 Methodology

Background Investigations:

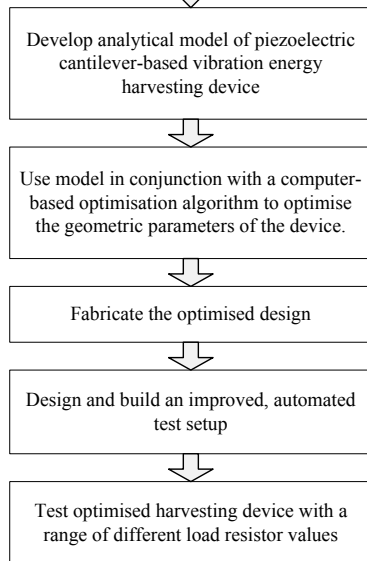


Preliminary Experiments:

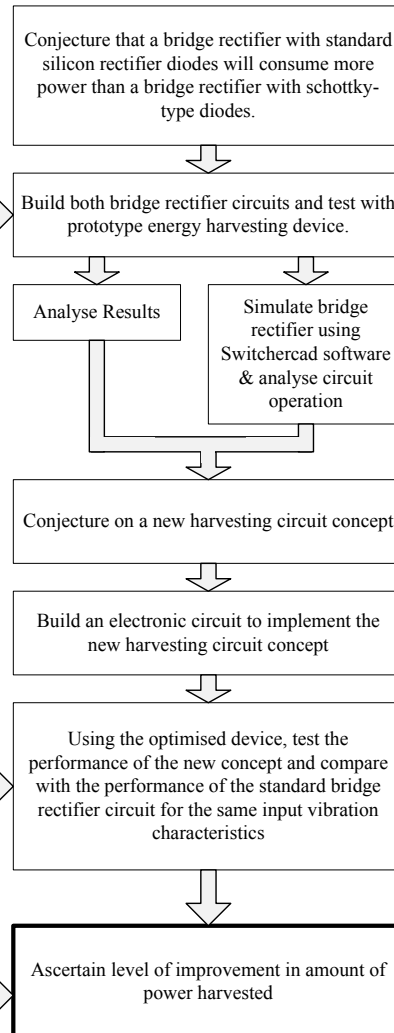
Piezoelectric Vibration Harvesting Device Optimisation



Main Body of Work:



Proposed New Harvesting Circuit Concept



1.7 Thesis Structure

Chapter two presents a literature review, which begins by examining the power requirements of a range of electronic devices and systems. Following this, an overview of the various energy harvesting technologies that can be used to extract energy from the different available sources (for example solar, thermal, or radio frequency) is given, paying particular attention to the power levels achieved in experiments to date. The two sets of data are then compared; i.e. the power levels that have been achieved by experiment are compared against the power requirements of electronic devices and systems, and justification is given for: a) piezoelectric conversion of vibration energy as the technology base chosen for this thesis, and b) focussing on power enhancement. Following this, an introduction to the concept of piezoelectricity is given, which encompasses both historical and technological contexts, and a history and state-of-the-art in power enhancement of piezoelectric generators is presented. The chapter ends with some brief conclusions.

Chapter three is concerned with the optimisation of the piezoelectric energy harvesting device. The chapter opens by describing the fundamental configuration of the device, before going on to describe some initial experiments that were carried out using a prototype generator and a prototype test setup built using commonly available laboratory equipment. After the findings from the initial investigations are discussed and conclusions are drawn, the development of the analytical model is given, and optimisation of the geometric dimensions of the device is then performed using the complex conjugate optimisation algorithm. Test considerations are discussed further, incorporating lessons learnt from the initial experiments, and an improved test setup is

built. The optimised device is fabricated and tested using the improved test setup and the results presented. The chapter ends with a discussion and conclusions of the work.

Chapter four is concerned with the development of a novel harvesting circuit concept. It begins by describing some initial experiments that were carried out using the prototype harvesting device of Chapter 3 and a bridge rectifier circuit. Findings from these experiments are discussed and conclusions are drawn. The evolution of the new harvesting circuit concept is then described and the advantages of it discussed, before a description of how the system was implemented in electronic circuit design is given. The circuit is built, compared through experiment with the standard bridge rectifier, compared through simulation with another circuit technique given in the literature, and the results presented. The chapter ends with a discussion and conclusions of the work.

Chapter five is the concluding chapter. It opens by reinstating the aims and objectives of the thesis, and then summarises the work undertaken in chapter 3, which is concerned with power enhancement through optimisation of the geometric dimensions of the harvesting device, and chapter 4, which is concerned with power enhancement through the development of a novel harvesting circuit concept. As the summary is given, the findings of the work undertaken are reiterated: namely that the power density of the optimised device is one of the highest reported in literature to date, and that by using the harvesting circuit concept proposed in this thesis rather than the standard bridge rectifier circuit, the amount of power harvested can be increased by 247%. Following this, the implications for the work are discussed, and the chapter ends with some recommendations for further work.

CHAPTER 2: LITERATURE REVIEW

Given the broad, cross-disciplined nature of the field of energy harvesting, it was deemed sensible that the literature review begin by focussing on the fundamentals. Therefore, this chapter first examines the power requirements of various electronic devices and systems, and then examines the state-of-the-art in energy harvesting technologies, evaluating the advantages and disadvantages of each technology and paying particular attention to their power generation capabilities. Following this, a decision regarding the technology that would form the basis of this project had to be made, and a research direction chosen. The choices made were: piezoelectric conversion of vibration energy and power enhancement, and accordingly, justification for each of these decisions is given following the above described literature examinations. After this, the literature review moves on to describe piezoelectricity. The reader is introduced to the concept by way of historical and technological contexts, and then guided through the advancements made to date toward power enhancement of piezoelectric devices. Lastly, the chapter concludes with some brief conclusions.

In summary, the aim of the literature review is to answer the following questions:

- 1) What is a ‘useful’ amount of power? What are the power consumptions of modern electronic components, devices and systems?
- 2) What is state-of-the-art in terms of power density for the different energy harvesting technologies? How does this compare with the power consumptions discovered in (1) above?
- 3) Which harvesting technology shows the most promise in terms of energy source availability, ease of implementation, and useful levels of output power?

- 4) When was piezoelectricity discovered and what major technological milestones are there in its history?
- 5) How does piezoelectricity work?
- 6) What has been achieved in terms of enhancing the power output of piezoelectric generators to date? What is left to be done?

2.1 Overview of Power Requirements of Electronic Devices and Systems

In order to understand what amount of power is a useful amount, and therefore what level of output power is to be aimed for when harvesting from environmental sources, a survey of the power consumptions of a range of modern electronic devices and systems has been performed. Figure 2-1 overleaf illustrates the results of this survey. The devices surveyed include: individual active (i.e. powered) components, such as a quartz oscillator or an accelerometer; some full systems that do not communicate wirelessly such as hearing aids or calculators; and a range of full systems that do communicate wirelessly, such as a tyre pressure monitoring sensor node, or an UWB transmitter for body area sensor networks.

Increasing power consumption

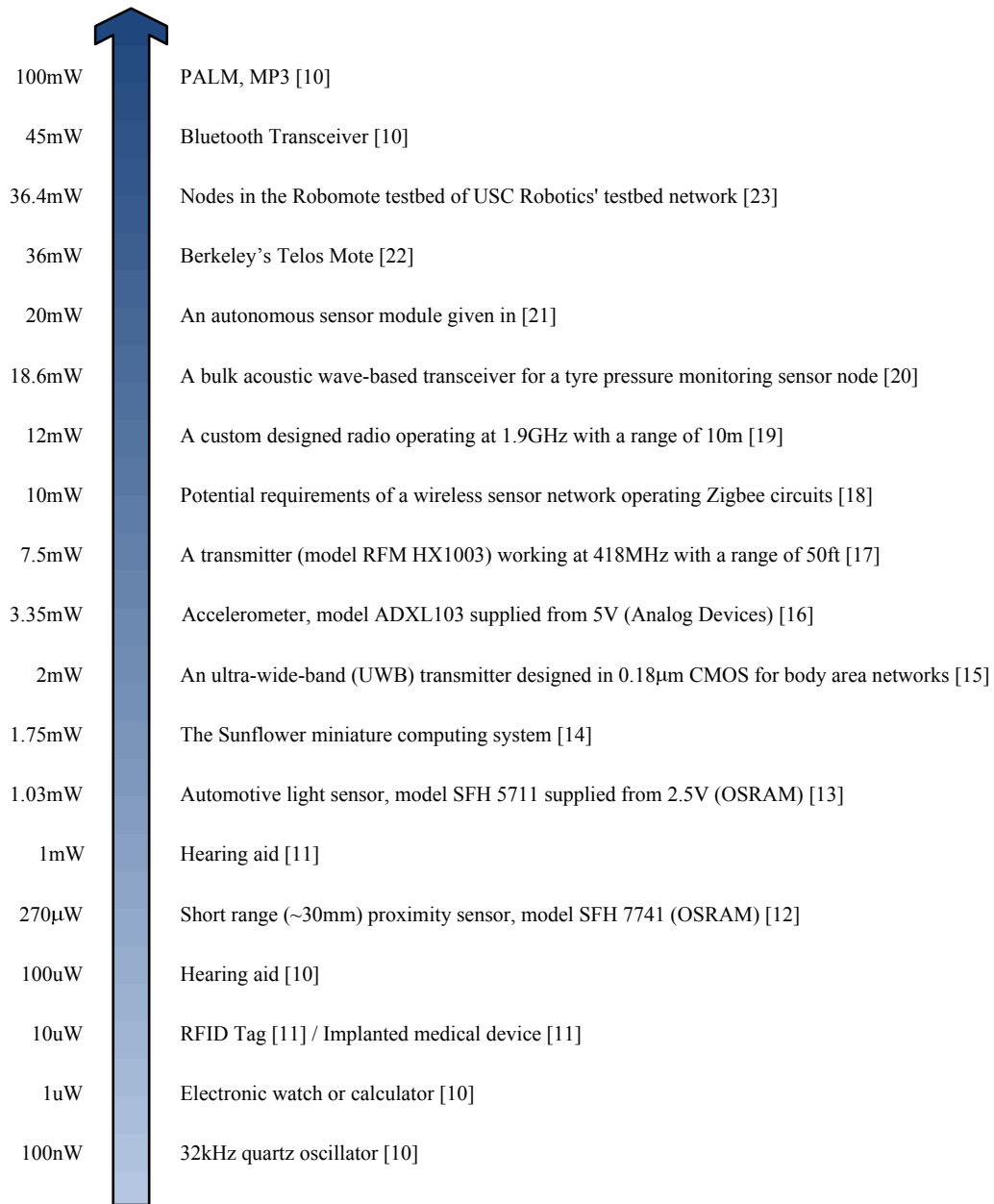


Figure 2-1 Power requirements of a range of modern electronic devices and systems (sources specified individually).

2.2 Overview of Energy Harvesting Technologies by Energy Source, with a focus on power generation capability

This section aims to provide an overview of the technologies available for harvesting from different environmental sources. Power output figures from tested devices where given in the literature are reported, and the advantages and disadvantages of harvesting from each environmental source are summarised.

2.2.1 Solar

All energy, with the exception of nuclear, is solar energy. The inhabitants of planet earth (both plant and animal) have been using energy from the sun since the beginning of their existence. Figures abound in the literature for the amount of power that is delivered to the earth from the sun: 10,000W per square metre [24], 100mW/cm² [25], 500W/m² (bright sunny day in Ireland) [26], and “1.5ZWh per annum {zeta (Z) is the SI unit for 10²¹}” [9]. Charles Fritz, an American who developed selenium photovoltaic cells in the 1800s, wrote in 1886 that the sun “*is both without limit and without cost and shall continue to stream down on earth long after we exhaust our supplies of fossil fuels*” [9]. Today this remains a sound argument for a focus on the development of solar energy harvesting technologies.

Conversion methods for solar energy are usually based on photovoltaic cells. Different materials have been used for photovoltaic cells throughout history: selenium was the first material discovered to have photoconductive properties, by Willoughby Smith in 1873, and the first selenium cell was developed by W. G. Adams and R. E. Day in 1877. At this stage typical cell efficiency was less than 1%, and so lack of affordable efficiency meant that the technology was not considered for use as a large-scale power

producer. After a period of about fifty years, the first silicon-based photovoltaic cells were reported, and by 1954 the efficiency of silicon solar cells reached 6%. Such cells were used in 1958 in America's second satellite, Vanguard 1, which had about 100cm² of solar cells and continued to transmit using solar power until 1964. By the 1970s gallium arsenide (GaAs) cells were being developed, though the relative scarcity of this material in comparison with the abundance of silicon made using GaAs cells prohibitively expensive for anything other than space applications (satellites), which were technologically coming of age in the 1970s. In 1972 an efficiency of almost 17% was reported from GaAs cells by Woodall and Hovel [27]. However, in 1985 efficiencies of laboratory-made silicon cells were pushed past 20%, as a group from the University of New South Wales (Australia) made several contributions by addressing the main loss mechanisms within the technology [28]. The most recent advances have allowed silicon photovoltaic cells to reach efficiencies nearing 24%.

The basic theory of operation of a photovoltaic cell is described in the following paragraph:

In general, modern photovoltaic cells are configured as a large-area pn junction made of silicon. First, consider a pn junction in an equilibrium condition; the excess free electrons from the n-doped semiconductor diffuse across the junction to recombine with the free holes in the p-doped semiconductor, and similarly, excess free holes from the p-doped semiconductor diffuse across the junction to recombine with free electrons in the n-type semiconductor. The recombination of the free electrons and holes results in the formation of a 'depletion zone' which is a layer that has no mobile charge carriers. Meanwhile, a net positive charge is left on the n-doped semiconductor due to an abundance of positive donor ions left behind after the departure of the electrons, and

similarly, a net negative charge is left on the p-doped semiconductor due to an abundance of negative acceptor ions left behind after the departure of the holes. These net charges serve to set up an electric field in the direction from n to p at the junction, prohibiting any further movement of any remaining charge carriers, thus the depletion region reaches its equilibrium dimensions.

The generation of a 'photocurrent' from a pn junction requires energy from a photon. When a photon (from sunlight) with energy higher than the silicon band gap value hits the silicon, it is absorbed into the silicon and its energy is given to an electron in the crystal lattice. The electron, which usually sits in the valence band where it is bound by covalent bonds, is then excited into the conduction band where it is free to move through the semiconductor and contribute to conductivity. Movement of the electron leaves behind a 'hole', thus, as photons hit the silicon, electron-hole 'pairs' are created. Those pairs that are created close to the pn junction migrate to it, where the electric field that was described earlier sweeps the electrons to the 'n' side and the holes to the 'p' side of the junction. The result (with the addition of electrical contacts and an external circuit) is that the device becomes a source of electromotive force.

Power levels that have been achieved from meso-scale solar energy harvesters are shown in Table 2-1 overleaf, and the advantages versus disadvantages of using photovoltaics for energy harvesting are summarised in Table 2-2.

Table 2-1 Power output levels of meso-scale solar energy harvesters

Power harvested	Voltage & Current Information	Space envelope	Load applied	Method	Source
Not specified	Open circuit voltage 150V. Short circuit current 2.8μA	1cm ²	1014Ω	A 100 cell array of hydrogenated amorphous silicon solar cells. Test conditions were air mass (AM) 1.5 illumination, which is a standard solar cell test	[29]
15mW	Not specified	1cm ²	Not specified	(Tabulated in the source)	[30]
5μW	Not specified	22500um ²	Not specified	Photodiode with integral CMOS storage capacitance (design "D3" in the source)	[31]
800nW	Not specified	3000um ²	230kΩ	(as above)	(as above)
76nW	Open circuit voltage 533mV. Short circuit current 230nA	338um ²	Not specified	(as above)	(as above)

Table 2-2 Advantages and disadvantages of solar energy harvesting

Advantages	Disadvantages
Mature/well established	Limitations on placement: must be in well-lit location and correctly orientated
Abundant energy source	Must be free from obstructions & kept clean
Inexpensive	Energy delivered for only part of the day
Highly compatible with electronics (provides voltage and current levels that can be easily matched with microelectronics)	If aiming for small-scale harvesters, difficult because power output directly linked to surface area
Relatively consistent efficiency over a broad range of wavelengths	Energy that can be harvested depends on latitude and atmospheric conditions
No moving parts	
Cells last for decades	

2.2.2 Air Flow

Air flow in the atmosphere (wind) is a result of pressure differences caused by the sun heating up different parts of the atmosphere. Approximately 2% of the sun's energy reaching the earth is converted into wind energy [32]. Humans have used wind as a power source for thousands of years: for propelling ships and boats by use of a sail, and for milling grain through the use of windmills. On a smaller scale air flow is readily available in a variety of environments, including ventilating and air conditioning ducts, convection from heating sources, and on moving vehicles. Figures stated in the literature for typical air velocities in these environments include: “*12m/s in large ducts, down to 1-2 m/s close to the exit in rooms*” [33], 10m/s [34] (for which the source specifies a power level of $256\mu\text{W}/\text{cm}^2$ may theoretically be possible), and 1200 feet per minute (6.1m/s) in an air conditioning duct [35]. The last of these three sources elaborates on the energy harvesting potential of the flow rate given: “*the kinetic energy flux (i.e. power) of air moving at that velocity through an area of one square centimetre is 12.4mW*” [35].

On examination of the literature, it appears that a very limited amount of work has been done on small-scale electrical power generation from air flow. The natural starting point for small-scale air flow harvesting devices is perhaps the large-scale wind turbine. The basic principle of operation of the wind turbine is as follows: the kinetic energy of the wind flow is turned into mechanical rotation energy via the vanes. There then usually exists a transmission system that comprises a hub, main shaft plus bearing, gearbox, and permanent coupling to a three-phase AC asynchronous generator (also known as a ‘squirrel cage induction motor’) that can be connected to the three-phase mains supply [36]. In the generator, the relative motion of the ‘squirrel cage’, which comprises short

circuiting coils and is mounted on the rotor (which in turn is connected to the rotating main shaft), and the rotating magnetic field of the stator, induces an electromotive force by Faraday's law of induction. The stator comprises a quantity of coils (the number of which must be divisible by three) that are connected to different phases of the national grid, and that are arranged inside a cylinder in a configuration that ensures a rotating magnetic field. The rotor sits on a shaft that spins inside this cylinder. In order for power generation to take place, the speed of the rotor needs to be higher than the speed of the rotating magnetic field of the stator, so that the stator rotating magnetic field is influenced or 'dragged' by the rotor magnetic field, hence producing a current in the stator coils that is dependant on the induced electromotive force and the connected resistance. In this way power is fed into the national grid.

While some small-scale air flow energy harvesting devices do consist of components akin to those in a large-scale wind turbine, and therefore generate power through Faraday's law of induction [35] [37] [33], it is perhaps a surprise to learn that a significant proportion of the devices developed utilise piezoelectric conversion instead [32] [34] [38] [39] [40]. In such a device, often the mode of operation is as follows: the mechanical rotation energy of the vanes (or rotor) assembly is transferred into sinusoidal mechanical motion either via a crankshaft attached to a rod, or by a camshaft mechanism, as shown in the two examples given in Figure 2-2:

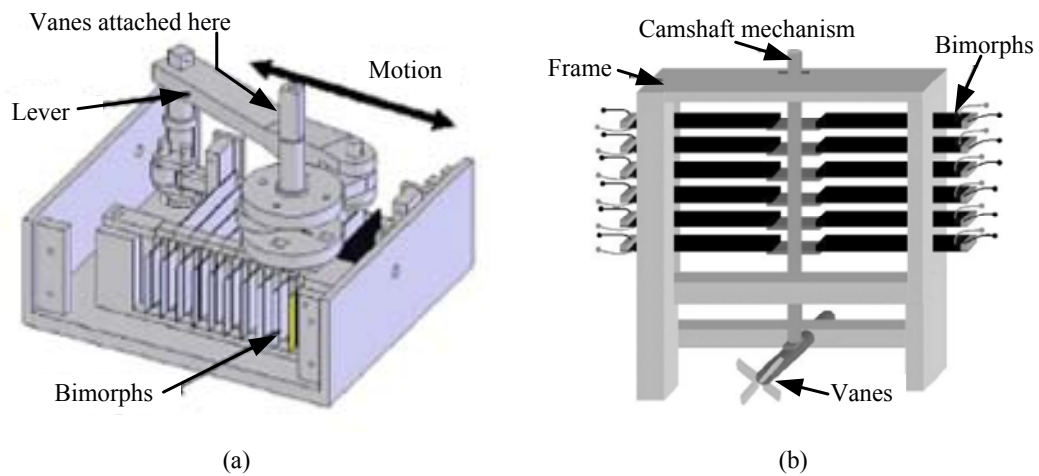


Figure 2-2 (a) Crankshaft design of a ‘Small scale windmill’ [40] (b) Camshaft design of an air-powered electric energy generator [32]

The rod is attached to some piezoelectric elements which are then subjected to time-varying strain at a given frequency and hence provide a charge output. It is not always made clear why this method is chosen over the conventional and more familiar rotation of electrical coils in a magnetic field, though this author suspects that part of the reason is that at small-scale, the force available from small sized vanes is not enough to overcome the initial ‘braking’ effect that the stator magnetic field has on the rotor. In addition, the voltage output using piezoelectricity is often already within the useable range of microelectronics (1-20V), whereas the voltage output from small-scale electromagnetic devices can be rather low, therefore requiring extra elements of power conditioning. Other configurations of air flow energy harvesting devices that are piezoelectric based include those that use bimorphs as the vanes of the turbine [38] [39], and one that operates using forces generated by a ‘von Kármán’s vortex street’ [34]. The latter device has the distinct advantage that it comprises no moving parts (see Figure 2-3):

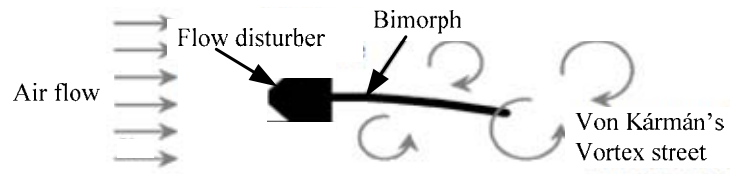


Figure 2-3 A piezoelectric bimorph in a von Kármán's vortex street [34]

Power levels that have been achieved from small-scale air flow energy harvesters are shown in Table 2-3, and the advantages and disadvantages of air flow energy harvesters are summarised in Table 2-4.

Table 2-3 Power output levels of small-scale air flow energy harvesters

Power harvested (mW)	Voltage & Current information	Space envelope information	Load applied (k Ω)	Air velocity (m/s)	Method	Source
"up to 0.1mW has been achieved"	"voltages of 0.8V have been achieved"	The bimorph is 14×11.8×0.35mm (<i>l</i> × <i>w</i> × <i>t</i>)	1.2	45	A bimorph in a 'von Kármán's vortex street'. Resonant frequency of the cantilever occurred at 600Hz ± 30%	[34]
2.4	0.6V	4.2cm diameter propeller	Not specified	5.5	A micro-windmill device	[33]
130	2.6V	4.2cm diameter propeller	Not specified	11.83	(as above)	(as above)
0.0045	Not specified	2.3in. diameter rotor (depth = 1.2 in.)	240	4.5	A device consisting of a 2.3in. diameter vertically mounted 'cup vane' rotor and 12 piezoelectric bimorph cantilevers	[40]
0.2	Not specified	3.8×4.2×2.6 in. (<i>w</i> × <i>l</i> × <i>h</i>) without vanes mounted. Each vane is 4 in. long.	30	4.5	A horizontally mounted rotor with four vanes spins a shaft with a crank arm attached to it. The crank arm pulls a bar which is attached to 9 bimorphs	(as above)
5	Approx' 12-15V _{pk} open circuit	7.6×10.2×12.7cm total size	"of the order of" 20"	4.5	Three 5-in. diameter fan rotors drive two rows of nine bimorphs via a crank assembly. Power figure quoted is combined rectified power of both rows	(as above)
1.2	(not specified for the air velocity figure given)	5.08×11.6×7.7 cm total dimensions	1.7	5.36	The rotary motion of a shaft with vanes attached is converted into the vertical motion of another shaft via a cam. The second shaft is attached to 12 bimorphs	[32]
10.2	6.9Vdc, 1.5mA (current figure is inferred from P=IV)	Each bimorph 'blade' has a free length of 53mm	4.6	Not specified	A piezoelectric windmill with 12 piezoelectric bimorph 'vanes' arranged along the circumference, a bridge rectifier, and a resistive load on the output	[39]

Power harvested (mW)	Voltage & Current information	Space envelope information	Load applied (k Ω)	Air velocity (m/s)	Method	Source
7.5	7.09V (inferred from $P=V_{pk}^2/R$)	(as above)	6.7	4.47	As above but with 10 piezoelectric bimorph 'vanes' around the circumference	[38]
1.1	Not specified	Approx' volume of 0.5cm ³	Not specified	40	An axial flow microturbine (with electromagnetic generator) device realised using MEMS processing technology	[37]
28	1.7Vdc, 16.5mA	Approx' 10cm diameter fan rotor	0.103	5.08	A miniature wind turbine with a brushless dc motor (without commutator) operated as a three phase AC generator, and a three-phase bridge circuit (to convert AC to DC) and a resistive load	[35]

Table 2-4 Advantages and disadvantages of air flow energy harvesters

Advantages	Disadvantages
	Large scale wind turbines can achieve efficiencies of 50% or more. The performance of miniature wind turbines is expected to be less good, mainly because of the relatively high viscous drag on the blades at low Reynolds numbers
	Friction forces increase with decreasing scale; for those air flow energy harvesters with bearings, the bearing losses will be greater at small-scale
	Can have many moving parts
	Quite complicated constructions
	Can not easily be miniaturised, due to complicated constructions, therefore tend to be quite bulky

2.2.3 Thermal

In principle, energy can be harvested wherever a difference in temperature exists. Such environments may include: human (or animal) skin, domestic radiators, and vehicle exhaust systems. It is known from medical research that about 80% of the energy spent on physical activity is turned into waste heat [41]; it is likely that a large fraction of that heat is transferred through the lungs and through sweating. One study [42] indicates that human energy expenditure is 407W while hiking at 4mph, and 175W while doing the housekeeping, which implies that about 326W and 140W is lost in the form of heat from each activity respectively. Another study [41] measured a figure for the average heat flow from a human wrist of 18.8mW/cm^2 for 158 volunteers sat at a desktop PC for half-an-hour. Recently, the car manufacturer Volkswagen has developed thermoelectric generators for recovering energy dissipated as heat from their vehicles. A prototype vehicle was shown at the “Thermoelektrik – Eine Chance Fur Die Atomobillindustrie?” event held in Berlin in 2008. Purportedly, the thermoelectric generator is capable of obtaining about 600W, which meets around 30% of the car’s electrical consumption requirements, saving about 5% of the fuel consumption [43]. Such a device is macro-scale however, which perhaps takes us outside our scope of small or ‘meso’-scale energy scavenging. There are lots of examples of further opportunities for small-scale thermal energy harvesting: the waste heat from the lamp in overhead projectors has been considered in one report [44], and dual-core processors in modern computers also produce waste heat. These last two examples have one thing in common: the excess heat generated can cause damage to the components of the equipment, unless it is removed by using yet more electrical energy to power a fan!

Most of the small scale thermoelectric generators detailed in the literature to date make use of thermopiles, which are devices that consist of a quantity of thermocouples (usually numbering in the hundreds) that are connected together electrically in series and thermally in parallel. Thermocouples operate using the ‘Seebeck principle’. In 1821 a German physicist, Thomas Seebeck, observed an electric current flowing in a series circuit that consisted of two dissimilar metals, the junctions of which were at different temperatures. The current flowing results from a potential difference which is set up when the temperature difference is applied. If the loop is opened at the cold junction (see Figure 2-4), an open-circuit voltage, V_{oc} , can be measured between the two conductors.

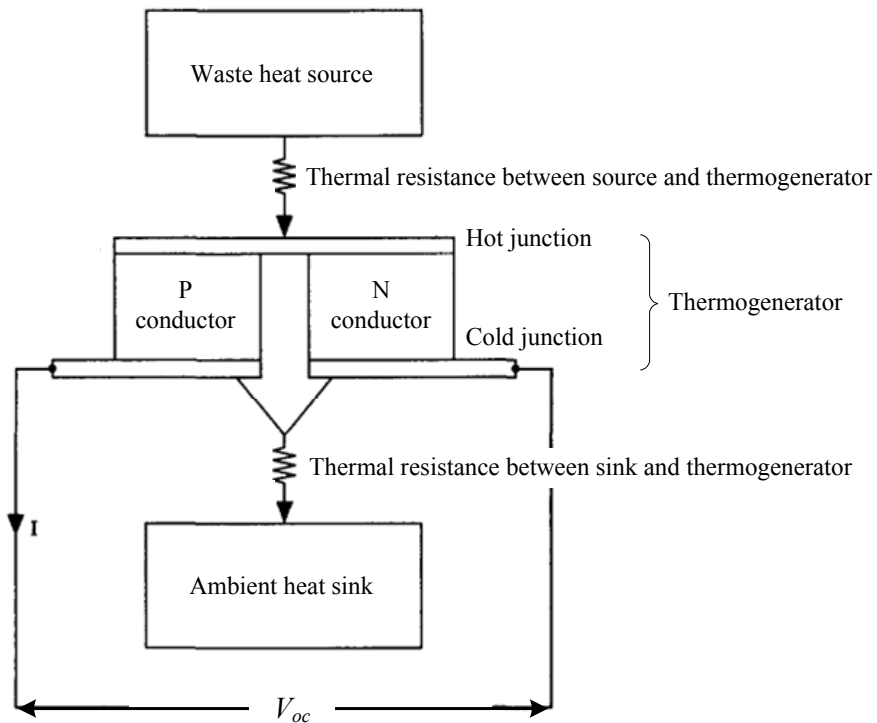


Figure 2-4 Working principle of a thermocouple [45]

The voltage V_{oc} is proportional to the temperature difference between the two junctions according to the following equation:

$$V_{oc} = \alpha_{pn}(T_{HJ} - T_{CJ}) \quad (1)$$

Where T_{HJ} is the temperature of the hot junction, and T_{CJ} is the temperature of the cold junction. The proportionality constant, α_{pn} , is known as the Seebeck coefficient.

Thermal energy harvesting devices may also operate using pyroelectricity, which is the ability of certain materials to develop an electric charge in response to a change in temperature. The effect is closely related to that of piezoelectricity, as both effects have their origins in the non-symmetric molecular structure of a material. In comparison with thermopile-based generators, there are currently relatively few pyroelectric based generators.

Looking at the literature on small-scale energy harvesting from temperature gradients, it seems that development of meso-scale thermoelectric energy converters has gradually evolved over the past fifteen years or so. There are now too many reports of thermoelectric devices developed in the last few years to show a comprehensive review of all of the power levels achieved here, but Table 2-5 does show a representative sample. In addition, the advantages and disadvantages of harvesting energy from thermal sources are summarised in Table 2-6

Table 2-5 Power output levels of small-scale thermal energy harvesters

Power harvested	Voltage & Current information	Space envelope information	Load applied(Ω)	Temperature difference (K)	Method	Source
100 μ W	Not specified	3 \times 3 \times 1cm	A power conditioning circuit	Not specified	An initial demonstration thermoelectric 'bracelet', built using MEMS fabrication processes	[41]
20 μ W	Not specified	Size of a small coin	Not specified	20	Thin-film thermoelectric generator; consists of 2250 thermocouples	[46]
250 μ W	\sim 1.8Voc	9 \times 3 \times 3mm	Not specified	Not specified, but corresponds to that between a human wrist and air	A 'multistage thermopile', comprising 158 thermocouples per stage and 32 thermopiles. The device is intended for wearing on a wrist.	[47]
22.5 μ W	300mV	2 \times 2 \times 1.3mm (overall size)	1000	Not specified, but corresponds to that between a human wrist and air	A generator designed for powering a wristwatch. The generator consists of ten 'modules' which are each comprised of 104 thermocouples	[48]
1.5 μ W	Not specified	Wristwatch-size	Not specified	1-3degC	A human-powered thermoelectric wristwatch	[49]
1.2 μ W	40Voc	1cm ²	Not specified	15	A Poly-SiGe thermoelectric generator consisting of 59,400 thermocouples and with cavities in the substrate. (Tests were done at wafer level)	[50]
0.6 μ W	25Voc	(as above)	Not specified	10	(as above)	(as above)
\sim 0.15 μ W	\sim 12.5Voc	(as above)	Not specified	5	(as above)	(as above)

Power harvested	Voltage & Current information	Space envelope information	Load applied(Ω)	Temperature difference (K)	Method	Source
$0.0417\mu\text{W}/\text{cm}^2$ K^2	$2.417\text{V}/\text{cm}^2 \text{K}$	$60\mu\text{m}\times 4\mu\text{m}$ (length \times width of thermolegs)	Probe station (Wentworth Lab) and multimeter	20	A thermoelectric energy harvester with thermal isolation cavity built in to prevent heat loss (i.e. to maintain the temperature gradient) and thus improve the power output.	[51]
$1.48\text{mW}/\text{cm}^2$	Not specified	$\approx 40\times 40\times 8.5\text{mm}$	5.5	10	A commercial thermoelectric module (TMG 254-1.0-1.3) designed for a cooling application. The device is comprised of 254 thermocouples.	[52]
$8.2\text{mW}/\text{cm}^2$	Not specified	(as above)	(as above)	22.5	(as above)	(as above)
$1.6\mu\text{W}/\text{cm}^2$	Not specified	7mm^2	Not specified	5	A silicon chip with 16000 thermocouples; envisaged for use in wearable fabrics	[53]

Table 2-6 Advantages and disadvantages of thermal energy harvesters

Advantages	Disadvantages
No moving parts	Available energy is affected by the thermal resistance of the source and sink of the thermal energy
Simple construction; can be miniaturised	Efficiency of conversion is limited by the Carnot efficiency
	Temperature differences tend to be small over miniature size scales such as meso-scale
	Relatively high cost

2.2.4 Pressure Variations

To this author's knowledge, there is very little research into using meso-scale devices to harvest energy from naturally occurring pressure changes. In theory this is possible. In 2003 Roundy [25] speculated that $7.8\text{nW}/\text{cm}^3$ could be gained from atmospheric pressure change through the day, and that $17\mu\text{W}/\text{cm}^3$ could be gained from a 1cm^3 closed volume of helium gas undergoing a 10°C temperature variation, where 10°C variation is what might be expected outdoors over a 24 hour period.

In regard to pressure changes existing in man-made structures, D Krähenbühl et al [54] in 2009 considered the use of an electric-motor driven compressor in reverse; i.e. as a compressed air-to-electric power converter. Their vision is that such a device could replace existing pressure reduction devices, such as throttles or valves, which are ordinarily present in many systems, including the mains gas supply infrastructure, automobile engines and cryogenic plants. The device, which is shown in Figure 2-5, has a total volume of 36.8cm^3 (dimensions of $l=4.3\text{cm}$, $d=3.3\text{cm}$ and $h=2.6\text{cm}$). In tests, the speed of the turbine exceeded 600 000 rpm and the output power exceeded 100W, indeed, a maximum power output of 170W was observed [54]. Concerning power density, such devices are obviously very attractive, since this level of power output equates to $4.62\text{W}/\text{cm}^3$.

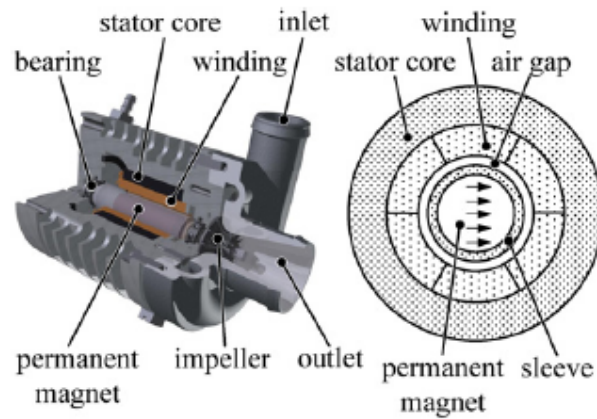


Figure 2-5 Machine cross-section of the compressed-air-to-electric power generator used in [54].

2.2.5 Radio Frequency Radiation

Radio frequency (RF) radiation belongs to the part of the electromagnetic spectrum that sits between about 10kHz and 300GHz. Like all electromagnetic waves, radio waves need no propagating medium, such as air or water, and are therefore able to travel through a vacuum. Indeed, a few space-related applications have been cited for RF energy harvesting, including inter-satellite power transmission and mechanical actuators for space-based telescopes [55]. It could be argued that radio frequency radiation is the most reliable ambient energy source for powering wireless sensors since, unlike solar or vibration, RF energy exists permanently, because multiple sources of different frequencies exist and radiate power in all directions. However, it suffers from a significant drawback in that the receiving module needs to be quite close to the transmitter (usually in the order of a few meters) in order to be able to harvest usable amounts of energy.

The fundamentals of radio waves are as follows: an oscillating charge in a piece of wire (e.g. an antenna) creates an electric field and a corresponding magnetic field. The

magnetic field induces another electric field which then induces another magnetic field, and so on. The nature of wave propagation is such that the magnetic and electric fields are mutually perpendicular, as can be seen in Figure 2-6, where the ‘*E*’ field is the electric field and the ‘*B*’ field is the magnetic field. The ‘field strength’ of the wave is measured by the change in potential per unit distance.

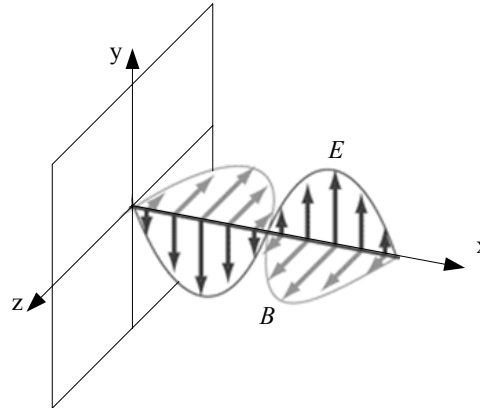


Figure 2-6 Electric and magnetic field components of an electromagnetic wave

The field strength of radio waves weakens as they travel. In free space, the field intensity of the wave deteriorates with the square of the distance travelled (i.e. at the rate of $1/d^2$, where d is the distance from the radiating source). This deterioration is known as ‘free space attenuation’ and occurs simply because the energy in the wave has to spread out further (over larger and larger spheres) as the distance from the source increases. In other media, such as air or water, energy in the wave is lost through ‘absorption’. For example, attenuation in the atmosphere is minor from about 10MHz to 3GHz, but at higher frequencies, absorption of some of the wave energy by the molecules in water vapour can result in significant attenuation of the signal. (As a side-note, domestic microwaves operate by using radiation near to 2.45GHz to excite the electrical dipoles in water molecules, thus causing heating by increasing the kinetic energy of the molecules through absorption of the wave energy).

After the RF power is transmitted through space to some distant point, the power is collected by a suitably placed antenna and converted back into DC. Since power transmission by radio frequency radiation requires three steps:

- 1) Convert DC power into RF power,
- 1) Transmit the RF power to some point,
- 2) Receive the RF power and convert it back into DC power,

the overall efficiency of the total power transfer is a product of the efficiencies associated with each of these stages [56]. Because of this, the literature available on harvesting energy from RF radiation tends to focus on efficient conversion technologies; i.e. on steps 1 and 3. Indeed, the bulk of the literature seems to report on improving the efficiency associated with converting the received RF energy back into DC energy.

As to actual figures reported for power transfer by radio frequency radiation, there are a few available, which are listed in Table 2-7. Table 2-8 reports on the advantages and disadvantages of harvesting from ambient radio frequency radiation.

Table 2-7 Power output levels of small-scale RF energy harvesters

Power harvested	Voltage & Current information	Space envelope information	Distance from transmitting antenna (m)	Frequency of radiation	Transmitted power	Load applied	Method	Source
220mW	Not specified	Not specified	0.08	Not specified, but somewhere between 2.2GHz and 2.7GHz	15W	A power meter	An antenna array connected to two circuits, each consisting of a filter, rectifier diode, and capacitor. The outputs of the two circuits were summed, and a power meter was connected directly to the output	[57]
15mW	Not specified	Not specified	0.6	(as above)	(as above)	(as above)	(as above)	(as above)
100 μ W	6.5V	30cm ²	1	902-928MHz	36dBm (4Watts EIRP)	0.33M Ω	An RF-to-DC power conversion system comprising: an antenna on a printed circuit board, an impedance matching network (utilising a high-Q resonator) and a voltage doubler rectifier	[58]
1 μ W	Approx 1.2Vdc	(as above)	10	(as above)	(as above)	1.32M Ω	(as above)	(as above)
135 μ W	1.9Vdc	Size of a small coin	1	915MHz	1W	WISP wireless sensing platform	A versatile, programmable, sensing platform: the "Wireless Identification and Sensing Platform" (WISP). Power figure quoted is the 'turn-on' power level for the full system	[59]

Table 2-8 Advantages and disadvantages of RF energy harvesters

Advantages	Disadvantages
The power level is controllable and predictable	Without a dedicated radiating source, ambient levels are very low and are spread over a wide spectrum
Power can be given over distance, unlike vibration for example, where the harvester has to make contact with the vibration source	The field strength drops off rapidly as distance from the source is increased
No moving parts	Efficient extraction using devices much smaller than the radiation wavelength is a challenge
	There is high power loss from RF wave propagation at UHF frequencies
	There is a limit to how much power can be transmitted by a source, because microwave power has adverse effects on biological systems. In the IEEE 802.11 standard, maximum allowable transmission power is 1000mW in the USA, 100mW in Europe, and 10mW/MHz in Japan [60]. This translates directly into a limitation on the amount of power it is possible to harvest.

2.2.6 Mechanical: Vibrations and Human Movement

Vibration energy perhaps represents the most abundant source next to Solar. Vibrations can be found in a wide variety of natural, industrial, commercial and transport environments, including: vehicle engine compartments, trains, ships, helicopters and bicycles; floors (offices, train stations, nightclubs), speakers, window panes, walls, bridges, kerbsides; household appliances (fridges, washing machines, microwave ovens), pumps and machinery, and humans (e.g. the human heartbeat).

Human movement, of course, is not necessarily directly related to vibrations. Other forms of mechanical energy come into play, particularly those that result from the bending of joints (knees and elbows) or those that result from impact: footfall during walking or running, or typing on a keyboard for example. Starner, in his landmark conceptual study [61], predicted that 6.9mW might be available from a moderately skilled typist typing at 40 words per minute, and that up to around 67W might be available from a person walking at 3.5m.p.h.

In terms of vibration energy, there are three very well-known methods of converting into electrical energy: electromagnetic, electrostatic, and piezoelectric, and a few other less well-known methods, including magnetostrictive. These different conversion methods can also be employed in harvesting non-vibration mechanical energy from human movement, although it can be seen from the literature that in this regard, piezoelectric and electromagnetic methods are most popular.

Table 2-9 on the next page gives the advantages and disadvantages of harvesting from vibrations and human motion, and Table 2-10 compares the advantages and disadvantages of each of the three main conversion methods.

	Advantages	Disadvantages
Vibrations	Abundant; possibly the most abundant energy source next to solar.	Sources can vary considerably in amplitude and dominant frequency.
		Sources can be intermittent, with periods of no vibration.
		Most vibration harvesting devices are resonant structures, and ambient environmental vibrations tend to have higher acceleration values at lower frequencies. The smaller the device, the more difficult it is to achieve a low resonant frequency.
Human Motion	Power outputs tend to be higher, because the harvesting device can be larger; e.g. the volume inside the sole of a shoe is larger than many vibration applications might allow for.	Inconvenience to the subject can only be avoided if low levels of power are extracted (the caveat to this is footfall, where a lot of energy is dissipated in normal walking anyway).

Table 2-9 Advantages and disadvantages of vibration and human motion energy harvesters

	Advantages	Disadvantages
Electromagnetic	Self contained (requires no external supporting accrements). Can have reduced mechanical damping over piezoelectric converters, depending on configuration (i.e. if not cantilever-based).	Voltage output levels can be rather low (hundreds of mV to $\approx 2V$), rendering the usual bridge rectifier AC-DC conversion method unusable.
		Can require complex fabrication and assembly of multiple small components.
		Not easily compatible with microelectronics. Can be quite bulky.
Electrostatic	Can be fabricated with existing silicon-based IC processes, making for ease of integration with microelectronics.	Usually requires some form of external voltage source to initially charge the capacitance of the harvesting device.
	Can be miniaturised easily, including to MEMS-scale.	May require relatively complex circuitry, in order to operate switches that are synchronised to the vibration (see Figure 2-12 on page 60 and accompanying explanation).
Piezoelectric	Self contained (requires no external supporting accrements).	Tend to have high output impedance.
	Voltage output levels tend to be in the useable range.	
	More compatible with microelectronics than electromagnetic harvesters, though not to the same extent as electrostatic converters.	Piezoelectric ceramic may suffer from fatigue over time and eventual cracking due to brittle nature.
	Can be miniaturised easily; there are examples of micro harvesters.	

Table 2-10 A comparison of the advantages and disadvantages of the three main vibration conversion methods

2.2.6.1 Electromagnetic Conversion

Electromagnetic (sometimes also called electrodynamic or electromechanical) conversion of vibration energy into electrical energy involves the construction of an assembly that facilitates relative movement between an electrical conductor and a magnetic field, hence the device makes use of Faraday's law of induction. The conductor is usually wound in a coil in order to maximise the area of conductor that is cut by the lines of magnetic flux. On examination of the literature on electromagnetic energy harvesters, it appears that a large proportion of them are configured as a cantilever beam where either the magnet/s form part of a seismic mass attached to the free end (in which case there is a static coil usually attached to the housing), or a coil is attached or patterned onto the cantilever (in which case the magnet remains fixed to the housing). Examples of such harvesters can be seen in Figure 2-7 (moving magnet type) and Figure 2-8 (moving coil type).

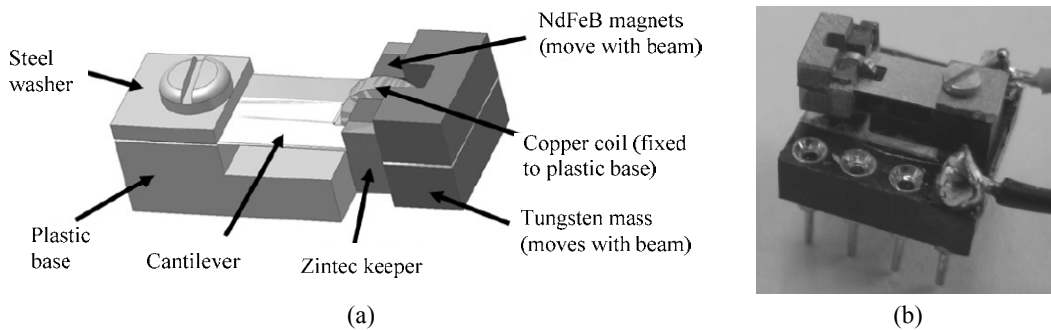


Figure 2-7 (a) 'Moving magnet' electromagnetic vibration energy harvester design given in [62] (b) Implementation of design [62]

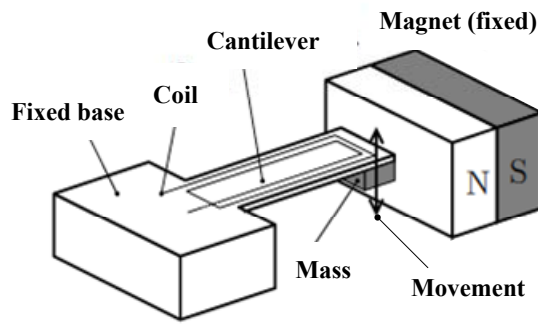


Figure 2-8 'Moving coil' electromagnetic vibration energy harvester design given in [63]

In some cases the generator does not take the form of a cantilever, but is a more literal interpretation of a classical spring-mass system [64] [65], as shown in Figure 2-9, where in (a), m is the mass, k is the spring constant (or stiffness), c is the damping coefficient, \ddot{y} is the acceleration of the host structure that results from the vibration environment, and $w_d(t)$ represents the displacement of the centre of the mass relative to y :

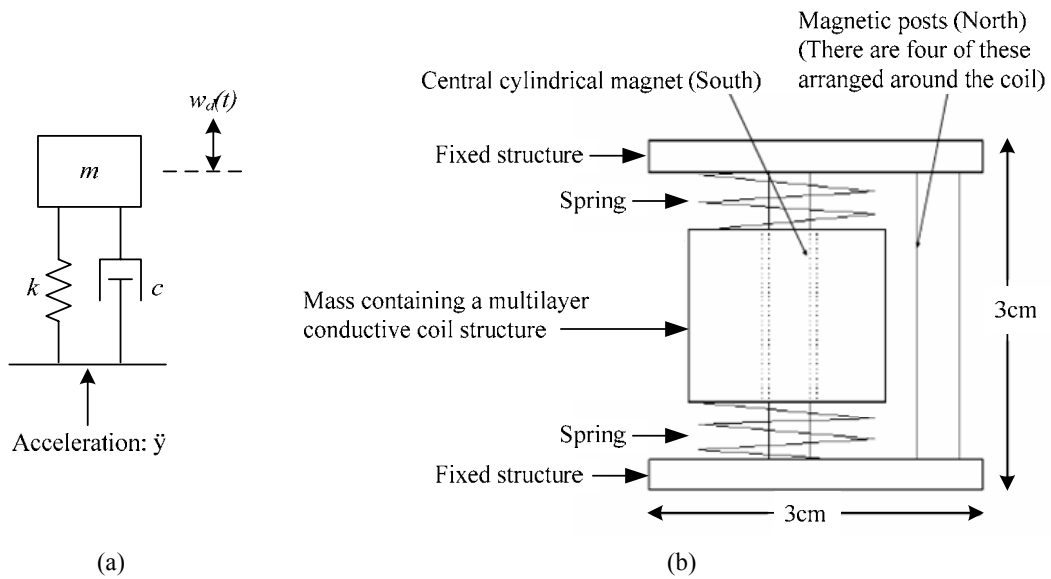


Figure 2-9 (a) A spring-mass system (b) Side view schematic of the electromagnetic vibration energy harvester presented in [65]

As with all resonant micro harvesting devices, the smaller the device, the more difficult it is to achieve a low resonant frequency, which has an important implication in regard

to miniaturisation, since frequencies found typically in the environment are usually low (below around 200Hz) [66] [67] [68] [69]. In one case, an attempt has been made to get around this problem by implementing a device that achieves mechanical ‘up-conversion’ [70].

A major problem concerning the use of electromagnetic converters is that the output voltage level is usually fairly low (typically a few hundred mV to a couple of V). Consequently, these types of converters tend to require some form of voltage up-conversion, such as a standard capacitor-diode voltage multiplier circuit.

There are very many electromagnetic generators reported in the literature, and it is not possible to report on the power outputs of all of them here, however Table 2-11 gives a representative sample. It was found, while examining the literature in detail, that it is difficult in some cases to extract the power and voltage figures. Vibration harvesters are often tested under a simple harmonic motion type of vibration, of a single frequency only, and hence the raw output of these generators when under test is usually AC. This provides scope for confusion when reporting these figures, since voltages and powers can be reported as either peak (pk), peak-to-peak (pk-pk), average, or root mean square (RMS), though this latter term does not represent any useful physical quantity when used in the representation of power, and it is not always evident which value is being used in the literature. In addition, some works report the power output after rectification, where the measured voltage becomes DC, and in these cases a true comparison with other converters is difficult because some of the raw output power from the generator is lost in the rectification process. Nevertheless, Table 2-11 aims to provide the reader with a good overview of power levels achieved by actual electromagnetic devices fabricated to date.

Table 2-11 Power output levels of meso-scale electromagnetic vibration energy harvesters

Power harvested	Voltage & Current information	Space envelope information	Load applied (Ω)	Vibration frequency (Hz)	Vibration acceleration or displacement information	Method	Source
17.8 μ W	52mV _{RMS}	<150mm ³	150	56.6	60mg	An electromagnetic micro generator based on a cantilevered inertial load. The intended application is an air compressor unit.	[62]
0.4nW	Not specified	Cantilever dimensions 25mm×10mm×1mm. Two masses (0.27g each)	128	700	0.64 μ m input	A cantilever beam with an integrated coil evaporated onto it and a fixed external magnet	[63]
0.3 μ W _{RMS}	Not specified	Bulk micro-machined device: circular membrane of 2.5mm, magnet mass of 2.4mg	39	4.4k	500nm input amplitude	The first micro-engineered inertial generator (to the best of this author's knowledge)	[64]
4nW	6mV	Cantilever dimensions 50×15×0.4mm. Magnet size: 20×20×5mm	Not specified	Upper diaphragm resonant frequency: 1, lower diaphragm resonant frequency: 25-50	n/s	A device that uses two resonant structures to achieve mechanical up-frequency conversion. The power figure shown is from a millimetre-scale mock-up.	[70]

Power harvested	Voltage & Current information	Space envelope information	Load applied (Ω)	Vibration frequency (Hz)	Vibration acceleration or displacement information	Method	Source
Not specified	180mV _{pk}	Proof mass = 0.5g	10	94	Mass given an initial displacement (value not specified) and then released	A prototype electromagnetic microgenerator	[71]
400 μ W	Not specified	(as above)	Not specified	2	Less than 2cm	For the same device as above; a " <i>best case mean power estimate</i> " for vibration from a human walking	(as above)
80mW _{pk}	4Vac	1cm ³	Not specified	60 to 120	\approx 200 μ m amplitude	A micro electromagnetic generator that uses laser micro-machined springs	[72]
\approx 100 μ W	2.3Vdc, 40 μ A	1cm ³	Not specified	60 to 120	\approx 200 μ m amplitude	For the same device as above. Figures shown are after a standard voltage quadrupler circuit is added to the output.	(as above)
0.53mW	Voltage is specified, but we don't know if it is open-circuit or not	240mm ³	0.28	322	25 μ m input amplitude	A cantilever beam device, fixed at one end and supporting a pair of NdFeB magnets (as a mass) on a c-shaped core at the free end.	[73]
830 μ W _{RMS}	1.8V _{pk-pk}	<1cm ³	1k	\sim 72	\approx 200 μ m input amplitude	A generator fabricated on a printed circuit board. The device uses laser micro-machined springs	[74]
2.5mW	0.5V _{RMS}	>1cm ³ (inferred from scale on picture)	100	102	0.4mm magnet displacement		[75]

Power harvested	Voltage & Current information	Space envelope information	Load applied (Ω)	Vibration frequency (Hz)	Vibration acceleration or displacement information	Method	Source
148nW	Not specified	<1cm ³ (inferred from photos)	Not specified	8.08k	3.9	An electromagnetic microgenerator on silicon with a wire-wound copper coil (fabricated using standard MEMS processing techniques)	[76]
23nW	Not specified	(as above)	52.7	9.83k	9.8	(as above)	(as above)
45 μ W _{RMS}	~450mV _{RMS}	≈150mm ³	4k	50	0.6	Building upon the previous work (from the line above)	[77]
122nW	Not specified	100mm ³	100	9.5k	3.9	An electromagnetic vibration powered silicon microgenerator	[78]
37 μ W	4.8V _{RMS}	0.84cm ³	0.6	322	13 μ m base amplitude	A two-magnet electromagnetic generator: the magnets are at the end of a cantilever beam; the coil is fixed.	[79]
3.9mW _{pk} instantaneous, 157 μ W average	Not specified	3.15cm ³	Not specified	Not specified	Not specified	(Related to the line above): A second prototype: a four-magnet electromagnetic generator aimed at improving the magnitude of the output voltage. The authors present results showing the response from the generator mounted on the engine block of a Volkswagen Polo. An instantaneous power of 3.9mW was measured during a journey of 1.24km (average speed 25km/hr) and the average power was found to be 157 μ W."	(as above)

2.2.6.2 Electrostatic Conversion

The basis of electrostatic conversion of vibration energy is the variable capacitor. The equation for the capacitance, C , of a capacitor is:

$$C = \frac{\epsilon_r \cdot \epsilon_0 \cdot A}{d} \quad (2)$$

where ϵ_r is the relative permittivity of the dielectric, ϵ_0 is the permittivity of free space (a constant of value $8.854 \times 10^{-12} \text{ C}^2/\text{N}\cdot\text{m}^2$), A is the area of one of the capacitor plates, and d is the distance between the two capacitor plates. The equation for the charge Q on either plate of the capacitor is:

$$Q = CV \quad (3)$$

where V is the magnitude of the potential difference (voltage) between the plates.

It is therefore the case that if a capacitor is charged by some external source, and the charge, Q , is then held constant, a change in the capacitance value, C , of the capacitor (caused, for example, by a change in the distance d between the plates of the capacitor) means that the voltage, V , across it will change. Similarly, if the voltage, V , across a pre-charged capacitor is held constant while distance between the plates, d , (and hence therefore the capacitance value, C , also) is changed, a change in the charge held within it, Q , will result. This is the working principle of the electrostatic vibration energy harvester. Usually, one plate of the capacitor is mechanically fixed in some way to the vibration source and therefore undergoes acceleration in phase with the vibration source, while the other plate is fixed to an inertial mass that is suspended by some spring mechanism, so that due to the inertia of the mass, this second plate moves out of phase with the plate fixed to the vibration source. As the plates move relative to one another, the energy stored in the initially-charged capacitor changes, thus providing the

mechanism for mechanical to electrical energy conversion. In its simplest form, this can be depicted by Figure 2-10, though in practice, there are different configurations of electrostatic converter, as shown in Figure 2-11.

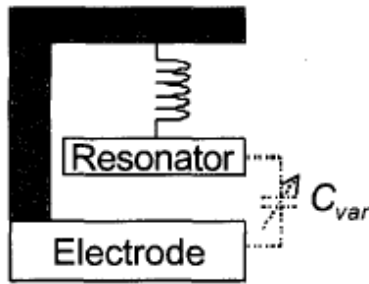


Figure 2-10 Working principle of an electrostatic vibration energy harvester [68].

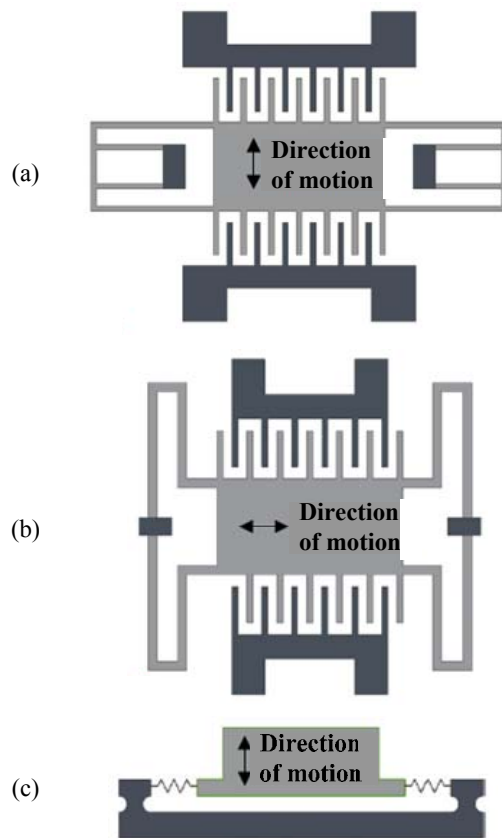


Figure 2-11 Three types of electrostatic converter (a) in-plane, overlap varying type (b) in-plane gap closing type (c) out-of-plane gap closing type [80].

Several problems need to be overcome in the practical implementation of an electrostatic vibration energy harvester: first, there is a need for an external voltage source to ‘prime’ (initially charge) the capacitor. Second, there is the very real mechanical problem of maintaining two conductors, which move relative to one another, at a very small separation in their closest-proximity state without letting them actually make contact. Third, depending on the mode being used (constant voltage or constant charge), the extraction of energy has to be accurately synchronised to the vibration. Figure 2-12 and the explanation that follows demonstrate this last point for a constant charge type of electrostatic converter [81]:

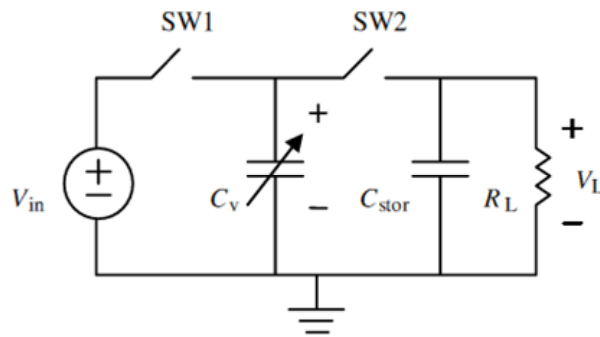


Figure 2-12 Schematic of a constant charge electrostatic vibration energy harvester [81]

Operation is as follows: SW1 is closed, and the variable capacitor C_v is charged to V_{in} while its capacitance is at its maximum value (i.e. minimum distance between the plates). Following this, SW1 is opened, and due to displacement resulting from the input vibration, the plates of C_v move further apart until its capacitance reaches its minimum value. The charge on the capacitor during this process remains constant. Due to $Q=CV$, this means that the voltage across the capacitor plates is increased, indicating an increase in the electrical energy stored in C_v . At the point where the capacitance of C_v reaches its minimum value, SW2 is closed and C_{stor} is charged by C_v through charge redistribution, thus current can flow through the external load resistor R_L and perform

work. The fact that this process requires switches that are synchronised to the vibration means that relatively complex supporting circuitry is required in the form of detection and switch driving circuits, which could be perceived as a disadvantage.

On the other hand, electrostatic conversion has some distinct advantages: the first and most often mentioned of which is the ease with which MEMS-fabricated electrostatic converters can be integrated with already existing silicon-based microelectronics. It is relatively easy to fabricate variable capacitors through mature silicon-based MEMS fabrication processes, so such devices would be readily compatible with electronic ICs available at the present time. Another less cited advantage is that, since the variable capacitor can convert mechanical work done by linear motion into electrical energy directly, it is possible to use electrostatic conversion to create non-resonant generators for use in either low-frequency applications (where achieving resonance may be difficult in small package sizes) or in other forms of kinetic energy harvesting, for example from the slow, large amplitude movements found in human beings.

Examination of the literature on electrostatic vibration energy harvesting devices reveals that relatively few examples of actual fabricated devices exist in comparison with electromagnetic generators. Table 2-12 shows a survey of power output levels achieved from fabricated electrostatic vibration energy harvesting devices.

Table 2-12 Power output levels of meso-scale electrostatic vibration energy harvesters

Power harvested	Voltage & Current information	Space envelope information	Load applied (Ω)	Vibration frequency (Hz)	Vibration acceleration (m/s^2)	Method	Source
$3.5\mu W_{RMS}$	$1V_{RMS}$ & $1.8\mu A_{RMS}$	$\approx 0.2cm^3$	Two load resistors (560k each)	1460	127.53	A fully packaged {in a Ceramic Leadless Chip Carrier (CLCC) package used for electronic devices} electrostatic MEMS microgenerator utilising two variable capacitors	[82]
$40\mu W_{dc}$	$10V_{pk}$	$20 \times 45mm$	7M	2	3.92	A microgenerator designed with $320\mu m$ microball-bearings (to maintain plate separation). Power was measured after rectification, but a voltage trace is given of the raw (without rectification) output	[83]
$80\mu W$	Not specified	(as above)	"optimum load" (value not specified)	6	3.92	(as above)	(as above)
$36\mu W$ mean power, $500\mu W$ peak power	$15\mu A$ at $2.4V_{dc}$	Not specified	Electronic circuit (input impedance not specified)	6	1	An out-of-plane gap closing generator that uses a 'honeycomb structure' to produce a variable capacitor. The generator was excited by a simulation of the movement produced by the left ventricular wall motion of a canine (beagle) heart	[84]
$5\mu W$	Not specified	Not specified	40M	500	9.81	An electrostatic generator making use of an electret in place of an external voltage source	[85]
$1.76mW$	Not specified	$18cm^3$	Not specified	50	~ 9.81	An electrostatic microgenerator with 100Hz bandwidth	[69]
$120nW$	Not specified	Not specified	10M	45Hz	0.08	A resonating capacitive generator. The device was tested on a wall that had a $1\mu m$ vibration displacement	[68]

Power harvested	Voltage & Current information	Space envelope information	Load applied (Ω)	Vibration frequency (Hz)	Vibration acceleration (m/s^2)	Method	Source
2.4 μ W (inferred from $P=E/T$)	220V	0.75cm ³	1012	~20	50	A 'Coulomb Force Parametric Generator (CFPG): a non-resonant electrostatic generator fabricated using MEMS processing techniques. Reported energy output is 120nJ per AC cycle	[86]
6 μ W	200V	0.8cm ³	1G	10	3.95	An in-plane, overlap varying, voltage constrained, variable capacitor polarised with a fluoro-carbon polymer electret	[87]
37.7 μ W	75V _{pk}	0.4cm ³	60M	20	15.79	(related to the line above and uses a similar device to conduct a series of power generation experiments)	[88]
278 μ W	60V _{pk}	Not specified	4M	20	9.47	(related to the two lines above; this work produces a model for the generator)	[89]

2.2.6.3 Piezoelectric Conversion

Certain materials, which can be either naturally occurring such as cane sugar, quartz, Rochelle salt and bone, or man-made such as barium titanate, lead titanate, and lithium niobate, are piezoelectric; that is: they will produce an electric charge when subjected to mechanical pressure or conversely, they will physically deform in the presence of an electric field. The first effect is termed the piezoelectric ‘direct’ effect whereas the latter effect is termed the piezoelectric ‘converse’ effect. Figure 2-13 illustrates these effects, where P indicates the direction of polarisation of the piezoelectric disc, F indicates an applied force, and E indicates the application of an electric field.

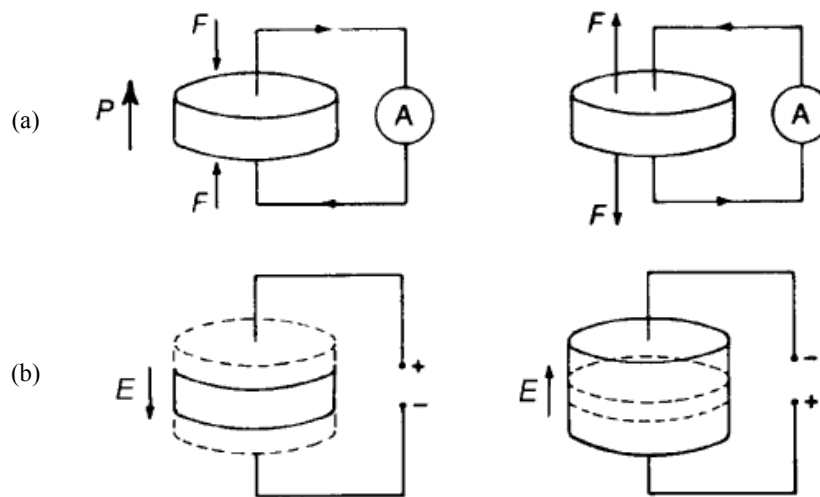


Figure 2-13 (a) The direct and (b) the indirect piezoelectric effects. The broken lines indicate the original dimensions [90].

The basis for the piezoelectric direct effect is the movement of charges within the piezoelectric material. When the material is forcibly deformed by application of an external mechanical pressure, its dimensions change, albeit only slightly ($\approx 4\%$ or so). This change in dimensions correlates directly with movement of the atoms within the material. Where electrical dipoles, which are a pair of point charges with equal magnitude but opposite sign, pre-exist within the arrangement of atoms the material is

said to possess ‘spontaneous polarisation’, and the dipoles are altered as the atoms move; i.e. the point charges either move further apart or closer together. Where no electrical dipoles are ordinarily present, they are created by the movement of the atoms. This alteration or creation of dipoles results in a change in the polarisation density (dipole moment per unit volume) of the piezoelectric material, and this effect manifests itself as a change in charge per unit area developed on an electrode attached to the external face of the material.

The prerequisite for a material to possess piezoelectricity can perhaps best be explained in terms of a piezoelectric crystal material: the necessary condition is the lack of a centre of symmetry in the crystal ‘unit cell’. In unit cells that have a centre of symmetry, the positions of average positive charge and average negative charge coincide, so that no dipole is ordinarily present. Furthermore, due to the symmetry of the unit cell application of a mechanical pressure in any direction cannot alter the average charge positions to form a dipole. Piezoelectric materials therefore, through the lack of a centre of symmetry, inherently directly couple a mechanical elastic property of the material such as stress or strain, to an electrical property such as dielectric displacement (polarisation) or electric field. This has the advantage that no external accrements are needed to achieve conversion of mechanical energy to electrical energy; a piezoelectric-based generator can be completely self-contained.

Piezoelectric materials have been integrated into many different types of structure for harvesting energy either from vibrations, or other sources of kinetic energy, such as human motion. Some of these structures are examined in section 2.4.1.1 (page 73) of this thesis. A summary of the power levels that have been achieved using piezoelectric generators is given in Table 2-13 on the following page.

Table 2-13 Power output levels of meso-scale piezoelectric vibration energy harvesters

Power harvested	Volume & Current information	Space envelope information	Load applied (Ω)	Vibration frequency (Hz)	Vibration acceleration (m/s^2)	Method	Source
39mW	Not specified	29mm diameter, 1mm thickness	400k	100	A cyclic force of 7.8N with a payload of 85g was applied. The velocity of the payload was measured to be 0.177m/s _{RMS}	A piezoelectric cymbal harvester placed between an engine and engine mounting. The device was connected to a bridge rectifier and load resistor. The power value given is the processed power.	[91]
3 μ W	Not specified	23mm wide at base, 23mm long, 0.3mm thick	333k	80.1	Only the beam motion amplitude is given: 0.8mm	A tapered (triangular) piezoelectric cantilever	[92]
18mW	20.57V _{DC}	0.987cm ³	24k	53.8	Not specified	A Mide Technology Corporation (Medford, MA, USA) Quick Pack model QP20W connected to a bridge rectifier and load resistor. The power value given is the processed power output.	[93]
80 μ W	6.3V _{pk}	\approx 1cm ³	250k	100	2.5	A bimorph poled for series, made with PZT and a centre steel shim, and with an end mass.	[66]
335 μ W	13V _{pk}	1cm ³	225k	60	2.5	A bimorph fabricated from a Piezo Systems Inc (MA, USA) bimorph part number T226-H4-103, with an end mass made from tungsten alloy.	[25]
207 μ W	8.3V _{pk}	1cm ³	180k	85	2.5	A bimorph fabricated from a Piezo Systems Inc (MA, USA) bimorph part number T215-H4-103, with an end mass made from tungsten alloy.	(as above)

Power harvested	Volume & Current information	Space envelope information	Load applied (Ω)	Vibration frequency (Hz)	Vibration acceleration (m/s^2)	Method	Source
500 μ W	Not specified	39cm ³	Not specified	113	9.81	A Mide marketed vibration energy harvesting device based upon a cantilevered QuickPack transducer.	[94]
900 μ W	Not specified	1.947cm ³	10k	30	Not specified	A Mide Quick Pack model QP40N: a bimorph actuator constructed from four piezoceramic wafers embedded in a kapton and epoxy matrix.	[95]
462 μ W	Not specified	(as above)	100k	30	Not specified	(as above)	(as above)
112.36 μ W	Not specified	(as above)	10k	25	Not specified	(as above)	(as above)
20mW peak, but \approx 1mW average	Peaks of \approx ±60V	The insole of a standard Nike trainer	250k	The test was carried out at a 1Hz walking pace	Not specified	A hexagonal multilaminate piezoelectric foil stave: two eight-layer stacks of 28-micron PVDF sandwiching a 2mm flexible plastic substrate bonded with epoxy. The PVDF sheets are connected so they appear in parallel.	[96]
8.4mW	44V	The heel of a US Navy work boot	500k	0.9Hz walking pace	Not specified	A non-bending compressible dimorph: two commercially available PZT transducers, a heel-shaped 0.025-inch beryllium-copper mid plate, and two aluminium rivets.	[97]

2.3 Justification for Focussing on Piezoelectric Conversion of Vibration Energy

The literature review began with an overview of the power requirements a variety of electronic devices and systems. It then detailed the energy harvesting technologies available for harvesting from the different types of energy source, paying particular attention to power output levels achieved in experiments to date. Energy sources covered included: solar, air flow, thermal, pressure variations, radio frequency radiation and mechanical (vibration and human motion).

From the tables detailing the power output levels achieved: Table 2-1 through Table 2-13, it can be seen that constructing a fair comparison of the technologies in terms of achievable power output is a difficult task: a wide variety of methods and devices sizes have been employed, a wide variety of environmental conditions have been simulated, and a wide variety of electrical loads have also been applied. In addition, the information required for comparison purposes is not always recorded, and it is not always clear for those devices with an AC output, whether the power and voltage figures reported are in the peak, peak-to-peak, average, or indeed conditioned (e.g. after processes such as AC-DC conversion) format. However, it may be possible to observe general trends, for example, it appears that meso-scale air flow energy harvesters have a consistency of power outputs in the mW range for air velocities generally in the range of 4.5m/s to 12m/s (see Table 2-3). In comparison, it appears that meso-scale thermal harvesters have a consistency of power outputs in the μW range for temperature changes in the range of 5K to 20K (see Table 2-5). Solar and RF harvesters seem to rank somewhere in between air flow and thermal in terms of power output, though it should be noted that for some of the solar devices the power figures reported are for devices with surface areas that are very tiny (i.e. much less than 1cm^2). Therefore if

these devices were scaled-up to 1cm^2 , their output power would be expected to be much higher. Vibration harvesters have been shown to generate power levels anywhere between 0.4nW (for a 0.1cm^3 cantilever-based electromagnetic generator operating at 700Hz under vibration displacement of $0.64\mu\text{m}$ [70]) to 56mW (for a 1cm^3 electromagnetic generator with operating between 60Hz to 120Hz under a vibration displacement of $\approx 200\mu\text{m}$ [72]). In regard to the different methods of harvesting from vibration energy, it seems that piezoelectric conversion tends to result in higher power outputs than electromagnetic or electrostatic conversion: typically in the hundreds of μW to a few mW region (e.g. $335\mu\text{W}$, $462\mu\text{W}$, $900\mu\text{W}$, 1.3mW), with voltages reaching high single figures to tens of volts DC or peak (e.g. 8.3V_{pk} , 13V_{pk} , 9.8V_{RMS} , $20.57\text{V}_{\text{DC}}$). It appears that electrostatic conversion can harvest lower power outputs: ranging from 124nW to $278\mu\text{W}$ for the devices examined in this study. In regard to electromagnetic generators, the output voltages are noticeably smaller than for the other two types of conversion method; the range observed in this study is between 6mV and 4.8V_{RMS} , with many occurring below 1V . This may have implications when considering the conditioning of the power output; for example, it would be difficult to convert a $450\text{mV}_{\text{RMS}}$ (636mV_{pk}) AC output to DC using a conventional bridge rectifier circuit, since the forward bias voltage of a diode can be between $\approx 0.2\text{V}$ to $\approx 0.6\text{V}$.

In terms of providing power to the various electronic devices and systems represented in Figure 2-1, the information collected in Table 2-1 through Table 2-13 might be represented as shown in Figure 2-14, where it should be made clear that, because figures reported in the literature are usually the raw output powers of harvesting devices (i.e. without any conditioning), the output powers quoted in the figure have been reduced by 20% to account for losses that will occur during the conditioning process.

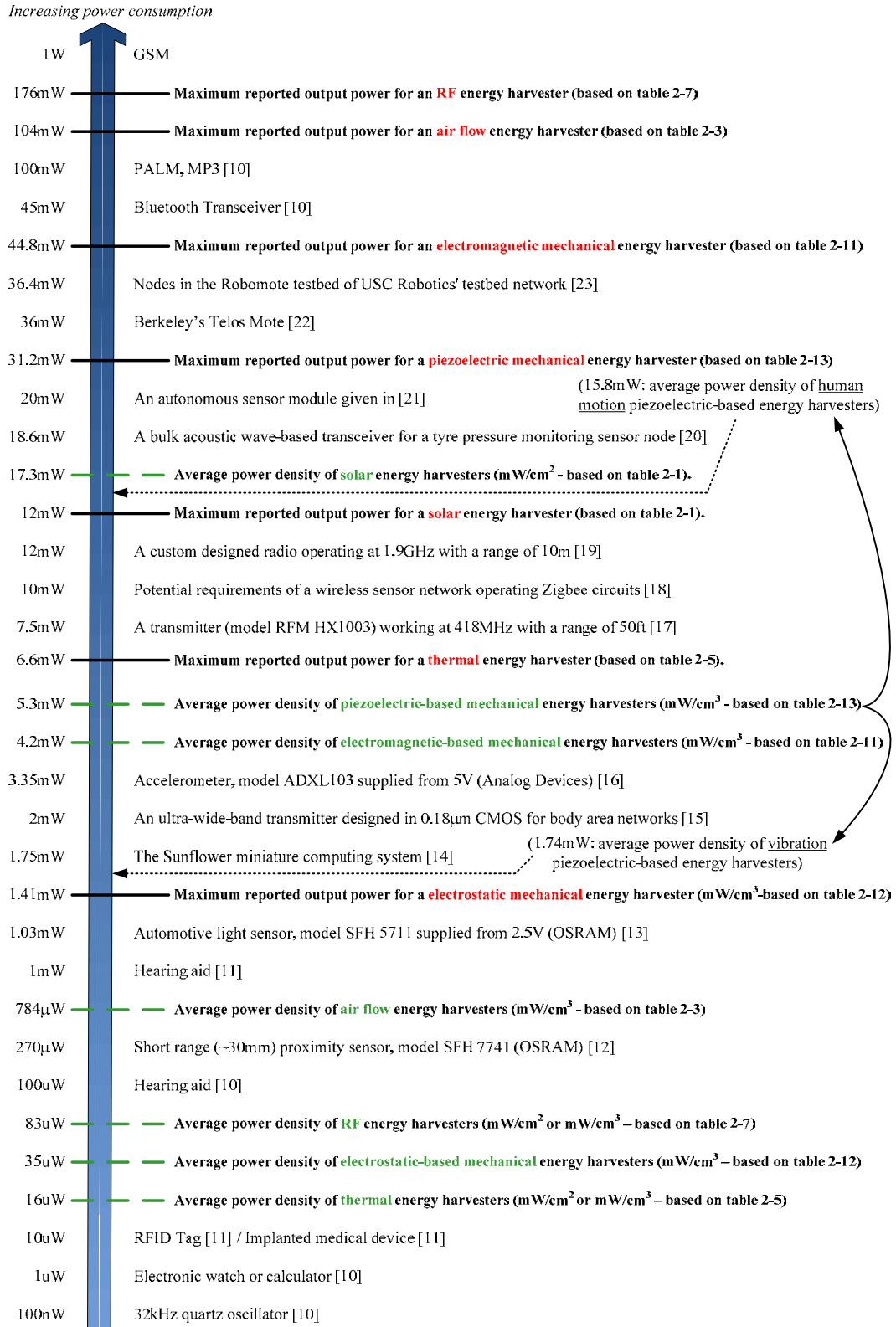


Figure 2-14 Power requirements of a range of electronic devices and systems, maximum output powers recorded for the different energy sources, and average power densities of meso-scale generators harvesting from the different energy sources.

Figure 2-14 provides an indication of what is feasible when considering energy harvesting technologies to power electronic applications. In the figure, the “Maximum reported output power for...” indicators (represented by the horizontal solid black lines) are just that; i.e. they are simply the maximum power value that has been reported for a meso-scale device of that technology tested to date. These maximum figures have not been normalised in any way to account for different device sizes, environmental conditions of electrical loading conditions; they are simply ‘as is’. The “Average power density of...” indicators (represented by the horizontal dashed green lines) were calculated by first calculating the power density; i.e. mW/cm^2 or mW/cm^3 , where possible, for each individual reported device, and then the average was taken for all of the devices in that category. For these average figures, variations in applied environmental conditions and electrical loading conditions have not been accounted for. The reason for this is that it was found to be near impossible to take into account variations in all aspects; i.e. electrical loading conditions and environmental inputs as well as device size, because the number of works that give sufficient information on all three aspects are few, leading to a very small sample size.

From the average power density figures calculated, it can be seen that photovoltaic converters and piezoelectric-based mechanical energy converters appear to represent the highest power density technologies, at $17.3\text{mW}/\text{cm}^2$ and $5.3\text{mW}/\text{cm}^3$ respectively, while thermal conversion seems to represent the lowest power density technology at $16\mu\text{W}/\text{cm}^2$.

It is interesting also to note the advantages and disadvantages of the various energy harvesting technologies given in Table 2-2 through Table 2-10; some are very distinct, for example, the ability of RF to give power over distance could be a significant

advantage in applications where a remote monitoring capability is required and no other environmental source is available. One can imagine food or medical industry applications such as automated chemical analysis or temperature control of the contents of vats or raw ingredient stores in factories, where the power level to the sensors could be controlled from one central RF transmitter. Similarly, both solar and thermal harvesting devices have the advantage of comprising of no moving parts, making them inherently more reliable than air flow or vibration harvesters whose moving parts may wear or fatigue over time. The high power density of photovoltaic and piezoelectric harvesting technologies has already been mentioned, but in addition, these two technologies have the advantage that they harvest from two of the most abundant sources of energy available: solar and mechanical. Indeed, the key advantage that harvesting from vibrations offers is the abundance of available vibration environments, which occur in all manner of transport vehicles (from bicycles to aircraft), buildings and other civil infrastructure, and industrial environments (see Table 1-1 on page 4 for an exhaustive list). Given the possibilities that this can offer in terms of application scenarios, and considering the discussion above on the merits of piezoelectric conversion, which include a high power output, useable output voltage range, and self contained power generation, the technology choice considered in this thesis is piezoelectric conversion of vibration energy.

2.4 Justification for Focussing on Power Enhancement

Given that piezoelectric conversion of vibrations is the technology choice of this thesis, the aim of this section is to discuss why investigating methods of enhancing the power output is a worthwhile research effort.

Other potential avenues of exploration that might have been considered include: geometric variations of the harvesters (for different purposes), wearable or implantable harvesters, tuned or wideband harvesters and durability of the harvesters. Each of these other categories will be briefly discussed here, before justification is given for focussing on power enhancement.

2.4.1 Other Potential Avenues of Exploration

2.4.1.1 Geometric Variations of Piezoelectric Harvesters

The most common geometric configuration used in the design of piezoelectric energy harvesting devices is the rectangular cantilever beam as shown in Figure 2-15.

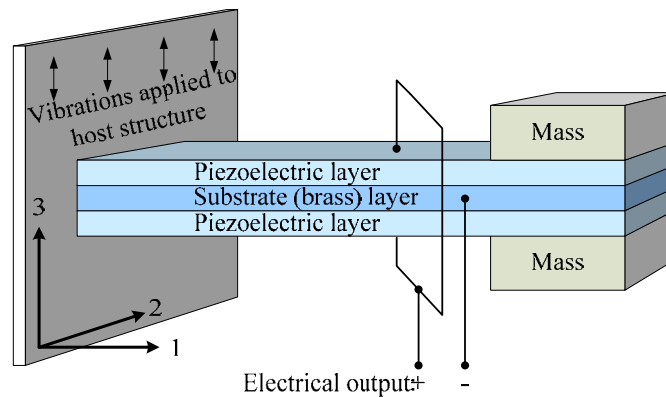


Figure 2-15 A rectangular piezoelectric bimorph cantilever.

This is because harvesting from steady-state vibrations is the concern for many researchers, and for this purpose the structure offers a large average strain for a given applied force and a low resonant frequency in a small package size. The latter point is important because vibrations that are commonly found in the environment tend to have higher acceleration values at the lower frequency range; i.e. below 200Hz or so [66] [67] [68] [69]. Other geometries have been explored however, for different purposes, including: improving the amount of power that can be harvested from vibrations,

improving the mechanical robustness of the device, and obtaining a design that is not resonant-based and so can harvest over a wide range of frequencies or from an impact. Table 2-14 on the next page summarises the different configurations developed to date, and identifies the purpose of each one, while Figure 2-16 gives examples of each type of device:

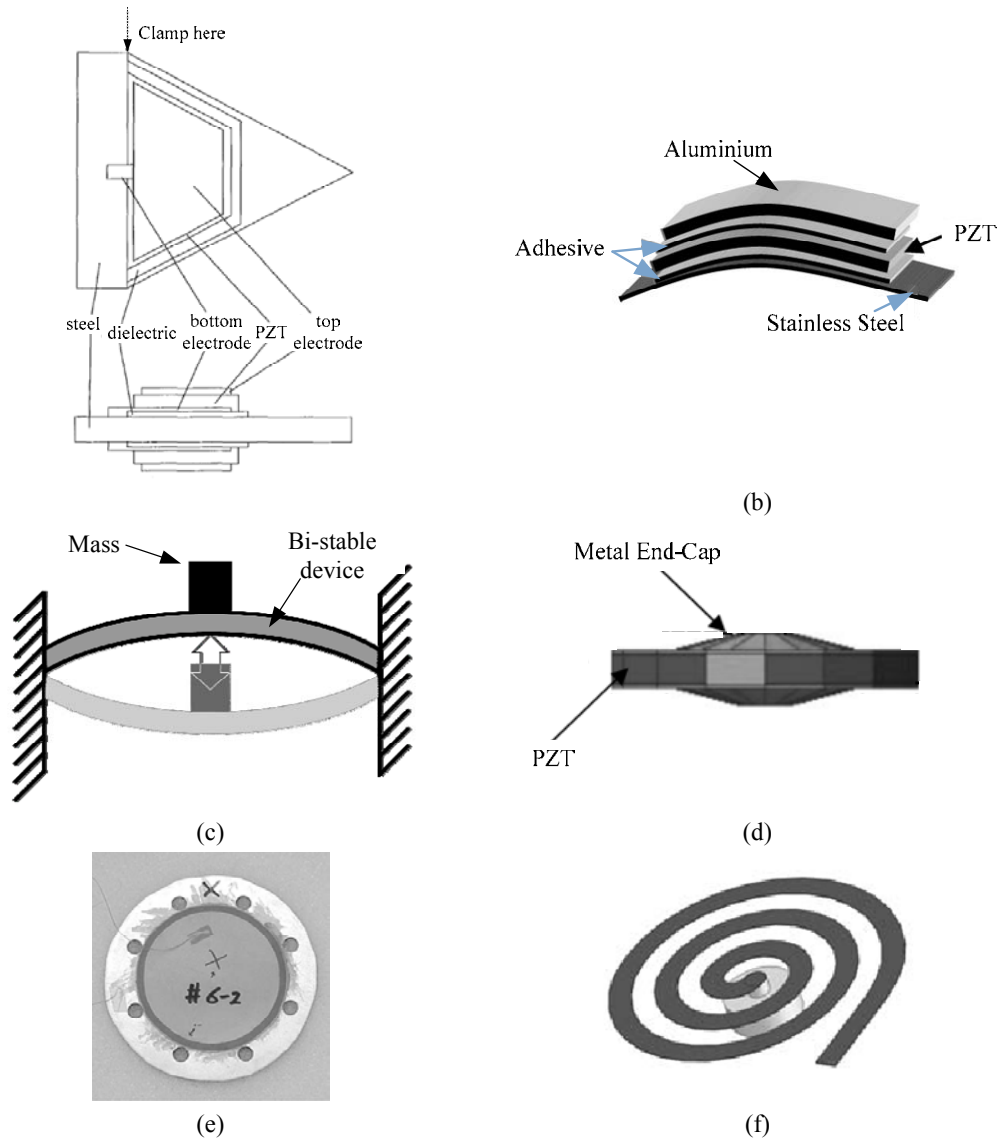


Figure 2-16 Schematics of the different configurations of piezoelectric energy harvesting device developed to date (a) a triangular cantilever [92] (b) a pre-stressed bender [98] (c) a bi-stable device [99] (d) a cymbal harvester [91] (e) a circular (disc) harvester [100] [101] (f) a spiral shaped harvester [102].

Table 2-14 Summary of piezoelectric harvesting device shapes and their purpose.

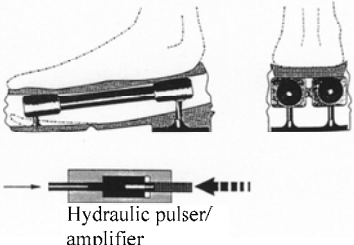
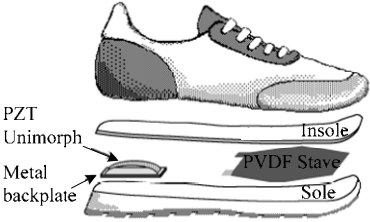
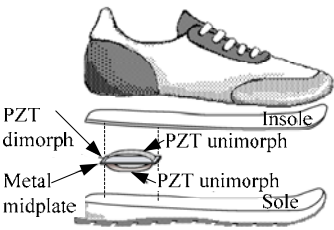
Device Shape	Investigated by	Purpose
Triangular cantilever	Glynne Jones et al in 2001 [92] Mateu and Moll in 2005 [103] Baker et al in 2005 [99]	For enhancing the power output: a higher maximum vibration amplitude can be applied to a triangular cantilever than for the same size rectangular cantilever.
Pre-stressed bender	Kymissis et al in 1998 [96] Mossi et al in 2001 [104], 2003 [105] and 2005 [98] Yoon et al in 2005 [106]	For harvesting from an impulse (i.e. from footfall), rather than from vibrations.
Bi-stable	Baker et al in 2005 [99]	For overcoming the problem of having to match the resonant frequency of the device with the (often changeable) frequency of the vibration environment.
Cymbal	Kim et al in 2004 [91]	For increased durability, since the device does not bend (bending causes fatigue in the piezoelectric material). The device is compressed instead.
Circular (disc) shaped	Kim et al in 2005 [100] [101]	For harvesting from a pressure source. With properly arranged electrodes, the power output can be enhanced.
Spiral shaped	Choi et al in 2006 [102] Yuantai et al in 2006 [107]	For lowering the resonant frequency of the device (a spiral is a very compact way of arranging a long beam length).



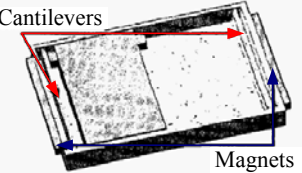
2.4.1.2 Wearable and Implantable Piezoelectric Harvesters

In regard to wearable piezoelectric harvesters, it is evident from reading the literature that most efforts are focussed on harvesting energy from footfall, probably because walking or running gives a plentiful source of waste energy [61] and because humans are already accustomed to the energy loss mechanism that occurs in shoes. Because the volume offered by the sole or heel of a shoe can be quite large (a few cm^3), the power output of shoe-based harvesters tends to be quite high, since the device can be fairly big and the forces applied to it can be high. Table 2-15 on the following pages provides a summary of work performed involving shoe-based generators to date.

In regard to implantable piezoelectric harvesters, the earliest example was possibly in 1963 when Myers (of Bell Telephone Labs., Inc) et al [108] developed a device to be placed about a large blood vessel such as the aorta. They tested the device with a circuit similar to a battery-powered pacemaker, by simulating the motion of the aorta by pumping water through tubing. More recent examples of implantable piezoelectric harvesters include Sohn et al in 2005 [109], who compared two 1cm^2 piezofilm (PVDF) pieces: one square and the other circular, for harvesting energy from fluctuating blood pressure in humans, and Platt et al [110] [111], who demonstrated the feasibility of using piezoelectric generators incorporated into the components of a total knee replacement (TKR) implant. Sohn et al found that the circular piezofilm outperformed the square piezofilm in terms of power generation by about 30%, and Platt et al found that one of their proposed piezoelectric stacks was capable of generating 1.6mW when subjected to a 900N ISO knee force profile. Interestingly, for use in KNRs expected lifetimes of 20-40 million cycles are expected, so Platt et al are one of the few researchers to consider the long term prospects of the device, testing it for 10^4 cycles.

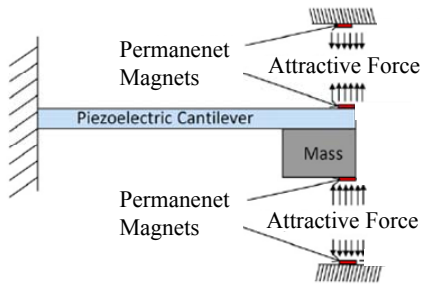
Table 2-15 Summary of work performed to date on shoe-based piezoelectric harvesters

Date	Investigated by	Device/Work carried out	Power Output/Findings
1995	Antaki et al [112]	 <p>A piezoelectric stack, comprising 18PZT slugs in a 1/17 scale model</p>	676mW while walking 2.1W while jogging (for a 75kg man)
1998	Kymissis et al in 1998 [96]	 <p>Two devices: 1) A PVDF elongated hexagon bimorph with a plastic substrate for harvesting from bending of the sole, 2) A piezoelectric patch adhered to a sprung steel strip for harvesting from a heel strike.</p>	PVDF Stave: peak = ±60V and 20mW, average = 1mW due to low duty cycle. Sprung steel strip: peak = 150V and 80mW, average = 2mW due to low duty cycle. (frequency of footfall ≈1Hz) (electrical load = 250kΩ)
2001	Shenck and Paradiso [97]	 <p>Expanded on the work of Kymissis (above), to produce a ‘dimorph’ for incorporating into the heel of a US Navy work boot.</p>	Average = 8.4mW for a ‘brisk walk’ (electrical load = 500kΩ)
2005	Mateu and Moll [103]	Carried out a comparison study on the different beam structures (e.g. triangular versus rectangular homogenous cantilevers, and simply supported beams with point or distributed loads) in order to analyse the advantages, disadvantages, and power outputs of each with the application of shoe-mounted scavengers in mind.	The best solution for a shoe insert is an asymmetric heterogeneous bimorph that is simply supported and subjected to a distributed load, though they did not experimentally validate their findings.

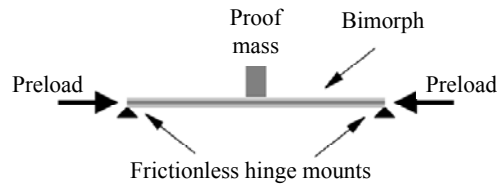
Date	Investigated by	Device/Work carried out	Power Output/Findings
2005	Yoon et al [106]	 <p data-bbox="934 414 1386 584">Developed an analytical model of a pre-stressed bender, and used the model to discover what the optimal design characteristics of the device are; i.e. what parameters to maximise or minimise in order to maximise charge generation.</p>	<p data-bbox="1417 365 1848 397">Several ‘rules of thumb’ were determined:</p> <ol data-bbox="1417 406 1879 625" style="list-style-type: none"> 1) Increasing the width is more effective than increasing the length, 2) Increasing the dome height is favourable, 3) Increasing the substrate (metal layer) thickness is favourable. Their analytical trends were borne out by experimental results based on nine different harvesters.
2008	Klimiec et al [113]	<p data-bbox="588 673 1396 779">Used a self-made piezoelectric product, based on polyethylene-propylene (PE-PP) copolymer, in a shoe-based generator. A foil sample of just 11μm thickness was placed between two 3mm thick electrodes; the completed structure was assembled into the sole of a training shoe with glue.</p>	<p data-bbox="1417 673 1879 779">340nW_{RMS} (for one 11μm thick active layer). (1Hz walking pace) (electrical load = 20mΩ)</p>
2009	Rocha et al [114]	 <p data-bbox="934 812 1386 950">Produced an injection-moulded shoe sole with both a number of PVDF elements and a small-scale (smaller than a one cent Euro coin) power conditioning circuit embedded within it.</p>	<p data-bbox="1417 828 1848 941">The piezoelectric generator power output, during experimental tests, was “tens to hundreds of mW” [114], depending on placement, geometry, and number of foils.</p>
2005	Renaud et al [115]	 <p data-bbox="934 1015 1386 1128">Developed a model of a non-resonant harvester for harvesting power when positioned on the wrist. The free-sliding mass collides with two piezoelectric cantilevers.</p>	<p data-bbox="1417 1047 1879 1096">Proposed output is 40μW for an arm swing of \approx10cm</p>

2.4.1.3 Tuned or Wideband Piezoelectric Harvesters

The accomplishment of non-resonant vibration energy harvesters is an obvious goal for researchers in the field of vibration energy harvesting, given that vibrations present in the environment rarely take the form of simple harmonic motion that maintains a single frequency value over time, and that most energy harvesting devices developed to date are resonant structures by nature. This need to match the natural frequency of the structure with the frequency of the vibration source is a pressing problem that is inhibiting the adoption of vibration energy harvesting as a feasible power source, and it is a problem common to all methods of conversion: electromagnetic and electrostatic as well as piezoelectric. Reports of non-resonant or tunable piezoelectric vibration energy harvesters began to emerge around 2005. An interesting variety of methods have been employed to achieve frequency tuning, though most at present seem to require human intervention in order to actively alter some physical aspect of the vibration harvester, which somewhat negates the objective of using energy harvesting devices in remote environments or embedded in structures. Figure 2-17 attempts to show six methods considered in the literature by which obtaining a tunable or non-resonant device has to date been achieved.

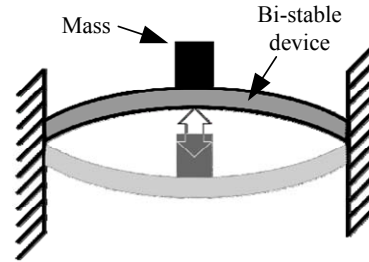


Challa et al (2008) [116]: A cantilever whose stiffness can be adjusted: the cantilever can be vertically displaced relative to the position of the two fixed magnets on the outer casing. The beam was successfully tuned between 22Hz and 32Hz (26.2Hz being its natural frequency without any magnetic force applied). Over this range the power output remained between $240\mu\text{W}$ and $289\mu\text{W}$.

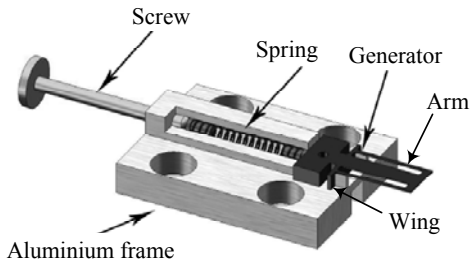


Leland et al in 2006 [118] aimed to tune a bimorph by applying a variable compressive preload. They found that as the axial preload on the device was increased:

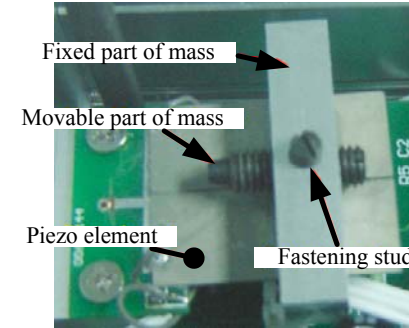
- 1) The resonant frequency reduced by as much as 24%,
- 2) The coupling coefficient increased by as much as 25%,
- 3) The power output maintained between $300\mu\text{W}_{\text{pk}}$ and $400\mu\text{W}_{\text{pk}}$ across frequencies that varied, depending on the axial preload, from 200Hz to 250Hz,
- 4) The damping ratio increased by approximately 67%.



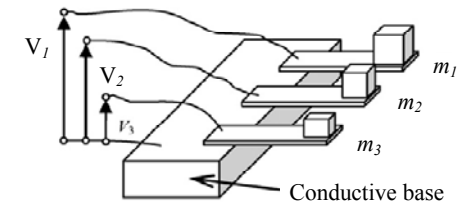
The bi-stable generates power when it snaps through from one stable state to the other. Baker et al [98] tested the bi-stable over 20Hz to 100Hz and compared its performance with that of an uncompressed beam. They found that the bi-stable demonstrated the ability to harvest larger amounts of power (30% to 100% more) off-resonance than the uncompressed beam.



Eichhorn et al (2008) [119]: A cantilever with a mechanism that enables a force to be applied to the free end. Turning the screw pushes the wings against two blocks (part of the aluminium frame) which provide a counter pressure that generates prestress in the arms, thus applying a force to the tip of the beam. A shift in the resonant frequency of more than 20% was achieved.



Wu et al (2008) [117]: A cantilever with a mass whose centre of gravity can be adjusted by means of a movable mass mounted into the fixed mass. The results given indicate a frequency adjustment of between 130Hz and 180Hz.



Ferrari et al (2008) [120]: A multi-frequency generator. The output of each cantilever was rectified separately. The use of three cantilevers shortened the time required to charge a capacitor from 25.8s (worst case with just one of the cantilevers) to 6.6s (best case with all three cantilevers). This trend was true regardless of which of the three resonant frequencies was used. Interestingly, the storage capacitor could be charged within 21s even if the excitation frequency was off resonance for all three of the cantilevers.

Figure 2-17 Six methods of achieving wideband or tunable piezoelectric vibration energy harvesters.

2.4.1.4 Durability of Piezoelectric Harvesters

It is rare to find published examples of work carried out to assess the long term life of energy harvesting devices. On reading the literature, this author has gained a sense that works are available that detail the effects of many cyclical stresses on piezoelectric materials, however, reports where the materials have been configured into an energy harvesting device and loaded cyclically over long periods of time are hard to find. It is certainly the case that for energy harvesting devices to be considered suitable for long term use (which is, after all, the goal if they are to replace batteries and provide maintenance-free operation), the reliability and long term prospects of them will have to be considered. It may simply be that at the present time this is not the priority. The sense this author has reached is that there are more important areas that need to be improved first, such as feasibility in some cases, wideband vibration harvesters and gaining increases in power, before elements such as cost and reliability come more into focus. A few researchers have examined long-term life as a sub-section of their main work, such as Platt et al [110] [111] (whose work is discussed in section 2.4.1.2), and du Plessis et al [121] but to this author's knowledge, there are no works whose main focus is on the performance of a device under long-life conditions.

2.4.2 Justification for Focussing on Power Enhancement

It is evident from the previous sections, which include: geometric variations of harvesters; wearable or implantable harvesters; tuned or wideband harvesters; and durability, that much progress has been made in piezoelectric energy harvesting over the last ten years. However, regardless of the form of energy harvesting device, it is usually the power output that is the foremost parameter to be considered. This is because the power output of the device is the fundamental parameter that dictates system feasibility;

e.g. if the harvesting device cannot generate enough power for the intended application, there is little point in continuing any further. Indeed, if confronted with a requirement for a remote monitoring application whose solution may lie in the utilisation of energy harvesting technology, it is likely that the first step taken by the system designer will be a feasibility study, and a fundamental part of that study will be a power budget to ascertain whether or not the energy harvesting solution is capable of supplying the remote monitoring application. Obviously, the higher the power density of the energy harvesting technology, the better chance the system designer has of being able to meet the requirement.

Given this reasoning, it is evidenced by Figure 2-14 (page 70), which shows a range of power requirements of electronic devices and systems and indicates the average power densities of the different energy harvesting technologies, that a pressing limitation of energy harvesting devices remains their low power outputs. The figure shows that the power consumptions of many of the most useful applications, including some of the most recently developed wireless sensor node platforms, remains above the power generation capability of most meso-scale energy harvesting devices. For example, the power requirement of the Sunflower miniature computing system developed in 2007 [14] represents one of the lower power systems available; its power consumption is around 1.75mW in active mode. If matched with a piezoelectric energy harvesting device, it appears that a device such as those incorporated into the sole of a shoe might be capable of providing power. However, the Sunflower system measures only 0.9×1.2 inches, so it is plain to see that in this case the harvesting device would take up the majority of the combined system weight and volume. Although keeping size to a minimum is not necessarily always important, it is reasonable to assume that in many

practical applications size is an issue, in particular for wireless sensor nodes. It is therefore important that the power output of an energy harvesting device is maximised for its size.

Given the discussed importance of the power parameter; i.e. that it fundamentally dictates system feasibility, and given the limitations that the low power output of harvesting devices is currently imposing on the adoption of energy harvesting technology, the aim of this thesis is to investigate and develop methods of enhancing the power output of a piezoelectric-based vibration energy harvester.

2.5 Overview of Piezoelectricity

Since piezoelectricity is the mechanism of energy transfer from mechanical (vibration) into electrical on which this thesis is based, it follows that a description of the concept is warranted, so that an understanding of the background and fundamentals of the phenomenon may be gained thus giving the reader a more complete and fully rounded picture. The two sections that follow describe the historical (2.5.1) and technological (2.5.2) contexts of piezoelectricity.

2.5.1 A Brief History of Piezoelectricity

The idea that some solids might exhibit an electrical response when subjected to pressure was first conjectured by Charles Augustin de Coulomb in the late eighteenth century [122]. This led the French minearologist René Just Haüy, and the French scientist Antoine César Becquerel, to investigate into the possibility in the early nineteenth century, though their experiments sadly proved inconclusive. The piezoelectric effect was first demonstrated conclusively by the brothers Pierre and Jaques Curie in 1880. Pierre was just 21 years old at the time, and Jacques was 24. The

brothers already had knowledge of the crystallographic origins of pyroelectricity (the ability of a solid to develop an electric charge in response to a change in temperature) and, based on their knowledge, they put forward the theory that there was a one-to-one interdependence between the electrical effects resulting from a change in temperature and the mechanical stress in a crystal. To prove this, they chose specific crystal cuts from crystalline solids that were known to exhibit pyroelectricity (among them, tourmaline, quartz, topaz, cane sugar, and Rochelle salt) for use in their experiments, and were able to prove the appearance of a surface charge on the crystals when the crystals were subjected to mechanical stress. This later became known as the piezoelectric ‘direct’ effect (piezo meaning “to press or squeeze”). The Curie brothers announced their discovery as follows:

“Those crystals having one or more axes whose ends are unlike, that is to say hemihedral crystals with oblique faces, have the special physical property of giving rise to two electrical poles of opposite signs at the extremities of these axes when they are subjected to a change in temperature: this is the phenomenon known under the name of pyroelectricity.

We have found a new method for the development of polar electricity in these same crystals, consisting in subjecting them to variations in pressure along their hemihedral axes.” [123]

The piezoelectric ‘converse’ effect, whereby a stress is exhibited in the material when an electric field is applied, was not predicted by the Curie brothers, but was verified by them after the existence of it was mathematically deduced from fundamental

thermodynamic principles by Gabriel Lippman, just one year later in 1881. Also in 1881, it was a German physicist: Wilhelm Gottlieb Hankel, who suggested the name “piezoelectricity”, which became the accepted name for the effect [122].

The Curie brothers continued to examine the properties of the new phenomenon they had just discovered, using just one type of crystal: tourmaline. The direction they took was to perform systematic quantitative experiments in order to discover the rules that govern the effect [123]. Such rules had already been discovered for pyroelectricity, and given the analogous links the two phenomena shared, the reasoning was that similar laws existed for piezoelectricity. Following their experiments, they concluded their new-found rules to the Academy of Science in January 1881:

“I. The two ends of tourmaline release equal quantities of electricity of opposite signs.

II. The quantity released by a certain increase of pressure is of the opposite sign and equal to that produced by an equal decrease of pressure.

III. This quantity is proportional to the variation of pressure.

IV. It is independent of the tourmaline’s length.

V. For a same variation of pressure [sic] per unit of surface area, it is proportional to the area.” [123]

In the 30 years or so after this, more work was done to further define both the crystal structures that exhibited piezoelectricity, and the macroscopic piezoelectric coefficients that are used in tensorial analysis of crystal solids. In 1893 Lord Kelvin, a British mathematical physicist and engineer, developed an atomic model to describe the effect,

and the French physicist Pierre Maurice Marie Duhem and German physicist Friedrich Carl Alwin Pockels both substantially contributed to the understanding of the phenomenon. In 1910 Woldemar Voigt published “Lehrbuch der Kristallphysik” (Textbook on Crystal Physics), which became a standard reference work that depicted all 20 natural crystal classes exhibiting piezoelectricity and all 18 piezoelectric coefficients.

The first practical application of piezoelectricity, to the best of this author’s knowledge, was in the development of sonar during World War I. The French physicist Paul Langevin and his colleagues used piezoelectric transducers to solve the problem of submarine detection [122]. They developed a transducer that comprised a number of thin quartz crystals glued between two steel plates. The device resonated at about 50kHz and was eventually successfully used to emit a ‘chirp’ underwater, the echo of which could be timed in order to derive a measurement of the depth of the submarine [124]. From these beginnings, the development of sonar transducers remains ongoing to this day.

Possibly the next major technological milestone in the advancement of piezoelectricity is the development of the ‘crystal oscillator’. A crystal exhibiting the piezoelectric effect can be made to resonate by driving it at its natural mechanical frequency. Because the frequency dependence on temperature is very low, such piezoelectric resonators can be used in applications that require very stable and accurate timing. In 1917 Alexander M. Nicholson (Bell Telephone Laboratories) first patented a crystal oscillator developed using Rochelle salt, and in 1921, Walter Guyton Cady developed the first oscillator based on Quartz crystal. Soon after that, in around 1926, a quartz oscillator was used for the first time to stabilize the frequency of a transmitter [125]. Today, such devices are

frequently used in everyday electronic systems such as wristwatches, radios, mobile phones and computers, as well as in test and measurement equipment such as oscilloscopes and signal generators.

During World War II, isolated research groups based in the US, Russia and Japan worked simultaneously on developing synthetic (man-made) piezoelectric materials that were demonstrated to have much improved piezoelectric properties over naturally occurring materials. A significant milestone of this time was the development of the first man-made piezoelectric substance: barium titanate (BaTiO_3), which later led to the development of the lead zirconate titanate family of piezoceramics in the 1950s [124]. A large number of applications and products for piezoelectricity emerged out of the research efforts during World War II, including: improved sonar devices, piezoelectric filters, piezo buzzers, phonograph ‘pickups’ for record players, igniters (similar to those used in gas grills), and microphones.

In the 1950s, Jaffe and his colleagues [125] established that the lead zirconate titanate family (named the ‘PZT’ family) exhibited strong piezoelectric effects, and since then, PZT materials, in their various chemical compositions, have become the dominant piezoelectric ceramic in use today. However, the story of piezoelectricity does not end there; in the 1960s discoveries were made concerning the piezoelectric properties of some polymer materials. Polyvinylidene was discovered to have piezoelectric properties, after being stretched during fabrication, by Kawai et al in 1969, and work continues on the development of polymer-based piezoelectric materials to this day.

Given that the movement of piezoelectric transducers is extremely small; i.e. a very high electric field corresponds to only a tiny change (~4%) in the width of a crystal,

piezoelectricity has emerged to be a science with an impressively large portfolio of applications. Aside from those applications mentioned previously, piezoelectric materials have been employed in many high technology applications, including: medical ultrasonic devices, engine management systems, acoustic emission testing systems, piezoelectric motors, laser mirror alignment systems, scanning probe microscopes, and for the ultrafine focussing of optical assemblies.

2.5.2 Basic Description of the Piezoelectric Effect

An understanding of the piezoelectric effect begins with an understanding of the internal structure of the solids that exhibit it. A solid (sometimes called a crystalline solid) is characterised by long-range order of the atoms, molecules, or ions that comprise it; that is: the atoms, molecules or ions are arranged in a recurring pattern that extends into all three spatial dimensions, thus the solid has a crystal ‘lattice’ structure. A ‘unit cell’ of the lattice structure can be described as the smallest divisible unit arrangement of atoms, which is tiled in three dimensions, that describes the lattice by having the same symmetrical characteristics that are unique to the lattice. For example, Figure 2-18 depicts the unit cell of a simple cubic lattice.

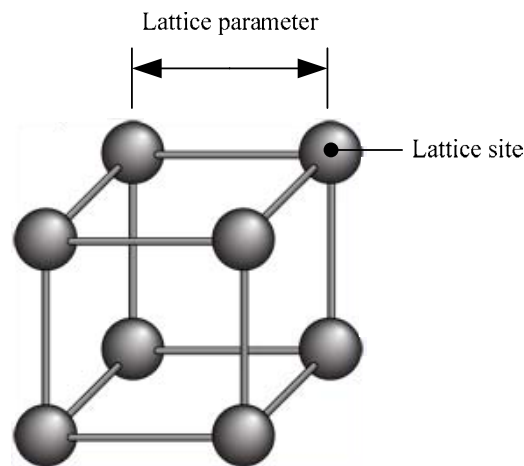


Figure 2-18 A unit cell of a simple cubic lattice

Crystallographers classify crystals according to their symmetry, and the cubic lattice is one of seven ‘lattice systems’. Each system is characterised by a unique arrangement of three axes, for example the cubic lattice system has three axes that are all perpendicular to each other and equal in length, as shown in Figure 2-19.

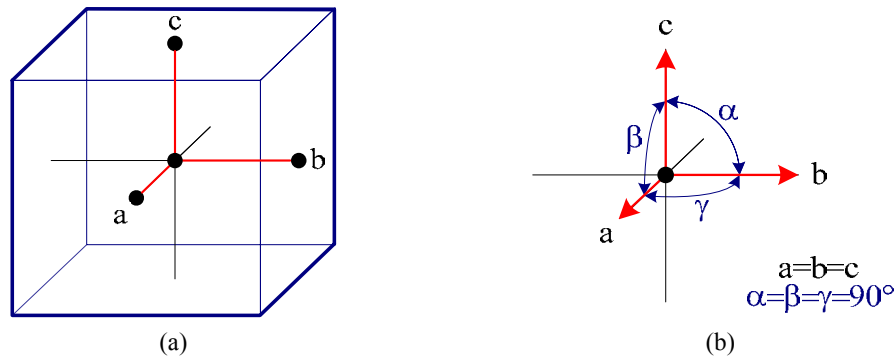


Figure 2-19 (a) Cubic unit cell geometry (b) crystallographic axes

The cubic lattice has a lattice ‘site’ at each corner of a cubic array (Figure 2-18). At each lattice site is an atom, molecule or ion, which identifies the ‘basis’ of the crystal structure; for a complete description of a crystal structure, both the basis and the lattice should be specified.

The seven lattice systems, in order of ascending symmetry, are: triclinic, monoclinic, orthorhombic, rhombohedral, tetragonal, hexagonal, and cubic. These systems are further sub-divided into thirty two ‘point groups’ according to their symmetry with respect to a point; i.e. symmetry operations about one unmoved point that leave the appearance of the crystal structure unchanged. Of these thirty two point groups, eleven are centrosymmetric (the unit cell has a centre of symmetry) and in one, a combination of symmetries leaves the cell such that it is akin to having a centre of symmetry. Twenty are thus classed as non-centrosymmetric, and all the crystals belonging to these twenty classes are piezoelectric.

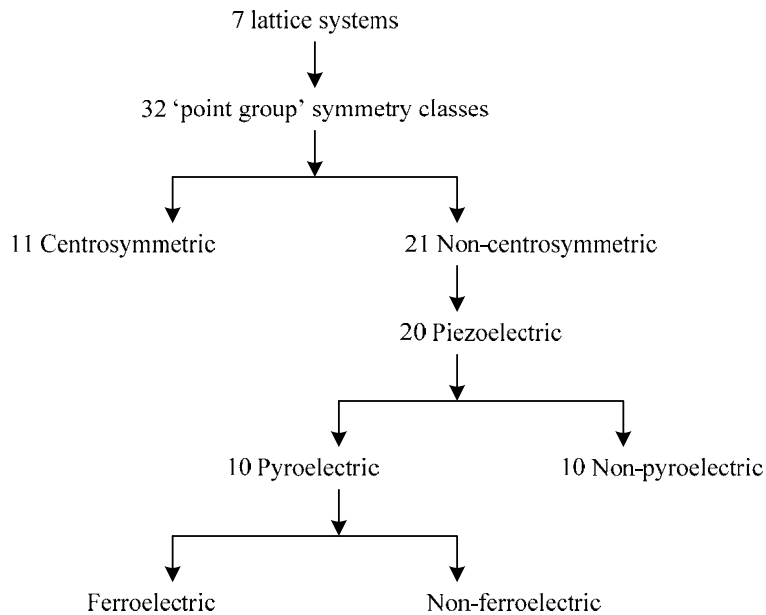


Figure 2-20 Categorisation of crystals belonging to the seven lattice systems

The lack of a centre of symmetry in a unit cell is a necessary condition for piezoelectricity, since this endows the crystal with the ability to form (or alter an already existing) dipole when put under pressure. The occurrence of a dipole within a unit cell is described as follows: the unit cell contains positive and negative charges, as a result of which there is a position of average positive charge and a position of average negative charge within the cell. If these two positions coincide, no electrical dipole is present. If the positions don't coincide, the cell encompasses an electrical dipole. Such a unit cell is said to contain 'spontaneous polarisation' and is labelled as being 'pyroelectric' as well as piezoelectric. All pyroelectric point group crystal classes (there are ten of them) are also piezoelectric, however not all piezoelectric crystal classes are pyroelectric (see Figure 2-20). For those crystals that are piezoelectric but not pyroelectric, applying pressure to the material is the only means by which dipoles are generated. For pyroelectric crystals, dipoles are ordinarily present and applying pressure

to the material alters the dipoles by the following process: as pressure is applied to a unit cell with no centre of symmetry, the cell physically distorts, resulting in a change in the distance between the positions of average positive and average negative charge, thus altering the ‘moment’ of the dipole (the electric dipole moment p is the product of the value of the point charge q and the separation between the two charges d). This alteration results in a change in the polarisation density (dipole moment per unit volume) of the crystal, which correlates directly with a change in charge per unit area developed on the external face of the crystal.

A key point to note in the understanding of piezoelectricity, is that long-range correlation must exist among the electric dipoles in a piezoelectric material. Initially, dipoles that are near each other tend to align in the same direction to form regions of local alignment known as ‘Weiss domains’. Weiss domains themselves, however, are randomly distributed throughout the material, as can be seen in Figure 2-21, and hence initially there can be no net dipole movement when the crystal is under pressure, since the orientation of dipoles in the Weiss domains cancel out the effects of each other.

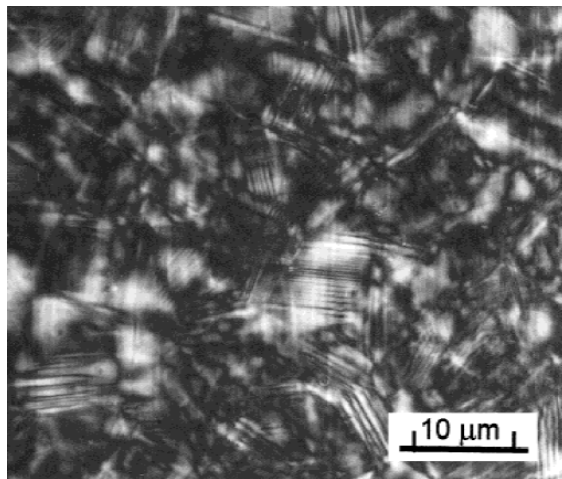


Figure 2-21 Weiss domain patterns in a tetragonal PLZT 12/40/60 ceramic [126].

For macroscopic piezoelectricity to be observed in the material (where charge separation can be observed across the whole of the material and used to perform work) a ‘poling’ process first has to be completed. The poling treatment involves exposing the material to a strong DC electric field at an elevated temperature; usually a temperature just below the Curie temperature of the material. Under these conditions, the electrical dipoles most nearly aligned with the direction of the applied field will grow and the dipoles that are not initially aligned will orientate themselves to become more in-line. On removal of the electric field and elevated temperature conditions, the dipoles remain locked in approximate alignment, thus giving the material ‘remanent polarisation’ and making it piezoelectrically active. Figure 2-22 illustrates this process.

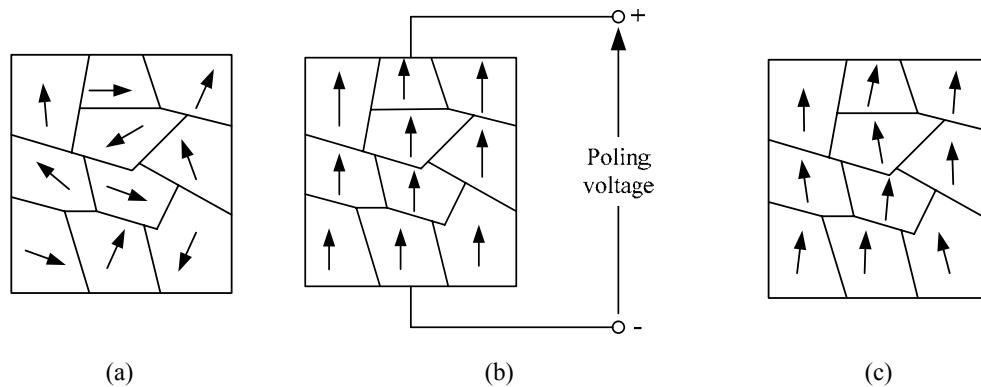


Figure 2-22 Weiss domains in the poling process of a piezoelectric ceramic (a) before poling (b) during poling, (c) showing remanent polarisation after poling

It was Gray [126] in 1945 who first made the significant discovery that an external electric field could orient the Weiss domains in a ceramic material. Previous to this, it was believed that ceramics could not be piezoelectrically active, because they lacked the long-range correlation of their electrical dipoles [126].

For the characterisation of a piezoelectric crystal or ceramic, a set of coefficients exists, and for these a sign convention is in place for both the coefficients and the axes sense.

Piezoelectricity directly couples a mechanical elastic property: stress or strain, to an electrical property: dielectric displacement (polarisation) or electric field, and the piezoelectric coefficients are used to connect either of the two mechanical variables with either of the two electrical variables. The choice of independent variables determines the particular piezoelectric constant to be used. A piezoelectric coefficient is usually given with superscripts and subscripts, for example: $\varepsilon^{\sigma}_{33}$. The superscripts denote a quantity held constant, for example ε^{σ} denotes that this ε coefficient was determined while the stress was held constant (meaning that the piezoelectric material was mechanically unconstrained). The subscripts denote the directional conditions under which the coefficient was determined, for example the piezoelectric charge coefficient, d_{31} , describes the generation of polarisation in the “3” direction per unit mechanical stress applied in the “1” direction (direct effect); *or*, it can describe the induced strain in direction “1” per unit electric field applied in direction “3” (converse effect). The axes sense is as shown in Figure 2-23, where the Cartesian “x” corresponds to “1”, “y” corresponds to “2”, and “z” corresponds to “3”.

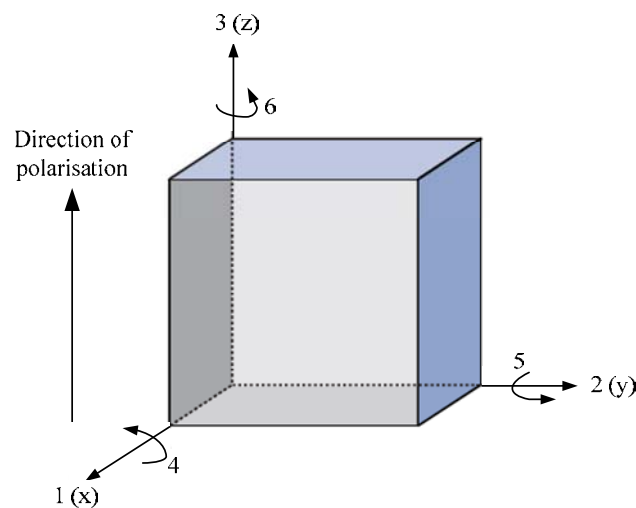


Figure 2-23 Orthogonal axes system used to describe the properties of piezoelectric materials [127].

The equations that govern the behaviour of piezoelectric materials are shown in matrix form in Table 2-16 [122], where a prime denotes transpose:

Table 2-16 Elasto-piezo-dielectric constitutive equations [122]

$$\begin{array}{ll}
 T = c^E S - e' E & D = e S + \varepsilon^S E \\
 T = c^D S - h' D & E = -h S + \beta^S D \\
 S = s^E T + d' E & D = d T + \varepsilon^T E \\
 S = s^D T + g' D & E = -g T + \beta^T D
 \end{array}$$

The third set within this table are the constitutive equations that describe the direct and converse piezoelectric effects:

$$D = d\sigma + \varepsilon^\sigma E \quad (\text{direct effect}) \quad (4)$$

$$S = s^E \sigma + dE \quad (\text{converse effect}) \quad (5)$$

Where: D is the polarisation, d the piezoelectric charge coefficient, σ the stress, ε^σ the absolute permittivity of the material under constant stress conditions, E the electric field, S the strain, and s the elastic compliance of the material under constant electric field conditions. The set of equations given in Table 2-16 in matrix form are actually simplified representations of second-order, three-dimensional tensors that relate the properties (i.e. the coefficient) along different orientations of the material. The mathematics, however, is complex and deeply involved. For the purpose of this thesis, only equation (4) is required.

2.6 History and State-of-the-Art in Power Enhancement of Piezoelectric Generators

On examination of the piezoelectric energy harvesting literature, it seems that there are a significant number of works that first develop a model of a proposed device, then build the device, and then quantify the power output. These works do not appear to be aiming to enhance the power output of the generators per se; rather, their focus is often

on either proving the feasibility of a new concept, such as a new device structure, or on proving the validity of the model so that it may be reliably trusted to make predictions of device characteristics (for example power output, resonant frequency or source impedance). Quantifying the power output is a necessary part of these proving process in these cases, and as such it does not mean that, if the achieved power values were high, they were necessarily aimed for. It is for this reason that works of this nature are omitted from this section. Only studies that directly concentrate on improving the power output of piezoelectric energy harvesters by some means are considered.

In regard to the generators themselves, there seems to be three main directions that have been explored in the quest for improved power performance: fundamental changes in the geometry of the device, mathematical optimisation of device parameters, and investigations that result in ‘design guidelines’ relating to physical and geometrical parameters. In addition to these, there are a number of circuit techniques that have been devised specifically to boost the power output of the harvesters. These include impedance adaptation and synchronised techniques; each of these will be explored here.

2.6.1 Power Enhancement through Design of the Harvesting Device

2.6.1.1 Geometric Advancements

For harvesting from vibrations, the cantilever beam with an end mass forms the basis of many harvesting devices. This is because the configuration offers large average strain in the piezoelectric material for a given applied force, and because low resonant frequencies can be achieved due to the low stiffness of the structure. Modifications to this form to gain improvements in power output have included triangular (tapered) shaped cantilevers [103] [99] and the introduction of a differently-shaped masses [128] [129].

2.6.1.1.1 Triangular-shaped Cantilevers

Although Glynne-Jones et al [92] used a tapered beam in their experiments in 2001, the focus of their work was on proving feasibility of the harvesting concept and on device fabrication rather than on the power enhancement benefits of this shape. The tapered shape was first analysed specifically for the purpose of enhancing power output, to the best of this author's knowledge, by Baker et al [99] in 2005. They predicted that a triangular shape could lead to a 50% increase in power output over a standard rectangular beam. In the case of a rectangular beam with an end mass, the maximum moment induced by the mass occurs at the fixed end of the beam, hence there is a large stress concentration at the base and very little stress at the free end. This means that much of the piezoelectric material at the free end does not contribute to charge generation (see Figure 2-24).

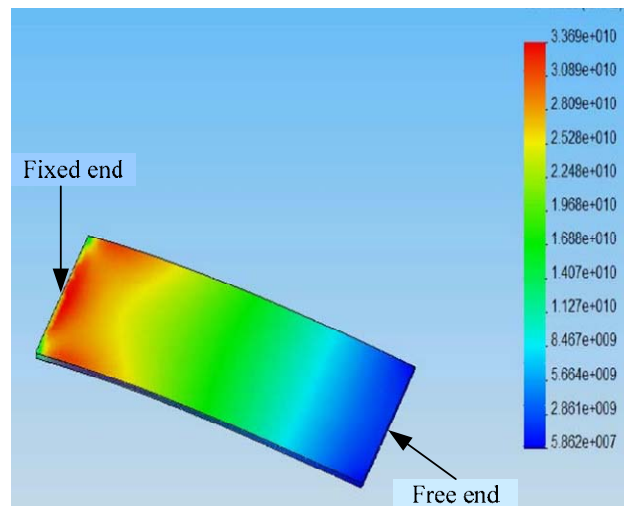


Figure 2-24 FEM analysis of a rectangular piezoelectric cantilever. The red areas denote areas of high stress [99].

In contrast, a triangular-shaped cantilever with an end mass can be made such that the radius of curvature along the length of the beam remains constant, hence the strain becomes uniform over the length of the beam and all of the piezoelectric material can

contribute to charge generation. The triangular geometry then, has the advantage that all of the piezoelectric material can be homogeneously stressed to a value just below the yield stress, which is in effect a way of maximising the strain in the material. By experiment, Baker et al were able to prove an increase in power of 30%, which was not quite their predicted 50%, but nevertheless is a big improvement by a simple means.

Mateu and Moll [103], also in 2005, showed by analytical investigation that for the case of a triangular cantilever, the radius of curvature can be made constant along its length, and so the strain along the length can also be made constant, which results in a higher average strain and beam deflection than a rectangular cantilever would experience for identical input conditions. Since higher strain in a piezoelectric material translates directly into higher charge output, the triangular design results in a higher power output per unit area than the rectangular design.

In 2008 the triangular design was again revisited by Goldschmidtboeing and Woias [130]. In their simulation study, which examined beam shapes ranging from rectangular to triangular; they ascertained that there is a trade-off to reach the optimum design shape, because:

- a) The mass distribution of the beam shape influences the efficiency of conversion of the excitation energy into mechanical energy, and in this respect a rectangular shape is more efficient than a triangular shape, since the distance between the centroid and fixed end of a rectangular beam is one half the length of the beam, whereas for a triangular beam it is only one third of the total length.
- b) The above effect is opposed by the previously-discussed advantage of curvature homogenisation that results from the triangular beam shape.

Goldsmidtboeing and Woias showed that, between the choice of rectangular and triangular beam shapes, these opposing effects of curvature homogenisation and mass distribution nearly cancel each other out in terms of efficiency of energy conversion. However, they conclude that the triangular beam shape has an advantage in that the maximum tolerable excitation amplitude is nearly double that for a rectangular beam. Hence it seems that the beam shape, while it has only a little influence on the efficiency, has a large effect on the maximum tolerable excitation amplitude; thus a triangular shape is preferred for an increased power output.

2.6.1.1.2 Geometric Variations of the Proof Mass

For the purposes of power enhancement, attention has also been given to optimising the proof mass. It could be considered that the overall volume of a traditional cantilever-based piezoelectric harvester is the product of the overall length, overall width, and overall height, such that the volume consists, in most cases, of a rectangular box that encloses both the beam and the seismic mass as shown in Figure 2-25. In this regard, there is a lot of wasted space within the box:

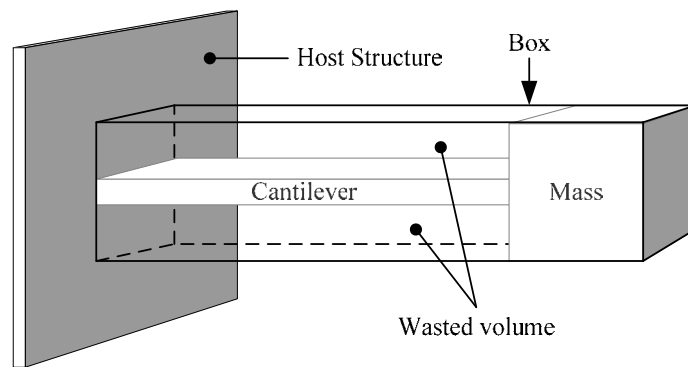


Figure 2-25 Schematic of a cantilever-based piezoelectric generator showing potentially wasted volume.

Some researchers have strived to make more efficient use of this space, usually by filling it in with more seismic mass material. Increasing the mass value has the combined effect of both lowering the resonant frequency of the device and increasing the power output. A U-shaped mass was considered by Roundy in his thesis of 2003 [128] (Figure 2-26):

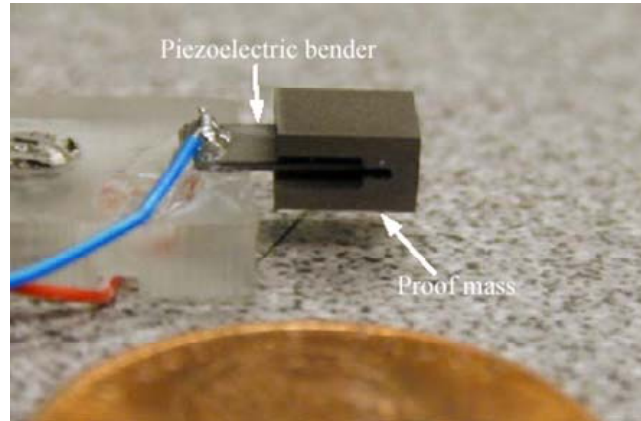


Figure 2-26 Rectangular piezoelectric cantilever beam with U-shaped mass [128].

The device was designed to harvest from the vibrations that are present on the inside of a car tyre. For this application, the space-envelope limit was $5\text{mm} \times 5\text{mm} \times 5\text{mm}$, and given such a small volume, the U-shaped mass design was adopted as a method of increasing the mass value. The device was tested by using a square wave drive to an electrodynamic shaker, and the result was a peak voltage of $\approx 1.75\text{V}$ across a $130\text{k}\Omega$ load resistor, giving a power output of $\approx 12\mu\text{W}$.

In 2009 Li et al [129] experimented with a curved L-shaped mass as shown in Figure 2-27:

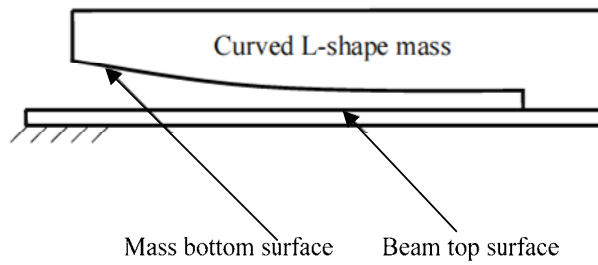


Figure 2-27 Cross section of a rectangular piezoelectric beam with a curved L-shaped mass [129].

The idea behind this shape is that the curved geometry makes better use of the otherwise wasted space than does the flat L-shaped mass (of which the U-shaped mass of Figure 2-26 comprises). This is illustrated in Figure 2-28:

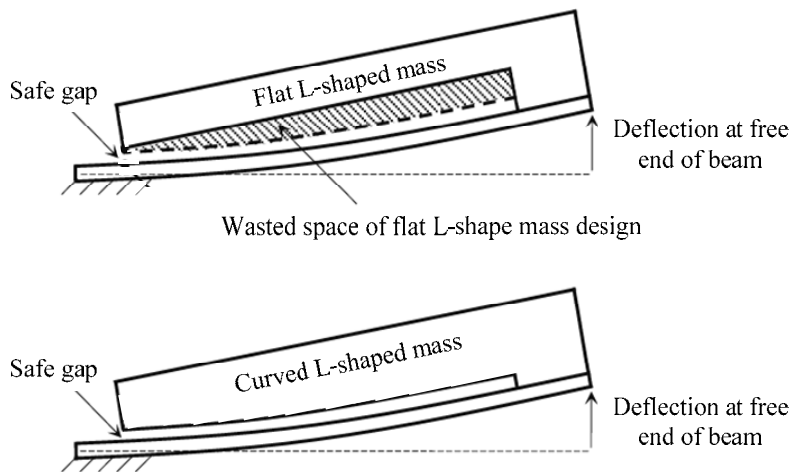


Figure 2-28 The curved L-shaped beam utilises more of the otherwise wasted volume than does the flat L-shaped beam [129].

When comparing the curved L-shape mass harvester with an equivalent volume block-shape and U-shape mass harvester, Li et al found that the fundamental frequency of the curved L-shape mass design was 24% and 26% lower than the block-shape and U-shape designs respectively. Their fabricated device had a volume of 0.242cm^3 (see Figure 2-29) and at $0.75g$ acceleration, generated $350\mu\text{W}$ at 64Hz with a $117\text{k}\Omega$ load, which is

a power density of $1.45\text{mW}/\text{cm}^3$. The equivalent volume block-shape harvester they tested generated $208\mu\text{W}$ at 86.5Hz with a $40\text{k}\Omega$ load, which is a power density of $860\mu\text{W}/\text{cm}^3$. The curved L-shaped mass design is thus very attractive for the purpose of enhancing the power density of the device.



Figure 2-29 Photograph of the rectangular piezoelectric cantilever with L-shaped mass [129].

2.6.1.2 Mathematical Optimisation

Optimisation means: “to make something as effective or advantageous as possible”. Some researchers have strived to optimise the design of a piezoelectric harvester through providing ‘design guidelines’, such as Yoon et al in 2005 [106], but not many have used an expression with a computer-based optimisation algorithm to produce an optimised device. Works that have used optimisation algorithms are detailed in this section, whereas those that provide design guidelines are discussed afterwards.

Roundy and Wright [19], in 2004, describe an analytical model of a cantilever-based piezoelectric vibration energy harvester, and then used their derived expression for power output as an objective function in one of Matlab’s built-in optimization routines. Not much detail about the optimisation process is given in [19], but more detail is given in [128] and [25]. ‘Reasonable constraints’ were set for the optimisation problem that dictated the maximum allowable device volume and allowable ranges for other device parameters such as lengths (of beam, electrodes, and mass), and the height of the mass. The formulation of ‘reasonable constraints’ was necessary since with only the bare

minimum of constraints, e.g. “the maximum device volume shall not exceed 1cm^3 ”, the optimiser was found to return values for the device parameters that made it impractical to manufacture (a design with an awkward aspect ratio or high electrical impedance for example) [25]. Two sets of reasonable constraints were formulated in this work, which resulted in two optimised designs. The power outputs of these designs were $375\mu\text{W}$ and $207\mu\text{W}$, each for a device that is 1cm^3 in volume.

Yoon et al [106], in 2005, developed an analytical model of a unimorph pre-stressed bender for harvesting energy from human footfall (this device is also mentioned briefly in Table 2-15 of section 2.4.1.2, and is discussed in more detail in the next section: 2.6.1.3). They suggest that their derived equation for the charge output of this device can be utilised directly in a numerical optimisation algorithm, though they do not perform this in the work.

The most recent work to consider the use of an optimisation algorithm is that performed by Kauffman and Lesieutre [131] in 2009. They developed a low order model that can be used to describe the behaviour of a unimorph or bimorph annular-shaped piezoelectric vibration energy harvester, and then successfully used the model in an optimisation problem to maximise the power output of the device while constraining the minimal inner radius and maximal outer radius. Details of which optimisation algorithm is used are not given, though some discussion is given about the process. Experiments were carried out, though neither of the two devices fabricated (one a bimorph and the other a unimorph), were the optimised design. The experiments done were for the purpose of validating the model, and the results did largely show good agreement with the model, though it is a shame they did not fabricate and test their optimised device.

2.6.1.3 Studies Providing Design Guidelines

The previous section discussed works that focused on the optimisation of piezoelectric energy harvesting devices through the use of computer-based optimisation algorithms. This section deals with those works that provide ‘design guidelines’ for piezoelectric energy harvesters. As an example of the type of work this author considers falling into this category, the reader is referred to the manuscript published by Yoon et al [106] in 2005 (this work is also discussed briefly in Table 2-15 of section 2.4.1.2). In this analytical and experimental study, an analytical model of a pre-stressed bender is described and used in order to discover the optimal design characteristics of the device; i.e. which parameters to maximize or minimize in order to achieve maximum charge generation. Yoon et al subsequently built and tested several devices, and emerged from the study with the following conclusions regarding the design of the device:

- 1) *“Increasing the width of the unimorph is more effective in charge generation than increasing the length.”*
- 2) *“Increasing the center height with a variation in manufacturing process is also very favourable for charge generation.”*
- 3) *“Increasing thickness of the substrate is effective in charge generation, which may be restricted by the available input force to deform the curved unimorph.”*

[106]

These are examples of what this author understands to be ‘design guidelines’, in that it is practical advice that leads to an increased power output. Further works that result in similar advice to designers is discussed in this section.

Lu et al [132], in 2004, provide some guidelines regarding the type of materials used in the design of a piezoelectric harvester. Their work describes an analytical model derived for a rectangular piezoelectric cantilever with an end mass. They subsequently build and test the device, and emerge from the study with the following conclusions:

- 1) *“At the higher frequency [sic], single crystal PZN-8% PT can achieve much higher output power in comparison to piezoelectric material PZT PIC255.”*
- 2) *“The performance of PZN-8% PT is more sensitive to operational frequency and that of PZT-PIC255 is more sensitive to external resistance.” [132]*

Their conclusions can be explained on examination of their derived expression for the power output of the harvesting device:

$$\bar{P} = vI = \frac{\omega^2 b^2 h^2 e_{31}^2 \bar{A}^2}{4(1 + bL\epsilon_{33} \frac{\omega R}{\Delta})^2} R. \quad [132]$$

The PZN-8% PT material has a larger ϵ_{33} coefficient, which is in the denominator of the expression, and the PZT-PIC255 material has a larger ϵ_{31} coefficient, which is in the numerator of the expression. At lower vibration frequencies, the smaller ϵ_{33} and larger ϵ_{31} from the PZT-PIC255 contributes to a higher power output, but as the frequency increases, the larger $\epsilon_{31}/\epsilon_{33}$ ratio of the PZN-8% PT material contributes to a higher power output.

The work of Kim et al [100] [101] has already been mentioned in Table 2-14 of section 2.4.1.1. In this analytical and experimental study, two circular ‘plate’ structures are analysed for harvesting from pressure sources. The first was a fully electroded version (shown in Figure 2-30), and the second was a ‘regrouped electrode’ version (Figure 2-31).

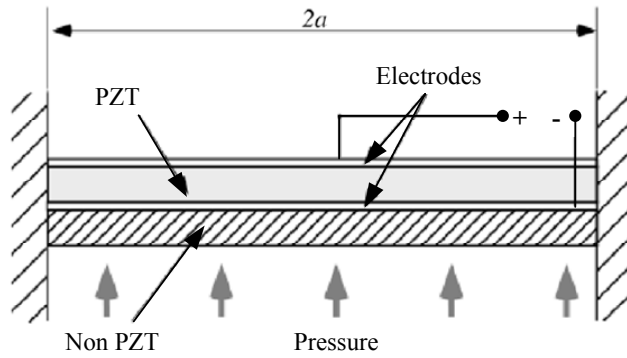


Figure 2-30 Cross section of a fully electroded clamped circular unimorph plate [100].

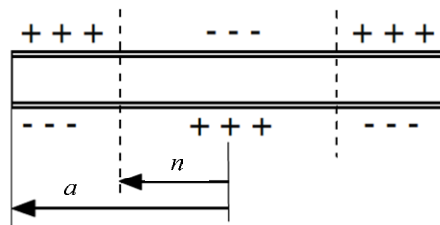


Figure 2-31 Cross section of the piezoelectric layer of the 'regrouped electrode' version of the clamped circular unimorph plate [100].

In Figure 2-31, a is the radius of the plate and n is the radius of the inner region. In the regrouped electrode version the electrodes were divided into areas that correspond to regions of positive and negative stress (and thus positive and negative charge) that exist along the radius of the plate as it undergoes a uniform pressure load, as is illustrated in Figure 2-32:

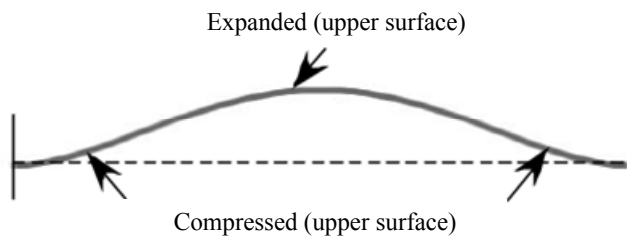


Figure 2-32 Deflection and stress of the clamped circular unimorph plate [100]

It was found that by regrouping the electrodes (or performing patterned polarisation of the piezoelectric material, which is what they did in practice) an enhanced level of output power was achieved. Specifically, the design guideline that results from this work, in the event that a plate structure is the concern, is:

- 1) *“The optimal pattern for a clamped circular unimorph plate with uniform pressure loading is to reverse polarity in the piezoelectric material beyond a radius of $0.707a$.”* [101]

where a is the radius of the plate.

2.6.2 Power Enhancement through use of the Harvesting Circuitry

A number of circuit techniques have been investigated to enhance the power output of piezoelectric energy harvesting devices. These include impedance adaptation methods, and synchronous techniques.

2.6.2.1 Impedance Adaptation

The principle of impedance adaptation is to provide a method by which the electrical load impedance can be matched to the source impedance of the piezoelectric generator, as from impedance matching theory these are the conditions under which maximum power transfer occurs. In 2002 Ottman et al [93] were the first to explore a method of interfacing to vibration-based piezoelectric generator with a matched impedance load through the use of a DC-DC converter. They first determined, through analytical modelling, that the peak output power from a piezoelectric generator when a bridge rectifier circuit is used occurs when the voltage at the output of the rectifier is approximately one-half the open-circuit voltage of the generator. To ensure that this condition was always met, Ottman et al used a DC-DC converter, not to provide output voltage regulation, which is the normal application for these converters, but instead to

control the optimal voltage point at the output of the rectifier. The circuit used to implement the concept is shown in Figure 2-33:

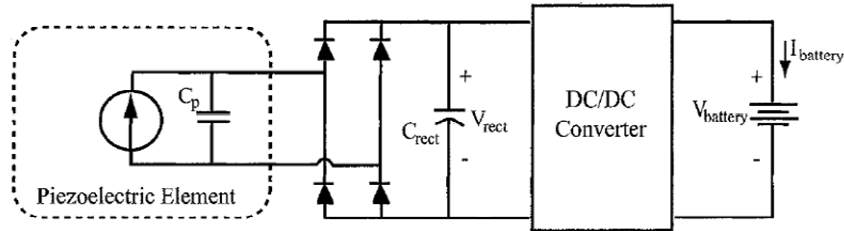


Figure 2-33 Adaptive energy harvesting circuit given in [93].

Because the load is a battery, the voltage at the output of the DC-DC converter is held constant, or changes very slowly. Therefore, in order to maximise power flow to the battery, current flow into the battery must be maximised. They achieved this by sensing the current flowing into the battery, $I_{battery}$, and then adjusting the duty cycle of the DC-DC converter accordingly (through means of a control circuit). In testing the circuit, they found that when the output of the piezoelectric generator was 45V open-circuit: (a) maximum current flow of 4.3mA was achieved, (b) the duty cycle was 3.18%, and (3) the voltage at the output of the rectifier was 20.4V (slightly less than one-half the open-circuit voltage), therefore verifying their analytical model. The implication of the work was that power transfer was increased from 4.5mW when a simple bridge rectifier circuit alone was used, to 13mW when the bridge rectifier circuit was used with the DC-DC converter technique, which is an improvement of 289%. Later, in 2003, [133] Ottman et al found that as the magnitude of the mechanical excitation to the harvesting device increased, the optimal DC-DC converter duty cycle became essentially constant, therefore the control of the converter was greatly simplified from its initial incarnation given in [93] in 2002.

2.6.2.2 Synchronised Techniques

In 2005 ‘synchronised techniques’ began to appear, so called because they are based on synchronisation between extraction of the charge produced by the piezoelectric element and the input vibrations. The first synchronised technique to make an appearance was the ‘Synchronised Switch Harvesting on Inductor’ (SSHI) technique, by Guyomar et al in April 2005 [1]. The second technique, Synchronous Electric Charge Extraction (SECE) appeared from the same research group later in 2005 [134].

2.6.2.2.1 Synchronised Switch Harvesting on Inductor (SSHI)

The technique is a way of processing the voltage delivered by the piezoelectric harvesting device in a non-linear manner, such as to take advantage of the mechanical position (displacement) of the generator in order to boost the power output of the device. The technique requires a switched inductor connected electrically in parallel with the capacitance of the piezoelectric harvesting device, as shown in Figure 2-34:

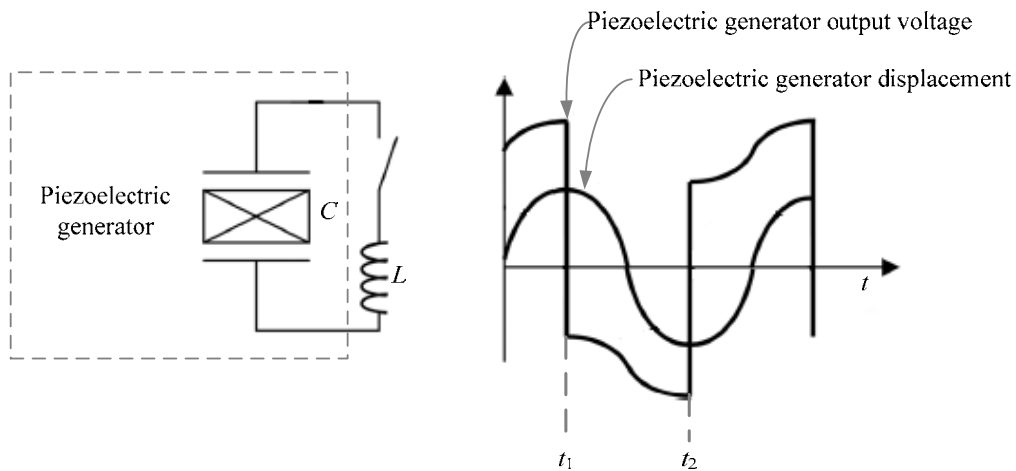


Figure 2-34 Required circuit components, and resultant voltage waveform, for the SSHI technique [1].

The switch is closed at times t_1 and t_2 (at the maxima and minima of transducer displacement), allowing the inductor and capacitance of the piezoelectric generator to form an oscillator with a frequency of:

$$\frac{1}{2 \cdot \pi \cdot \sqrt{L \cdot C}} \quad (6)$$

The value of the inductor is chosen such that the oscillator frequency is much higher than the generator vibration frequency. This has the advantage that the technique does not require a large-value inductor, and thus the circuit can remain small-scale. After a half-period of the LC oscillator the polarity of the charge on the generator has been reversed, and the switch is then opened. This has the effect that, except during the inversion process, the generator voltage is always increasing, as can be seen in Figure 2-34. Since the output voltage is greatly enhanced by this technique, there is a related increase in the power transferred to the load, through the relationship:

$$P = VI \quad (7)$$

Since SSHI is a technique upon which this thesis is based, the following description attempts to take a more in-depth look at the physical operation of the charge inversion process:

Consider a bimorph cantilever-based vibration harvesting device as shown in Figure 3-2 (b) on page 120 (repeated overleaf for clarity).

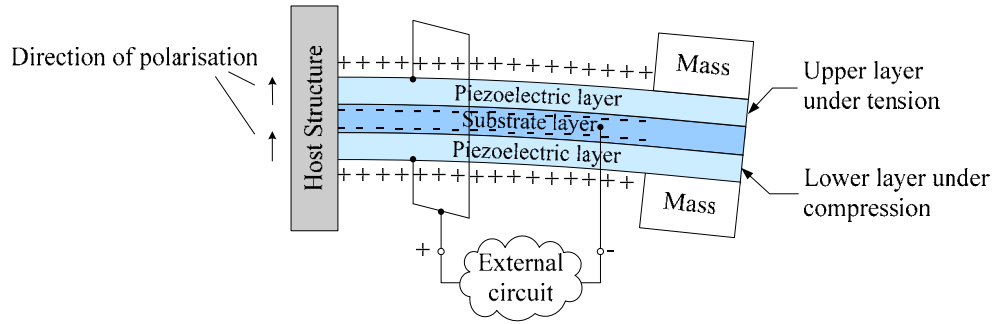


Figure 3-2 Schematic of a cantilever-based vibration energy harvesting device arranged as a bimorph poled for parallel.

Under steady-state vibration conditions, the tip (free end) of the cantilever moves up and down repeatedly with respect to the fixed end, which is attached to a host structure that is situated in a vibration environment. As the tip moves downwards, the top piezoelectric layer is put under tension which, for the direction of polarisation given in Figure 3-2, means that the charge generated on the top surface electrode is positive with respect to the charge generated on the centre (substrate layer) electrode. Similarly, the bottom piezoelectric layer is put under compression which, for the direction of polarisation given, means that the charge generated on the bottom surface electrode is positive with respect to the charge generated on the centre electrode. If, at the minima extremum of tip displacement, these charge polarities are reversed almost instantaneously; i.e. as the tip remains at its minima displacement, then the centre substrate electrode becomes positive with respect to the two outer electrodes. As the tip then moves upwards, the top piezoelectric layer moves from a state of tension to compression, which means that the new charge generated on the centre electrode is positive with respect to the charge generated on the top surface electrode, but the centre electrode is already positively charged with respect to the two outer electrodes, as a result of the SSHI process, and therefore this newly generated positive charge is added

onto the existing positive charges on the centre electrode. Thus the technique can be said to be taking advantage of the mechanical position; i.e. the displacement, of the device in order to maximise its power output.

The power output of a piezoelectric energy harvesting device can be most easily characterised through the use of a load resistor. Since a load resistor has no reactive components; it is purely resistive, the power dissipated by the load resistor in watts is easily calculated and wholly represents the useful power output from the generator; i.e. output power that can perform useful work. Many piezoelectric harvesting devices are characterised this way, including the one presented in Chapter 3 of this thesis. A direct comparison can be made of the power output of a piezoelectric harvester with a load resistor connected directly across its output terminals, and the power output of the same harvester using the SSHI technique and a resistive load, as illustrated in Figure 2-35. This is the ‘AC comparison case’ since the current experienced by the load resistor is alternating.

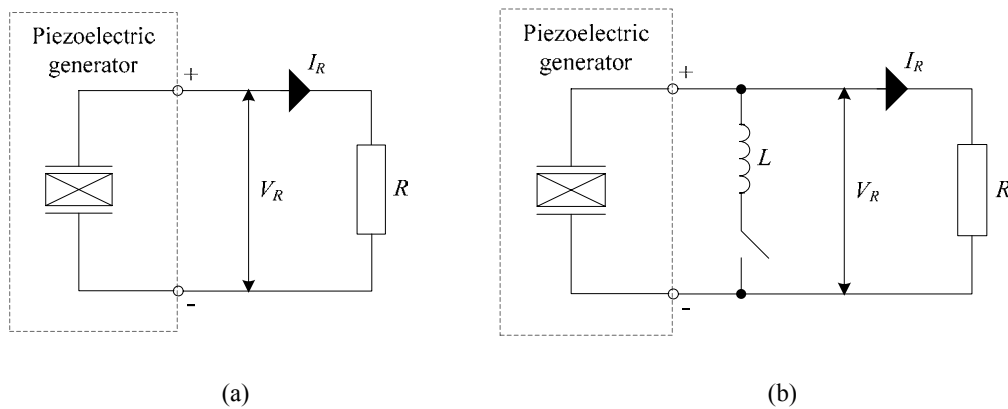


Figure 2-35 Method of measuring the effect of the SSHI technique for the AC case (a) circuit for measuring the power output of the generator without the use of SSHI (b) circuit for measuring the power output of the generator with the use of SSHI.

Similarly, the technique can be used with a bridge rectifier to form the ‘DC comparison case’ as shown below:

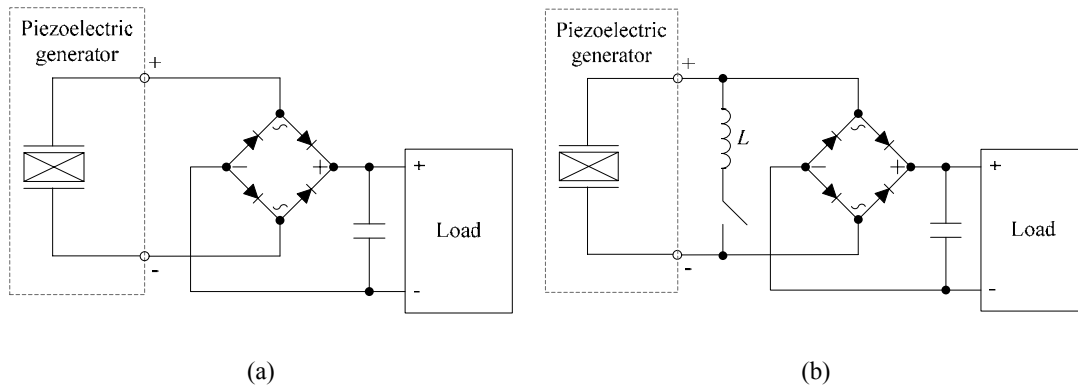


Figure 2-36 Method of measuring the effect of the SSHI technique for the DC case (a) circuit for measuring the power output of the generator without the use of SSHI (b) circuit for measuring the power output of the generator with the use of SSHI.

Guyomar et al carried out these experiments in the work that first introduced the SSHI technique in 2005 [1] and found that the power increase using the SSHI technique was greater than 900% for the DC case, and around 380% for the AC case. The power improvement that can be achieved then is significant, making the technique worthy of investigation and further development.

Component-wise, the technique appears at first to be very simple, as only an inductor and switch are needed. However, in order to operate the switch at the correct times; that is, whenever a displacement extremum occurs, ‘peak’ and ‘trough’ detection circuitry needs to be developed in addition to switch driving circuitry. A further consideration for the circuit designer is that the switch must be bidirectional, since charge inversion in both directions is required for the technique to work. These extra circuit functions are often overlooked in the literature, but they are necessary if the technique is to be implemented in practice.

2.6.2.2.2 Synchronous Electric Charge Extraction (SECE)

This technique is different to SSHI, in that where SSHI inverts the voltage on the piezoelectric generator in order to achieve an increased transfer of power from generator to load, SECE evacuates the charge available on the generator at the times when it is at a maximum, and then uses a flyback converter to push the evacuated charge round an external circuit. The circuit that implements the technique in [134] is given in Figure 2-37:

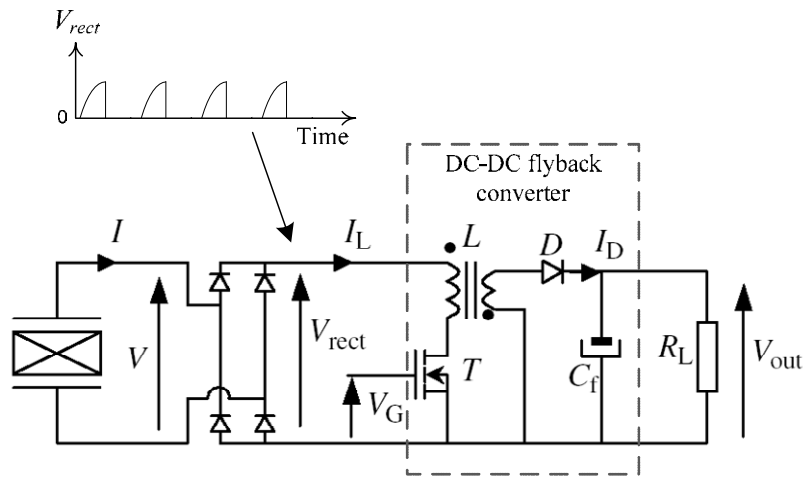


Figure 2-37 Circuit that performed SECE in [134].

The rectifier in the circuit does not include a smoothing capacitor, hence V_{rect} is not flat. Whenever the rectified voltage reaches a maximum, the MOSFET is switched on and charge is transferred to the inductor. When the charge is completely transferred (identified by V_{rect} being cancelled to 0V), the MOSFET is switched off again. After the MOSFET is switched off, the magnetic field around the inductor collapses, pushing charge round the external circuit (i.e. the capacitor and load resistor).

In experiments the SECE technique was shown to increase power transfer by over 400% compared to an impedance adaptation method, where maximum power is transferred

through matching the load impedance to the source impedance of the generator. However, the SECE technique has another advantage: the harvested power is not influenced by the load characteristics. This is because the generator is left in the open-circuit configuration for most of the time. In the experiments performed in [134] the generator was open-circuit for 8.3ms, while the duration of the charge extraction phase was just 10 μ s.

In summary, this author's understanding of the technique is that it uses the flyback converter to perform two functions:

- 1) Evacuate charge from the piezoelectric element when it is at its maximum. By doing this, similar to the SSHI technique, the output voltage is artificially increased. Figure 2-38, given in [134] indicates this:

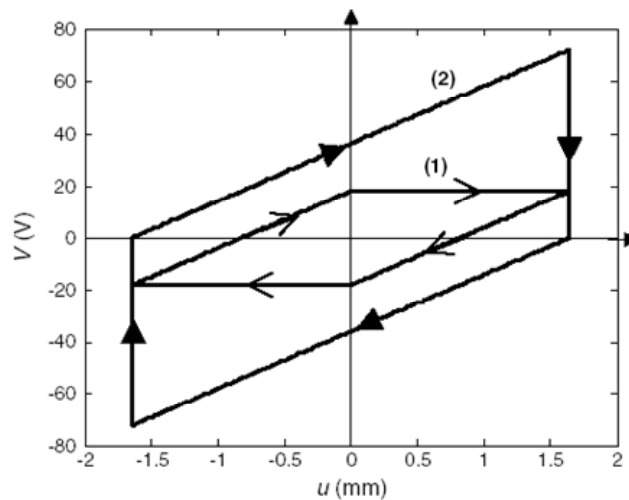


Figure 2-38 Theoretical cycles of the piezoelectric voltage as a function of the displacement (1) impedance adaptation technique (2) SECE technique [134].

- 2) Act as a buffer between the piezoelectric generator and load impedance. This means that the load applied does not affect the dynamic behaviour of the

piezoelectric generator. However, that is not to say that the technique itself does not affect the behaviour of the generator; it is simply that the technique, as it performs the increase in transferred power, has a consistent or ‘fixed’ effect on the performance of the generator, whereas different value load impedances have different effects on the output voltage amplitude and frequency of the piezoelectric generator.

2.7 Conclusions of the Literature Review

The literature review began with a survey of the power requirements of some modern electronic devices and systems. Following this an overview of the various energy harvesting technologies that can be used to extract energy from the different available sources (for example solar, thermal, or radio frequency) was given, paying particular attention to the power levels achieved in experiments to date. The two sets of data were then compared; i.e. the power levels that have been achieved by experiment to date were compared against the power requirements of electronic devices and systems.

It was found that even though the power levels obtained from harvesting devices has increased over the last six years or so, there is still a gap between the amount of power that can be harvested, and the amount of power that is ‘useful’ for powering an application. Currently, unless the harvesting device is quite large, such as solar panel, or a kinetic energy generator installed in a shoe for example, the power output is quite low; usually below the mW level, and many of the most useful applications (e.g. transmitters, miniature computing systems and wireless sensor nodes) have power consumptions in the mW range. This, coupled with the fact that the power output of a harvesting device is the fundamental parameter that dictates energy harvesting system feasibility, led to the focus on enhancement of the power as the research problem.

The harvesting technology chosen as a basis for the research problem was piezoelectric conversion of vibrations, since vibrations are one of the most abundant sources of energy available (see Table 1-1 on page 4), offering many possible application scenarios, and piezoelectric conversion tends to result in higher power outputs than electromagnetic or electrostatic conversion: typically in the hundreds of μW to a few mW region (e.g. $335\mu\text{W}$, $462\mu\text{W}$, $900\mu\text{W}$, 1.3mW), with voltages reaching high single figures to tens of volts DC or peak (e.g. $8.3V_{\text{pk}}$, $13V_{\text{pk}}$, $9.8V_{\text{RMS}}$, $20.57V_{\text{DC}}$). In addition, piezoelectric converters do not require any external accruements, so are completely self-contained.

Following these decisions, an introduction to the concept of piezoelectricity was given, which encompassed both historical and technological contexts, and a history and state-of-the-art in power enhancement of piezoelectric generators was presented, which covered both power enhancement through advances in the design of the generator (e.g. tapered cantilever shapes and different mass shapes) and power enhancement through use of the harvesting circuitry (focussing on impedance adaptation and synchronised techniques).

CHAPTER 3: DEVELOPMENT OF THE ANALYTICAL MODEL, OPTIMISATION, AND TEST OF THE PIEZOELECTRIC GENERATOR

Given the justification for focussing on enhancing the power density of a piezoelectric energy harvester, discussed in sections 2.3 and 2.4, the aim of this chapter is to ascertain a method of enhancing the power output by considering the design of the device. The chapter begins with a description and discussion of the fundamental configuration of the generator. Following this, some experiments conducted with a prototype cantilever-based piezoelectric harvester, which was fabricated from a commonly available piezoelectric buzzer, are described. The experiments necessitated the development of a test setup, therefore a prototype test setup, which was built using commonly available electronics laboratory equipment (e.g. a function generator, power amplifier and oscilloscope), is also described. Conclusions concerning both the prototype generator and prototype test setup are drawn, and then a way forward is proposed: namely to develop an analytical model that can be used with computer-based optimisation software to optimise the geometric parameters of the device, so that maximum power possible output can always be achieved for the space-envelope allowed in a given application. The analytical modelling is presented and is used with the complex conjugate optimisation algorithm (utilising Mathcad 2000 Professional software) to obtain the dimensions for a device that is optimised for maximum power output given an allowed volume of 1cm^3 . The optimised device is fabricated, an improved test setup is developed, and the device is tested. It is shown that the optimised device is capable of producing $370.37\mu\text{W}$ at a resonant frequency of 87Hz . The chapter ends with a discussion and conclusions of the work.

3.1 Description of the Design

From the literature review (Chapter 2), it can be surmised that piezoelectric-based vibration energy harvesting devices are very often configured as a cantilever beam with an end mass, as shown in Figure 3-1:

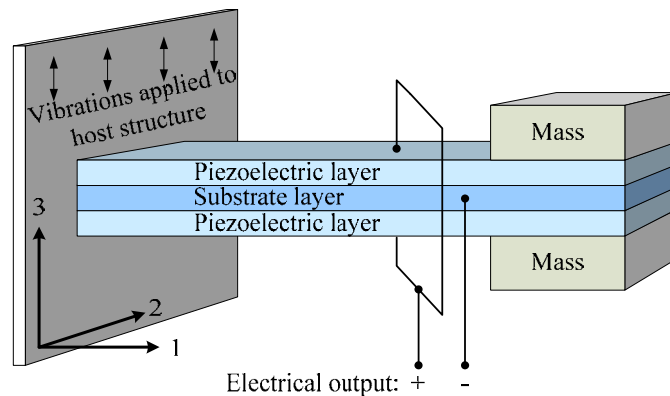


Figure 3-1 A piezoelectric vibration energy harvester configured as a cantilever beam

There is good reason for this: a cantilever results in one of the least stiff structures for a given volume. This means that the cantilever offers both a low resonant frequency and a high average strain in its materials for a given volume. Both of these characteristics are useful for a vibration energy harvester; a high average strain in the piezoelectric layers translates directly into a high power output and, from information gleaned from the literature review, it seems that the higher acceleration amplitude vibrations tend to occur at the lower frequency values, i.e. below 200Hz or so [66] [67] [68] [69]. Furthermore, as discovered from the ‘power enhancement’ section of the literature review (section 2.6.1.1.1), if the cantilever is configured to be triangular in shape rather than rectangular, then the maximum tolerable excitation amplitude can be much higher because all of the piezoelectric material can be homogeneously stressed to a value just below the yield stress. In the case of a rectangular cantilever, if the material near the fixed end of the beam is stressed to a value just below the yield stress, the material at

the free end is not stressed to the same degree. This means that, for the same size of device, a triangular-shaped beam is capable of outperforming a rectangular-shaped beam in terms of power output.

Cantilevers operate in the '31 mode'; that is, charges are collected in the "3" direction - through the electrodes (in-line with the polarisation of the material, which is conventionally denoted as the "3" direction), and the mechanical strain acts in the "1" direction (see Figure 3-1). While this is not the most efficient mode of use for a piezoelectric material (the '33 mode', where both the electric field and mechanical strain act in the "3" direction, usually has larger coefficient values; i.e. d_{33} and k_{33} are usually larger than d_{31} and k_{31}), use of the '31 mode' enables the benefits brought about by the low stiffness of the cantilever configuration, thus making it more effective. Cantilever-based piezoelectric energy harvesters work in the following way: when the host structure is subjected to acceleration from a vibration environment (for clarification, acceleration in the "3" direction only is assumed), the inertia of the mass causes the mass to move out of plane with the host structure. This relative displacement of the mass with the host structure results in curvature of the beam, which causes stress in the "1" direction within the piezoelectric layers. This in turn results in an electrical output through the electrodes of the device in the "3" direction as a consequence of the piezoelectric direct effect.

Cantilever-based piezoelectric harvesters can be arranged either as a unimorph, bimorph, or multi-layer bimorph, as shown in Figure 3-2:

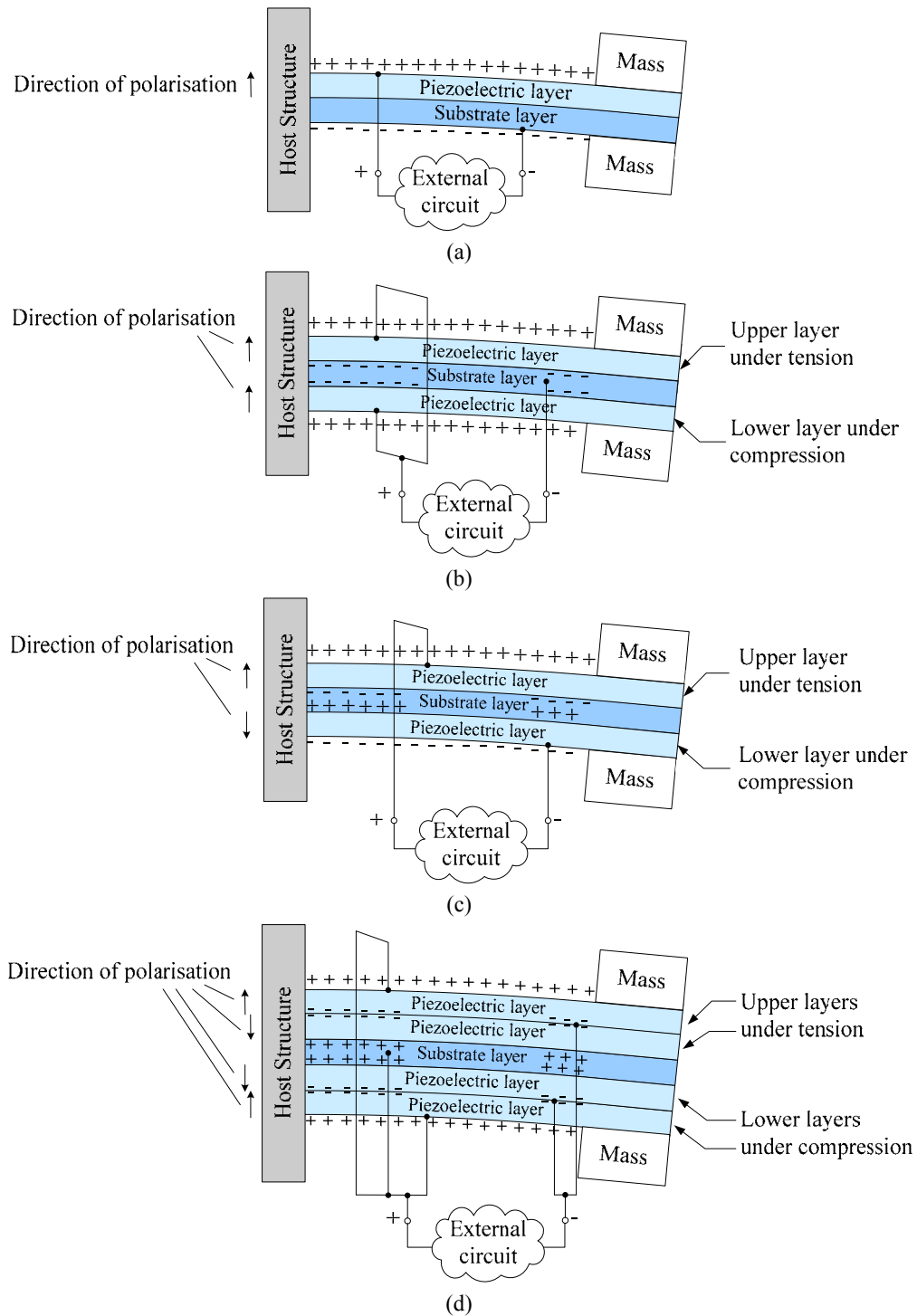


Figure 3-2 Schematics of differently arranged piezoelectric cantilever-based vibration energy harvesting devices (a) a unimorph (b) a bimorph poled for parallel (c) a bimorph poled for series (d) a multilayer bimorph poled for parallel

In bimorph and multilayer bimorph arrangements the device can be physically wired so that the piezoelectric layers are connected either in parallel or in series. Taking the case of a bimorph as an example, parallel connection requires that the piezoelectric layers are poled in the same direction so that, when subjected to acceleration from a vibration source, charge of the same polarity appears on the outer electrodes of the device. Thus the outside electrodes are connected together to make one electrical output terminal, and the centre layer constitutes the other electrical output terminal. Series connection requires that the piezoelectric layers are oppositely poled, such that when acceleration is applied, charge of one polarity exists on one of the outer electrodes while charge of the opposite polarity exists on the other outer electrode. In this case each outer electrode becomes an electrical output terminal. For the same size of device, the power output remains the same regardless of whether the device is poled for parallel or series. However, the ratio of current to voltage changes: for a device poled for series the output voltage is double that of a device poled for parallel; and for a device poled for parallel the output current is double that of a device poled for series [135]. This is because in the parallel case, the surface area of electrode able to output current directly to the circuit is double that for the series case, and in the series case the floating voltage output of each piezoelectric layer are connected in series (akin to connecting two batteries in series).

3.2 Initial Investigations

In order to conduct some initial investigations, an experimental approach was adopted. A cantilever-type harvester was fabricated, and experiments were performed with a simple load resistor. The purpose of these experiments was to begin to build up some physical intuition in order to better understand this type of device. The objectives were to get a feel for what can be expected regarding the power and voltage, and what (if

any) factors should be taken into account in the fabrication and testing of such a device. Because the aim of this thesis is to enhance the power output of the harvesting device, it was thought that a simple experiment could be undertaken where the fabricated prototype could be tested with a series of load resistors varying in value.

3.2.1 Prototype Device Fabrication

For the initial investigations, a simple ceramic-disc ‘buzzer’ transducer (part number YU83E) was obtained from Maplin Electronics (Rotherham, South Yorkshire, UK), as shown in Figure 3-3:



Figure 3-3 A buzzer transducer

The known data for the buzzer is as follows:

Manufacturer:	Bell Piezo (Taiwan)
Manufacturer’s part no.:	FT-20T-6A1
Metal plate thickness:	0.2mm
Total thickness:	0.4mm
Metal material:	Brass

This buzzer was cut using a small ceramic disc cutter powered from a Dremel (Robert Bosch Tool Corporation, Mount Prospect, IL, USA) multitool to form a rectangular

beam with dimensions of 20mm×3mm (length×width). These dimensions were arbitrary values, based on the idea that the total volume of the device should not exceed 1cm³ as this would fit within the context of this thesis; i.e. meso-scale energy harvesters. Cutting the buzzer transducer in this manner proved difficult. The main difficulty arose because of the fragility of the piezoceramic layer; the greatest care had to be taken when cutting to ensure that the ceramic did not crack. It was found that the best method was to use the dremmel tool to make a cut into the transducer some 2-3mm away from the desired cutting line, and then file away the rest with a fine needle-file, periodically checking the dimensions with vernier callipers. Even then, despite best efforts, some cracking did result.

In considering the type of material to use for the end mass, the literature was consulted. It is known that a greater mass value leads to a device with a lower resonant frequency and higher power output. Therefore, it is conducive to use a material with a high density, since this allows for a greater mass value in a restricted volume. Gold, platinum, lead and silver offer high densities at 21,450; 19,300; 11,340 and 10,500kg/m³ respectively. Since these materials are obviously hard to obtain, steel was a good compromise at 7,930kg/m³. The steel was obtained from some old brackets, which were first cut using a junior hacksaw and then again filed down to size. Two masses were fabricated, each with dimensions of 10mm×3mm×2mm (length×width×thickness). The total mass value of the two combined masses was 0.95g.

The masses were attached to the end of the beam using Loctite (Henkel, Düsseldorf, Germany) superglue, and connections to both the electrode on top of the piezoceramic and the brass layer were made using Circuitworks (Chemtronics, GA, USA) conductive

epoxy adhesive. The finished prototype device is shown, inserted into a specially designed aluminium holder, in Figure 3-4:

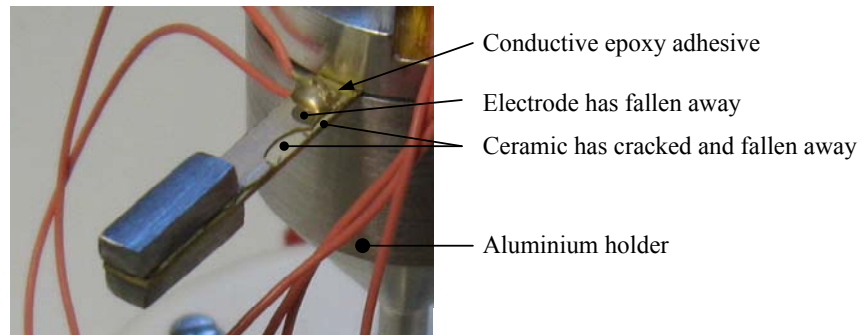


Figure 3-4 First prototype vibration energy harvesting device in aluminium holder.

3.2.2 Prototype Test Setup

In order to perform preliminary tests with this device, it was necessary to build a test setup. An easy way of simulating vibration, and one that is used repeatedly in the literature, is through the use of an electrodynamic shaker. A small Gearing & Watson (Data Physics, San Jose, CA, USA) electrodynamic shaker (model no. V2) was readily available at Cranfield, and an aluminium fixture was designed to transmit the acceleration of the shaker armature to the fixed end of the cantilever. This setup is shown in Figure 3-5:

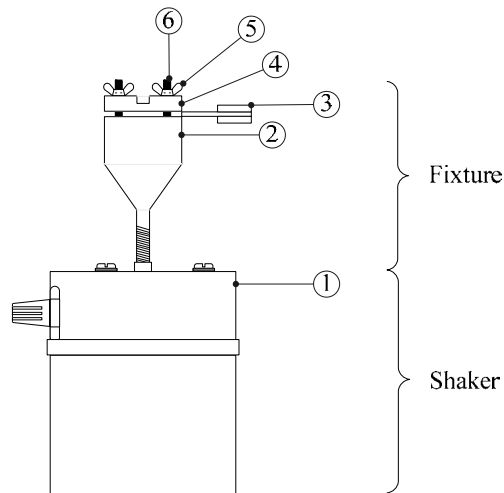


Figure 3-5 First shaker & aluminium fixture.

In the figure:

- 1) = Gearing & Watson (Data Physics) model V2 electrodynamic shaker,
- 2) = Shaker armature,
- 3) = Aluminium fixture (lower part),
- 4) = Prototype piezoelectric vibration energy harvester,
- 5) = Aluminium fixture (upper part),
- 6) = M3 Wing nut ($\times 2$),
- 7) = M3 Studding ($\times 2$).

Since the prototype harvester is a resonant device, a method of performing a frequency sweep had to be devised so that the resonant frequency could be ascertained and used to power any prototype circuitry that might be developed. However, since a resonance condition can magnify acceleration forces, it is important that the response of the test system itself (i.e. the shaker plus aluminium fixture) is flat over the test frequency range, so that the response obtained from the harvesting device can be trusted as a true output of the device. In order to examine the response of the shaker plus fixture, an accelerometer was fixed onto the fixture. Obviously, while considering the response of

the shaker plus fixture, it is also important that the accelerometer itself does not have a resonant frequency that falls within the test frequency range. The accelerometer chosen was Analog Devices (Norwood, MA, USA) part no. ADXL103. Pertinent details of it are as follows:

Measurement range: $\pm 1.7g$
Sensitivity: $1000mV/g$
Resonant frequency: $5.5kHz$

The accelerometer required some peripheral circuitry, mainly in order to set the bandwidth of it. The bandwidth was set, using an external capacitor, to be -3dB at 227Hz, which is adequate for the vibration energy harvesting application considered in this thesis. Appendix A shows a circuit diagram for the accelerometer and supporting components. It was also considered that the position of the accelerometer on the aluminium fixture might be important. Ideally, the accelerometer should be placed as close to the fixed end of the cantilever as possible, so that it can be used to show the actual acceleration applied to the energy harvesting device [136]. The nearest that it was practical to get to this ideal was to mount it onto the top piece of the fixture as shown in Figure 3-6:

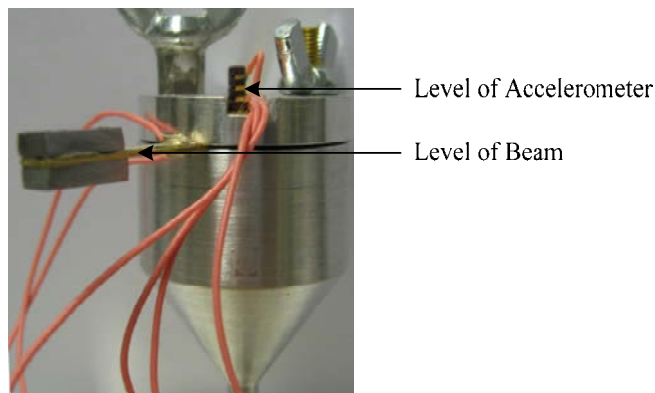


Figure 3-6 Location of accelerometer relative to location of beam.

In an optimal test setup, the output of the accelerometer would be used as part of a feedback loop to calibrate the input to the electrodynamic shaker, so that a constant acceleration is applied over the test frequency range; e.g. as in a closed loop system. However, this was not available, so it was considered that an open-loop system could be used if the frequency response of the shaker plus fixture remained flat over the test frequency range. The open-loop system depicted in Figure 3-7 was initially devised to obtain both frequency responses; i.e. that of the shaker plus fixture (to check that it remained flat), and that of the prototype harvesting device:

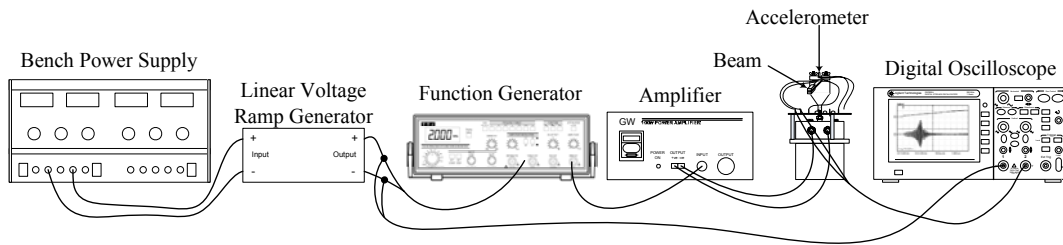


Figure 3-7 First developed test system.

The system is based around the ‘sweep in’ function of the function generator. This function correlates an input voltage level with an output frequency value, so that if a ‘voltage ramp’ can be applied, a frequency sweep is the resulting output. The linear voltage ramp generator is a custom built circuit board that produces a voltage that starts at 0V and increases linearly to 5V. This output is connected to the “sweep in” input of the function generator which responds by outputting a linear frequency sweep from 0Hz to 200Hz as shown in the oscilloscope trace given in Figure 3-8:

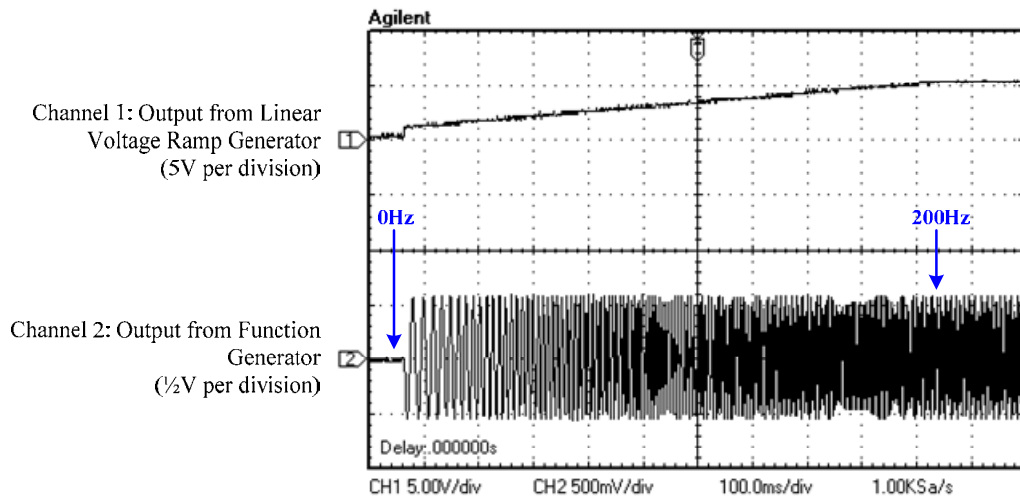


Figure 3-8 Oscilloscope trace of use of the ‘sweep in’ input of the function generator to obtain a frequency sweep from 0Hz to 200Hz.

The system therefore implements a crude form of voltage-controlled oscillator. The linear voltage ramp generator was designed so that the time taken for the voltage to increase from 0V to 5V was approximately 1 second. This value was chosen to make it possible to capture the full output response (over the 0-200Hz sweep) from both the accelerometer and prototype harvester on the oscilloscope in one test ‘run’ while maintaining enough resolution to represent the data accurately.

In order to make sense of any data collected from the prototype harvesting device using this test setup, it was necessary to know what value of voltage input to the function generator equates to what value of frequency output. This was achieved by manually connecting various voltages to the ‘sweep in’ input using the bench power supply, while recording the frequency of the output waveform observed on the oscilloscope. In this way the transfer function of the voltage-controlled oscillator can be plotted, as shown in Figure 3-9:

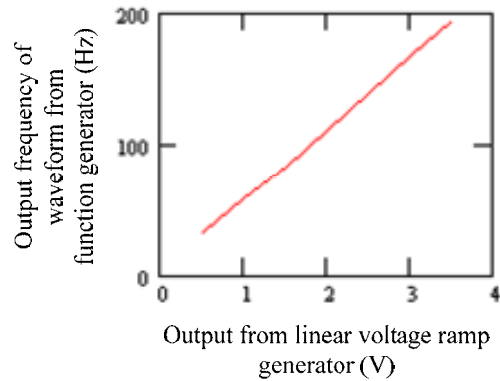


Figure 3-9 Transfer function of the voltage-controlled oscillator

3.2.3 Testing the Prototype Device

Once the test setup of Figure 3-7 was built and the transfer function obtained, the responses of the shaker plus aluminium fixture and the prototype harvester could be captured, as shown in Figure 3-10:

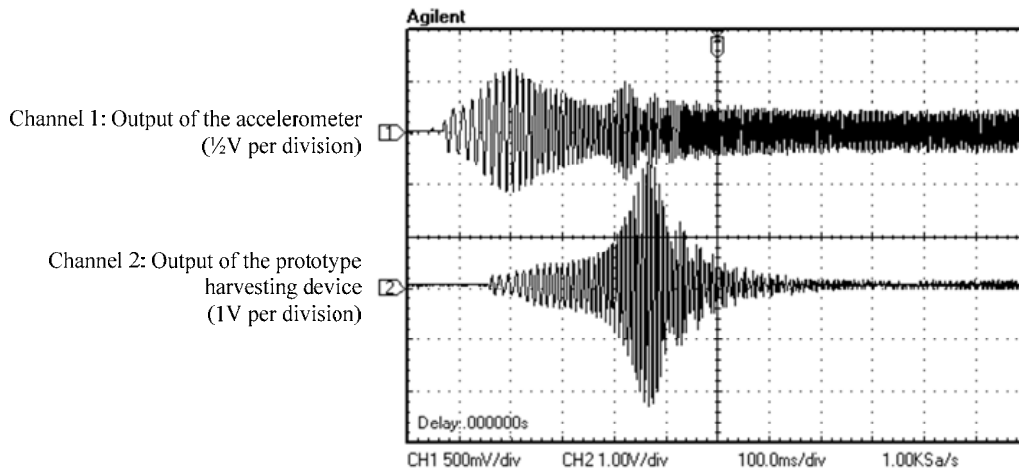


Figure 3-10 Oscilloscope trace showing the responses of the shaker plus aluminium fixture and the prototype harvesting device.

From Figure 3-10, it is apparent that the shaker plus fixture does not have a flat frequency response over the test frequency range. Fortunately though, despite this

uneven response, it is very obvious that the prototype harvester does have a resonant frequency somewhere below 200Hz. In order to find the resonant frequency, the test was repeated, this time with Channel 1 of the oscilloscope connected to the output of the linear ramp voltage generator and Channel 2 connected to the output of the prototype harvesting device. Figure 3-11 shows this:

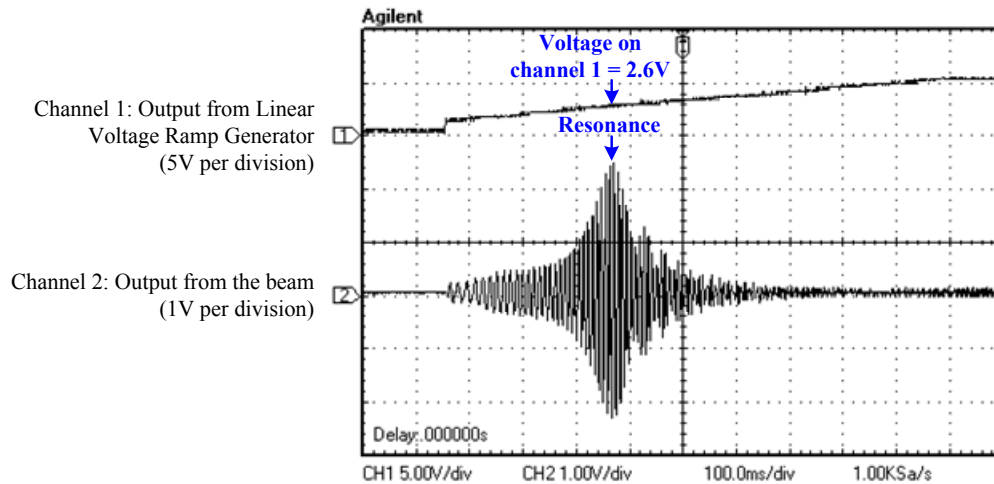


Figure 3-11 Oscilloscope trace showing the output of the linear voltage ramp generator and response of the shaker plus aluminium fixture.

The voltage measured on Channel 1 at the point where the beam is at resonance was found to be 2.6V which, according to the data collected for Figure 3-9, corresponds to a frequency of 160.29Hz.

The purpose of finding the resonant frequency of the prototype harvesting device was so that the device could be characterised in terms of maximum power output. Since the resonance condition dictates maximum displacement of the cantilever, maximum power output occurs at the resonant frequency, thus characterisation in terms of the maximum power output should be done at resonance.

The power output of a piezoelectric energy harvesting device can be most easily characterised through the use of a load resistor. Since a load resistor has no reactive components (it is purely resistive) the power dissipated by the load resistor in watts is easily calculated and wholly represents the useful power output from the generator; i.e. output power that can be used to perform work. Therefore, in order to characterise the power output of the prototype harvesting device, a series of load resistors (each resistor with a different value) was connected directly to the output of the device while it was excited at its resonant frequency. The voltage across each load resistor was measured using the oscilloscope. The average power dissipated by each load resistor can be found either from Equation (8):

$$P_{ave_in_R} = \frac{V_R^2}{2 \cdot R} \quad (8)$$

Where R is the value of the load resistor and V_R is the peak (or amplitude) of the voltage across the load resistor. The results of these tests are shown in Figure 3-12:

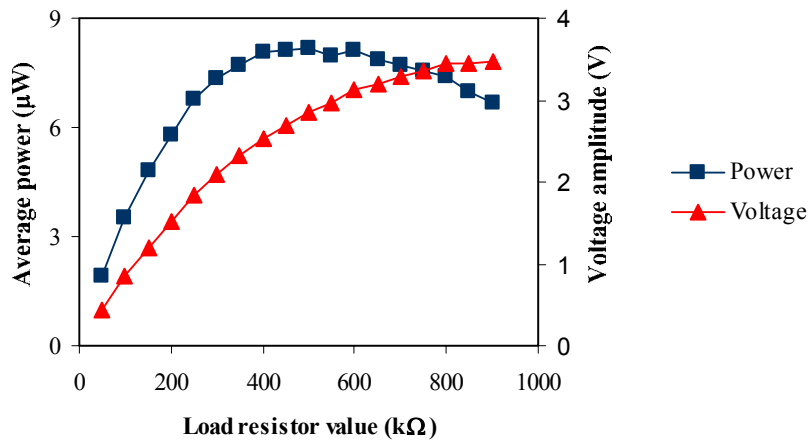


Figure 3-12 Peak voltage and average power output of the prototype harvesting device.

The results show that the voltage measured across the load resistor increases as the value of the load resistor increases. This is expected, because the value of the internal

impedance of the generator remains constant while the value of external load resistor is increased; a proportionally greater voltage is dropped across the load resistor. The voltage increase is not linear however, because the voltage is proportional to the ratio of internal source impedance value to external load resistance value, which varies inversely with the external load resistance value. This can be explained more thoroughly through the use of a circuit diagram, where the piezoelectric generator is represented as an AC voltage source in series with its own internal impedance:

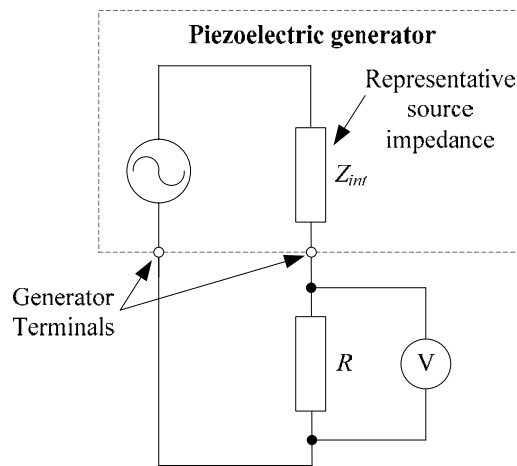


Figure 3-13 A piezoelectric generator represented as an AC voltage source in series with its own internal impedance.

In Figure 3-13, Z_{int} represents the internal impedance of the generator, R is the external load resistor, and V represents a voltmeter that is measuring V_R , which is the peak (or amplitude) of the voltage across the load resistor. If Z_{int} is, for example, $500\text{k}\Omega$, which is a reasonable estimate based on impedance-matching theory and the experimental results given in Figure 3-12, and R is increased from $50\text{k}\Omega$ to $900\text{k}\Omega$ in $50\text{k}\Omega$ steps, the ratio Z_{int} to R is as shown in Figure 3-14:

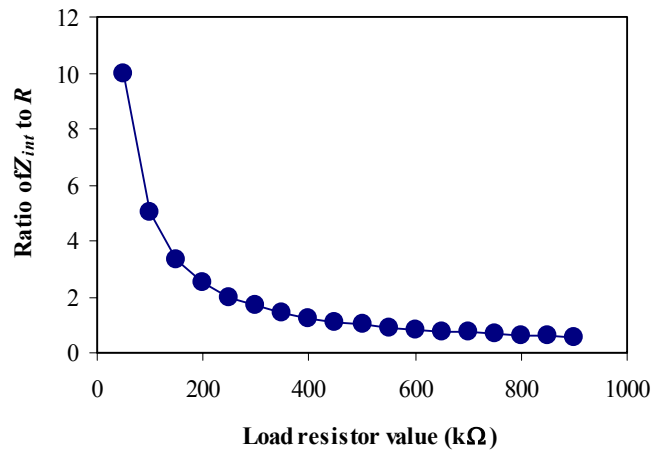


Figure 3-14 Ratio of internal impedance value to external load resistor value versus external load resistor value.

This graph shows that initially, the value of internal impedance is high with respect to the value of external load resistance. This means that the greater portion of voltage available from the AC voltage source will be dropped across the internal impedance while the lesser portion of the voltage available will be dropped across the external load resistor. As the value of resistive load is increased, the value of internal impedance reduces with respect to the value of load resistance in an inversely proportional manner, meaning that proportionally less voltage will be dropped across the internal impedance (in an inversely proportional manner) and proportionally more voltage will be dropped across the external load resistor (in a non-linear increasing manner). Figure 3-15 shows this trend:

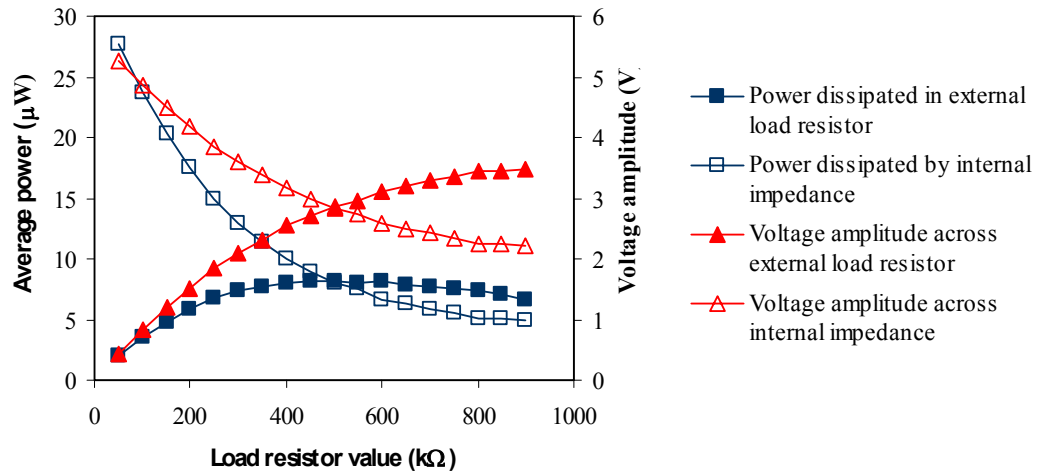


Figure 3-15 Graph showing trends of the voltages generated across and powers dissipated by both the fixed-value internal impedance of a piezoelectric generator and the varying-value external load resistance.

Figure 3-15 also shows that the power dissipated by the external load resistor increases with load resistor value until it reaches a maximum value, after which it decreases. This is also expected, since from the equation for power, equation (8) on page 131, if the voltage across the load resistor follows the type of curve shown in Figure 3-12 and Figure 3-15, and the load resistor value R increases linearly, then at the higher load resistor values the value of R dominates meaning that the resultant curve for power shows an increase followed by a decrease. In contrast to the power dissipated by the external load resistor, the power dissipated by the internal impedance of the generator can only decrease, since the internal impedance value Z_{int} remains constant while the voltage across it decreases.

In regard to the actual voltage and power levels that were obtained from the prototype generator, the maximum voltage measured was $3.47V_{pk}$, which occurred with a load resistor value of $900k\Omega$, and the maximum power was $8.18\mu W$, which occurred with a

load resistor value of 500k Ω . The voltage at the maximum power point was 2.86V_{pk}. This amount of power is very low, and when compared with the values obtained from other fabricated devices reported in the literature (see Table 2-13 on page 66) is amongst the bottom few. Accordingly, the voltage achieved at the maximum power output is also quite low, and again is below those obtained from other reported devices.

3.3 Conclusions of the Initial Investigations

The purpose of the initial investigations was to gain some physical intuition in the use of a cantilever-based piezoelectric energy harvesting device and its capabilities. There were several outcomes of these investigations:

Regarding the fabrication of the device:

Fabricating a device by hand is difficult. In this case, a section of the piezoceramic cracked and fell away. In addition, some of the electrode material on the top surface of the piezoceramic also fell away (see Figure 3-4 on page 124). This will no doubt have affected the performance of the generator in a negative manner. It was considered that for the next iteration of device, purchasing and making use of a ready-cut actuator would prove more reliable. Such devices are commercially available in both unimorph and bimorph forms, and in the bimorph form are available in both poled for parallel and poled for series formats. The difficulties experienced in hand-cutting the cantilever meant that it was also unlikely that a triangular-shaped beam could be easily obtained, since fabricating one would be significantly problematic, and triangular-shaped actuators are not readily available commercially. Thus, for the next iteration of device, it was decided that the rectangular shape should remain.

Regarding the power output:

In comparison with the reported values given in the literature for piezoelectric energy harvesting devices (see Table 2-13 on page 66), the power output of the prototype harvester is very low. There may be several reasons for this: firstly, the material characteristics of the piezoceramic are unknown, since the manufacturer does not supply this information. It is possible that, since the buzzer is manufactured in large quantities, and since it is designed for the sole function of providing an audible sound, the buzzer does not require a very good quality piezoelectric material with high piezoelectric coefficients, as might an energy harvesting device, and thus it seems likely that the piezoceramic used may be low quality. Therefore, in considering the next iteration of piezoelectric vibration energy harvester, a more optimal choice of piezoceramic material is required. Secondly, the device was built with no guidance on how the dimensions of it affect its power output. The power output might significantly be improved if, for example, the thickness of the piezoceramic material is increased, or the ratio of brass layer to piezoceramic layer thicknesses is changed, but with no knowledge of how the dimensions affect the power output, these ideas are only conjecture. Without guidance, the only option is to rely on a trial-and-error approach, which is usually both costly and very time consuming. Therefore, in considering the next iteration of piezoelectric harvester, it is considered that a modelling approach would be useful. However, the model should not simply predict outputs of the device (e.g. power or voltage) when provided with dimensions and material characteristics, since this still would not provide guidance on how to design a harvester for an increased power output; i.e. the designer still has to rely on a trial-and-error approach (albeit this time with the aid of a model). Instead, the model should be able to provide a device design; i.e. to

provide the dimensions for a device that has been optimised for maximum power output. In addition, it would be useful if the model has the capability to allow the designer to see how each dimension affects the power output, so that for a given space-envelope, the designer can make informed choices about the device design.

Considering the above discussion, it was considered that a modelling approach would be valuable for obtaining a design for a device that is optimised in terms of power output. This was the next step to be carried out, and it is detailed in the next section of this thesis: section 3.4.

Regarding the test setup:

While the test setup presented is capable of performing a ‘frequency sweep’ test, it is considered that it is rather a crude, non-ideal setup. There are several problems associated with it, which can be listed in brief as follows:

- 1) The test ‘runs’ do not result in data. Rather, a trace on an oscilloscope screen is obtained. This obviously leads to difficulties in accurate analysis.
- 2) The test ‘runs’ are non-repeatable; i.e. the frequency sweep is not done in a controlled, incremental manner. This is simply a product of relying on the ‘sweep in’ function of the function generator. Its significance is that, even if data could be collected, the output of the prototype device could not be recorded for exact frequency points, for example at 20Hz, then 21Hz, then 22Hz etc.
- 3) Each test ‘run’ was designed to last 1 second in order that the entire frequency sweep be displayed on the oscilloscope. However, there is a possibility that this is too fast given that there is likely to be some latency in the system. This can be described as follows: measurement of the voltage output of the linear voltage ramp

generator and the output of the harvesting device occurs simultaneously (through use of the oscilloscope); however, there will be some time-lag in the system between the linear voltage ramp generator setting a certain voltage level and the harvesting device responding to the corresponding frequency value. This means that the response captured for the harvesting device is slightly delayed from the recorded output of the linear voltage ramp generator, giving an inaccuracy if corresponding measurements of the two signals are recorded simultaneously; i.e. on a ‘same time basis’, as was done in these initial investigations.

- 4) The response of the shaker plus aluminium fixture is not flat over the test frequency range, and this will have an influence on the harvesting device output.

Considering the above discussions, it was considered that for the next iteration of harvesting device, an improved test setup should be designed and built. The improved test setup is discussed in section 3.7.1 on page 188.

3.4 Analytical Modelling

3.4.1 Background

As mentioned and depicted by Figure 1-1 in the introduction section (page 11), an energy harvesting system can be portrayed by three basic functional blocks: the energy transducer, some conditioning (and possibly also power management) circuitry, termed under the umbrella term of ‘harvesting circuitry’, and the end application system. Elaborating on these basic functions, the full energy harvesting system might appear as shown in Figure 3-16, where (a) shows a basic system that requires only power conditioning, and (b) shows a more complex system that requires both power

conditioning and power management. Of course, the type of energy harvesting system implemented will be largely dependent on the end application system.

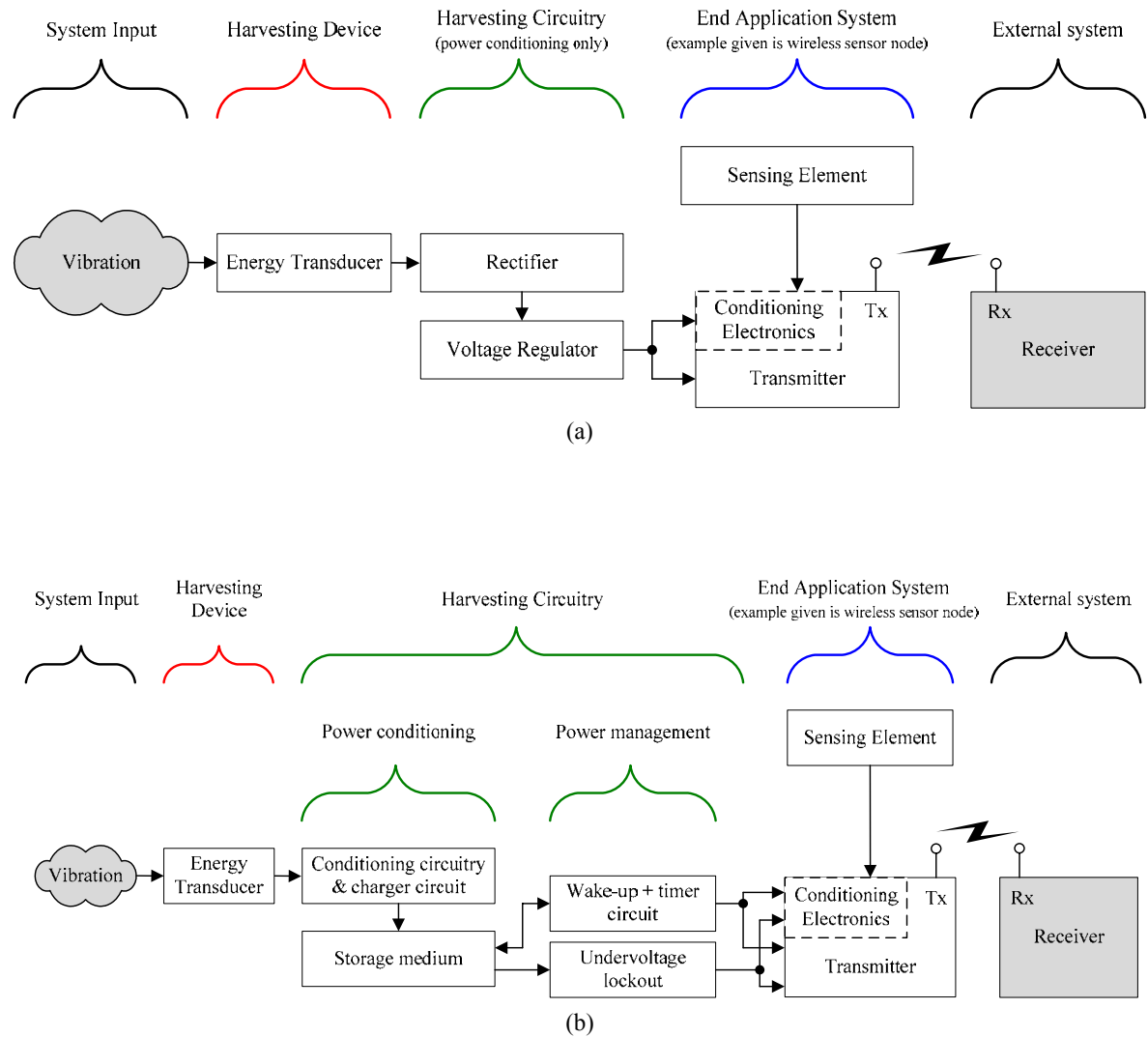


Figure 3-16 Possible block diagrams for basic energy harvesting systems; (a) requiring power conditioning only (b) requiring both power conditioning and power management.

With regard to the development of the energy harvesting device, it is wise to consider its immediate neighbours in the block diagram; i.e. the ‘input’ side, which in this case is vibration energy, and also the ‘output’ side, which in this case is the harvesting

circuitry. This is because the energy harvesting device is not necessarily independent of these functions, rather, these functions can affect the performance of the device: the input side puts bounds on the device design in terms of the resonant frequency/frequencies to aim for, and the output side (the harvesting circuitry) can feed back to influence the dynamic behaviour of the device. For example, it is known, in the case of a piezoelectric generator that takes the form of a resonant mechanical structure (for harvesting from vibrations), that attaching an electrical load results in a shift in the resonant frequency of the device, as a result of the piezoelectric backward coupling effect. The following sections attempt to describe the considerations given to each of the main functions depicted in Figure 3-16, and their interrelationships, for the case given in this thesis.

3.4.1.1 Source Vibrations

The characteristics of the source or ‘input’ vibrations are dictated by the intended application environment. Simply put: they are what they are; i.e. an input to the system, and as such dictate the fundamental limit on the amount of energy available to be harvested. The goal is to convert as much of the vibratory input energy as possible into useful electrical energy; where the implication of the term “useful electrical energy” here is not simply that all electrical energy is useful, but more specifically that electrical energy of a particular format is the goal: usually a regulated DC voltage supply. In vibration environments, the vibration might take one of several possible forms; examples are: transient type vibration, continuous but non-cyclic and simple harmonic motion. Figure 3-17 below provides a diagrammatic view of these types of vibration:

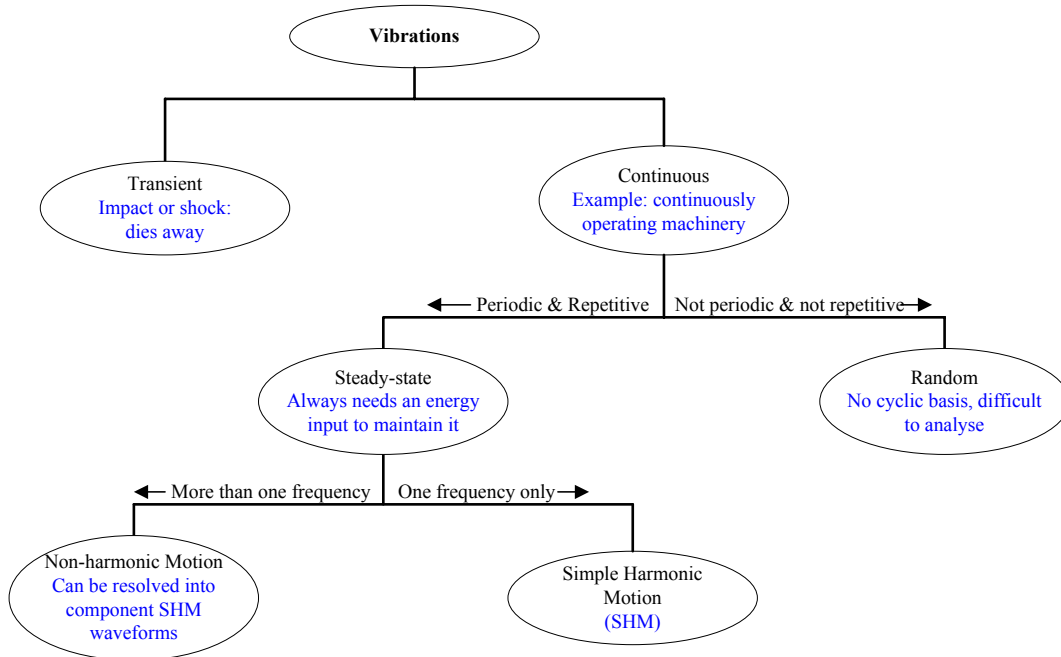


Figure 3-17 Different vibration types.

In the literature, the most commonly used form of input vibration is simple harmonic motion (SHM). This is because SHM enables simple, uncomplicated analysis, fitting in neatly with the familiar concept of a mechanical resonant system. In this thesis also, a simple harmonic motion-type of vibration is considered.

Also in regard to the vibration input, the vibration is usually transmitted to the harvesting device by the harvesting device being attached to a host structure. The host structure itself might be the source of vibration or the host structure might be attached to the source of vibration. The higher the amplitude of host structure motion, the greater the power output from the harvesting device, because the greater will be the relative displacement of the salient parts of the harvesting device, e.g. in the case of a piezoelectric cantilever, the greater will be the relative displacement between the tip (free end) and fixed end, leading to more strain in the piezoelectric material and hence more charge generated.

3.4.1.2 Transducer (Energy Harvesting Device)

As mentioned in section 3.4.1.1, a simple harmonic motion-type of vibration is assumed to be the input to the system, thereby enabling the employment of a mechanical resonant structure for the energy harvesting device. Many ways of modelling such a structure have been reported in the literature to date, including equivalent electric circuit methods, finite element methods and analytical methods.

In lumped element equivalent circuit methods, a piezoelectric vibration generator might be represented as follows [137]:

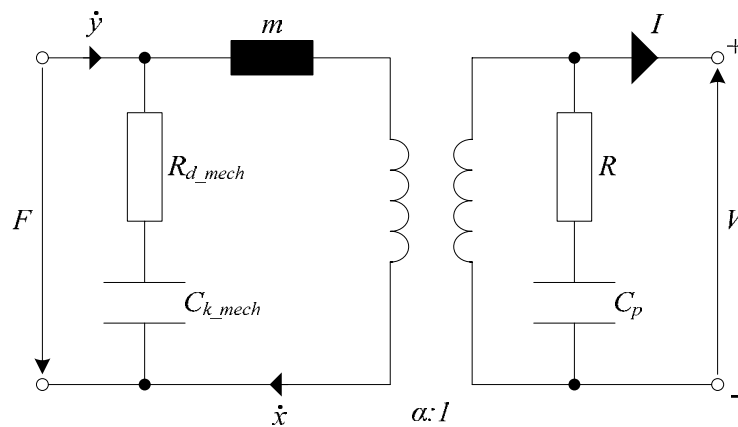


Figure 3-18 Equivalent electric circuit of a piezoelectric generator with base excitation [137].

where: y is the displacement of the host structure, R_{d_mech} represents mechanical damping, C_{k_mech} is the structural stiffness, m is the mass, x represents the displacement of some generalised coordinate of the device (e.g. in the case of a cantilever-based structure, it could be the tip of the cantilever), a is the electromechanical coupling factor (and the transformer is assumed to be ideal), R represents dielectric losses, C_p represents the capacitive behaviour of the piezoelectric element, I is the current output, and V is the voltage generated across the output ports. In using equivalent circuit methods to

represent piezoelectric conversion, the force, F , is usually considered to be analogous to voltage, and velocity is usually considered to be analogous to current. In a base excited case, the force, F , is equal to zero. This type of model can be used to model the dynamics of a piezoelectric energy harvesting device. However, the model parameters, which are represented by the discrete entities in the model (for example, the capacitor C_{k_mech} represents the mechanical structural stiffness of the device) are independent of the geometrical shape and material parameters of the device, making the model unsuitable for the purpose of this thesis, which is to optimise the geometry of the device in order to make the best use of a space envelope that the device may utilise in a proposed application. For this purpose, some method of relating the values of the model parameters (e.g. mass, stiffness, or capacitive behaviour of the piezoelectric element) to the dimensions of the device is required.

Finite element analysis (FEM) is an advanced numerical modelling method that has a good reputation for reliably producing accurate results when modelling and simulating different types of structures. It also has the particular strength that it enables detailed visualisation of the modelled structure. However, it is usually used for prediction purposes; i.e. for predicting how structures will behave in given environments. The designer is often given objective values for the model parameters, and will work toward these goals in order to produce an ‘optimal’ design. However, it can be argued that an ‘optimal’ design created in this manner is not actually optimised, rather, it has only been calculated to a sufficient level; i.e. one that is simply *good enough* to fit the function required. For the aim of this thesis, which is the optimisation of the geometric parameters of the harvesting device, a method by which a computerised optimisation algorithm can be applied to the geometric parameters is required.

Analytical methods, while more labour intensive than computerised numerical methods, have several advantages. Firstly, the sometimes complex relationships between input variables (e.g. geometric or material parameters) and structure characteristics (e.g. stiffness or resonant frequencies) are made more transparent; i.e. the designer has the opportunity to gain insight not only into *how* a change in an input parameter affects the dynamic behaviour of the structure (this can also be done with FEM analysis), but may also immediately learn *why* the change has the effect that it does. It therefore leads to greater intuition in device design, through an increase in the designer's knowledge. The designer does not have to rely on a trial and error approach to establish relationships between input variables and structure behaviour. Secondly, analytical models have the advantage that they can be used with computerised optimisation algorithms, since a mathematical equation can be derived for the parameter to be optimised and used as an objective function in an appropriately formulated optimisation problem. It is for these reasons that an analytical approach has been chosen in this thesis, for the purpose of optimising the geometry of the piezoelectric generator in order to enhance the power output.

In designing and prototyping an energy harvesting device, some means by which the electrical outputs can be characterised needs to be considered. In the literature presently available, a simple load resistor is often connected across the output of the generator. Use of a load resistor in this way enables very easy measurement of the power output of the generator; it is therefore a simple and convenient way of characterising the output of the generator. Moreover, if many research groups characterise the power outputs of their devices using this method, it can make for easy comparison between different structure types and conversion methods.

A resistive load is also useful for examining another phenomenon associated with vibration energy piezoelectric energy harvesters: the shift in the resonance frequencies of the harvester structure that occurs with different resistive load values. As the value of load resistance is increased from a low value to a high value (i.e. in the direction of zero to infinity), the output of the harvesting device moves from short-circuit to open-circuit conditions. This has the effect of shifting the modal frequencies of the device from those that in the literature are now commonly referred to as the ‘short-circuit resonance frequencies’ to the ‘open-circuit resonance frequencies’. Several research groups have noted this effect in recent years [135] [138] [139] [140]. One of the most notable discussions occurs in the work of Ertuk and Inman [140]. They point out that this variation in modal frequencies with changes in load resistor value indicates that piezoelectric electromechanical coupling has more effects than just the sole viscous damping effect that is often assumed; that it is actually more complicated. They discuss the fact that piezoelectric electromechanical coupling is often misrepresented in the literature when single-degree-of-freedom models are used, which results in inaccuracies in the predicted electrical outputs of the generator and misrepresentation (or non-representation) of the variation of modal frequencies with load resistance. Their paper appeared in late 2008 which, in relation to the project instigated in this thesis, came after the work on the proposed analytical model was completed. Therefore, while correctly, they point out the misnomers of using a single-degree-of-freedom model to model a piezoelectric-based harvester, the model developed in the following sections of this thesis does indeed use this method. Moreover, for reasons of simplicity, it also does not include the piezoelectric backward coupling effect. The philosophy behind the model presented in this thesis is that it is developed in such a way that the relationships

between the harvesting device parameters such as stiffness or stress, and the harvesting device geometry are taken into account. If the structural parameters can be linked to the device geometry, the electrical outputs can also be linked to the geometry, by definition of piezoelectric electromechanical coupling, and hence the model can be used to perform an optimisation (for maximum power output) of the geometric parameters in order to enhance the power output. The practical implication of this is that through this method, the best use can be made of a volume, or ‘space envelope’, that a device may utilise in a given application. However, in the development of such a model, since it has been simplified by necessity for this purpose, it is difficult to represent the full effects of the piezoelectric coupling. Therefore, it is this author’s intention that the model developed in this thesis is good enough for a ‘first pass’ attempt for the proposed purpose, and that the inclusion of the full effects of the piezoelectric coupling could be included at a later date as the next stage. Obviously, this places some limitations on the model developed here: it will tend to overestimate the power output, as is discussed in [140]. In addition, the prediction of the optimal load resistance will be inaccurate by some degree since the equation used in the model is $R_{opt} = 1 / 2\pi f C_p$ (where f is the vibration excitation frequency and C_p the internal capacitance of the piezoelectric harvesting device) because, of course, only one set of modal frequencies can result from the model if the backward piezoelectric coupling effect is not included; i.e. the variation in modal frequencies is not seen as the load resistance changes. However, it was considered possible that some of these limitations might be tolerable when considering the later development of the harvesting circuitry, given in Chapter 4. For example, concerning the value of optimal load resistance: Ertuk and Inman in [140] show that for the bimorph cantilever presented in their later work, [141], the use of $R_{opt} = 1 / 2\pi f C_p$

leads to a source impedance value of $84.6\text{k}\Omega$ rather than the more accurate value of $35\text{k}\Omega$ that they predict through the use of their distributed parameter model, leading to an overestimation error of 142%. This may seem significant, but from an electronic viewpoint, it may be possible that the choice of circuit topology for the power conditioning circuitry will not vary as a result of a factor of 2.4 error in the source impedance value: in this case at least, the values of load resistance considered are all of the same order.

3.4.1.3 Harvesting circuitry

The harvesting circuitry serves at least one, but sometimes two, main functions: power conditioning and power management. The former is required since the power output of an energy harvesting device is rarely in a readily useable form. For example, in the case of a vibration energy harvesting device, the output may vary in frequency and amplitude, and might also be intermittent, depending on the particular vibration environment under consideration. Many electronic applications such as wireless sensor nodes or portable devices at present require a regulated DC supply, therefore the output from the harvester, at a minimum, must be rectified and voltage regulated. If the voltage output of the generator is too low, it might also require boosting through the use of a voltage multiplier, charge pump or other similar voltage-boosting circuit. If the current output of the generator is too low, one solution might be to build up a charge reservoir over time, and then connect the application electronic circuit only when sufficient charge has been stored. Power conditioning therefore refers to conversion of the power into a format that is useful for the intended end application.

The latter mentioned function of the harvesting circuitry: power management, is needed if some means of controlling the delivery and/or storage of power is required, e.g. for an end application that operates in ‘burst’ mode rather continuously; or the power management might, for example, control the delivery of power to an application when it is needed, and at all other times divert the generated charge to a storage medium for use at a later date. The power management function is therefore an active management function, involving some measurement and decision making activities for a processor or other controlling device, whereas power conditioning is more likely to be a process that requires no active control and continuously operates whenever energy is available from the environmental source.

In many of the available works present in the literature, a simple load resistor is often used to connect to the output of the generator. This is done not necessarily with the intention that the load resistor is to represent the harvesting circuitry, but instead is simply a method whereby the electrical outputs can be characterised for those works whose scope does not include any harvesting circuitry elements of the full system. A simple load resistor connected across the output terminals of the generator allows for easy measurement of the voltage and easy calculation of the average power output of the device; it is simply a convenient way of characterising the electrical outputs of the generator. Indeed, if many research groups characterise the power outputs of their devices in this way, it may be possible to compare different structure types and conversion methods. However, utilising a simple resistor as a load is not, in reality, useful in terms of the representation of a real energy harvesting system as depicted in Figure 3-16. A load resistor obviously cannot represent the sometimes complex power conditioning that needs to be done, nor does it require any power management. It cannot

show the effect that a non-linear load might have on the energy harvesting device, and it cannot show the losses that might be associated with power conditioning circuitry. Therefore, while it is indeed useful as a means of characterising the power output of an energy harvesting device, and can provide a method by which comparison between energy harvesting devices might be carried out, for real life purposes, a load resistor could be considered to be too simplified; that is, it could be argued that the load on the energy harvesting device is likely to be more complicated than can be represented by a simple load resistor.

3.4.1.4 Conclusions of the background to the analytical modelling

Given the discussions in the previous three sections then: 3.4.1.1 for discussion of the source vibrations, 3.4.1.2 for the energy transducer and 3.4.1.3 for the harvesting circuitry, it seems that when developing a piezoelectric-based harvesting device for a vibration energy harvesting system, there are many factors to be considered, and also, that many variables external to the device itself; i.e. from other functions such as the harvesting circuit or input vibrations, have an influence. Some of the outside influences might be:

- Consideration of the input vibrations: what form do they take, e.g. continuous steady-state or random? How much energy is available to the energy harvesting system?
- Given the particular application environment being considered, what is the allowable space-envelope for the system? What is the volume value and what three-dimensional shape does it take?

- Consideration of the harvesting circuitry: what kind of power conditioning is required? This will largely depend on the end application electronic system, e.g. the wireless sensor node or portable device. Is power management and/or some form of storage medium needed in addition to power conditioning? Will the load attached to the harvesting device affect the dynamic response of the harvesting device to the input vibrations, by affecting its mechanical structural parameters, such as stiffness? If so, *how* will it affect the dynamic response/structural parameters? Can the effects be tolerated, or maybe even used to an advantage?

And some of the factors in the development of the harvesting device might be:

- Choice of appropriate modelling method to best suit the purpose, e.g. numerical, equivalent circuit, analytical or other.
- Considerations concerning the representation of the effects of the piezoelectric electromechanical coupling: is it an important feature for the purpose being considered? If so, how best to represent it?
- Considerations concerning the electrical characteristics of the piezoelectric generator, e.g. capacitive behaviour, dielectric losses and source impedance characteristics.

In the section that follows, 3.4.2, an analytical model of a cantilever-based piezoelectric vibration energy harvesting device is developed for the purpose of this thesis: that is to optimise the geometric parameters of the device in order to enhance the power output, and therefore power density ($\mu\text{W}/\text{cm}^3$). In the development of the model, the geometry of the device (i.e. the dimensions) are linked to the mechanical (e.g. mass value or stiffness), and ultimately electrical (e.g. current output or capacitance of the

piezoelectric element), parameters so as to enable the derivation of a final equation for power output that can be used as an objective function in an optimisation problem, to optimise the geometry of the device for maximum power output. The input vibration considered is a SHM-type of vibration, and the power output is characterised through the use of a simple load resistor. The full piezoelectric backward coupling effect is not included at this stage, for reasons of simplicity, and the electrical damping has been included, along with the mechanical damping, in the viscous damping term in the SDOF approach used. Dielectric losses in the generator are also ignored. However, whereas in other models found in the literature the mechanical and electrical parameters are simply represented by values which are independent of the dimensions of the device, here the dimensions of the generator are taken into account, such that their effect on the mechanical and electrical parameters is considered. As will be seen, one effect of this, in regard to the mass dimensions in particular, is that the gravity centre of mass, instead of being represented by a point mass on the end of a cantilever (which is the approach commonly used), more properly results in one more bending moment acting on the cantilever compared with the ‘point mass’ approach. This results in a representation within the model of how the mass geometry affects the spring constant of the system, and thus also how it affects the resonant frequency of the device. To this author’s knowledge, no other model available in the literature takes this effect into account. Indeed, in the coupled distributed parameter model built by Ertuk and Inman [141], which was built to represent a cantilevered piezoelectric energy harvester with a tip mass, the tip mass is considered as a lumped mass without dimensions. Meanwhile another work [142] has shown that the output performance of the harvesting device can be greatly influenced by not only the mass value of the tip mass but also the geometry

of it, in particular the length. The analytical model that will be developed in the following section takes into account the effect of the mass dimensions, including the length, on the harvesting device electrical outputs.

3.4.2 Development of an Analytical Model for Optimisation of the Geometric Parameters of the Harvesting Device

3.4.2.1 Modelling Approach

For reasons discussed in sections 3.1 (Description of the Design) and 3.2 (Initial Investigations) of this thesis, the piezoelectric energy harvesting device to be considered is a rectangular piezoelectric cantilever with seismic masses symmetrically attached at the free end. As shown in Figure 3-2 in section 3.1, the cantilever can be configured in a number of ways, including a unimorph design, a bimorph design or a multilayer design, and for the bimorph or multilayer designs, the piezoelectric layers can be poled either for series connection or parallel connection. The particular configuration chosen for the harvester detailed by this analytical model is a bimorph poled for parallel, as shown in Figure 3-1 on page 118 (repeated here for convenience):

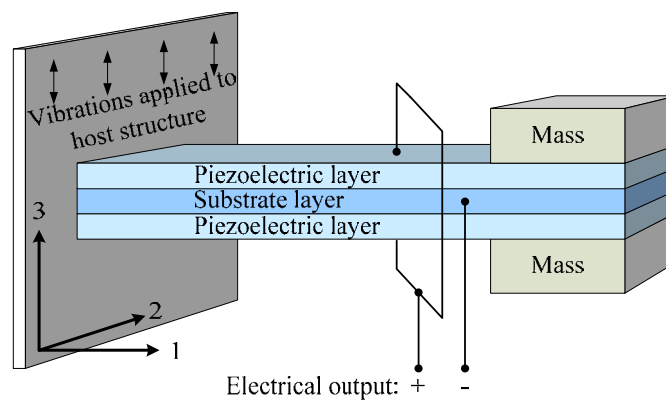


Figure 3-1 A piezoelectric vibration energy harvester configured as a cantilever beam.

The surfaces (both top and bottom) of each piezoelectric layer are covered by a thin electrode (not shown in the figure) except for those portions of the layers that lie between the two masses. For convenience, all of the dimensional parameters considered in the derivation of the analytical model are shown in Figure 3-19:

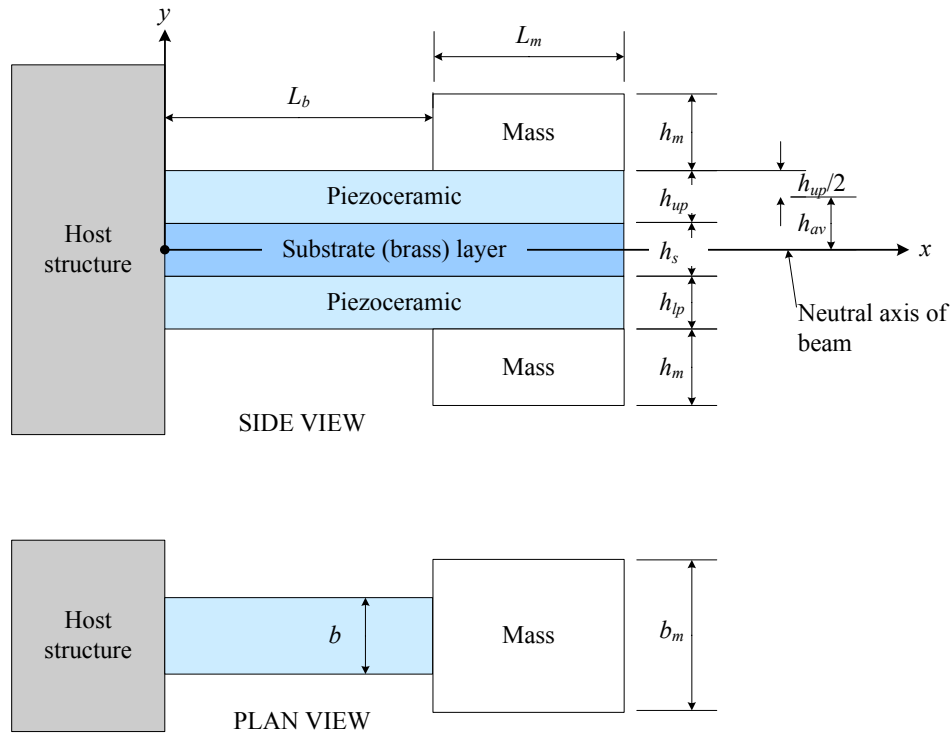


Figure 3-19 Schematic of the harvesting device showing the notation of the dimensional parameters used in derivation of the model.

Figure 3-20 shows a representative circuit for the piezoelectric energy harvesting device, which is used to determine the electric outputs (current, voltage and power) in the model:

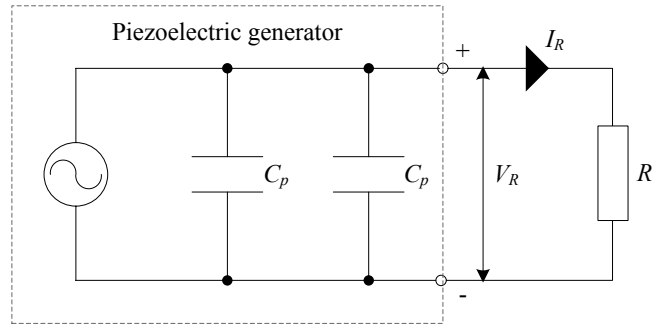


Figure 3-20 Representative circuit of the harvesting device, where: C_p is the capacitance of each piezoelectric layer.

A simple load resistor is used to represent a circuit external to the device; this was done because, as mentioned before, it allows for easy calculation of the amount of power transferred from the piezoelectric harvester to the electrical load. In constructing the model, the following assumptions are made:

- 1) The mass of the beam is ignored, and so the beam is assumed to behave like a spring. The justification for this is that the mass value of the beam is negligible when compared with the mass value of the attached symmetrical masses. Therefore, the device is treated as a spring-mass system in the model.
- 2) The adhesive layers that exist between the substrate and piezoelectric layers are ignored because these layers are very thin.
- 3) The backward piezoelectric coupling effect is ignored in order to decrease the complexity of the model.

Since the cantilever employs d_{31} coupling between the mechanical and electrical domains; that is, the electrical axis is always “3” because charge is always transferred through the electrodes, while the mechanical axis is always “1” because the acceleration of the host structure generates stress in the “1” direction, the electrical charge density

generated by the piezoelectric cantilever can be calculated by using the following piezoelectric constitutive equation:

$$D_3 = d_{31}\sigma_1 + \varepsilon_p^\sigma E_3 \quad (9)$$

where D_3 is the charge density present on the electrodes; d_{31} is the piezoelectric charge coefficient, σ_1 is stress generated in the “1” direction, ε_p^σ is the absolute permittivity of the piezoelectric material under constant stress conditions, and E_3 is the electric field developed in the “3” direction. The physical meaning of the first term within Equation (9), $d_{31}\sigma_1$, is that of the piezoelectric direct effect; hence it represents the total charge generated. The second term, $\varepsilon_p^\sigma E_3$, relates to the effect of a dielectric in a capacitor (since piezoelectric ceramic is also a dielectric). To understand this it is useful to consider from an electrical viewpoint the type of source a piezoelectric generator constitutes. Conventional electrical sources are one of two types: constant voltage or constant current. Simplistically speaking, the constant voltage source theoretically generates as much current as is needed to maintain a constant voltage across its output terminals, and a constant current source is as its name describes, so that the voltage at its output terminals is a function of the constant current and the impedance of the external circuit. A piezoelectric generator however, simply generates *a finite amount of charge*. In this way it can be likened to a current source, but not a constant current source. The introduction of a dielectric between the plates of a capacitor in a circuit poses no problem to a conventional constant voltage or current source, since either is able to provide the extra energy required to charge the extra capacitance. However, for a piezoelectric generator with a finite charge output, the same introduction of a dielectric results in a decrease in voltage across the capacitor plates, caused by the apparent decrease in charge density on them due to the induced charges of opposite polarity that

appear of the surfaces of the dielectric. This second expression therefore represents charge that is ‘locked’ into the piezoelectric (capacitive) element that cannot be accessed. In summary then, the first term, $d_{31}\sigma_1$, in equation (9) represents the total charge generated; the second term, $\varepsilon_p^\sigma E_3$, represents charge that remains inside the generator, and D_3 represents charge that is free to flow through a connected external circuit, which in this case is represented by a simple load resistor.

The total charge available to flow through the external load resistor, Q_3 , is the product of D_3 and the surface area of the electrodes:

$$Q_3 = 2 \cdot \int_0^{L_b} D_3 b dx \quad (10)$$

where b is the width of the beam and L_b is the length of the electrodes, which coincides with the length of the beam. The factor of two occurs because the parallel connection of two piezoelectric layers is being considered.

The current I_R flowing through the load resistor is therefore:

$$I_R = \frac{dQ_3}{dt} \quad (11)$$

And the voltage V_R developed across the resistor is equal to:

$$V_R = I_R \cdot R \quad (12)$$

where R is the value of the resistor.

The electric field across the piezoelectric layers, E_3 in equation (9), can be determined from the voltage developed across the piezoelectric layers:

$$E_3 = \frac{V_3}{h_p} \quad (13)$$

where V_3 is the voltage developed across the piezoelectric layers and h_p is the thickness of one of the layers. It should be noted here that V_3 in equation (13) is equal to V_R in equation (12) (see Figure 3-20). Therefore, there is interdependence between D_3 and E_3 within equation (9). This can be described as follows: stress in the mechanical domain, σ_1 , results in an electrode charge density, D_3 , and hence current flow, I_R , and a voltage across the piezoelectric layers, V_R (or V_3) in the electrical domain through equation (9). However, the voltage developed, V_R (or V_3), then feeds back into equation (9) via E_3 equation (13). Throughout the rest of this thesis, the voltage developed across the load resistor will be denoted by V_R .

In equation (9), the stress generated in the piezoelectric layers, σ_1 , can be determined from:

$$\sigma_1 = E_p \cdot y \cdot \frac{d^2 w_d(x,t)}{dx^2} \quad (14)$$

where E_p is the Young's modulus of the piezoelectric material, y is any distance from the neutral axis that falls within the region of the piezoelectric layer, and $w_d(x,t)$ is the out-of-plane deflection of the neutral axis at any distance x along the length of the beam.

It is assumed that the displacement of the neutral axis of the cantilever, $w_d(x,t)$, takes the form of a conventional equation of motion; i.e.:

$$w_d(x,t) = W_d(L_b) \cdot f(x) \cos(\omega t - \theta) \quad (15)$$

where x is any point along the length of the beam, $W_d(L_b)$ is the out-of-plane displacement at the end of the beam, $f(x)$ is a normalised shape function that satisfies the boundary conditions of the cantilever, and θ represents the relative phase lag between the movement of the mass and movement of the host structure.

The terms defined thus far are as yet undetermined functions. However, from equations (9) to (15) it can be deduced that D_3 , and hence I_R and V_R , are dependent on σ_1 , since d_{31} and ϵ_p^σ are constants and, due to the interdependence between E_3 and D_3 , E_3 is only dependant on the thickness of one of the piezoelectric layers: hp . Equation (14) shows that in order to determine σ_1 , $w_d(x,t)$ is required, which is given by equation (15). Therefore, the key to determining D_3 is to determine equation (15): $w_d(x,t)$. The remainder of this section is devoted to finding the undetermined functions in equation (15).

3.4.2.2 Determination of $W_d(L_b)$ for Equation (15)

The assumptions made thus far are such that the piezoelectric energy harvester is treated as a spring-mass system, as shown in Figure 3-21:

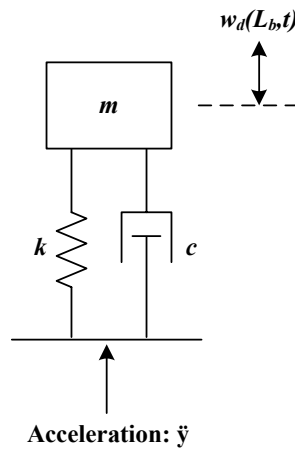


Figure 3-21 Cantilever with an end mass represented as a spring-mass system.

In Figure 3-21, m represents the combined value of the symmetrical masses attached to the free end of the cantilever, c is the damping coefficient, k is the spring constant (or stiffness) of the cantilever, \ddot{y} is the acceleration of the host structure (resulting from the vibration environment), and $w_d(L_b, t)$ is used to represent the displacement of the neutral

axis at the end of the beam (at $x = L_b$) relative to y . At present, both k and c are undetermined parameters. The derivation of k will be given later in section 0 and c is not derived; instead a figure for the damping ratio: ζ , which is related to c by:

$$\zeta = \frac{c}{2m\omega_n} \quad (16)$$

where ω_n is the resonant frequency of the cantilever, is obtained in section 3.4.2.3.

Conversion of the cantilever structure into a spring-mass system allows an equation for the motion of the mass relative to host structure motion to be written as:

$$m \ddot{w}_d(L_b, t) + c \dot{w}_d(L_b, t) + k w_d(L_b, t) = -m \ddot{y}(t) \quad (17)$$

Let:

$$w_d(L_b, t) = W_d(L_b) \cos(\omega t - \theta) \quad (18)$$

where $W_d(L_b)$ is the amplitude of mass motion relative to host structure motion.

Substituting (17) and its derivatives into (18), and solving for $W_d(L_b)$ gives:

$$W_d(L_b) = \frac{Ym\omega^2}{\sqrt{(k - m\omega^2)^2 + (c\omega)^2}} \quad (19)$$

where Y is the amplitude of the host structure motion. Equation (19) can be further evolved, through use of equation (16), into equation (20):

$$W_d(L_b) = \frac{Ym\omega^2}{k \sqrt{\left[1 - \left(\frac{\omega}{\omega_n}\right)^2\right]^2 + \left(2\zeta \frac{\omega}{\omega_n}\right)^2}} \quad (20)$$

Determination of k for Equation (20)

The previous section dealt with the determination of $W_d(L_b)$ for equation (15). However, two more undefined parameters arise as a result: k and ζ in equation (20). The aim of this section is to determine k . A figure for ζ will be obtained in the next section.

The spring constant k in equation (20) is the stiffness of the cantilever, which is determined by the geometry of the structure and the Young's modulus of the materials used in construction of the device. Unlike the spring-mass system depicted in Figure 3-21, the spring constant of a cantilever varies, as each point along the length of the beam is displaced vertically by a different amount. For a cantilever without an end mass, the spring constant can be easily found from a relevant text book. However, for a cantilever with an end mass such as the case considered here, the spring constant needs to be derived. In Figure 3-21, the spring constant can be found from the applied force per unit deformation at the mass central point, and since this point is used to represent deflection at the free end of the cantilever (at $x = L_b$), k at $x = L_b$ is equal to:

$$k = \frac{12EI}{L_b(4L_b^2 + 6L_mL_b + 3L_m^2)} \quad (21)$$

where E is the Young's modulus of the cantilever material, I is the area moment of inertia, and L_m is the length of the mass. However, it should be noted here that since the beam being considered is a composite structure; the determination of E is non-trivial since two values exist: E_p , which is the Young's modulus of the piezoelectric material, and E_s , which is the Young's modulus of the brass centre shim material. Therefore, the question of how to incorporate both E_p and E_s into equation (21) needs to be considered; this is discussed later in section 3.4.2.4. As the spring constant is an important

parameter, the derivation of equation (21) is given in detail here. For a cantilever without an end mass, the internal bending moment, M_{int} , is:

$$M_{int} = FL_b - Fx \quad (22)$$

Where F is the force acting on the tip of the free end of the beam. In this case, the deformation at $x = L_b$ (represented by w_l) is:

$$w_l(L_b) = -\frac{FL_b^3}{3EI} \quad (23)$$

which is based on the standard beam equation for the bending moment [143]:

$$\frac{M}{EI} = \frac{d^2w(x)}{dx^2} \quad (24)$$

However, for a cantilever with an end mass, it becomes apparent that an additional moment, $\frac{1}{2}FL_m$, is present that gives the beam more deflection. The detailed force analysis is given using Figure 3-22:

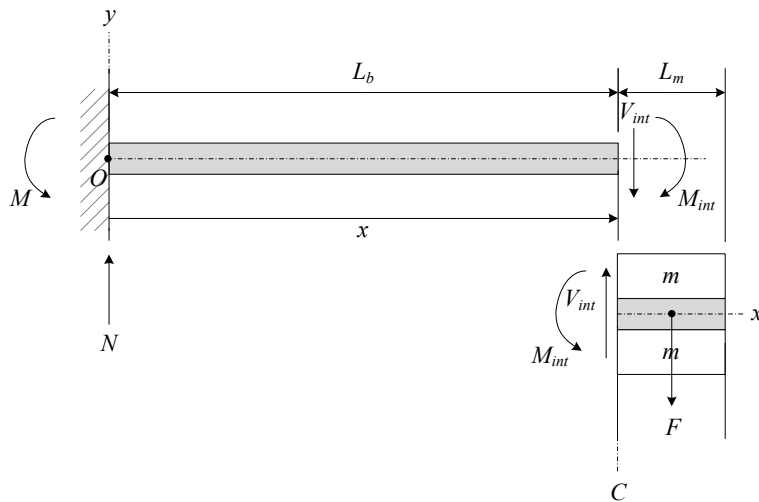


Figure 3-22 Force analysis for a cantilever with an end mass.

Analysing the left-hand portion for the summation of moments about the section C gives:

$$\sum M_c = M - Nx - M_{\text{int}} = 0 \quad (25)$$

and, as the beam is in equilibrium:

$$M = F\left(L_b + \frac{L_m}{2}\right) \text{ and } N = F \quad (26)$$

The internal bending moment for the beam with an end of mass is therefore:

$$M_{\text{int}} = F\left(L_b + \frac{L_m}{2}\right) - Fx \quad (27)$$

It can be seen that the difference between equations (27) and (22) is:

$$F \frac{L_m}{2} \quad (28)$$

Use of equation (24) [143] for equation (28) obtains the additional deformation, w_2 , present at $x = L_b$:

$$w_2 = \frac{FL_m L_b^2}{4EI} \quad (29)$$

Adding the result of (29) to (23) and making that result equal to 1 (since k is the applied force *per unit* deformation) yields the expression for k given in equation (21).

3.4.2.3 Determination of ζ for Equation (20)

The previous section dealt with finding the first undefined parameter: the spring constant k , for equation (20). This section deals with obtaining a value for the second undefined parameter: the damping ratio ζ .

The damping ratio cannot be found by theoretical analysis, only by experiment. In models previously reported, the separate effects of mechanical damping and ‘electrically induced damping’ (i.e. that caused by the piezoelectric coupling) of piezoelectric generators have often been represented as a combined entity in the viscous

damping term c for reasons of simplicity. Therefore a value of 0.05, inferred from the literature, has been used here, where 0.025 is due to mechanical damping and 0.025 is due to electrically induced damping [25].

3.4.2.4 Determination of EI for Equation (21)

The previous two sections: 0 and 3.4.2.3, dealt with the determination of k and ζ for equation (20) respectively. Since the cantilever studied here is a composite structure comprised of two different materials, each with its own Young's modulus value, the resultant equation for the spring constant k , equation (21), has one further undetermined parameter in it: E . As mentioned in section 0 the question of how to incorporate E_p , which is the Young's modulus of the piezoelectric material, and E_s , which is the Young's modulus of the brass centre shim material into equation (21) in place of E needs to be considered. This is the purpose of this section.

According to mechanics of materials theory, the area moment of inertia, I , of a rectangular area, (such as the end-face of the beam considered here) about its centroidal axis, can be found from [143]:

$$I_x = \int y^2 dA \quad (30)$$

where the subscript x indicates that the moments are to be taken about the x-axis, which is made coincident with the centroidal axis. Also according to mechanics of materials theory, the neutral axis for a symmetrical beam is at half the height of the beam, which coincides with the centroidal axis for the present case. The above two facts imply that equation (30) can be used to find I for equation (21). However, implementing equation (30) in its present form does not allow for inclusion of the effects of two different Young's modulus values, as discussed above.

Therefore, a different approach is employed for the composite case: considering EI as one combined entity that is ΣEI . An expression for ΣEI can be determined by using Figure 3-23 and equation (30), and is:

$$EI = E_p \int_{-h_n}^{-h_n+h_{ip}} y^2 b dy + E_s \int_{-h_n+h_{ip}}^0 y^2 b dy + E_s \int_0^{h_s+h_{ip}-h_n} y^2 b dy + E_p \int_{h_s+h_{ip}-h_n}^{h_s+h_{ip}+h_{ip}-h_n} y^2 b dy \quad (31)$$

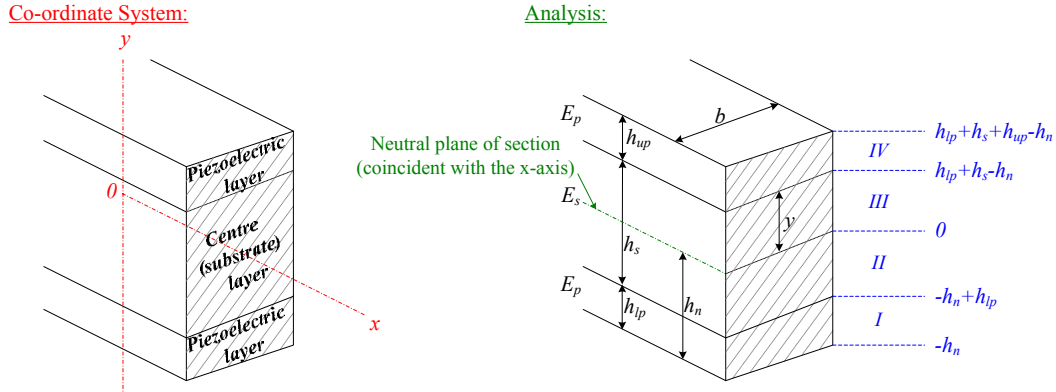


Figure 3-23 Method of finding the area moment of inertia for a composite beam.

3.4.2.5 Determination of $f(x)$ for Equation (15)

The previous three sections determined the undefined parameters: k , z , (and EI for k) for the expression that calculates the out-of-plane displacement at the end of the beam, $W_d(L_b)$, which is equation (20). Remembering that the key to determining D_3 is to derive equation (15), $W_d(L_b)$ from equation (20) can now be substituted into equation (15), leaving only $f(x)$ that remains undetermined. The purpose of this section is to determine $f(x)$.

The function $f(x)$ is a normalised vibration-mode shape function that satisfies the boundary conditions of the cantilever. It is:

$$f(x) = -\frac{3}{2L_b^2} x^2 \left(\frac{x}{3L_b} - 1 \right) \quad (32)$$

where x is any point along the length of the beam. In deriving equation (32), the following assumption was made:

- 1) The shape of the beam under dynamic conditions is the same as the shape of the beam under static conditions.

An equation from statics that describes the maximum deflection at the end of a cantilever is [143]:

$$W_s(L_b) = -\frac{FL_b^3}{3EI} \quad (33)$$

and an equation from statics that describes the deflection at any length x along the length of a cantilever is:

$$w_s(x) = \frac{FL_b}{2EI} x^2 \left(\frac{x}{3L_b} - 1 \right) \quad (34)$$

The normalisation can be performed by:

$$f(x) = \frac{w_s(x)}{W_s(L_b)} \quad (35)$$

Which results in equation (32). This normalisation satisfies the boundary conditions $f'_{(x=0)} = 0$ and $f_{(x=L_b)} = 1$.

3.4.2.6 Determination of Equation (14) for σ_1

Sections 3.4.2.2 through 3.4.2.4 describe the derivation of various functions needed for the determination of $W_d(L_b)$, which is required for equation (15). Section 3.4.2.5 derived $f(x)$, which is also required for equation (15). Successful derivation of equation (15) means that σ_1 , and therefore D_3 , can be calculated through equation (14). For completeness, the derivation of equation (14) is given in this section.

Equation (14) provides the link between the out-of-plane displacement, $w_d(x,t)$, in the “3” direction and stress generated in the “1” direction within the piezoelectric layers of the cantilever:

$$\sigma_1(h_{av}) = E_p \cdot h_{av} \cdot \frac{d^2 w_d(x,t)}{dx^2} \quad (14)$$

The parameter h_{av} represents the height at half the thickness of the piezoelectric layer (as shown in Figure 3-19; page 153). This value was chosen as an estimation of the position of average strain. The derivation of equation (14) is based on mechanics of materials theory [143], and in particular on equations (24), which were previously introduced, (36) and (37), which are: the standard beam equation for the bending moment in a beam, the formula for Young’s modulus, and the flexure formula, respectively:

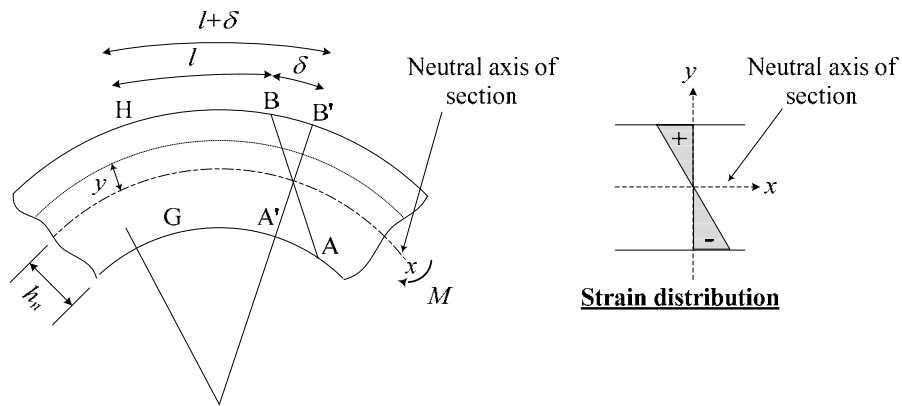
$$\frac{M}{EI} = \frac{d^2 w(x)}{dx^2} \quad (24)$$

$$E = \frac{\sigma}{\varepsilon} \quad (36)$$

$$\sigma_x(y) = \frac{My}{I} \quad (37)$$

where the subscript x in equation (37) indicates that stress in the x -direction, which is synonymous to the “1” direction, is the subject, and ε in equation (36) represents strain.

Figure 3-24, which shows the strain distribution through the thickness of the beam, is used in the derivation of equation (14):



*Notes:

- 1) Figure shows a homogenous beam for simplicity,
- 2) y is any distance from the neutral axis,
- 3) Due to the curvature a section AB , which was originally parallel to GH , has rotated to $A'B'$.

Figure 3-24 Strain distribution in a curved beam.

Since strain is the change in length, δ , divided by the original length, l , maximum strain occurs at the top of the beam (at hp). Strain in the “1” direction, ε_1 , as a function of vertical distance, y , is:

$$\varepsilon_1(y) = \frac{\varepsilon_1(hp)}{hp} y \quad (38)$$

Applying equation (36) for Young’s modulus yields an expression for stress in the “1” direction:

$$\sigma_1(y) = E \frac{\varepsilon_1(hp)}{hp} y \quad (39)$$

Substitution of equation (37), which is the flexure formula, into equation (39) yields:

$$\frac{\varepsilon_1(hp)}{hp} y = \frac{My}{IE} \quad (40)$$

From equation (38), the left hand side of equation (40) is equivalent to the strain present in the “1” direction. By substitution of equation (24), which is the bending moment, into equation (40), and application again of equation (36) for Young’s modulus, the resulting expression forms the basis of equation (14):

$$\sigma_1(y) = Ey \frac{d^2w}{dx^2} \quad (41)$$

The parameter y , which represents any distance from the neutral axis (as shown in Figure 3-24) is replaced by h_{av} in equation (14) which, as mentioned before, represents the height at half the thickness of the piezoelectric layer. The Young’s modulus E takes the value of the Young’s modulus of the material at height h_{av} ; i.e. that of the piezoelectric ceramic material: E_p .

3.4.2.7 Determination of the Electrical Outputs

Successful derivation of $w_d(x,t)$ in equation (15) means that D_3 , and hence Q_3 , I_R and V_R can now be calculated. Substituting equation (12) into (13) (remembering that $V_R=V_3$), (13) into (9), and (9) into (10) obtains:

$$Q_3 = 2 \cdot b \cdot \int_0^{L_b} \left(d_{31} \cdot \sigma_1 + \varepsilon_p^\sigma \cdot \frac{I_R \cdot R}{h_p} \right) dx \quad (42)$$

Differentiating equation (42) with respect to t and then substituting it into equation (11) yields:

$$I_R = \frac{dQ_3}{dt} = \omega \cdot 2 \cdot b \cdot \int_0^{L_b} \left(d_{31} \sigma_1 + \varepsilon_p^\sigma \frac{\frac{dQ_3}{dt} \cdot R}{h_p} \right) dx \quad (43)$$

By substitution of equation (14) for the stress generated at h_{av} :

$$I_R = \omega \cdot 2 \cdot b \cdot \int_0^{L_b} \left(d_{31} \cdot E_p \cdot h_{av} \cdot \frac{d^2 w_d}{dx^2} + \varepsilon_p^\sigma \cdot \frac{dQ_3}{dt} \cdot R \right) \cdot b \cdot dx \quad (44)$$

Substituting equation (15) into (44) (requiring further substitutions of equations (20) and (32) into equation (15)) yields:

$$I_R(f) = \frac{3 \cdot d_{31} \cdot E_p \cdot h_{av} \cdot b \cdot Y \cdot m \cdot \omega(f)^3}{L_b \cdot k \cdot \sqrt{\left[1 - \left(\frac{\omega(f)}{\omega_n} \right)^2 \right]^2 + \left(2\zeta \frac{\omega(f)}{\omega_n} \right)^2}} + \frac{2 \cdot \varepsilon_p^\sigma \cdot b \cdot L_b \cdot \omega \cdot \frac{dQ_3}{dt} \cdot R}{h_p} \quad (45)$$

Finally, substituting equation (21) into (45) gives:

$$I_R(f) = \frac{d_{31} \cdot E_p \cdot h_{av} \cdot b \cdot Y \cdot m \cdot \omega(f)^3 \cdot (4L_b^2 + 6L_b L_m + 3L_m^2)}{4 \cdot EI \cdot \sqrt{\left[1 - \left(\frac{\omega(f)}{\omega_n} \right)^2 \right]^2 + \left(2\zeta \frac{\omega(f)}{\omega_n} \right)^2} \cdot \left(1 + \frac{2 \cdot \varepsilon_p^\sigma \cdot b \cdot L_b \cdot \omega(f) \cdot R}{h_p} \right)} \quad (46)$$

Equation (46) describes the amplitude of the current flowing through the external load resistor. The voltage amplitude across the load resistor can be found from equation (12):

$$V_R(f) = I_R(f) \cdot R = \frac{d_{31} \cdot E_p \cdot h_{av} \cdot b \cdot Y \cdot m \cdot \omega(f)^3 \cdot (4L_b^2 + 6L_b L_m + 3L_m^2) \cdot R}{4 \cdot EI \cdot \sqrt{\left[1 - \left(\frac{\omega(f)}{\omega_n} \right)^2 \right]^2 + \left(2\zeta \frac{\omega(f)}{\omega_n} \right)^2} \cdot \left(1 + \frac{2 \cdot \varepsilon_p^\sigma \cdot b \cdot L_b \cdot \omega(f) \cdot R}{h_p} \right)} \quad (47)$$

The average power dissipated in the load resistor (i.e. ‘useful’ power transferred to the load) can then be determined from:

$$P_{ave_in_R}(f) = \frac{V_R(f)^2}{2 \cdot R} \quad (48)$$

Therefore, substituting equation (47) into equation (48) obtains the average power dissipated in the load resistor:

$$P_{ave_in_R}(f) = \frac{E_p^2 \cdot d_{31}^2 \cdot Y^2 \cdot \omega(f)^6 \cdot b^2 \cdot h_{av}^2 \cdot m^2 \cdot (4L_b^2 + 6L_b L_m + 3L_m^2)^2 \cdot R}{32 \cdot (EI)^2 \cdot \left[\left[1 - \left(\frac{\omega(f)}{\omega_n} \right)^2 \right]^2 + \left(2\zeta \frac{\omega(f)}{\omega_n} \right)^2 \right] \cdot \left(1 + \frac{2 \cdot \varepsilon_p^\sigma \cdot b \cdot L_b \cdot \omega(f) \cdot R}{h_p} \right)^2} \quad (49)$$

All of the parameters in equation (49) that aren't (or don't rely on) geometric parameters can be easily found from data sheets or determined through equations (16) - (35). The parameter Y is a function of the driving vibration characteristics:

$$Y(f) = \frac{a}{\omega(f)^2} \quad (50)$$

where a is the acceleration value of the driving vibrations. Equation (49) is an expression for the average power dissipated in any value load resistor connected to the output terminals of the generator; i.e. a resistor with value R . Conventional circuit theory dictates that maximum power transfer from source to load occurs when their impedances are matched, making it conducive to aim for this condition. According to convention then, for maximum power transfer R should be made equal to the source impedance of the generator, when it might then be called the optimal load resistance value, R_{opt} . It is well known that a piezoelectric generator can be represented as a current source in parallel with its own internal capacitance, as shown in Figure 3-20, and this leads intuitively to equation (51) as an expression for the source impedance value, and hence as an expression for R_{opt} :

$$X_c(f) = R_{opt}(f) = \frac{1}{\omega \cdot (C_1 + C_2)} \quad (51)$$

where $X_c(f)$ is the capacitive reactance (and C_1 and C_2 the capacitance values) of the piezoelectric layers:

$$C_1 = C_2 = \frac{\varepsilon_r \cdot \varepsilon_0 \cdot A}{h_p} \quad (52)$$

where A is the area of one of the electrodes (i.e. $L_b \times b$), and h_p is the thickness of one of the piezoelectric layers. If the value of load resistance, R , in equation (49) is made optimum by substitution of equation (51) into (49), then the expression to obtain the average power dissipated in the load resistor becomes:

$$P_{ave_in_R}(f) = \frac{E_p^2 \cdot d_{31} \cdot Y^2 \cdot \omega(f)^5 \cdot h_{av}^2 \cdot m^2 \cdot (4L_b^2 + 6L_b L_m + 3L_m^2)^2 \cdot b \cdot h_p}{256 \cdot (EI)^2 \cdot \left[\left[1 - \left(\frac{\omega(f)}{\omega_n} \right)^2 \right]^2 + \left(2\zeta \frac{\omega(f)}{\omega_n} \right)^2 \right] \cdot \varepsilon_r \cdot \varepsilon_0 \cdot L_b} \quad (53)$$

Therefore, whereas equation (49) is an expression for the average power dissipated in *any* value load resistor, R , equation (53) is an expression for the average power dissipated in an *optimal* value load resistance; i.e. when $R = R_{opt}$.

3.5 Device Optimisation

The analytical model described in the previous section, 3.4, resulted in an expression for the average power that is dissipated in an optimum-value load resistor placed across the output terminals of a rectangular bimorph cantilever vibration energy harvester. The amount of power dissipated by the resistor represents the useful power output of the piezoelectric energy harvesting device. A particular strength of the derived expression for power, equation (53), given by this model is that it can be very easily used as the objective function in a computer-based optimisation algorithm to optimise the geometric parameters of the device, because it has within its arguments all of the geometric parameters of the device. To this author's knowledge, no other model results in an expression for power that in its final form includes the influence of all of the geometric parameters of the device. It would be very easy for a designer who is considering using

an energy harvesting system to pick up this expression, input to it the vibration characteristics of the intended application environment, set constraints in regard to the space-envelope available in the application, and then use an optimisation routine in order to determine the optimum dimensions for achieving maximum power output. In addition, once the optimum dimensions have been obtained, their values can be put back into equation (47) to obtain the voltage output, back into equation (46) to obtain the current output if required, and into (51) to give the source impedance value, thus providing information that allows for the development of power conditioning circuitry.

The aim of this section is to provide an example of this kind of scenario, where the vibration characteristics and space-envelope constraints are dictated by a particular application, and the optimum dimensions for maximum power output are required. This section is split into sub-sections as follows:

- 1) Section 3.5.1: Discussion of the vibration characteristics (dictated by the application environment),
- 2) Section 3.5.2: Discussion of the space-envelope constraints (dictated by the application environment),
- 3) Section 3.5.3: Discussion of the material characteristics, which can be categorised either as inputs (as per the vibration characteristics) or as additional parameters to be optimised,
- 4) Section 3.5.4: Details of the software and optimisation algorithm used,
- 5) Section 3.5.5: Optimisation results.

3.5.1 Vibration Characteristics of the Intended Application Environment.

Two pieces of information regarding the vibration environment that the generator is to be placed in are needed: the target frequency, and the acceleration amplitude of the vibrations. As this thesis does not consider as part of its focus a specific application for the harvesting system, this author has turned to the available literature for suitable information concerning these two values. Vibration environments have been previously measured and reported in [66] and [67] for the purpose of vibration energy harvesting. Roundy et al. [66] found that for ‘low level’ ambient vibrations, it is common to see a large peak in magnitude somewhere below 200Hz, and that for four of the twelve vibration sources they examined, that peak centred somewhere close to 120Hz. For this reason, 120Hz was chosen as a target frequency for the generator. Regarding the second piece of information required: the acceleration level, a value of $\pm 2.25\text{m/s}^2$ was chosen because this is representative of real-world vibration environments [66].

3.5.2 Space-envelope Constraints

A simple space-envelope of 1 cm^3 was allowed for the generator, simply because “power output per volume” has emerged as one comparison metric for generators recently (i.e. the ‘power density’ of the generators is compared), and 1cm^3 is not an unreasonable volume for the generator to occupy for many applications, for example for pipeline monitoring, or monitoring of road, rail or bridge structures. In addition to an overall volume constraint, a constraint on the beam length to mass length ratio was added, because without it the optimiser (which always prefers to increase the mass value to obtain more power) returns a minute beam length value and a massive mass length value, and this form of structure is no longer representative of a spring-mass system, rendering the model invalid.

3.5.3 Material Characteristics

In addition to the vibration characteristics and space-envelope dictated by the application environment, a further consideration not mentioned thus far is the characteristics of the materials that the cantilever comprises. These exist in the objective function, equation (53), as:

- E_p Young's modulus of the piezoelectric ceramic,
- d_{31} Piezoelectric charge coefficient of the piezoelectric ceramic,
- ρ_m Density of the mass material – required for m (the mass value is the product of density \times volume),
- ρ_p Density of the piezoceramic material – required for m (the section of the beam that lies between the masses constitutes part of the mass value),
- ρ_s Density of the substrate material – required for m (comment as for ρ_p above),
- ϵ_r Relative permittivity of the piezoceramic material – required for R_{opt} (see equation (51) and accompanying discussion),
- E_s Young's modulus of the substrate material – required for EI (see equation (31)),
- ϵ_p^σ Absolute permittivity of the piezoceramic material,

These material characteristics can be either dictated at the start as per the vibration characteristics, and therefore categorised as inputs to the objective function, or they can be made to be additional outputs of the optimisation process; i.e. to be optimised for maximum output power, as per the geometrical parameters. There are many types of piezoelectric ceramic available commercially, and if a device design is to be made in large quantities, there would almost certainly be some gain to be had in putting the material parameters into the latter category so that they are optimised. However, for the

purposes of demonstrating the optimisation process, which requires the fabrication of only one or two devices, it is most efficient simply to use a readily available commercial bimorph actuator; though by doing so of course, some of the device parameters (for example thicknesses of the piezoelectric and shim layers in addition to all of the material characteristics) are automatically dictated. A survey was done on commercial bimorph actuators that are currently available. A difficulty experienced in carrying out this survey, was that quite often not all of the data required was provided by the manufacturers. It was found that Piezo Systems Inc (MA, USA) not only offers comprehensive data sheets, but their part no. T226-H4-103Y uses a piezoelectric ceramic with a very high piezoelectric charge constant (d_{31}) value at -320×10^{-12} m/V. A high piezoelectric charge constant, from the piezoelectric constitutive equation (9) given on page 155, implies a high conversion of mechanical energy to electrical energy. For the mass material, tungsten alloy with a density of 18100kg/m^3 (M&I Materials Ltd/Wolfmet, Manchester, UK) was chosen. Using a high density material such as tungsten alloy is advantageous because it means that a greater mass value is achievable in a small space, leading to a low device resonant frequency in a small package size and hence making it easier to match the low frequencies typically found in ambient vibration environments. Appendix B provides a full summary of the material properties for the device optimised and fabricated in this thesis.

3.5.4 Optimisation Software

To solve the optimisation problem, the engineering calculation software “Mathcad 2000 Professional” (Parametric Technology Corporation/Mathsoft, MA, USA) was used. The objective function of the optimisation problem was the derived expression for the average power output of the harvester with an optimal load resistance; i.e. equation (53)

on page 171. However, it should be noted that in order to perform the optimisation procedure with Mathcad 2000 professional, several substitutions of underlying equations had to be made into equation (53); for example: the variable for mass, m , in the numerator of (53) actually needs to be represented by expression (54) below:

$$m = \left[(L_m \cdot h_m \cdot b_m \cdot \rho_m) + (L_m \cdot h_s \cdot b \cdot \rho_s) + \left[L_m \cdot (h_{lp} + h_{up}) \cdot b \cdot \rho_p \right] \right] \quad (54)$$

since mass is equal to density \times volume, and the mass in this case consists of the two tungsten-alloy masses, plus the mass of the beam in between; i.e.:

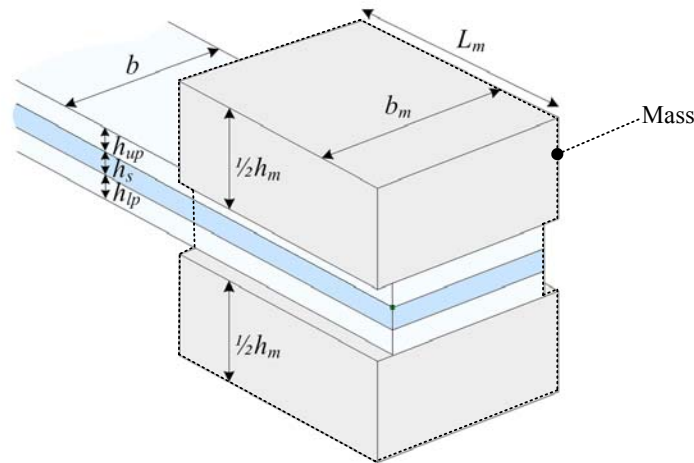


Figure 3-25 Origin of equation (54) for the value of the mass, m .

The reason for doing this is that it is much easier to put the expression into its ‘base’ form (i.e. until no more substitutions can be made), rather than a ‘nested equation’ form for two reasons: 1) because the user can see exactly where each input variable lies in the expression for power output, and 2) because it greatly helps to eliminate the possibility of making a mistake, since the user interface of Mathcad is a blank sheet in which equations need to be written sequentially. If the nested equation form of the objective function were to be used, it might quickly become complicated, with layers of variables feeding into the hierarchy of equations. By keeping it simple by making the

substitutions, the input variables and their values can be listed first, and the objective function (expression for power) can follow immediately afterwards. A full list of the substitutions required is given in Table 3-1. Table 3-2 lists the input variables for the optimisation problem, Table 3-3 lists the output variables, and Table 3-4 lists the constraints.

Table 3-1 List of substitutions into the objective function: equation (53), in Mathcad 2000 professional.

Variable in eqn. (53)	Description	Substituted by:
ω	Angular frequency of input vibration	$2 \cdot \pi \cdot f$
h_{av}	The height, from the neutral axis of the beam, at half the thickness of the upper piezoelectric layer (as shown in Figure 3-19 on page 153). This position was chosen as an estimate of the position of average strain, as discussed in section 3.4.2.6	$\frac{h_s}{2} + \frac{h_{up}}{2}$ (refer to Figure 3-19 on page 153 for an explanation of h_s and h_{up})
m	Value of the seismic mass	$(L_m \cdot h_m \cdot b_m \cdot \rho_m) + (L_m \cdot h_s \cdot b \cdot \rho_s) + [L_m \cdot (h_{lp} + h_{up}) \cdot b \cdot \rho_p]$ (refer to equation (54), Figure 3-25, and surrounding text for an explanation of variables)
EI	ΣEI (as per section 3.4.2.4)	$EI = E_p \int_{-h_n}^{-h_n+h_{lp}} y^2 b dy + E_s \int_{-h_n+h_{lp}}^0 y^2 b dy + E_s \int_0^{h_s+h_{lp}-h_n} y^2 b dy + E_p \int_{h_s+h_{lp}-h_n}^{h_s+h_{lp}+h_{up}-h_n} y^2 b dy$ (section 3.4.2.4 on page 163 provides an explanation of the derivation of this expression)
ω_n	Natural frequency of the piezoelectric cantilever harvester structure	$\sqrt{\frac{12EI}{L_b \cdot (4L_b^2 + 6L_m L_b + 3L_m^2)} \cdot m}$ (this originates from $\sqrt{\frac{k}{m}}$, where k is the spring constant of the cantilever and m is the seismic mass value. In the case considered here, k was derived in section 0 as: $\frac{12EI}{L_b (4L_b^2 + 6L_m L_b + 3L_m^2)}$)

Table 3-2 Input variables for the optimisation problem.

Material Variables	
Variable	Description and value input to the optimisation problem
E_p	Young's modulus of the piezoelectric ceramic, value: $62 \times 10^9 \text{ N/m}^2$ (obtained from the data sheet for actuator part no. T226-H4-103Y)
E_s	Young's modulus of the brass centre layer, value: $100 \times 10^9 \text{ N/m}^2$ (obtained from [144])
ρ_m	Density of the mass material, value: 18100 kg/m^3
ρ_s	Density of the brass centre layer, value: 8780 kg/m^3 (obtained from [144])
ρ_p	Density of the piezoelectric ceramic material, value: 7800 kg/m^3 (obtained from the data sheet for actuator part no. T226-H4-103Y)
d_{31}	Piezoelectric charge coefficient, value: $-320 \times 10^{-12} \text{ m/V}$ (obtained from the data sheet for actuator part no. T226-H4-103Y)
ϵ_r	Relative permittivity of the piezoceramic material, value 3800 (obtained from the data sheet for actuator part no. T226-H4-103Y)
Dimensional Variables	
Variable	Description and value input to the optimisation problem
$h_{lp}, h_{up} \text{ \& } h_p$	<p>h_{lp} = height of the upper piezoelectric layer h_{up} = height of the lower piezoelectric layer h_p = height of either piezoelectric layer (i.e. h_{lp} and h_{up} are identical in the case considered here, since the bimorph under consideration is symmetrical). h_p occurs in equation (53) rather than h_{lp} or h_{up}, simply because the expression for optimal load impedance (equation (51) on page 170) involves the calculation of two like capacitive reactances in parallel.</p> <p>In all cases, the value (0.278mm) was dictated by the purchase of actuator part no. T226-H4-103Y from Piezo Systems Inc.</p>
h_s	Height of the brass centre layer, dictated by the purchase of actuator part no. T226-H4-103Y. Value: 0.102mm (obtained from the data sheet)
h_n	<p>Height of the neutral axis of the beam. In the case considered here, since the bimorph under consideration is symmetrical, h_n could be found simply from:</p> $h_n = \frac{h_{lp} + h_s + h_{up}}{2}$ <p>Value: 0.329mm</p>
b	Width of the beam, dictated by the purchase of actuator part no. T226-H4-103Y. Value: 3.2mm (obtained from the data sheet)

Vibration Environment Variables

Variable	Description and value input to the optimisation problem
Y	<p style="text-align: center;">Amplitude of acceleration, found from:</p> $Y = \frac{2.25}{\omega_n^2}$ <p style="text-align: center;">As per equation (50) on page 170, where 2.25 is the acceleration value chosen based on the discussion in paragraph 3.5.1; i.e. $\pm 2.25 \text{m/s}^2$ ($\pm 0.23\text{g}$).</p>

Structure Variables

Variable	Description and value input to the optimisation problem
ζ	<p style="text-align: center;">Damping ratio. As discussed in paragraph 3.4.2.3 on page 162, the damping ratio can only be found by experiment; therefore a value of 0.05, inferred from literature, was input to the optimisation problem.</p>

Table 3-3 Output variables of the optimisation problem

Variable	Description
L_b	Length of the beam
L_m	Length of the mass
h_m	Height of the mass
b_m	Width of the mass

Table 3-4 Constraints of the optimisation problem

Constraint	Entry into Mathcad
Length of the beam to be greater than zero	$L_b > 0$
Length of the mass to be greater than zero	$L_m > 0$
Height of the mass to be greater than zero	$h_m > 0$
Width of the mass to be greater than zero	$b_m > 0$
Cantilever to fit into volume of 1cm ³ or less:	$\left[\left((h_{lp} + h_s + h_{up} + h_m) \cdot L_m \cdot b_m \right) + \left((h_{lp} + h_s + h_{up}) \cdot L_b \cdot b \right) \right] \cdot 1 \cdot 10^6 \leq 1$
Length of beam to be at least half the length of the mass	$L_b \geq \frac{1}{2} \cdot L_m$
Natural frequency of the beam to be 120Hz	$\sqrt{\frac{12EI}{L_b \cdot (4L_b^2 + 6L_m L_b + 3L_m^2)} \cdot m} = 2 \cdot \pi \cdot 120$ <p>120Hz was chosen as the target resonant frequency based on the discussion given in paragraph 3.5.1. (Note that this requires substitutions for EI and m, as described in Table 3-1)</p>
Frequency of input vibrations to be kept in the range 60-140Hz inclusive	$f \geq 60$ $f \leq 140$

Note that for the purpose of optimising the geometry of the harvesting device, the desired output variables of the optimisation process are the dimensions of the device, as shown in Table 3-3. Because an actuator was bought in: part no. T226-H4-103Y (Piezo Systems Inc, MA, USA), some of the dimensions, for example the height of the piezoceramic and brass layers, were automatically dictated, which is why they appear as

input variables in Table 3-2, rather than as output variables in Table 3-3. The parameters that remain that can be optimised are listed in Table 3-3. If a bimorph is to be custom fabricated rather than bought in, then more dimensions could be included in the output variables list, with the possibility of obtaining results that might lead to an even greater power output. However, as mentioned in section 3.5.3 it was most efficient to obtain a bought-in bimorph for this project, since only a one-off device was required.

Note also that included in Table 3-4, which lists the constraints of the optimisation problem, is a constraint that requires the input driving vibration frequency, f , to remain within the bounds of 60 to 140Hz inclusive. This was done as a ‘self-check’. Since the constraint set for the natural frequency of the harvesting device was that it be fixed at 120Hz (again, see Table 3-4), it was reasoned that if given the input frequency variable, f , as a parameter to be optimised, the optimiser should return 120Hz as the optimal value, thus providing a self-check that the optimiser, in conjunction with the derived expression for power; i.e. equation (35), was indeed performing as intended.

In regard to the type of optimisation algorithm used, Mathcad has an “auto select” feature that automatically determines an appropriate algorithm for solving the type of problem it is presented with. In this case the software automatically applied the conjugate gradient method. A print-out of the Mathcad file used is given in appendix C.

3.5.5 Optimisation Results

The dimensions for the optimised design are listed in Table 3-5. In order to give a visual effect, a schematic of the optimised device is also shown in Figure 3-26:

Table 3-5 Dimensions of the optimised vibration energy harvester.

Dimension	Value (mm)
Beam length L_b	6.033
Beam Width b	3.2
Mass length L_m	12
Mass width b_m	8.159
Total Mass height h_m	9.374
Thickness of each piezoelectric layer h_{lp} and h_{up}	0.278
Thickness of centre shim layer h_s	0.102

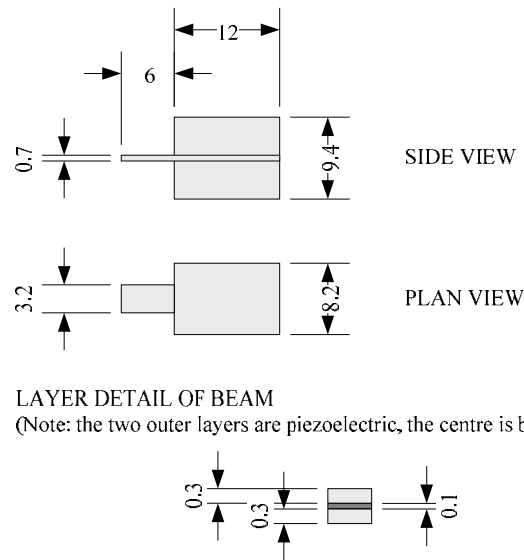


Figure 3-26 Schematic of the optimised device (all dimensions are in mm).

The results show that in order to achieve a higher level of output power, a smaller beam and larger mass is preferred in the design of the device. The optimised geometric dimensions were put back into equation (47) to obtain the predicted voltage amplitude, and into equation (51) to obtain the source impedance (and hence optimum load

resistance) values. Figure 3-27 shows the predicted output power and voltage of the device as a function of frequency:

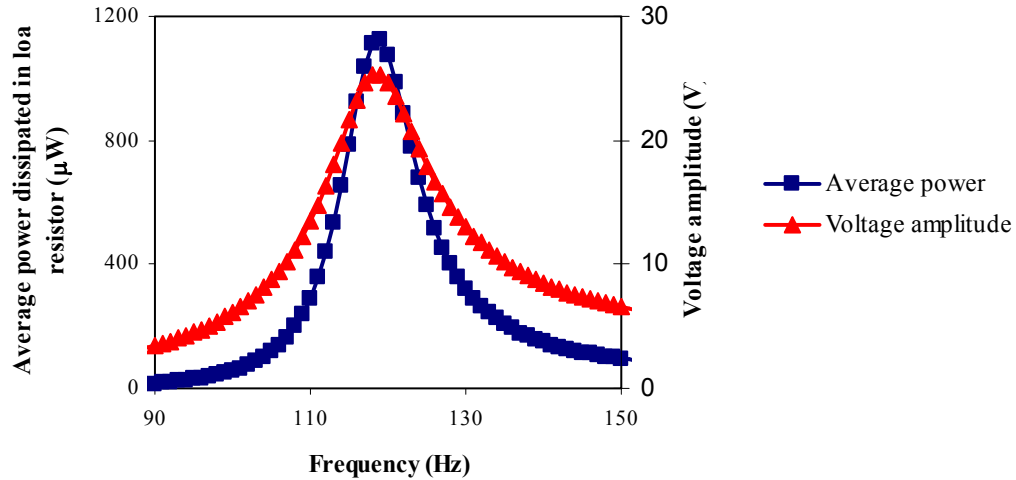


Figure 3-27 Simulated values of the power and voltage outputs of the optimised device.

The model predicts a maximum output power of 1.1mW at resonance into an optimum resistive load. The predicted voltage amplitude at resonance across the optimum resistive load is 25.43V. The optimum resistive load value predicted is 288.1kΩ.

In order to gain trust that these results are indeed an optimum design, and that the optimiser, in conjunction with the equation (35) (the expression for power derived in this thesis) were performing as intended, some sensitivity analysis is required. However, care must be taken in this process, since it is not simply a straightforward task of adjusting some dimensional parameter, the length of the beam say, and then examining the output. A change in any dimensional parameter results in a change in the resonant frequency of the device, which in turn will result in a predicted power output that will no longer bear any relevance, because the aim was to obtain a harvesting device with a resonant frequency of 120Hz. One cannot simply change a dimensional parameter,

without first considering that the volume constraint (i.e. the cantilever must fit into a volume of 1cm^3 or less), and the resonant frequency constraint (i.e. the natural frequency of the beam is to be 120Hz) must both be adhered to, otherwise the comparison would not be ‘like-for-like’; it would be meaningless.

Given the above considerations then, it was decided that one method by which a sensitivity analysis could be carried out, was to fix one of the output variables at a value other than that given as the result in Table 3-5, and then repeat the optimisation process. In this way, if say, the length of the beam is fixed at 6.433mm, which is 0.4mm longer than the optimum value given by the optimisation process, then the dimensions of the mass can remain as output variables, and the constraints will still apply. This procedure was performed twice: once where the length of the beam was altered by 0.4mm, as just described, and once for a case where the length of the mass was shortened by 0.3mm. The results are shown in Table 3-6 and Table 3-7 respectively.

Table 3-6 Results from a sensitivity analysis where the length of the beam, L_b , is constrained to 6.433mm but the resonant frequency remains constrained at 120Hz and the device volume constrained within 1cm^3 .

Dimensions	
Dimension	Value (mm)
Beam length L_b	Fixed at 6.433
Beam Width b	3.2
Mass length L_m	12
Mass width b_m	7.985
Total Mass height h_m	9.162
Thickness of each piezoelectric layer h_{ip} and h_{up}	0.278
Thickness of centre shim layer h_s	0.102
Electrical Characteristics	
Maximum power output at resonance	895 μ W
Voltage amplitude at resonance	22.3V
Optimum resistive load value	279 Ω

Table 3-7 Results from a sensitivity analysis where the length of the mass, L_m , is constrained to 11.7mm but the resonant frequency remains constrained at 120Hz and the device volume constrained within 1cm^3 .

Dimensions	
Dimension	Value (mm)
Beam length L_b	6.207
Beam Width b	3.2
Mass length L_m	Fixed at 11.7
Mass width b_m	7.086
Total Mass height h_m	11
Thickness of each piezoelectric layer h_{lp} and h_{up}	0.278
Thickness of centre shim layer h_s	0.102
Electrical Characteristics	
Maximum power output at resonance	1.03mW
Voltage amplitude at resonance	24V
Optimum resistive load value	281 Ω

It can be seen that in neither sensitivity analysis case does the output power exceed that obtained, 1.1mW, from the original optimisation problem. This provides a degree of trust that the results originally obtained are indeed those for an optimum design.

With some confidence then, we can return to an analysis of the predicted electrical outputs of the optimised device. In comparison with the experimental results obtained from the first prototype harvesting device (detailed in section 3.2 from page 129 onwards) 1.1mW is an improvement in the power output of the device by a factor of 134, and 25.43V is an improvement in the voltage output by a factor of 9. In addition, the resonant frequency of the device has been lowered to that of a more practical value (120Hz) for harvesting from vibrations which, as discussed before, based on the literature review appear to have larger amplitude values at lower frequencies (below 200Hz or so). These simulated values suggest that through the use of the model developed in this thesis, the power output of a cantilever-based vibration energy

harvesting device can be significantly enhanced. The next stage is to fabricate the device and to test it.

3.6 Fabrication of the Optimised Design

As mentioned in section 3.5.3, a commercially available bimorph actuator: Piezo Systems Inc (MA, USA) part no. T226-H4-103Y, was purchased. Ferric Chloride solution, FeCl_3 , was used to remove the nickel electrode material from the areas where the symmetrical masses were to be attached. The reason for removing the electrode material from these areas is that the portions of the piezoceramic layers that lie between the masses do not contribute to charge generation, since they can not be deformed due to the thickness of the masses, and leaving the electrode material in place in these areas would increase the capacitance of the piezoelectric generator, which in turn would decrease the voltage output through the relationship:

$$Q_3 = C \cdot V \quad (55)$$

where Q_3 is the charge developed on one electrode of the piezoelectric harvesting device, C is the total capacitance of the device, and V is the voltage developed across the output terminals of the piezoelectric generator. Since the portions of the piezoceramic layers that lie between the masses do not contribute to charge generation, the amount of charge generated, Q_3 , remains the same regardless of whether the sections of electrode are removed or not. In this case, increasing the capacitance, C , results in a decrease in the voltage generated: V . Decreasing the voltage output of the generator would lead to a decrease in the amount of power output, therefore it is favourable to remove the electrodes from this portion of the cantilever.

Following the removal of the electrode sections, wires were then attached to both outer electrodes and the centre shim by using Circuitworks (Chemtronics, GA, USA)

conductive epoxy resin, and the masses were attached using Loctite (Henkel, Düsseldorf, Germany) superglue. A photo of the fabricated device is shown in Figure 3-28:

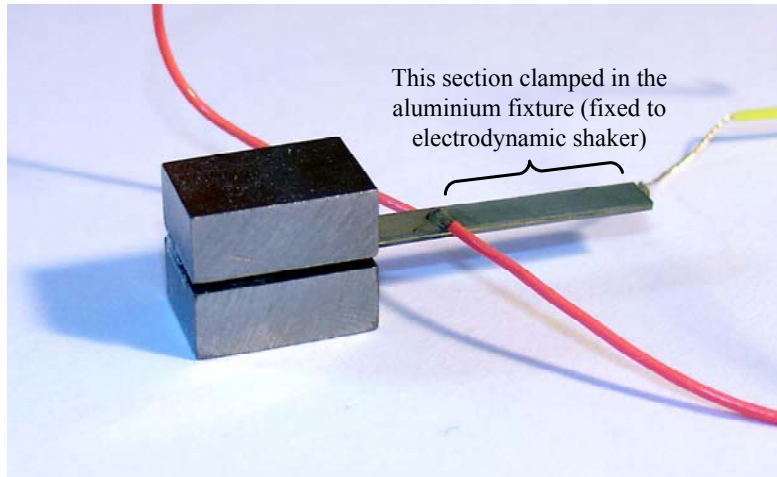


Figure 3-28 Photo of the optimised vibration energy harvester.

3.7 Testing of the Optimised Design

The purpose of this section is to detail the improved test setup and equipment, and describe the procedure used with the improved test setup to test the optimised device.

3.7.1 Improved Test Setup and Equipment

In the initial investigations carried out in section 3.2, a first test setup was built that could perform a frequency sweep of 0-200Hz in approximately 1 second. However, although some results were obtained using this test setup, from the discussions given in the conclusions section 3.3 (page 135) there was clearly a need for a better, more considered testing approach. The main problem concerning the approach taken in the initial investigations was the lack of control of the frequency sweep. Ideally, the frequency that is applied to the harvesting device needs to be incremented in a controllable manner, where the length of time spent at each frequency can be adjusted

as required. In addition, automated collection of data would be useful, rather than simply observing traces on an oscilloscope. This latter point implies the use of data acquisition hardware. Since such hardware was not immediately available, the first attempt to make an automated system, by necessity, involved many self-built component parts, as shown in Figure 3-29:

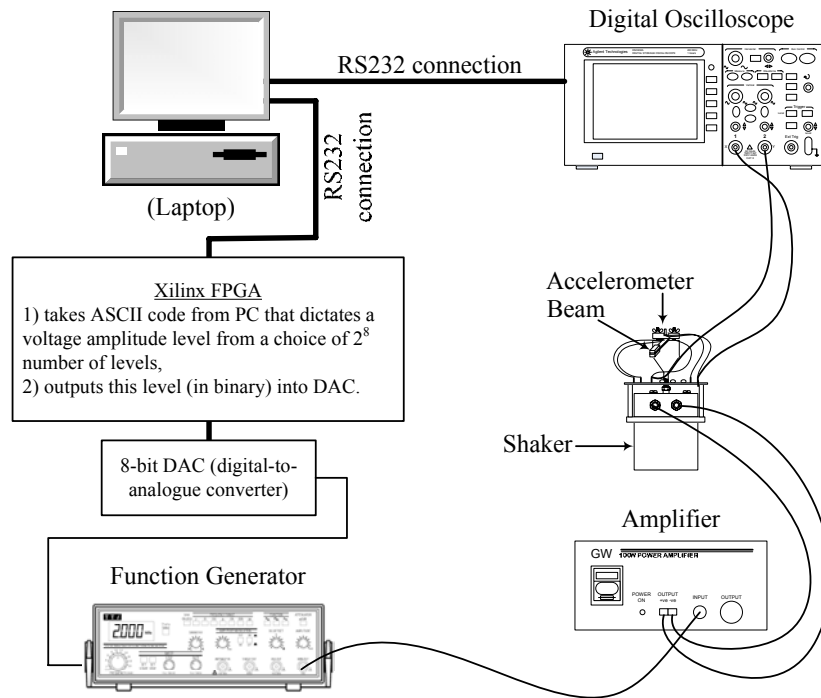


Figure 3-29 First automated test system.

All computer programming for the system of Figure 3-29 was done in Tool Command Language (TCL), and both the 8-bit DAC and the Hardware Description Language (HDL) for the Xilinx FPGA were self-designed; i.e. not commercial equipment. A basic description of operation of the system is as follows:

- 1) The PC (via a TCL program, a Xilinx FPGA and a DAC) presents an analogue voltage to the 'sweep in' input of the function generator,

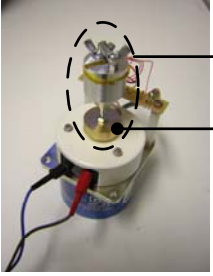
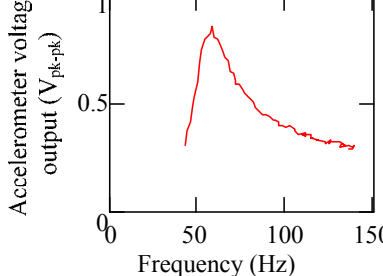
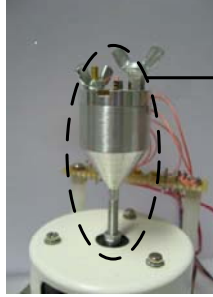
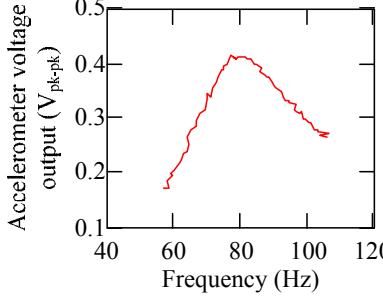
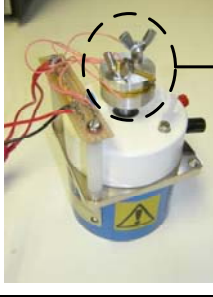
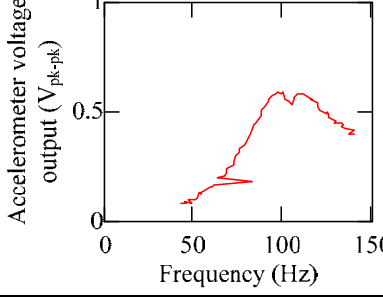

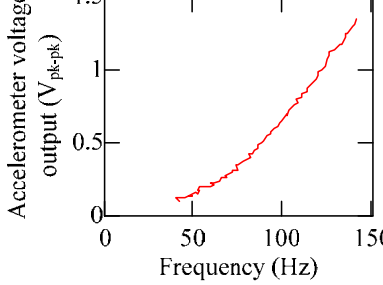
- 2) The function generator outputs a frequency that corresponds to the analogue voltage present at its input,
- 3) The PC leaves the system to settle for a time (this time was set to 2 seconds but it is adjustable),
- 4) The PC then requests voltage amplitude and frequency measurements of the beam or accelerometer response (or both) from the oscilloscope. The measurements are recorded in a comma separated values (CSV) type of file on the PC.
- 5) The PC (via the Xilinx FPGA and DAC) increases the analogue voltage amplitude input into the function generator,
- 6) The function generator responds by increasing the frequency of its output,
- 7) The PC leaves the system to settle again for 2 seconds,
- 8) The PC again requests and records voltage amplitude and frequency measurements from the oscilloscope,
- 9) The loop repeats over and over.

This system offered significant benefits over the initial test system: firstly the rate of change of frequency could be much more closely controlled because the length of time spent at each frequency increment could be specified. Secondly, both the amplitude and frequency of the voltage output of the harvesting device were automatically recorded, leading to a collection of data that could be properly analysed. Combined, these two benefits eliminated two of the four problems associated with the initial test setup; i.e. problem numbers 1 and 3 of those listed in listed in section 3.3 (page 135).

The first task for the improved system was to be of use in investigating one of the other problems mentioned in section 3.3: that of the uneven response of the shaker plus fixture (problem number 4). From the response trace recorded in the initial

investigations (see Figure 3-10 on page 129), the shaker plus fixture appeared to have some resonance effects in the 0Hz to 100Hz region. In an effort to investigate these effects, with a view to perhaps shifting or moving them further away from the test frequency range of interest, a series of different fixtures and weights were explored, the responses of which were captured using the improved test system. The results of these tests are shown in Table 3-8 in the order of heaviest fixture first.

Table 3-8 The effect of different fixtures on the frequency response of the shaker plus fixture

Type of mounting	Response of shaker plus fixture
 <p>Fixture is 75 grams (Additional brass piece)</p>	
 <p>Fixture is 39 grams (no modifications)</p>	
 <p>Fixture is 22.5 grams (shorter design)</p>	
 <p>Fixture is 6 grams (top piece only – mounted on a screw fitted to the armature)</p>	

These results clearly show that the mass of the fixture had a direct bearing on the resonance effects observed, and that lower mass values of the fixture shifted the resonant frequency of the system to a higher value. Unfortunately, from these results it appeared that it was not possible by practical means to move these resonance effects far

enough away from the test frequency range, such that they would not affect the response of the piezoelectric harvesting device. Therefore, the decision was taken to obtain another shaker.

By performing these tests, the improved test setup was proven to be capable of obtaining a frequency response. However, in addition to the non-flat frequency response of the shaker plus fixture, a further significant problem also still remained, and that was the non-repeatability of tests, which was problem number 2 discussed in section 3.3 on page 135. Since the ‘sweep in’ input of the function generator was still being used in this test system, the ‘test runs’ were still not repeatable. This is illustrated in Table 3-9, which shows a random sample of the data recorded when performing the shaker plus fixture response tests.

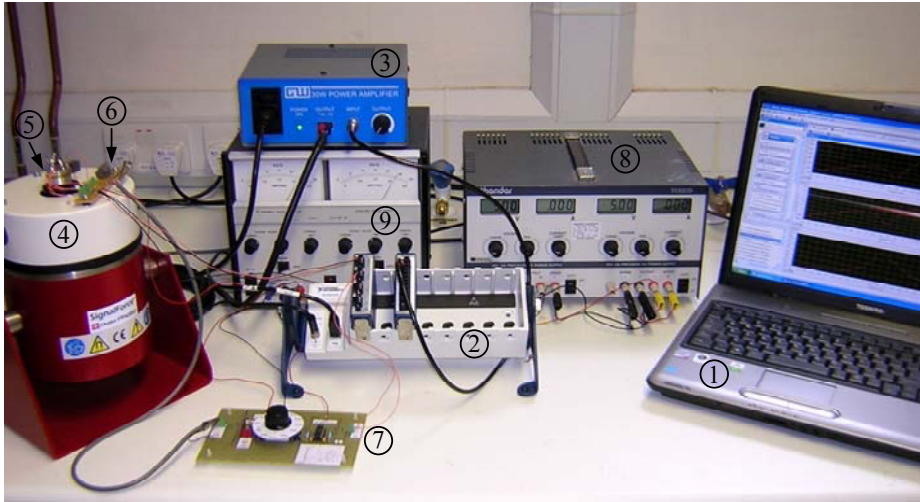
Table 3-9 A sample of the data recorded when performing shaker plus fixture response tests using the first automated test setup

DAC input	Accelerometer voltage output (V_{pk-pk})	Frequency of accelerometer voltage output (Hz)
300	0.204	56.18
310	0.212	56.65
320	0.224	59.64
330	0.236	59.06
340	0.248	60.19

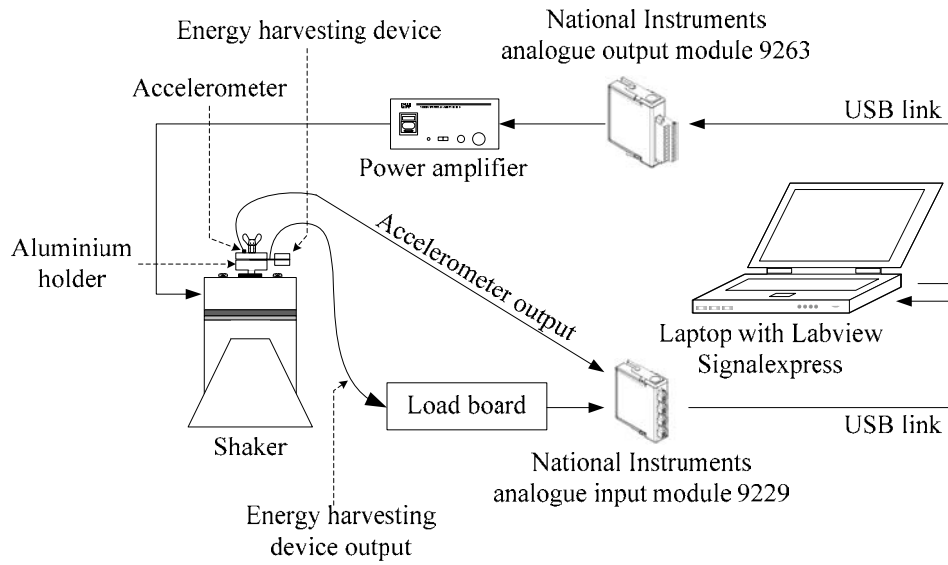
In the right-hand column, it can be seen that the frequency did not increase in even, controllable steps, for example: 56Hz, 57Hz 58Hz etc. This is simply a function of making use of the ‘sweep in’ input of the function generator, but it means that one test run cannot be made identical to another.

Following the experiences gained by using the improved automated test system to perform the shaker plus fixture response tests, it was decided that a complete overhaul

of the test system should take place in order to try to finally eliminate the problems encountered. This involved the purchase of new equipment and the development of the final version of the test setup, which largely used commercially available components. The final version of the test system developed by this author is based on National Instruments (NI; Austin, TX, USA) hardware and software. Figure 3-30 shows a photo and schematic of this test equipment setup. The laptop PC interfaces via USB to a NI CompactDAQ chassis that contains two modules: an NI 9263 analogue output module (containing a digital-to-analogue converter) that drives the power amplifier that drives the shaker, and an NI 9229 analogue input module (containing an analogue-to-digital converter) that connects to the accelerometer output, and to the energy harvesting device output via a custom-built load board.



(a)



(b)

Figure 3-30 (a) Photo of the final experimental test setup (b) schematic of the final experimental test setup.

In the photo:

- 1) = Laptop PC with National Instruments LabVIEW SignalExpress,
- 2) = National Instruments CompactDAQ chassis with 9229 and 9263 modules installed,
- 3) = Power amplifier,
- 4) = Electromagnetic shaker,
- 5) = Aluminium fixture with energy harvesting device and accelerometer,
- 6) = Circuit board for accelerometer supporting components,
- 7) = Custom-built load board,
- 8) = Power supply for accelerometer.
- 9) = Power supply for load board.

The CompactDAQ chassis has eight available slots, in which can be positioned modules from a range provided by National Instruments. From this range, the NI 9229 analogue input module was chosen for the following reasons:

- 1) It can accept input voltages of up to $\pm 60V$, which means that it is suitable for piezoelectric energy harvesting devices, whose outputs have been known to reach up to $44V_{RMS}$ (see Table 2-13 on page 65).
- 2) It has 24-bit input resolution. This means that it can measure with very high precision over a very wide range. For example, if the input signal is $\pm 60V$ (which would be a worst case scenario) the minimum voltage that could be measured would be $7\mu V$; i.e. 1 binary bit can represent $7\mu V$.
- 3) It can simultaneously sample data on all connected channels (as opposed to multiplexing data from connected channels).

- 4) It has an input impedance of $1\text{M}\Omega$ which, while not as good as the $10\text{M}\Omega$ that can be achieved with an oscilloscope input, was still favourable compared to the other choices available.
- 5) It has a sample rate of 50kSamples/s , which is more than 125 times the sampling rate dictated by the nyquist sampling theorem.

The choice of analogue output module was easier, since the number of available options from NI was not so great. The NI 9263 analogue module was chosen because:

- 1) It has a 16-bit output resolution and a $\pm 10\text{V}$ voltage range, which means that, worst case, the minimum voltage ‘increment’ that can be output is $305\mu\text{V}$. However, since the test system uses a power amplifier (for the shaker), the output from the module need only be set very low (down to a hundred or so mV), meaning that the minimum voltage increment that can be applied is more likely to be only around $5\mu\text{V}$ or so; i.e. 1 binary bit can represent $5\mu\text{V}$.
- 2) The update rate is 100kSamples/s , which is more than enough for driving at frequencies of 200Hz or below.

In this final version of the test setup, the output of the energy harvesting device is connected to a custom-built load board, which serves two purposes. Firstly, it allows different load resistor values (from $25\text{k}\Omega$ to $550\text{k}\Omega$ in $25\text{k}\Omega$ steps) to be connected to the harvesting device output. Secondly, through the use of an instrumentation amplifier, it isolates the $1\text{M}\Omega$ input impedance of the 9229 analogue input module from the energy harvesting device output, presenting instead a $10\text{M}\Omega$ input impedance to the harvesting

device output. Figure 3-31 shows a photo of the custom-built load board; a circuit schematic is given in appendix D.

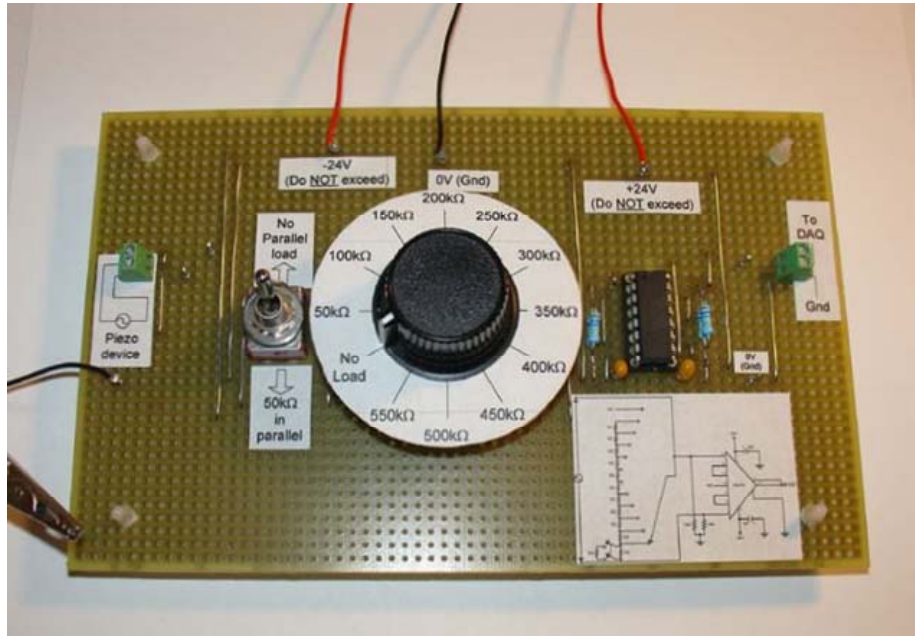


Figure 3-31 Photo of the custom-built load board.

NI LabVIEW SignalExpress, which is the software on the laptop PC, was used to build a program that performed a similar function to that provided by the previous self-built automated test setup; i.e. it performed the following logical sequence:

- 1) Set the shaker running at a specified frequency,
- 2) Wait for 2.5 seconds,
- 3) Record the amplitude of the accelerometer output waveform, and the amplitude of the energy harvesting device output waveform,
- 4) Increment the frequency to the next value specified,
- 5) Wait for 2.5 seconds,
- 6) Again record the amplitudes of the waveforms,
- 7) The loop repeats over and over until the last specified frequency is reached.

In LabVIEW SignalExpress, programs are built by assembling together a sequence of ‘steps’. For example, steps exist to create an analogue signal or to perform filtering on an acquired analogue signal. The steps used in the program developed by this author include (in sequential order): the “Create Analog Signal” step, the “DAQmx Generate” step (for sending the created signal out to the 9263 driver module), the “DAQmx Acquire” step (for acquiring signals; i.e. the response of the accelerometer and harvesting device, from the 9229 input module), and the “Tone Extraction” step (for extracting the detected frequency and amplitude of each of the input signals). Finally, a “Sweep” execution control step was wrapped around the series of sequential steps in order that once the sequence has been completed for one driving frequency value, it can be performed for the next incremented frequency value. For each of the steps, appropriate settings and configurations also had to be set. The details of the particular configuration of each step used will not be discussed here, but a JPEG of the user interface showing the configuration of each step is given in appendix E.

It can be seen from this sequence that the final version of the test setup eliminates one more of the major problems associated with both previous test setups: that of non-repeatability of tests. The final test setup version allows full control over the driving frequency, amplitude, time spent at each frequency increment and which output parameters to measure.

A further change made in this final version of test setup involved the choice of a different electrodynamic shaker. The shaker chosen is a Data Physics (San Jose, CA, USA) V20 model, that should offer a more flat response over the test frequency range, according to the data sheet, than the V2 model previously used. In order to check this, as before, the first task for the new test setup was to obtain the response of the shaker

plus fixture over the test frequency range. The response was obtained without the energy harvesting device present, as shown in Figure 3-32:

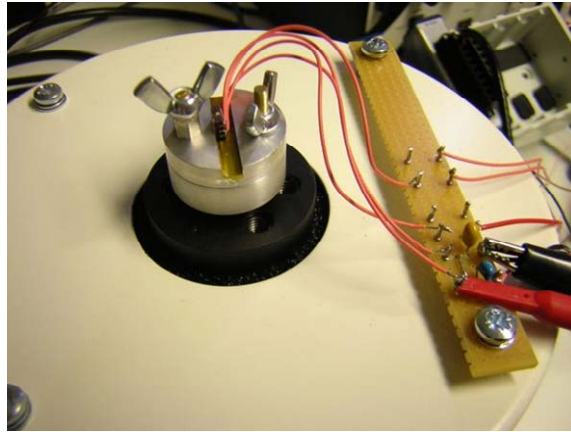


Figure 3-32 V20 electrodynamic shaker and fixture with no energy harvesting device installed.

The results of this test were as follows (the figure shows a direct printout from the NI LabVIEW SignalExpress software):

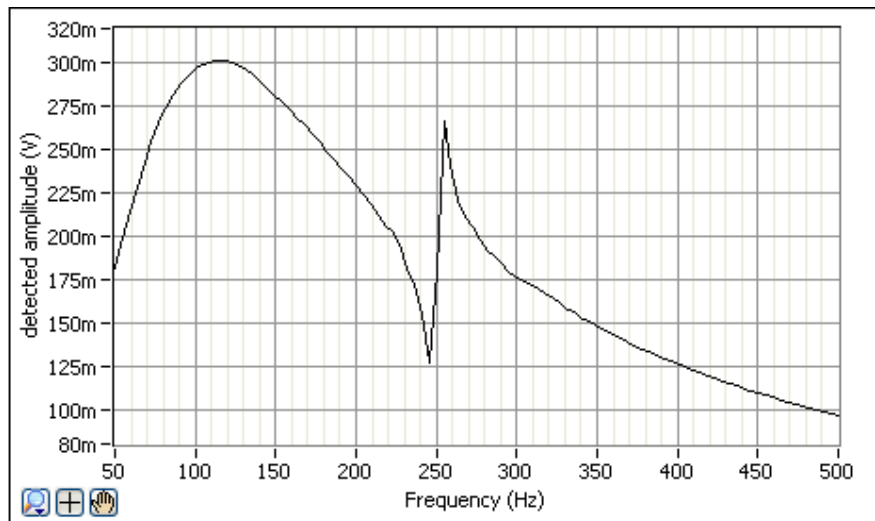


Figure 3-33 Response of V20 electrodynamic shaker plus fixture from 50Hz to 500Hz

This shows that, unfortunately, the response of the shaker plus fixture was not flat over the frequency range of interest. However, it should be noted that the response obtained here was from 50Hz to 500Hz, whereas the frequency range of interest in this thesis

extends only to 200Hz, which means that the sudden rise in amplitude that occurs around 250Hz will never be experienced by the energy harvesting device. It was decided to pursue with the V20 shaker and account for the non-flat response by other means; the process by which this was done is described in the following section.

3.7.2 Testing Procedure

The aim of this section is to detail the testing procedure that was used with the final version of test setup to test the optimised harvesting device.

LabVIEW SignalExpress software was used to first drive the shaker at a given frequency (chosen at the expected resonance frequency: 120Hz) while the amplitude of excitation was manually adjusted using the control on the power amplifier until the chosen acceleration value of $\pm 0.23g$ was recorded on the accelerometer output ($\pm 0.23g$ was chosen as representative of acceleration levels found in ambient vibration environments, as discussed in section 3.5.1).

LabVIEW SignalExpress was then used to perform a series of frequency sweeps from 30Hz to 150Hz while the load board was used to increment the value of load resistance applied to the energy harvesting device with each successive sweep. The responses from the accelerometer and energy harvesting device were recorded at every half-frequency within this range for each value of load resistance applied, resulting in two collections of data: acceleration applied to the energy harvesting device versus frequency, and voltage output of the energy harvesting device versus frequency. The data from the accelerometer showed that the acceleration applied at the fixed end of the cantilever did not exactly maintain the required value of $\pm 0.23g$ over the 30 to 150Hz range (as a result of uneven shaker dynamic response, as discussed in the previous section: 3.7.1),

but it was considered that the data from the accelerometer could be used to re-scale the output voltage data from the energy harvesting device, so that any deviation from $\pm 0.23g$ was accounted for, thus ensuring the voltage data obtained from the harvester was representative of a constant acceleration amplitude value over the whole frequency range. This re-scaling technique is only valid if the output voltage of the energy harvesting device is linearly proportional to the acceleration amplitude applied. Therefore, an experiment was performed to ensure that this was the case: an arbitrary frequency was chosen: 60Hz, and an acceleration amplitude sweep was performed from 0.045g to 0.311g while the output voltage of the energy harvesting device was recorded. The test was performed twice; each time with a different value of load resistor, the values of which were chosen arbitrarily: 250k Ω and 550k Ω . Figure 3-34 shows the results:

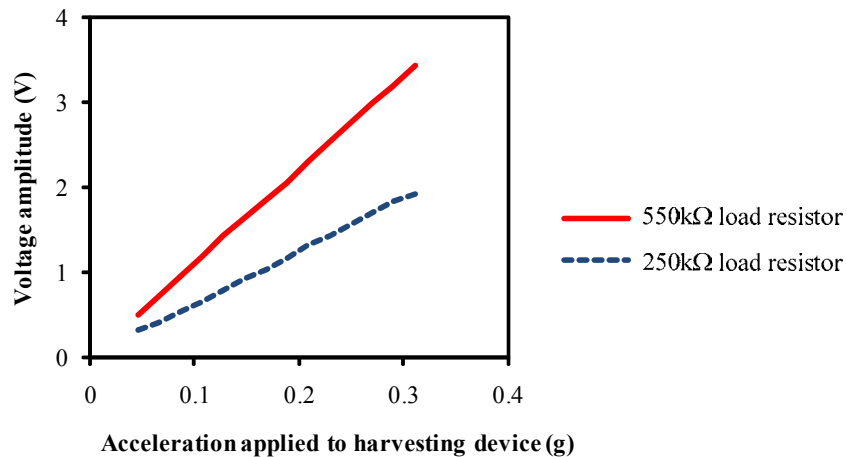


Figure 3-34 Measured output voltage of the optimised device versus vibration acceleration amplitude (frequency of vibration = 60Hz)

The results show that the output voltage of the prototype harvester is linearly proportional to the acceleration amplitude applied, which means that the re-scaling

technique is valid. To rescale the output voltage of the harvesting device, a reference data point was chosen at which the vibration acceleration amplitude applied was known to be the required application value; i.e. 0.23g. In this case the reference point was at 120Hz, since the acceleration was initially set to be $\pm 0.23g$ at this frequency. The ratio of reference acceleration value, 0.23g, to acceleration value for each of the other data points (i.e. at each half-frequency) was then calculated. This ratio was then applied, for each measurement, to the measured harvesting device output voltage. The result is that the voltage data obtained from the harvester becomes representative of a constant acceleration amplitude value over the whole frequency range. The average power output of the device could then be calculated using equation (48):

$$P_{ave_in_R}(f) = \frac{V_R(f)^2}{2 \cdot R} \quad (48)$$

Where $P_{ave_in_R}$ is the power output, R is the load resistor value, and V_R is the output voltage amplitude (peak voltage) of the energy harvesting device measured across the load resistor.

3.8 Test Results for the Optimised Design

Figure 3-35 shows the voltage amplitude (i.e. V_R) measured across each of the resistive loads for the frequency range of 70Hz to 110Hz and under a constant acceleration of $\pm 0.23g$:

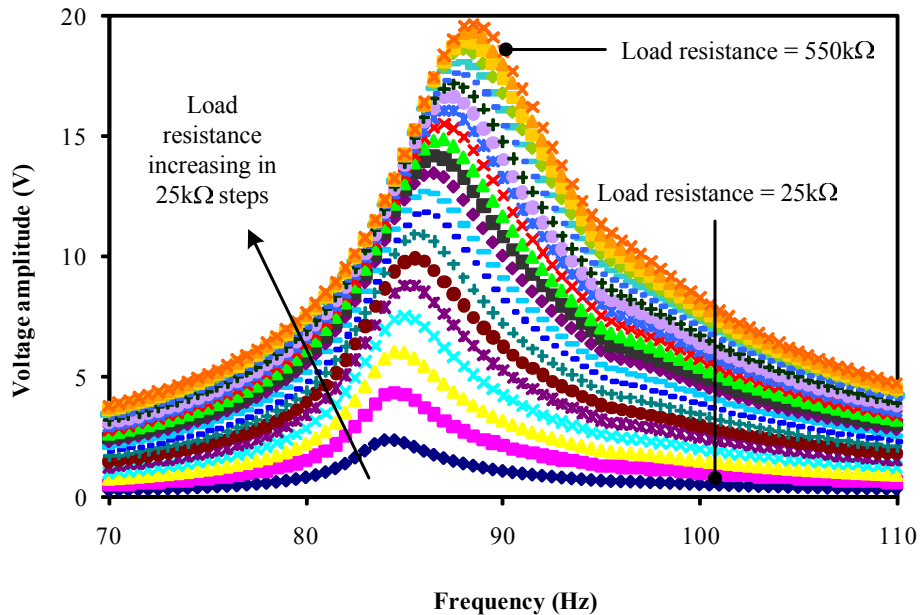


Figure 3-35 Measured output voltage of the optimised device with different load resistor values (constant acceleration of $\pm 0.23g$).

The highest output voltage measured was 19.68V, which occurred with a load of 550k Ω . Also of interest is the increase in device resonant frequency with the increase in load resistance value. Over the 25 to 550k Ω load resistance range the resonant frequency changed by 4.5Hz; it was 84Hz with a 25k Ω load, and 88.5Hz with a 550k Ω load. The effect implies that some degree of tunability of the device can be achieved by interfacing a variable electrical impedance to its output.

Figure 3-36 shows the voltage amplitude measured across the load resistor and the average power dissipated by it (i.e. useful power output from the harvesting device) versus load resistance value, where the data were extracted at the resonant frequency for each of the resistive loads (i.e. at the frequency of the peak of each curve shown in Figure 3-35):

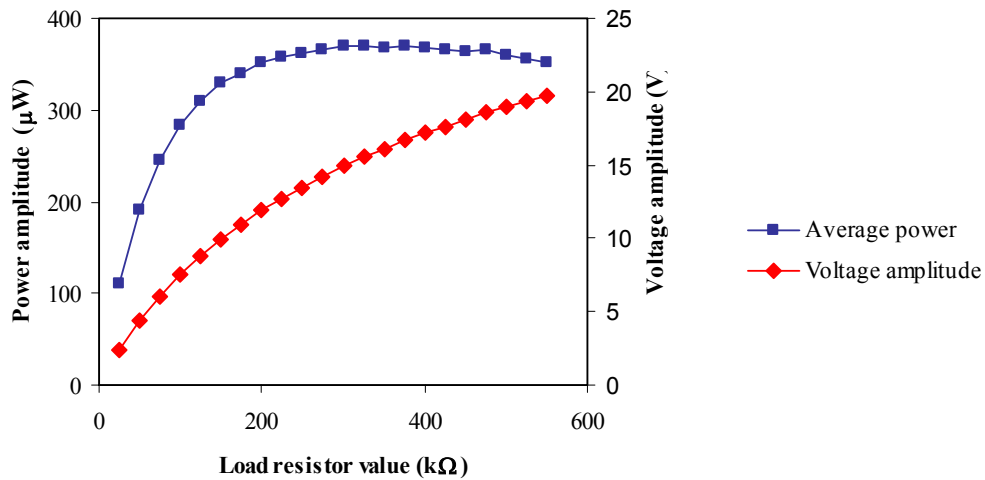


Figure 3-36 Measured output voltage and power of the optimised device versus load resistor value.

The maximum power generated was $370.37\mu\text{W}$, which occurred with a $325\text{k}\Omega$ resistive load. A voltage amplitude of 15.52V was measured at this maximum power level, and the resonant frequency of the device with a $325\text{k}\Omega$ load was 87Hz . These results compare with the experimental results from the prototype harvesting device and the simulated results from the modelling in the following way:

Table 3-10 Comparison of experimental results from the optimised device with simulated results from modelling of the optimised device and experimental results from the prototype device.

Parameter	Optimised device; experimental results	Optimised device; simulated results	Prototype device; experimental results
Maximum power output (μW)	370.37	1100	8.18
Voltage at maximum power output (V_{pk})	15.52	25.43	2.86
Optimal load resistance ($\text{k}\Omega$)	325	288.1	500
Resonant frequency (Hz)	87	120	160.29

The power obtained from the optimised harvesting device, $370.37\mu\text{W}$, is a factor of 45 greater than the power obtained from the prototype harvesting device. This is largely a result of the fact that the prototype device was fabricated without any guidance on how to arrange the geometric dimensions of the device so that a high power output could be obtained. By using the analytical model developed in this thesis, a method of determining what the geometric parameters should be in order to attain a high power output was used in the design of the optimised device, and the result is a vastly improved power output. However, even though the maximum output power obtained from the optimised device was $370.37\mu\text{W}$, this does not match the power level predicted by the simulation: 1.1mW . Some of the reason for the discrepancy may be due to slight inaccuracies in the fabrication of the device. It was fabricated by hand and it is very difficult to achieve more than a 0.5mm accuracy (see Table 3-5 on page 183 for the device dimensions that resulted from the optimisation process) by eye. Also, the addition of an amount of conductive epoxy resin on each outer electrode of the device, positioned near the fixed end of the beam for the purpose of making wired electrical connections, must have had some effect on the stiffness of the cantilever. However, aside from possible fabrication inaccuracies this author suspects that the main reason for the discrepancy between simulation and real-life is based on the fact that the model, in its present simplified form, does not take into account the backward piezoelectric coupling effect. Due to the electromechanical coupling dictated by the piezoelectric constitutive equation, which is given in equation (9) in this thesis (page 155), stress applied to the piezoelectric material results in a change in charge density displacement across the piezoelectric layers, which in turn results in the generation of an electrical field. However, the electrical field generated affects to an extent the motion of the

cantilever through the piezoelectric converse effect; i.e. as in the case for an actuator; therefore dampening the response of the generator to some degree and lessening its voltage output. This effect is not accounted for in the model, and so it is likely that the predicted values given by the simulations would over-estimate the power output of the device.

3.9 Conclusions

This chapter began with some initial experimental investigations into vibration energy harvesting, which were performed by using a prototype cantilever-based generator that was fabricated from a commonly available piezoelectric buzzer. The maximum power output of the prototype was just $8.18\mu\text{W}$, and the investigations revealed some factors to be considered regarding the test setup. Following this work, an analytical model of the device was built for the purpose of finding an expression for the power output that included all of the dimensional parameters of the device. The reason for obtaining an expression for power whose arguments included all of the dimensions was so that it could be used as an objective function in a computer-based optimisation algorithm to obtain a device design that was optimised for maximum output power.

An example of how the model can be used to optimise the device design was given in section 3.5. The generator was optimised in terms of its dimensions in order to gain maximum power output for a volume of 1cm^3 and the resulting design was fabricated. In order to eliminate some of the problems associated with the first test setup used for the prototype device, which included a non-flat response of the electrodynamic shaker assembly, non-repeatability of tests, not accounting for latency in the test system and the lack of data acquisition, two further iterations of automated test setup were constructed. The second iteration, which was based on National Instruments hardware

and software, was the final version used to test the optimised device. As per the prototype device, the tests consisted of applying different resistive loads to the output of the generator in order to characterise its power generation capability. The results were presented in section 3.8. The maximum power output achieved from the optimised vibration energy harvester was $370.37\mu\text{W}$, which is an improvement by a factor of 45 over the power produced by the prototype harvester. In summary, the following conclusions can be surmised:

- 1) An analytical model of a piezoelectric cantilever-based vibration energy harvesting device has been developed. The model results in an expression for power output whose arguments include all of the geometric dimensions of the device. The expression was successfully used as an objective function in an optimisation problem formed for the purpose of obtaining optimised dimensions for a vibration energy harvesting device with a volume restriction of 1cm^3 .
- 2) In terms of optimising to obtain maximum power output for a device volume of 1cm^3 , the developed model performed well. The maximum power output obtained, $370.37\mu\text{W}$, is state-of-the-art (see Table 2-13 on page 65) and as mentioned before, is 45 times greater than the power output of the prototype harvester, which was fabricated without the aid of a computer-based optimisation algorithm.
- 3) In addition to an improved power output, the model developed allows a target frequency to be specified as the resonant frequency of the generator. For the prototype harvester, the resonant frequency was a function of the device design; i.e. the geometry of the device and the characteristics of the materials used in its construction. However, for the optimised generator this relationship is reversed: the

device design is a function of the specified resonant frequency. This allows control over the resonant frequency of the device at the design stage.

- 4) The voltage developed across the load resistor at maximum power output was 15.52V amplitude (or $\pm 31.04V_{pk-pk}$), which is a level that is within the voltage range used for electronics. It is well above the forward bias voltage threshold of silicon conduction devices such as diodes, which are typically used to convert an AC voltage into a DC voltage.
- 5) In terms of verifying the analytical model developed, the measured values do not match the simulated values very well (see Table 3-10 on page 205). It is likely that the main reason for the discrepancy between the simulated and experimental results is the non-inclusion, for reasons of simplicity, of the piezoelectric backward coupling effect in the analytical model.

CHAPTER 4: DESIGN AND TEST OF THE NEW HARVESTING CIRCUIT CONCEPT

Given the justification for focussing on enhancing the power output of a piezoelectric energy harvesting device, discussed in sections 2.3 and 2.4, the aim of this chapter is find a way to design the harvesting circuitry (i.e. the circuitry that is usually connected to the generator to condition and/or manage the generated electrical power) such that it boosts the output power level of the device. The chapter begins with an initial experimental investigation into the operation and performance of a bridge rectifier circuit. In addition to the experimental investigation, an analysis of the operation of the bridge rectifier circuit is carried out using the circuit simulation tool Switchercad (Linear Technology, Milpitas, CA, USA). The purpose of these initial investigations was to try to ascertain an aspect in which the bridge rectifier circuit can be improved, in order to gain a higher efficiency in the AC-DC power conversion process. As a result of the experiments and simulations, the focus shifted to consider the use of the SSHI technique in conjunction with a charge pump-type circuit, and development of the new harvesting circuit concept progressed from that point forward.

The chapter is laid out as follows: the initial investigations that were carried out using the prototype harvesting device of Chapter 3 (section 3.2.1; page 122), and a bridge rectifier circuit are first described. The findings from the initial investigations are discussed and conclusions are drawn, and then a new harvesting circuit concept is proposed and the advantages of it are discussed. Following this, a description of how the proposed concept was implemented in electronics is given; i.e. a circuit design to perform the concept is detailed. The circuit is built and tested and the performance of

the concept is compared with the performance of a standard bridge rectifier circuit. The chapter ends with a discussion and conclusions of the work.

4.1 Initial Investigations

In order to conduct some initial investigations into the harvesting circuitry aspect of the project, for the purpose of finding ways to boost the power output of the piezoelectric generator, an experimental approach was first adopted. The prototype cantilever-type harvesting device that was fabricated in Chapter 3 (see section 3.2.1, page 122) was initially used as a vibration-powered generator since this was the only harvesting device available at the time of performing the investigations (the optimised device was not yet developed). The initial investigations performed were preliminary explorations, done before the focus for the harvesting circuitry aspect of the project was shifted towards the newly proposed harvesting circuit concept, which makes use of the SSHI technique. Therefore, the investigations served as a starting point in the quest to explore potential methods of enhancing the power output either by somehow boosting the voltage output of the generator, or by improving the efficiency of the power conditioning circuitry. The investigations led to the decision to focus on the use of the SSHI technique in combination with a charge pump-type circuit, which is why they are described in this thesis. The first part of this section details the experimental tests done for these investigations and the results obtained. Analysis of the results is aided by circuit simulation in order to gain an in-depth understanding of the operation of the circuit, and then the rationale behind the decision to focus on the use of the SSHI technique in combination with a charge pump-type circuit is discussed at the end of the section.

As a starting point in looking for an area in which savings in power dissipation could be made, consideration was given to the AC to DC conversion process. This is usually performed by using a bridge rectifier circuit, but it was thought that perhaps a synchronous rectifier circuit might instead prove to be more efficient. The reason why this might be so is that in traditional bridge rectifier circuits, some power is lost due to the forward bias voltage drop of the diodes, whereas in synchronous rectifier circuits MOSFETS either replace, or are put in parallel with, the diodes. This is shown in Figure 4-1:

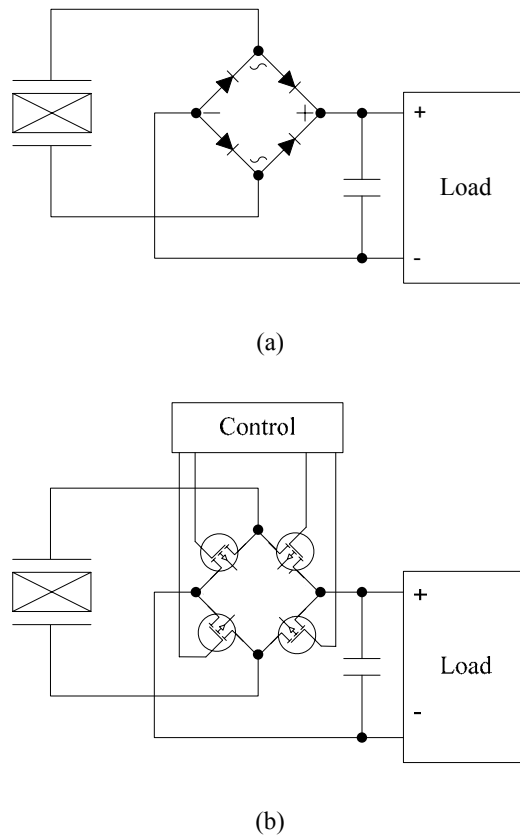


Figure 4-1 (a) Traditional bridge rectifier circuit and (b) synchronous rectifier circuit.

While MOSFETS, when switched on, also dissipate power, their power dissipation mechanism is purely resistive, and since the 'on' resistance of a MOSFET is very small,

the voltage drop across the drain-source terminals is low for small current flows, thus the power dissipation is also small. Therefore, the power dissipation of MOSFETS at low currents is much lower than that of diodes. Figure 4-2 illustrates this point:

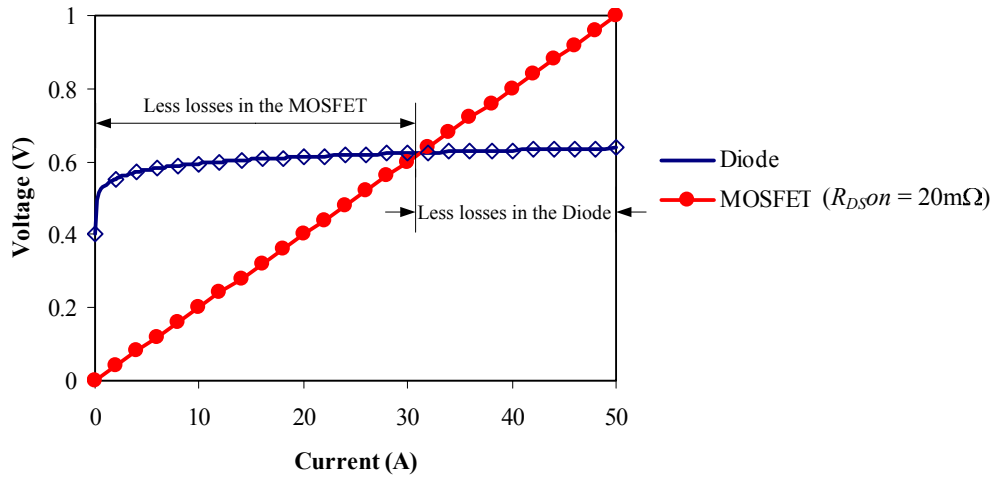


Figure 4-2 Graph showing the current versus voltage curves of a diode and a MOSFET operating in the ohmic region.

where the MOSFET current-voltage characteristic was calculated from:

$$V = I \cdot R_{DSon} \quad (56)$$

(where R_{DSon} is the “on” resistance between the drain and source terminals of the MOSFET), and the diode current-voltage characteristic was calculated from:

$$V = \frac{\ln\left(1 + \frac{I}{I_s}\right) \cdot k_B \cdot T_{amb}}{e} \quad (57)$$

Where I_s is the reverse bias saturation current of a diode, k_B is Boltzmann’s constant, T_{amb} is the ambient absolute temperature, and e is the charge carried by an electron.

Figure 4-2 shows the ‘trade-off point’; i.e. when it becomes beneficial to use a synchronous rectifier rather than a traditional diode rectifier. Indeed, first impressions

are that synchronous rectifiers seem suited for use with piezoelectric vibration energy harvesting devices, for the following reasons:

- 1) Higher supply voltages and lighter load currents enhance the efficiency of synchronous rectifiers, and in regard to piezoelectric generators, the load current is likely to be low and the voltage likely to be high (see Table 2-13 on page 65). The conditions could therefore be considered to be well-matched. Indeed, though they were not available at the time of these investigations, the results later obtained from the optimised harvesting device (detailed in Chapter 3) show that the voltage amplitude, which is synonymous with the peak voltage, at the maximum output power level of the generator was 15.52V, which is high in regard to conventional modern electronics.
- 2) Much of the power loss in MOSFETs occurs during switching: in the process of switching from off to on the MOSFET operates through a linear region, where the majority of power is dissipated. This means that the higher the frequency the MOSFET is switched at, the greater the losses. Fortunately, the frequency range of environmental vibrations (as reported in the literature) is 1Hz to 385Hz [66] [67] [68] [69], which is extremely low with regard to conventional switching circuitry, meaning there will be less losses due to this mechanism.

In order to ascertain how much energy is lost through the use of diodes used in a traditional bridge rectifier circuit, and hence to determine whether or not the synchronous rectifier direction was worth pursuing, it was thought that a simple experiment where two bridge rectifier circuits, one with normal silicon rectifier diodes and one with schottky-type diodes, could be investigated. While silicon rectifier diodes

have a forward bias voltage of ≈ 0.6 to 0.7V , schottky-type diodes are noted for their lower forward bias of $\approx 0.2\text{V}$. This means that in theory less power should be lost in the rectifier built from schottky diodes. The purpose of the first experiment was to verify this.

4.1.1 Design of Two Bridge Rectifier Circuits

For convenience and practicality when carrying out the tests the two bridge rectifiers were built in one simple switched circuit, as shown in Figure 4-3:

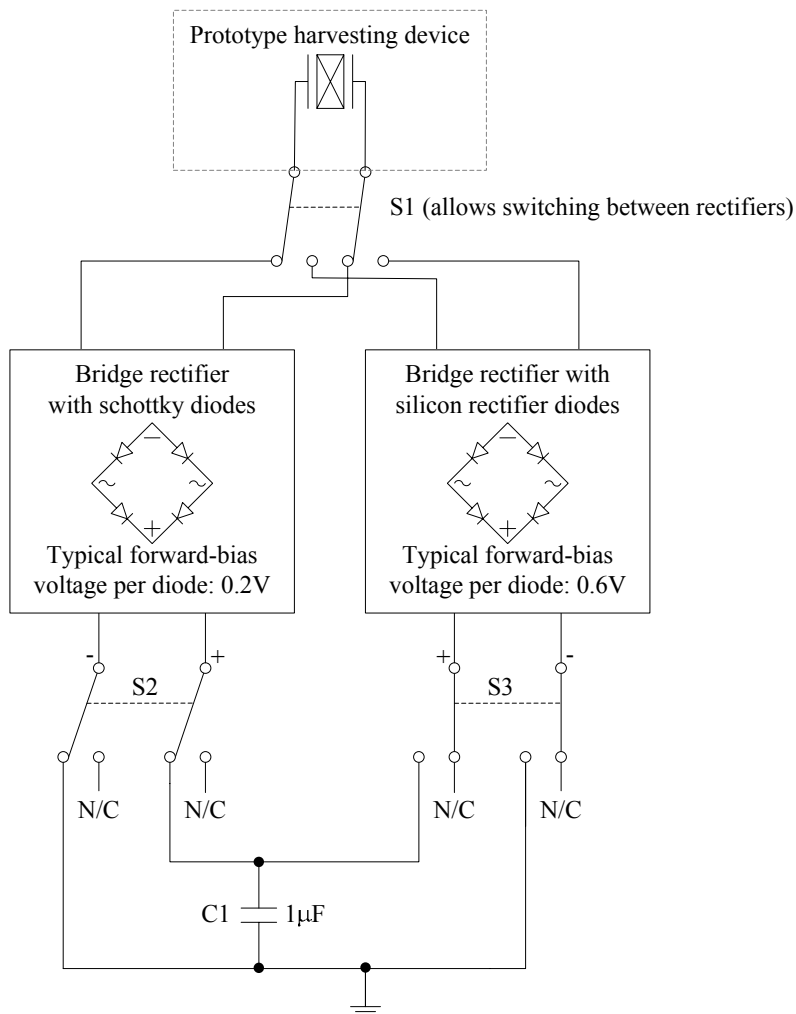


Figure 4-3 Circuit incorporating the two bridge rectifiers.

The signal diodes used were General Semiconductor (Vishay, Malvern, PA, USA) 1N4001 and the schottky diodes used were Vishay 1N5817. The $1\mu\text{F}$ capacitor was a 50V electrolytic type.

4.1.2 Bridge Rectifier Circuit Test Setup

The experimental setup shown in Figure 4-4 was used to perform the investigations with the two bridge rectifiers:

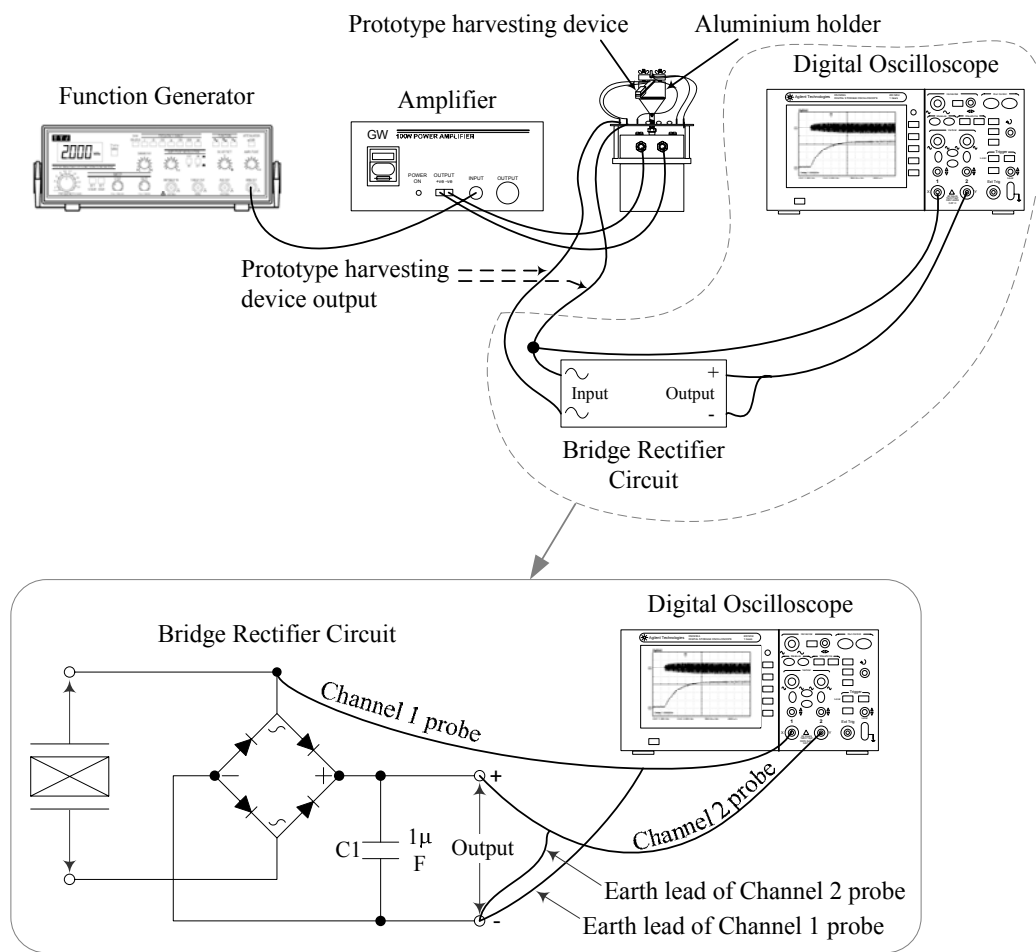


Figure 4-4 Test setup used for testing the bridge rectifier circuits.

As can be seen in Figure 4-4, the probe for channel 1 of the oscilloscope was connected to one output terminal of the prototype piezoelectric vibration energy harvesting device,

while its ground reference was connected to the minus of the DC output, and channel 2 was connected such as to measure the voltage across the smoothing capacitor of the bridge rectifier circuit. Channel 1 could not be connected directly across the output of the prototype generator (i.e. with the earth lead of its probe connected to one generator terminal and the probe itself connected to the other terminal), since this would short out one of the diodes of the bridge rectifier through the ground reference connections on the probes of the oscilloscope.

4.1.3 Testing the Bridge Rectifier Circuits

It was previously found, through experiment, that the resonant frequency of the prototype piezoelectric harvesting device was 160Hz. The method by which this was done is discussed in Chapter 3 (section 3.2.3, page 129). The function generator therefore, was set to provide an AC driving signal of 160Hz. The bridge rectifier made from silicon rectifier diodes was connected to the harvesting device through the use of switch S1 (in Figure 4-3), and the 1 μ F electrolytic capacitor connected to the bridge rectifier by using switch S3. The 1 μ F capacitor was allowed to charge to its full potential. The results of this test can be seen in Figure 4-5:

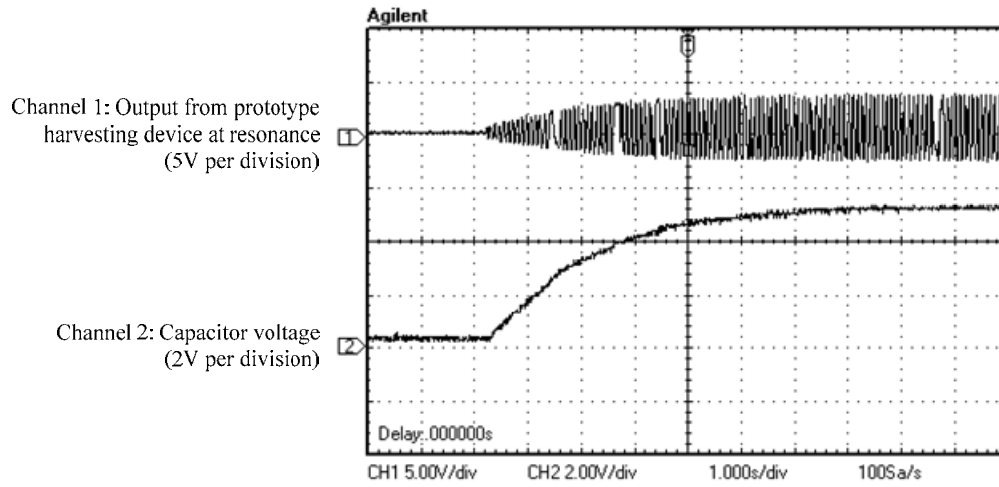


Figure 4-5 Charging curve of the $1\mu\text{F}$ capacitor using the bridge rectifier with silicon rectifier diodes.

The circuit was then disconnected from the piezoelectric generator by using S1, and the $1\mu\text{F}$ capacitor was allowed to self-discharge before the bridge rectifier made from schottky diodes was instead connected. Again, the $1\mu\text{F}$ capacitor was allowed to charge to its full potential. Figure 4-6 shows the results:

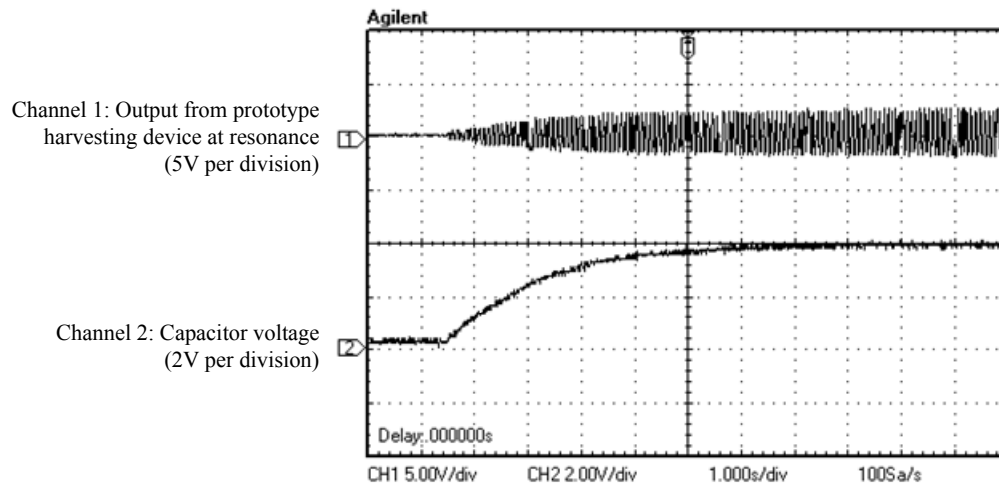


Figure 4-6 Charging curve of the $1\mu\text{F}$ capacitor using the bridge rectifier with schottky diodes.

Measured values for the voltages, and calculated energies and powers achieved are compared in Table 4-1:

Table 4-1 Comparison of measured voltages and the calculated energies and powers obtained using the two bridge rectifier circuits.

Parameter	Silicon rectifier diodes	Schottky diodes
Maximum pk-pk output voltage of prototype generator (V)	6.4	5.4
Maximum voltage, V_{max} , achieved on capacitor (V)	5.2	3.9
Total energy held (harvested) in the capacitor (calculated from $\frac{1}{2} CV^2$) (μJ)	13.5	7.6
Power available from the capacitor over 1 second (μW)	13.5	7.6
Power available from the capacitor over 5 seconds (μW)	2.36	1.45

The results show that the schottky diodes, which have the lower forward bias voltage, allowed *less* energy to be harvested into the capacitor: $7.6\mu\text{J}$, compared with $13.5\mu\text{J}$ when the silicon rectifier diodes were used.

Since the focus of the tests has thus far been on the amount of energy that can be harvested into the capacitor, the next step is to perhaps include some kind of representative load, such as a resistor connected across the $1\mu\text{F}$ capacitor, so that average power output over time can be plotted. The tests were therefore repeated, but with the addition of a variable resistive load. Conveniently, the load board that was designed for verifying the power output of the optimised device (see Figure 3-31 on page 198 and preceding accompanying discussion) could be used; however it was found that it had to be modified slightly to encompass a wider range of resistor values: $50\text{k}\Omega$ and $700\text{k}\Omega$ in $50\text{k}\Omega$ steps (rather than $25\text{k}\Omega$ to $550\text{k}\Omega$ in $25\text{k}\Omega$ steps). This modification was easy to carry out and does warrant great discussion here. For each resistive load value applied to the circuit, the voltage amplitude across the resistor was

recorded under steady-state conditions. The average power dissipated by the load resistor could then be calculated using equation (48):

$$P_{ave_in_R}(f) = \frac{V_R(f)^2}{2 \cdot R} \quad (48)$$

Where $P_{ave_in_R}$ is the average power dissipated, R is the load resistor value, and V_R is the voltage amplitude measured across the load resistor. The results are shown in Figure 4-7:

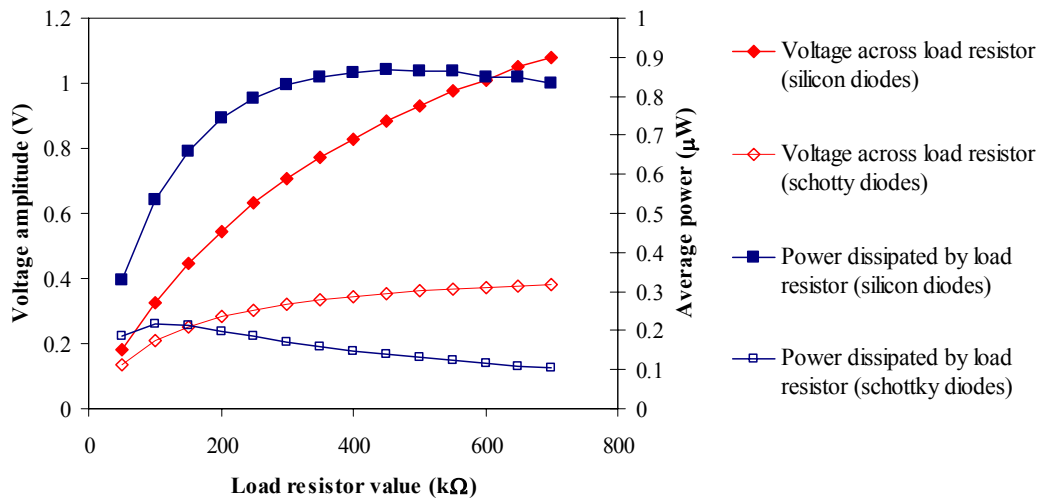
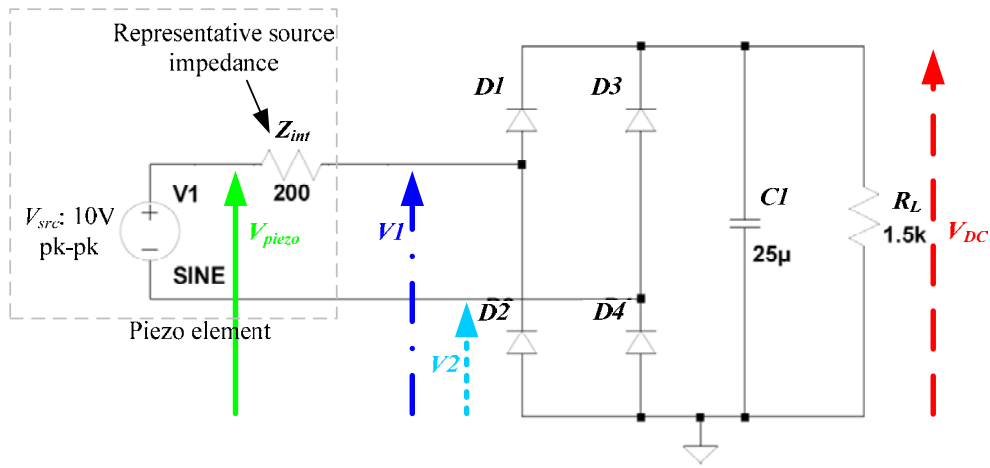


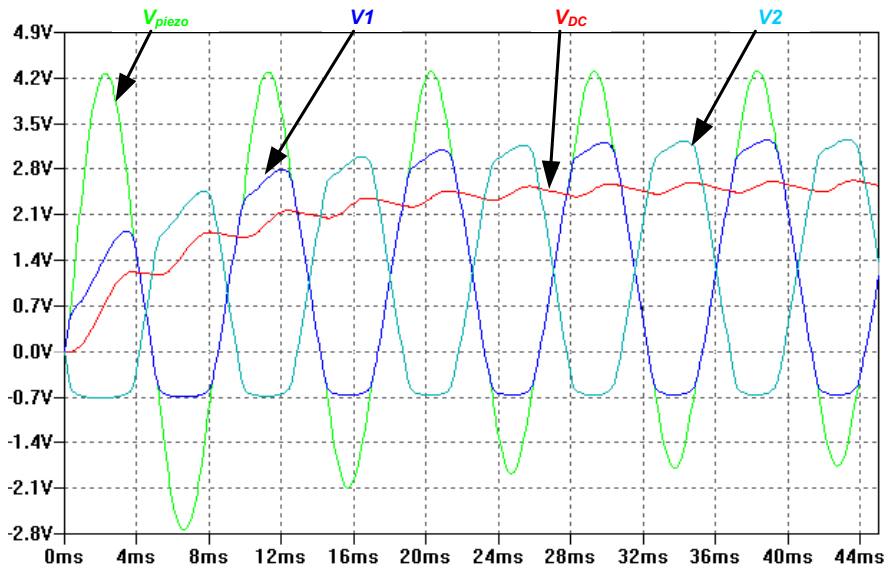
Figure 4-7 Measured voltage amplitude across, and calculated power dissipated by, different value load resistors for two different types of rectifier circuit: one with silicon rectifier diodes, the other with schottky diodes.

The results again show that *less* power was dissipated by the load resistors when the rectifier with schottky diodes was used: the maximum average value was $0.22\mu\text{W}$, which occurred with a load resistor value of 100Ω , whereas the maximum value when the silicon rectifier diodes were used was $0.87\mu\text{W}$, which occurred with a load resistor value of $450\text{k}\Omega$.

Analysis of these results can be done in a more in-depth manner by examining the waveforms obtained in Figure 4-5 and Figure 4-6. From these captured waveforms it can be seen that for both rectifier cases the AC_{pk-pk} output voltage of the harvesting device (shown on channel 1) increases steadily until it reaches a steady-state value. This pattern occurs because it takes a number of cycles of the AC output for the $1\mu F$ capacitor to charge to its full potential, and as the capacitor charges, it changes from representing a short-circuit condition to representing an open-circuit condition, thus the voltage output of the generator is initially at a decreased level and later reaches a higher, steady-state value. For the purpose of gaining further depth of understanding of the operation of the bridge rectifier circuit, a analysis will be performed by building and simulating the circuit in a circuit simulation tool, such as Switchercad (Linear Technology, Milpitas, CA, USA), as shown in Figure 4-8:



(a)



(b)

Figure 4-8 (a) Bridge rectifier circuit built in Switchercad (b) Simulated waveforms in Switchercad.

It should be noted here that the component values in Figure 4-8 (a) are not identical to those used for the experiments. The reason for this is that the purpose of the simulation is to allow insight into the operation of the bridge rectifier circuit, and for this purpose,

convenient and easy visual inspection of the voltage waveforms is important; the values were chosen such that steady-state circuit conditions could be reached in only a few AC cycles of the generator output, for convenience when viewing the various voltage waveforms. Despite the changes in component values, the way that the circuit operates remains the same. The aim is to gain an understanding of circuit operation.

Figure 4-9 shows the first cycle of the simulated waveform of Figure 4-8 (b), where the cycle has been broken down into sections A through D:

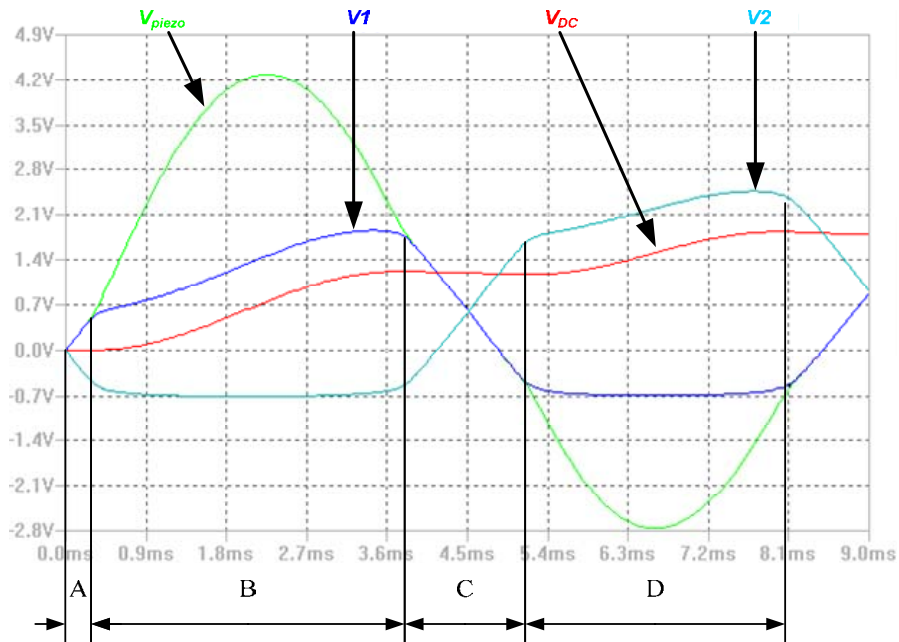


Figure 4-9 First cycle of the simulated waveforms.

Section A:

In section A, the diodes are blocking, so that the output from the voltage source representing the piezoelectric harvesting device, V_{piezo} , is essentially open-circuit. This is why the voltage at the output terminal of the generator, $V1$, simply follows V_{piezo} . Then, when the voltage across $D1$ reaches 0.6V, the diode starts conducting and the output of the generator is no longer open-circuit; it has the $25\mu\text{F}$ smoothing capacitor

and $1.5\text{k}\Omega$ load resistor across it. This can be seen at the point where $V1$ begins to separate from V_{piezo} . This is the start of section B.

Section B:

The circuit is now as follows, where the greyed out parts are non-conducting:

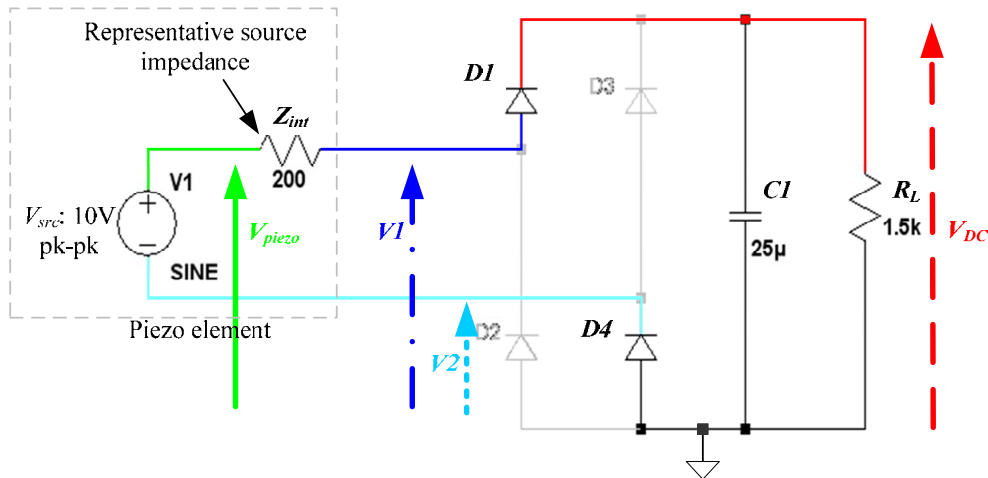


Figure 4-10 Circuit during the positive half-cycle of the piezoelectric generator output voltage.

As current flows through the $25\ \mu\text{F}$ smoothing capacitor energy is stored in the electric field around it and the voltage across it, V_{DC} , increases. Meanwhile, because diode $D1$ is now conducting, $V1$ and V_{DC} are linked by a difference of only one diode-drop between them, which is why they appear to track each other but are always 0.6V apart. Similarly, because diode $D4$ is now conducting, $V2$ and 0V are linked by a difference of only one diode-drop between them, which is why $V2$ sits at -0.6V throughout the duration of section B.

For proper analysis of section B, the voltage difference between V_{piezo} and $V1$ should also be questioned; i.e. why does it exist? This can be done by redrawing the circuit in a simplified form as per Figure 4-11 and analyzing the various voltage drops at a

particular point in time. Choosing the point in time when V_{piezo} is at its peak; i.e. at time 2.3ms in Figure 4-9, allows for a simplified theoretical analysis:

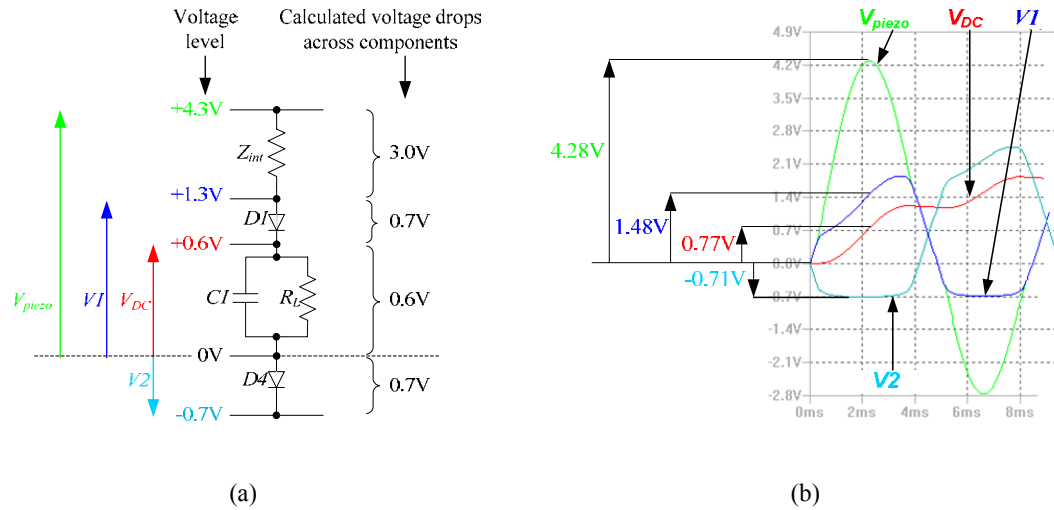


Figure 4-11 (a) Simplified circuit of the positive half-cycle showing calculated voltages across components (b) Simulated voltage waveforms for the circuit of Figure 4-10 showing simulated voltages across components.

The calculations to find the voltage drops were performed as follows:

- $V2$ sits at $\approx -0.7V$ due to the forward bias of $D4$,
- From the circuit of Figure 4-10, the pk-pk voltage of the voltage source, V_{src} , is 10V.

The amplitude of V_{piezo} therefore, can be calculated from:

$$V_{piezo} = \frac{V_{src(pk-pk)}}{2} - (\text{forward bias of } D4) \quad (58)$$

- $\approx 0.7V$ is dropped across $D1$,
- The reactance, X_{c1} , of the $25\mu F$ smoothing capacitor is calculated from:

$$X_{c1} = \frac{1}{2 \cdot \pi \cdot f \cdot C1} \quad (59)$$

Where f is the frequency of the AC output of the harvesting device and CI is the value of the smoothing capacitor. The total impedance of the capacitor and load resistor network, Z_L , can then be found from:

$$Z_L = \frac{X_{c1} \cdot R_L}{\sqrt{X_{c1}^2 + R_L^2}} \quad (60)$$

Where R_L is the value of the load resistor.

e) The remaining voltage drops; i.e. those across the source impedance, V_{int} , and across the parallel capacitor and load resistor network, V_L , can now be found from equations (61) and (62) respectively:

$$V_{int} = \frac{V_{piezo} - (\text{forward bias of } D1)}{Z_t} \cdot Z_{int} \quad (61)$$

$$V_L = \frac{V_{piezo} - (\text{forward bias of } D1)}{Z_t} \cdot Z_L \quad (62)$$

where Z_t is the total impedance of the circuit, which can be found simply from:

$$Z_t = Z_{int} + Z_L \quad (63)$$

The similarities between the calculated voltages and the simulated voltages for the circuit of Figure 4-10 are clearly evident in Figure 4-11. The analysis shows that the reason for the voltage difference between V_{piezo} and V_I (that can be seen in Figure 4-11 (b)) is the source impedance of the piezoelectric generator. In the case considered; i.e. with the component values chosen for the simulation, and for the first half-cycle of the circuit in its transient state; i.e. just after start-up, only 0.6V of the 5V available from V_{src} is ‘useful’; i.e. only 0.6V is used to power the load, which consists of CI and R_L in parallel. The losses due to the source impedance and diodes are therefore quite

significant in the first half-cycle of V_{src} after circuit start-up; together, they total 88%. However, it is expected that as the circuit reaches steady-state conditions, the losses due to the source impedance of the generator will decrease in significance, because as the smoothing capacitor, CI , charges, there will be less demand for electrical current from the voltage source, V_{src} .

Continuing the analysis of section B in Figure 4-9: after V_{piezo} peaks, it then decreases. When it approaches V_{DC} and reaches the point where it is equal to V_{DC} plus one diode drop, diodes $D1$ and $D4$ switch off again, meaning that the output from the generator is again open-circuit. This can be seen at the point in Figure 4-9 where V_I re-converges with V_{piezo} , and this signifies the beginning of section C.

Section C

During section C the diodes are off, no power is transferred from the harvesting device to the capacitor and load resistor, and the load resistor is dissipating power supplied only from the smoothing capacitor, hence V_{DC} decays a little. V_{piezo} also crosses into the negative half-cycle of the waveform.

Section D

Section D begins when $D3$ and $D2$ become forward-biased, and it follows the same pattern as section B but with one major difference: the capacitor is still holding some residual charge from the charging it received during section B (minus the slight decay that occurred during section C). In section D, the circuit is as follows:

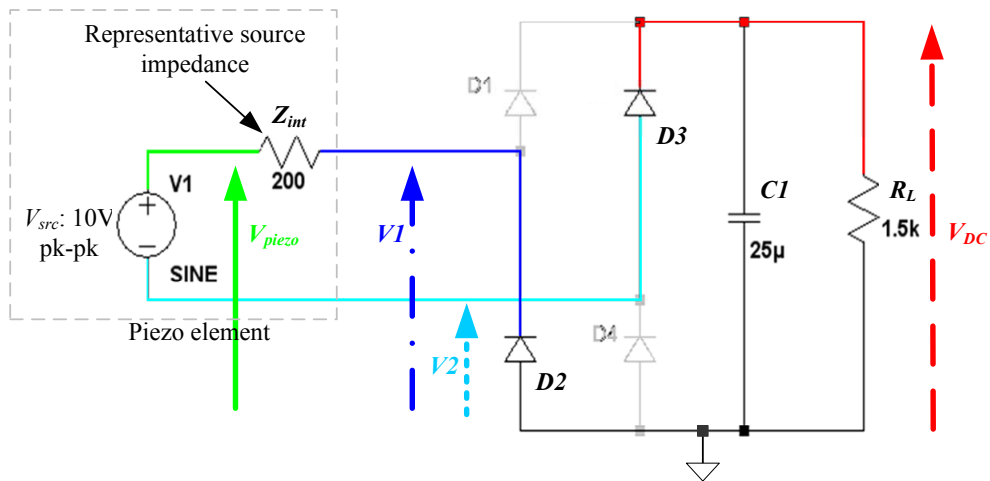


Figure 4-12 Circuit during the negative half-cycle of the piezoelectric generator output voltage.

Performing a similar analysis to that given for section B, the calculated and simulated voltages across the circuit components are as follows:

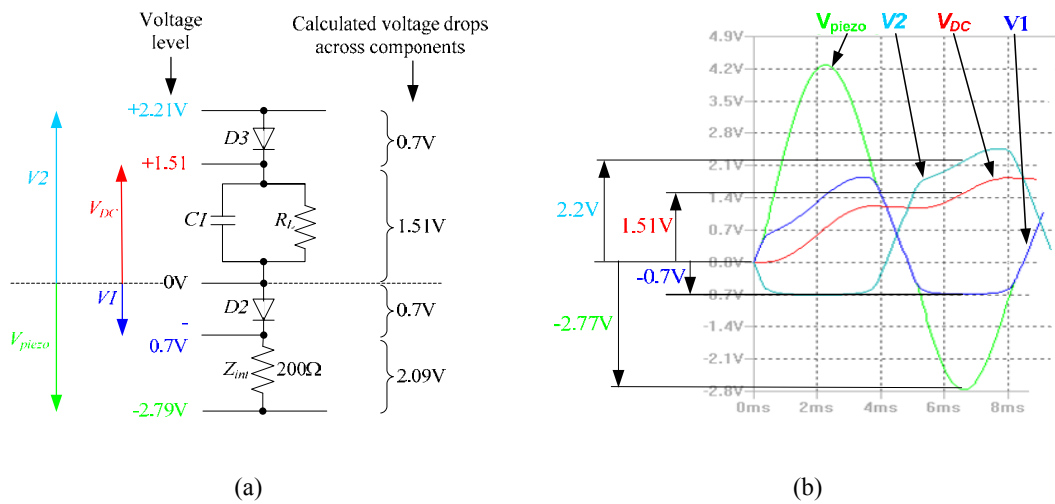


Figure 4-13 (a) Simplified circuit of the negative half-cycle showing calculated voltage drops across components (b) Simulated voltage waveforms showing simulated voltage drops across components.

Again, it can be seen that some of the voltage available from the piezoelectric generator is dropped across the internal source impedance of the generator, though not as much as

in the case of the first half-cycle of the AC output of V_{src} , because of the residual charge held in CI .

In order to prove that the amplitude difference between V_{piezo} and $V1$ (or V_{piezo} and $V2$, depending on whether the positive or negative cycle is being considered) is due to the source impedance of the piezoelectric generator, the value of the source impedance, Z_{int} , was changed in the simulation tool from 200Ω to 50Ω . Figure 4-14 shows the resulting waveforms for the two circuits:

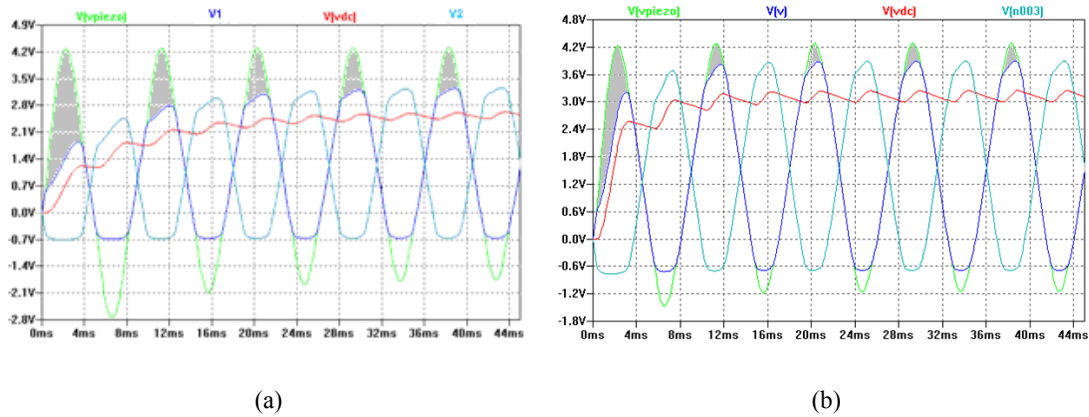


Figure 4-14 Simulated waveforms of the bridge rectifier circuit; (a) with a piezoelectric generator that has 200Ω source impedance (b) with a piezoelectric generator that has 50Ω source impedance.

It can clearly be seen that the difference between V_{piezo} and $V1$ (indicated by the shaded areas) has reduced, and V_{DC} reaches a higher voltage level in the circuit with 50Ω source impedance: around 3.11V , compared to 2.39V in the circuit with 200Ω source impedance. In addition, this higher voltage level is reached more quickly. Figure 4-14 also illustrates the fact that less power is dissipated by the source impedance of the generator as the circuit nears steady-state operating conditions.

The analysis just performed identifies three mechanisms by which power transfer from the harvesting device to the load can be inhibited, as follows:

- 1) Some of the voltage generated by the piezoelectric generator is dropped across its own intrinsic source impedance. This means that some power dissipation occurs in the harvesting device itself. This is perhaps not a surprise, since all forms of electrical supply have some form of source impedance. For example, it is well known that loading a battery heavily to obtain a high current output results in the battery becoming warm due to the power being dissipated by its internal source impedance.
- 2) Power is also lost through dissipation in the diodes of the rectifier. The forward bias voltage of the diodes themselves contribute to power loss, and this loss mechanism, since the forward bias voltage is fixed, becomes more significant if the output if the output voltage of the piezoelectric generator is low (around 1 to a few volts) rather than high.
- 3) The third reason for a potentially low amount of useful power delivery from the harvesting device is the bridge rectifier configuration itself. In the bridge rectifier circuit there is a 'charging' or 'transient' period, where the AC generator charges the smoothing capacitor before steady-state circuit conditions are reached. As the capacitor charges, the output of the piezoelectric generator is in the open-circuit condition more and more, because the diodes are in their reverse-bias state more and more. This can be seen in Figure 4-15:

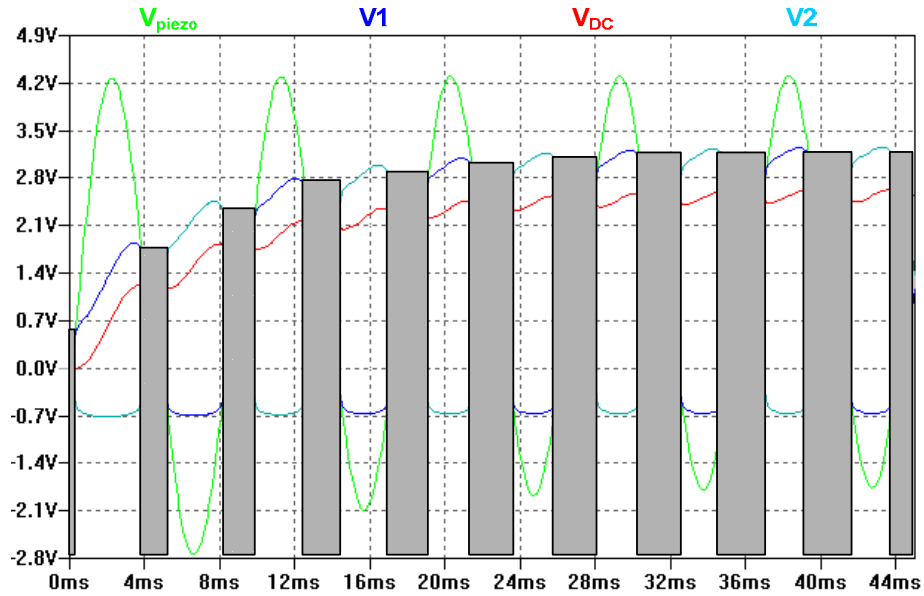


Figure 4-15 Operation of the circuit showing times (shaded) when no power is transferred from the piezoelectric harvesting device to the smoothing capacitor and load resistor.

During the times when the diodes are in the reverse-bias condition (indicated by the shaded areas), there is no power transfer between the piezoelectric generator and the capacitor and load resistor. It can be seen that when the circuit reaches steady-state operation, the proportion of time spent when there is no power transfer is at its greatest (the shaded areas are at their widest), and this is the main reason why this author believes that the bridge rectifier is not the most efficient method of converting AC into DC for an energy harvesting application.

Referring back to the experimental results given in Figure 4-5 and Figure 4-6, and Table 4-1 and Figure 4-7 (pages 218 to 220), the aim was to determine whether or not diodes with a lower forward bias voltage would allow more energy to be harvested into the $1\mu\text{F}$ smoothing capacitor than diodes with a higher forward bias volt drop. From Table 4-1 it appears that the schottky diodes, which have the lower forward bias voltage, allowed

less energy to be harvested into the capacitor: $7.6\mu\text{J}$, compared with $13.5\mu\text{J}$ when the silicon rectifier diodes were used. This translates into $7.6\mu\text{W}$ of available power for a time of 1 second, in comparison with $13.5\mu\text{W}$ of available power for 1 second when the silicon rectifier diodes are used. From Figure 4-7 also, less average power was dissipated by the load when the schottky diodes were used: a maximum average of $0.22\mu\text{W}$, compared with a maximum average of $0.87\mu\text{W}$ when the schottky diodes were used.

This is the opposite of the expected outcome. Since, in the case of energy stored in the capacitor (i.e. no load), the decrease in the power available from the capacitor corresponded with a decrease in the maximum voltage, V_{max} , achieved across it: from 5.2V with the silicon rectifier diodes to 3.9V with the schottky diodes, a hypothesis for this result (given the knowledge obtained from the analysis that has just been performed) is that more current is being taken either by the internal source impedance of the generator or by the diodes in the schottky bridge rectifier circuit. Since the source impedance of the generator is unlikely to have changed between experiments, the focus is directed to the diodes. An ideal diode in the reverse-bias condition does not allow current to flow through it. However, in reality, there is always a small amount of reverse leakage current; this parameter is sometimes referred to in diode data sheets as ‘the maximum average reverse current at rated DC blocking voltage’, and for the two different kinds of diodes used in the initial investigations performed here, these values are specified as below:

- 1N4001 silicon rectifier diode: $5\mu\text{A}$ for a reverse voltage of 50V at 25°C ,
- 1N5817 schottky diode: 1mA for a reverse voltage of 20V at 25°C .

It is not hard to imagine that even when scaled down to the reverse voltage levels that the diodes experienced in these investigations (3.2V was the maximum measured amplitude), this difference in reverse leakage current values is significant enough to cause the voltage output of the harvesting device (since the prototype generator has a high source impedance: $\approx 500\text{k}\Omega$ according to the results shown in Figure 3-12 of Chapter 3) to drop from $6.4V_{\text{pk-pk}}$ with the signal diodes, to $5.4V_{\text{pk-pk}}$ with the schottky diodes. Similarly, this difference in reverse leakage current could account for the lower power dissipations of the load resistors when the schottky diodes were used, compared with when the silicon rectifier diodes were used.

4.2 Conclusions of the Initial Investigations

The initial investigations, which comprised experiments with the prototype harvesting device and two types of bridge rectifier circuit, served as a starting point in the quest to explore potential methods of enhancing the power output of the harvesting device; either by somehow boosting the voltage output of the generator, or by improving the efficiency of the power conditioning circuitry. Several outcomes of these investigations were observed:

Regarding the improved performance of the bridge rectifier with the silicon rectifier diodes:

The result was the opposite of that expected: the power harvested using the bridge rectifier made from schottky diodes, which have a lower forward bias voltage than silicon rectifier diodes, was less than the power harvested using the bridge rectifier made from silicon rectifier diodes. It is likely that the reason for this is the higher reverse leakage current of the schottky diodes. Unfortunately, this causes difficulties in

proving the postulation that lower voltage drops across the switching components; i.e. the diodes (or MOSFETs in the case of a synchronous rectifier) of the bridge rectifier lead to more efficient AC-DC conversion. However, the in-depth circuit simulation analysis of the bridge rectifier circuit, performed as a result of the experimental investigation for the purpose of understanding the circuit further, did lead to some insight into the direction that might be taken next, as described in the next paragraph.

Considerations concerning the bridge rectifier circuit in general:

From the analysis of the bridge rectifier circuit presented in the previous section, it appears that this type of circuit is perhaps not the most efficient method of converting AC to DC for an energy harvesting application. There are two reasons for this: (1) the power loss caused by the diodes, and (2) because under steady-state conditions, the output of the piezoelectric generator spends much of its time in the open-circuit condition, where there is no power transfer from generator to load. Another mechanism for power loss was identified in the analysis: power is lost through dissipation by the source impedance of the generator, although it could be argued that some power loss will occur by this mechanism regardless of whether the bridge rectifier circuit is used or not; i.e. it will still occur if another circuit is used in place of the bridge rectifier. Point number (2) mentioned above would be true even if a synchronous rectifier were used, employing MOSFETS in place of the diodes. It was considered therefore, that it might be more beneficial if a circuit could be developed where energy is taken during the whole of each AC voltage cycle of the piezoelectric generator output, rather than for just part of it.

A second consideration regarding the bridge rectifier circuit, is that the output of the circuit is not in the format that is preferred for most electronic devices and systems: the output of the bridge rectifier circuit is simply DC (albeit with a certain amount of ripple), whereas most electronic devices and systems prefer a regulated DC supply. The distinction is that in a regulated DC supply the voltage remains constant regardless of the amount of current taken, whereas in the case of a simple bridge rectifier the output voltage cannot maintain a constant value; it either rises with a very light (high impedance) load or decreases with a very heavy (low impedance) load, and a change in amplitude of the AC supply side (which could feasibly occur in vibration environments!) directly influences the DC output amplitude.

A further consideration concerning the bridge rectifier-type circuit is that if the synchronous rectifier route were to be followed, potentially complex voltage detection circuitry might be required for the purpose of detecting the zero-volt crossover point of the piezoelectric generator output voltage waveform. In addition, switch driving circuitry would also be required for the purpose of driving the MOSFETs. The combined power consumption of these two additional circuit functions might negate the efficiencies made by replacing the diodes with MOSFETS. It was therefore considered that if the inclusion of voltage detection circuitry and switch driving circuitry is for some reason a necessity, then the rewards probably need to be greater; i.e. need to lead to more efficiencies or a greater boost in the output voltage of the generator than can be achieved by the simple elimination of the ≈ 0.6 -to- 0.7V forward bias voltage of the diodes.

Considering the above discussion, it was considered that a finding a method by which power can be harvested during the whole of each AC voltage cycle of the piezoelectric

generator, rather than for just part of it, should constitute a major driving factor behind any further investigations involving the harvesting circuitry aspect of the project. In this way it was considered that the energy output could be enhanced. In addition, it was deemed necessary that some method of converting the power into a regulated DC format needs to be developed, so that the power becomes truly useful; i.e. so that it can readily be used for powering electronic devices and systems.

As an aside, an interesting observation to note is that around the time of establishing this reasoning, a work appeared in the literature that did focus on the development of a synchronous rectifier implemented in CMOS for the purpose of achieving a more efficient AC-DC converter. Dallago et al [145] developed a voltage doubler rectifier circuit whose two diodes were replaced with MOSFETs which were driven from comparators. The whole circuit was implemented in BCD6s technology, and the result was an AC-DC converter with 91% efficiency [145]. The efficiency of a standard bridge rectifier can reach 81.2% [146]. Later in the literature (in 2008), Seeman et al. [147] also used a synchronous full wave rectifier for use with an electromagnetic energy harvester and achieved an efficiency of 88%.

4.3 A Proposed New Harvesting Circuit Concept

4.3.1 Background

Considering the discussion given in the conclusions at the end of the previous section, this author decided at this stage to try a different approach for the harvesting circuitry part of the thesis. Looking at the power consumptions of electronic devices and systems (some of which are given in Figure 2-1 on page 28), and looking at the present power output capabilities of current state-of-the-art harvesting devices (reported in Figure 2-14 on page 70), there remains a mismatch. The initial investigations done so far have assumed that an application system, e.g. a wireless sensor node or portable device, will be powered continually from the harvester whenever vibration is present. However, given the mismatch in power requirements versus power availability, it perhaps makes more sense to instead build up an energy reserve over time, such that a large energy reservoir is eventually obtained, from which the application device can then be powered. This makes sense from a vibration environment point of view also: given the uncertain nature of some vibration sources, much of the uncertainty could be taken out of the supply to the application. The energy reservoir, when full, could be turned into a regulated DC supply for a known length of time; the only uncertainty remaining being how long it would take to charge the next iteration of the charge/discharge cycle of the reservoir, since this is the process that would then depend on the vibration environment. The application system itself is therefore given a degree of protection from the uncertainties of the vibration environment. Other advantages of this approach are that a higher power application could be powered than would otherwise be possible with a continuous powered approach, and if the application does not need to switch on often, sufficient reserves could be built up to ensure a supply is always available when needed.

This differs from the continuous operation case in that if the application system is powered almost directly from the harvesting device (e.g. with just an AC-DC converter in between), the times when the application might need to switch on may not necessarily correspond with the times when sufficient vibration is present. For these reasons, from this point forward this author made the choice to adopt the philosophy of collecting charge over time in a storage reservoir, such that when the reservoir is full, it can be disconnected from the charging circuit and connected instead to an end application system; and the process can be repeated with the reservoir being alternately connected to the charging circuit and application system so that it is repeatedly charged and discharged.

4.3.2 The New Concept

In an effort to establish a method of harvesting power from the piezoelectric generator during the whole of each AC output voltage cycle, the idea of a charge pump-type circuit was considered, where the output of the harvesting device is connected directly to a load capacitor, as shown in Figure 4-16:

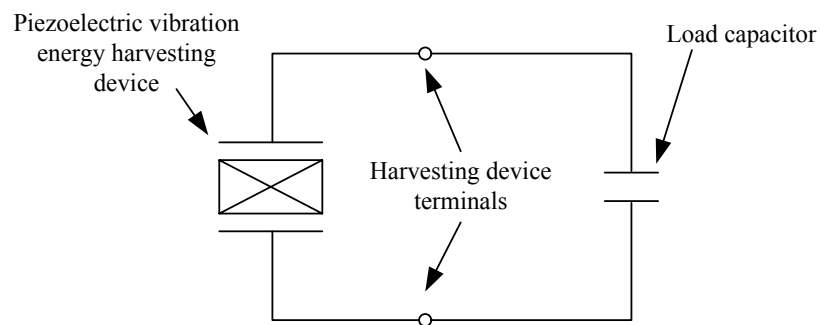


Figure 4-16 Piezoelectric vibration energy harvesting device connected directly to a load capacitor.

It was considered that the value of the load capacitor should be the same as the capacitance of the harvesting device, in order that maximum power be transferred in accordance with impedance matching theory. The impedance of the harvesting device can be found from equation (51), in Chapter 3, on page 170. Since the values of capacitance are the same, and since the AC frequency of the supply is of one value for both capacitances, the load impedance value is, in theory, guaranteed to match the source impedance value. In this configuration, as stress is generated in the piezoelectric material as a result of deflection of the energy harvesting device through application of an input vibration, the charge generated by the piezoelectric mechanism is distributed equally between the capacitance of the harvesting device and the capacitance of the load capacitor. It could be considered advantageous then to disconnect the load capacitor from the harvesting device at the point in time when the maxima (or minima) of the output voltage waveform of the harvesting device is reached, in order that the charge stored in the load capacitor can be extracted and held in an electrical storage medium, e.g. a supercapacitor or battery. If two load capacitors are used: one for collecting charge during the positive half-cycle of the harvesting device voltage output, and one for collecting charge during the negative half-cycle, then the result could be an accumulation of charge over time in two electrical storage mediums, as shown in Figure 4-17.

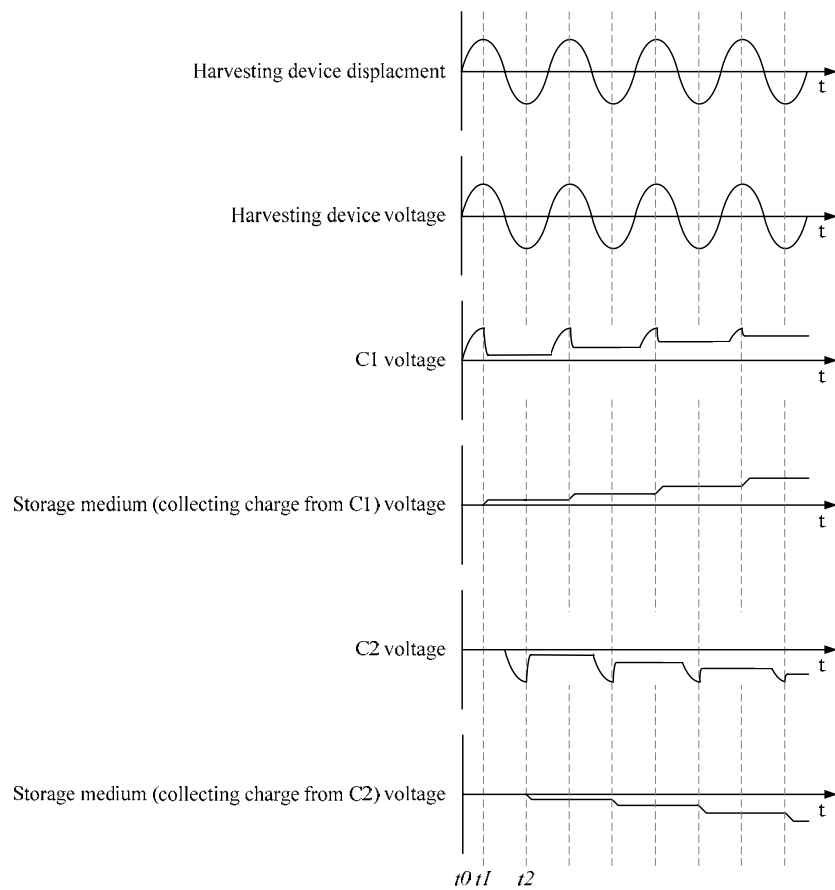
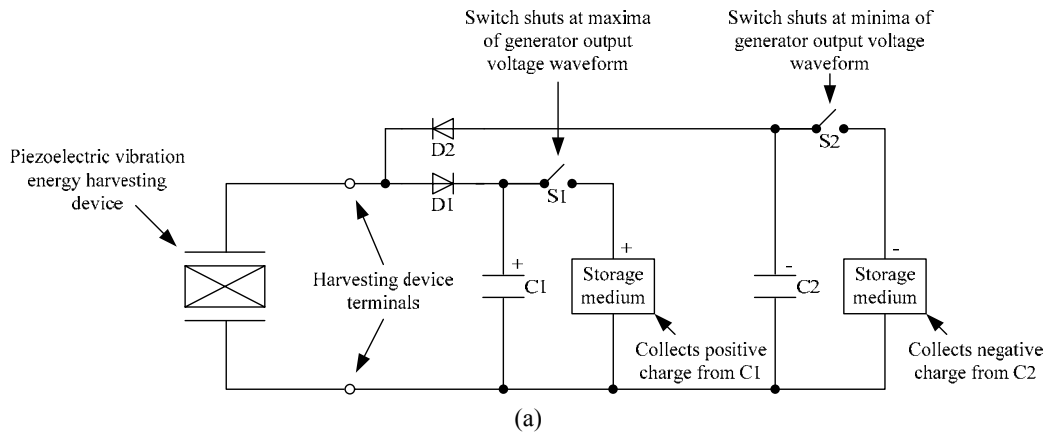


Figure 4-17 (a) Charge pump circuit for collecting positive generated charge in one storage medium and negative generated charge in another storage medium (b) Hypothesised voltage waveforms for the circuit showing charge accumulation in both storage mediums.

However, the problem remains with this circuit that charge is not harvested throughout the whole of the piezoelectric generator AC output voltage cycle. During the second half of the positive half-cycle and during the second half of the negative half-cycle, which are both times when the voltage output is decreasing in amplitude, the piezoelectric generator is again essentially in an open-circuit condition, thus no power transfer occurs during these times.

It was considered that the problem could be resolved if the charge storage concept of Figure 4-17 was implemented in conjunction with another technique which has been previously reported in the literature: the SSHI technique, the operation of which is described in section 2.6.2.2.1 (page 108) of this thesis. As described in section 2.6.2.2.1, the SSHI technique results in an artificial increase in the voltage output of the piezoelectric generator, leading to a related increase in the transfer of power. It does this by inverting the voltage on the piezoelectric generator at every maxima and minima of the generator displacement, through the use of a switched inductor placed electrically in parallel with the capacitance of the piezoelectric harvesting device. Figure 2-34 on page 108 shows the general working principle of the technique (repeated here for clarity):

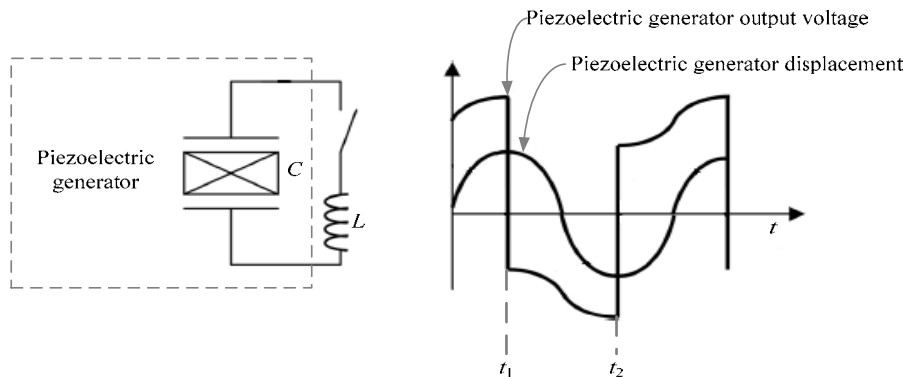


Figure 2-34 Required circuit components and resultant voltage waveform for the SSHI technique [1].

The switch is closed at times t_1 and t_2 (at the maxima and minima of transducer displacement), allowing the inductor and capacitance of the piezoelectric generator to form an oscillator. The value of the inductor is chosen such that the oscillator frequency is much higher than the generator vibration frequency. After a half-period of the LC oscillator the polarity of the charge on the generator has been reversed, and the switch is then opened. Since the SSHI technique instantaneously inverts the voltage at the maxima and minima of the piezoelectric generator displacement, it could be considered that the voltage output of the generator when using this technique has in effect phase-shifted such that it becomes leading by 90° . This is illustrated more clearly in Figure 4-18:

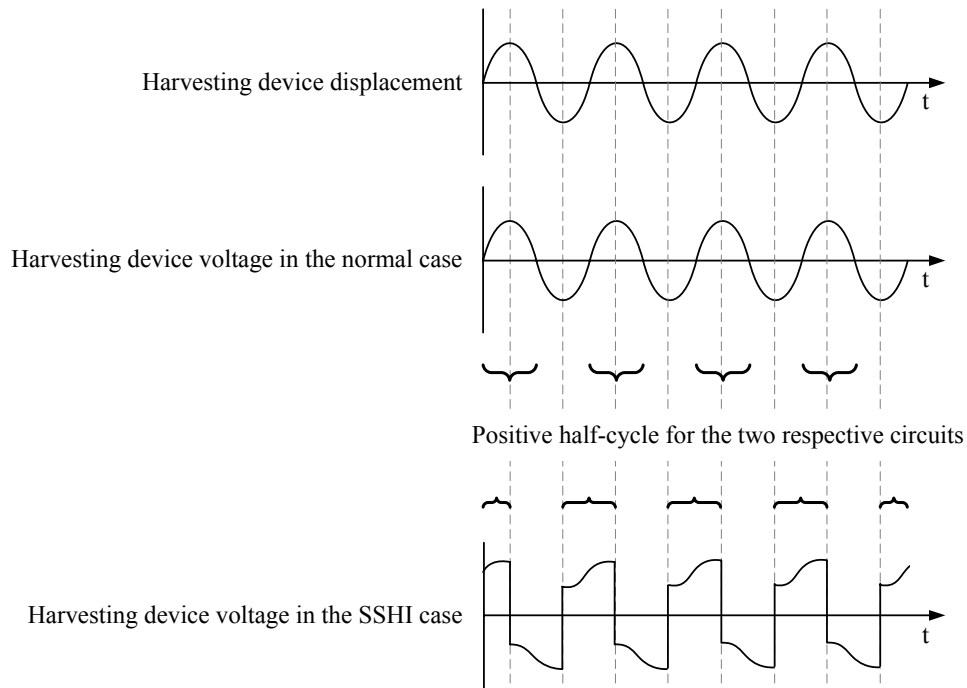


Figure 4-18 Comparison of the voltage output waveforms of the piezoelectric generator in the normal case and in the SSHI case.

This characteristic of the SSHI technique has the distinct advantage that, except for during the (almost instantaneous) charge inversion process, the output voltage of the

generator is always increasing. Since essentially the amount of time spent where the voltage is decreasing in amplitude is zero, use of the charge pump circuit of Figure 4-17 in the SSHI case allows charge to be harvested during the whole of the piezoelectric generator AC output voltage cycle. In addition, the voltage boosting effect of the SSHI technique can be utilised. The charge pump and SSHI functions therefore become mutually conducive to the aim of enhancing the power output of a piezoelectric generator.

The combined circuit also offers one other distinct advantage over the bridge rectifier circuit: since the circuit results in charge accumulation in two storage mediums (one holding positive charge accumulated from C1, and the other holding negative charge accumulated using C2) it is a simple matter to connect these two storage reservoirs, when they are both fully charged, such as to form a circuit from which a switched-mode DC converter can be supplied, as follows:

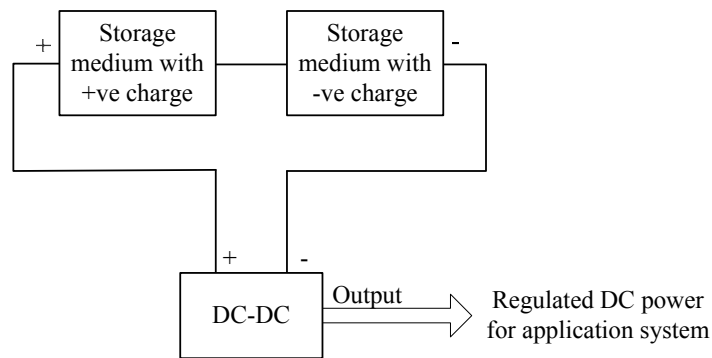


Figure 4-19 Circuit that can be formed to supply a DC-DC converter.

The advantage of powering a DC-DC converter from a charge reservoir is that it ensures enough current is available for proper operation of the converter. Since a switched-mode DC-DC converter operates by pulse-width modulation of its power input (by means of a solid state switch), the current taken from the power source supplying the

converter is not constant; rather, more current is taken when the solid state switch is in its 'on' state (i.e. when power is switched into the converter) than when the switch is in its 'off' state. Such an uneven current load is best supplied from a capacitive reservoir with a low equivalent series resistance (ESR), since the capacitor is able to provide the 'gulps' of current required for proper operation of the converter. If the DC-DC converter is to be supplied from a bridge rectifier powered from a piezoelectric generator, any variations in the frequency and amplitude of the vibration source might affect the operation of the converter, since it is possible that the charge provided by the smoothing capacitor will no longer be adequate.

In regard to an appropriate choice of storage medium, it is considered that for this application a pair of supercapacitors would be preferable to a pair of batteries. This is because, in addition to the above discussion on the use of a capacitive reservoir for powering a DC-DC converter, supercapacitors are also suited to being charged using a 'bucket'-type method, which is the method used by the charge pump storage concept developed here; repeated emptying of the charge from a small capacitor into the supercapacitor can eventually 'top up' the supercapacitor. Rechargeable batteries tend to require more careful charging methods, for example: nickel-cadmium and nickel-metal hydride batteries usually require a constant current supply that rapidly recharges the cells, then are trickle-charged in order to maintain full battery capacity. Lithium-ion technologies require even more specific charging methods: typically a constant current source is used until maximum cell voltage is reached, after which the voltage on the cells is held constant until the charging current drops to around 10% of its initial value, and a 'topping up charge' is then applied about once every 500 hours. If rechargeable battery cells are charged incorrectly, often the lifespan of the battery is dramatically

shortened. A comparison between the charging and discharging profiles for a battery and a supercapacitor is given in Figure 4-20 [148]:

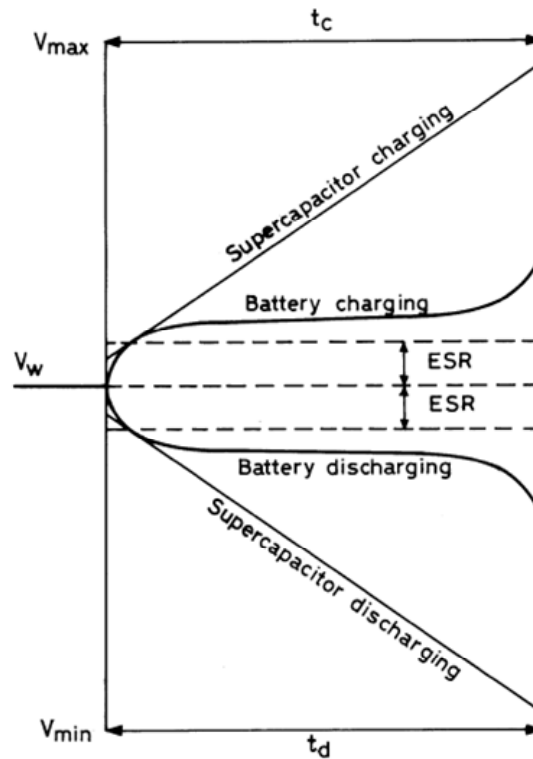


Figure 4-20 A comparison between the charging and discharging profiles for a battery and a supercapacitor for similar charge [148].

In Figure 4-20, t_c and t_d represent charge and discharge times respectively; V_w represents the operating voltage of the supercapacitor, akin to the open-circuit voltage of a battery; V_{max} and V_{min} represent the end of charge and end of discharge respectively, and ESR is the equivalent series resistance of the capacitor [148]. It can be inferred from Figure 4-20 that as charge is accumulated in a supercapacitor, the voltage across it increases linearly, and that as charge is extracted from a supercapacitor, the voltage across it decreases linearly. Therefore, the choice of a buck-boost DC-DC converter seems appropriate, as during the times when the voltage available from the

supercapacitors is higher than the voltage required by the application system (i.e. required by the wireless sensor node or portable electronic device) the converter can operate in buck-mode, and during the times when the voltage is lower than that required, the converter can operate in boost mode, thus power can be provided throughout the range of the supercapacitor's charge holding capacity, until it becomes exhausted.

This means that the final form of the proposed new harvesting circuit concept, incorporating the charge storage concept, the SSHI technique, and the components required for connection of a DC-DC buck-boost converter, is as shown in Figure 4-21:

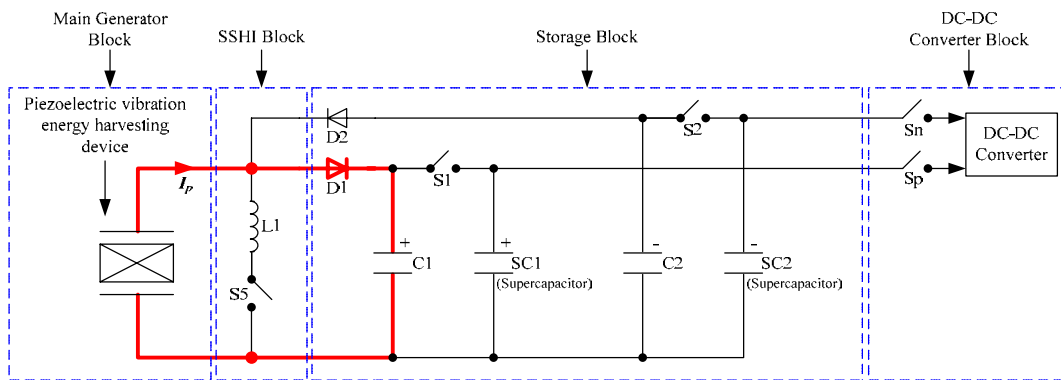


Figure 4-21 Schematic of the final form of the proposed harvesting circuit (showing current flow in the positive half-cycle of the piezoelectric generator AC voltage output).

Operation of the circuit can be described by using Figure 4-21 in conjunction with Figure 4-22 and the waveforms presented in Figure 4-23, as follows:

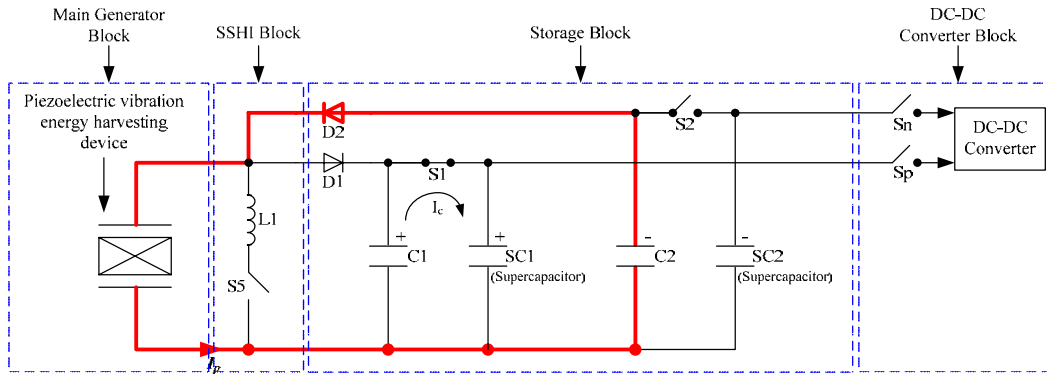


Figure 4-22 Schematic of the proposed harvesting circuit showing current flow in the negative half-cycle of the piezoelectric generator AC voltage output.

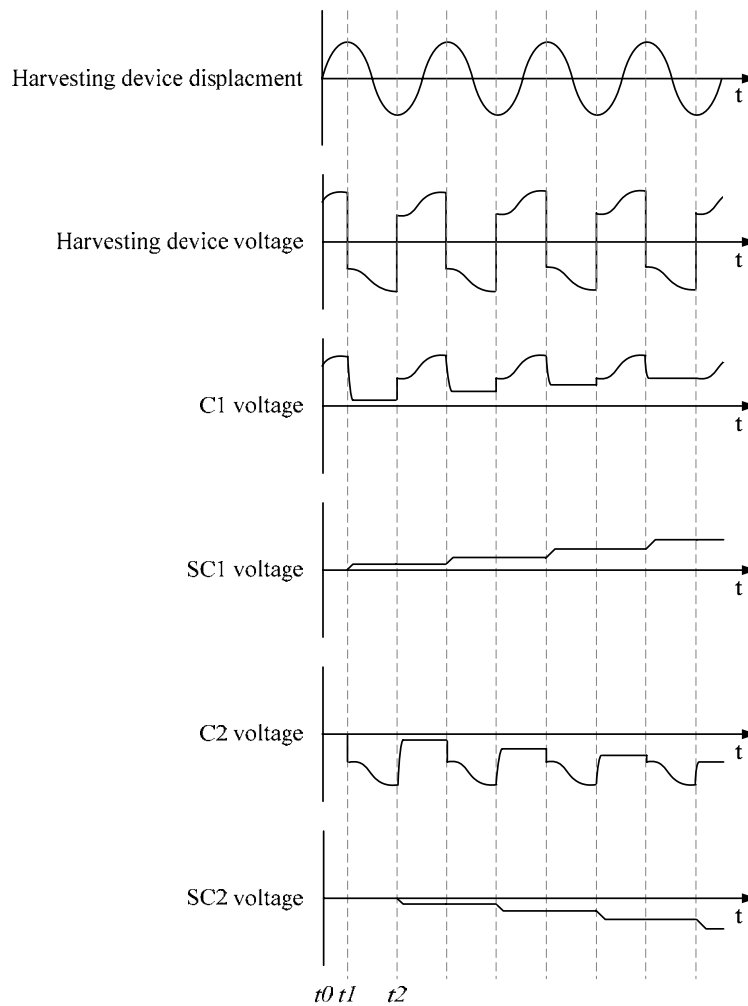


Figure 4-23 Hypothesised voltage waveforms for the proposed harvesting circuit, showing charge accumulation in both supercapacitors.

In regard to Figure 4-23: from t_0 to t_1 current from the piezoelectric generator, I_p , flows in the direction indicated in Figure 4-21, and C1 charges as shown in Figure 4-23. At time t_1 switch S5 is operated enabling charge inversion on the piezoelectric harvesting device (that results from the SSHI technique) and diode D1 becomes blocking. At the same time switch S1 is also closed, and charge is evacuated from C1 into SC1.

Between t_1 and t_2 the harvesting device voltage increases negatively. Current from the piezoelectric generator, I_p , now flows as indicated in Figure 4-22 and C2 is charged. At t_2 switch S5 is again operated completing the charge inversion process, switch S1 is opened (thereby preserving the charge in SC1), and switch S2 is shut causing the charge on C2 to be evacuated into SC2.

This process is repeated for every time-period (i.e. cycle) of the piezoelectric generator displacement, resulting in a net positive charge gain in supercapacitor SC1 over time, and a net negative charge gain in supercapacitor SC2 over time, as shown in Figure 4-23. A predetermined charge level (identified by measuring the voltage) in either supercapacitor SC1 or supercapacitor SC2 is the required condition for connection of the DC-DC converter. At this time, both switches S1 and S2 are opened, and Sp and Sn are closed. This forms a circuit thus:

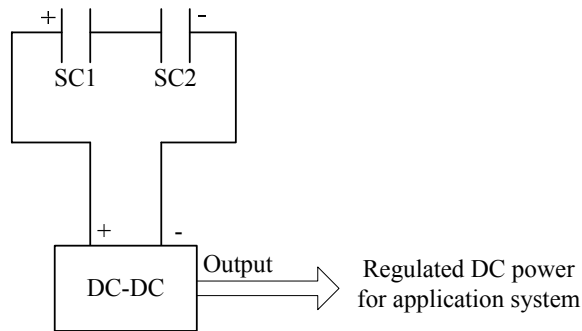


Figure 4-24 Circuit formed by the series connection of two charged supercapacitors, to supply a buck-boost DC-DC converter.

The DC-DC converter provides a regulated DC supply to the end application electronics.

4.3.2.1 Voltage detection and switch driving considerations

In order to achieve the above described switching at the appropriate times, detection circuitry has to be developed for the purpose of detecting the maxima and minima points of the piezoelectric generator voltage waveform. The advantage of combining the SSHI technique with the charge storage concept developed here is that both functions can use the same detection circuitry, since both require detection of the same points; i.e. the maxima and minima of the piezoelectric generator voltage waveform. This means that the only extra voltage detection circuitry required is that needed to detect a voltage threshold level that indicates a full charge on either supercapacitor SC1 or supercapacitor SC2, in order that the DC-DC converter might be connected and used to provide a regulated DC supply to the end application.

In addition to the required detection circuitry, switch driving circuitry also has to be developed for the purpose of driving switch S5 (for operation of the SSHI technique), switches S1 and S2 (for charge transfer to the supercapacitors), and Sp and Sn (for connection of the DC-DC converter). The function of control of these switches in terms of timing could easily be implemented through the use of a micro-power microcontroller. The processing overhead required would be very small indeed, since the control functions are very simple; i.e. the microcontroller only has to 'read' a detected voltage and then make the decision to operate a switch. In addition, the microcontroller could operate with a very low clock rate, because the output of the piezoelectric harvesting device is very low frequency due to the low frequency

environmental vibrations. These factors (low processing overhead and operation at a low clock rate) mean that power consumption of the microcontroller would be very low. In addition, modern microcontrollers incorporate many other features, such as internal comparators, ADC converters and a number of Input/Output (I/O) terminals, which could be used to implement some of the detection circuitry of the system, so that the need for separate detection functions in the system is negated further. It therefore seems that a micro-power microcontroller in a small package size would be well suited to this task. As an example, a microcontroller available from Microchip (Chandler, AZ, USA): part no. PIC16F688, has all of the above mentioned features and has an operating current of $11\mu\text{A}$ at an operating frequency of 32kHz with a 2V_{DC} supply; this equates to a power consumption of $22\mu\text{W}$. In sleep mode the power consumption drops to only $0.1\mu\text{W}$. Given the $370.37\mu\text{W}$ power output of the optimised harvesting device presented in Chapter 3, it is apparent that this microcontroller could easily be provided with power while leaving enough left over to power an end application system.

4.3.2.2 Block diagram of the new system topology

It is envisaged that the proposed harvesting circuit concept, represented in block diagram form with management electronics and an end application system, might appear thus:

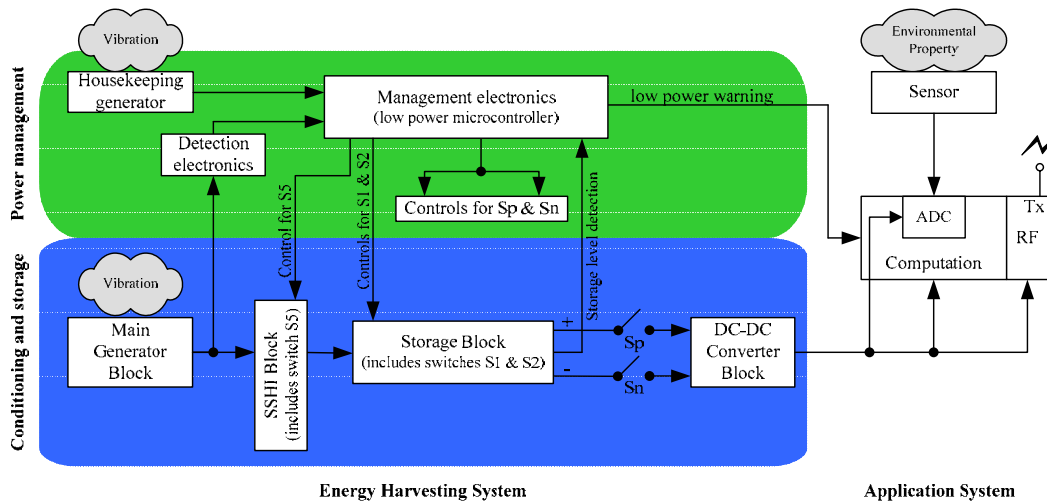


Figure 4-25 Block diagram of the proposed harvesting circuit and envisaged power management circuitry.

In Figure 4-25, the proposed harvesting circuit discussed thus far and given in Figure 4-21 (page 246) is represented by the blocks shown in the “Conditioning and Storage” part of the “Energy Harvesting System”.

It should be mentioned here that since the goal is obtaining an enhanced level of output power from a piezoelectric-based vibration energy harvesting device while considering the need for a regulated DC output, the focus during the experimental work that follows remains on the development of the “Conditioning and Storage” elements of the system. The “Power Management” blocks, although depicted in Figure 4-25 in their carefully envisaged end form, have been implemented so far only in prototype form (i.e. using a mixture of discrete and integrated components), because proving the new harvesting circuit concept, with its perceived improvements, was deemed to be of more importance than implementing the management electronics by elegant engineering design. The “Application System” is outside the scope of this thesis, but an example is depicted in Figure 4-25 in order to illustrate what might be done.

4.3.3 Advantages of the New Concept

The perceived advantages of using the new harvesting circuit concept developed in this thesis can be summed-up as follows:

- 1) Power is harvested from the piezoelectric energy harvesting device during the whole of its AC output voltage cycle, rather than just for part of it, as occurs with the bridge rectifier circuit.
- 2) The concept inherently converts from AC to DC, by the accumulation of charge in two storage supercapacitors (one collecting the positive charge generated by the harvesting device, and one collecting the negative generated charge) which are then connected together in series to form an energy reservoir with a positive terminal and a negative terminal. This negates the need for a conventional bridge rectifier and allows for the connection of a buck-boost DC-DC converter, since a capacitive reservoir is an ideal way of supplying power to a DC-DC converter.
- 3) The concept takes advantage of the increase in the voltage output of the harvesting device that results from using the SSHI technique.
- 4) The concept uses pre-existing maxima and minima detection circuitry (since it is already required for the SSHI technique) therefore a minimum of extra components need be added.
- 5) The concept is simple. For example, if a microcontroller were used to perform power management, only a few functions need be fulfilled and it can operate with a very low clock rate, therefore it can be very low power and a small size.

- 6) The concept provides a method of fully integrating the SSHI technique into a circuit that fulfils the traditional requirements of electronic devices and systems; i.e. it provides a regulated DC supply. The SSHI technique alone can result in an improvement in the power output of the device, it cannot convert from AC to DC or provide a regulated DC output.
- 7) The impedance match of the load capacitor (i.e. C1 or C2 of Figure 4-21) with the source (i.e. the piezoelectric generator) in theory results in maximum power transfer at all times, since if the frequency of the driving vibration sources changes, resulting in a change in frequency of the harvesting device voltage output, the impedance remains matched because the load attached to the generator is always purely capacitive.

4.4 Implementation of the Concept (Electronic Circuit Design)

The circuit designed to implement the proposed harvesting concept of Figure 4-21 and its associated detection, control, and switch driving functions is presented on the following page in Figure 4-26. This aim of this section is to describe the design of this circuit, detailing the considerations taken into account during design. The section is split into subsections that follow the functional blocks depicted in both Figure 4-21 and the system block diagram shown in Figure 4-25; that is:

- 1) Section 4.4.1: Design of the Main Generator Block
- 2) Section 4.4.2: Design of the SSHI Block
- 3) Section 4.4.3: Design of the Storage Block

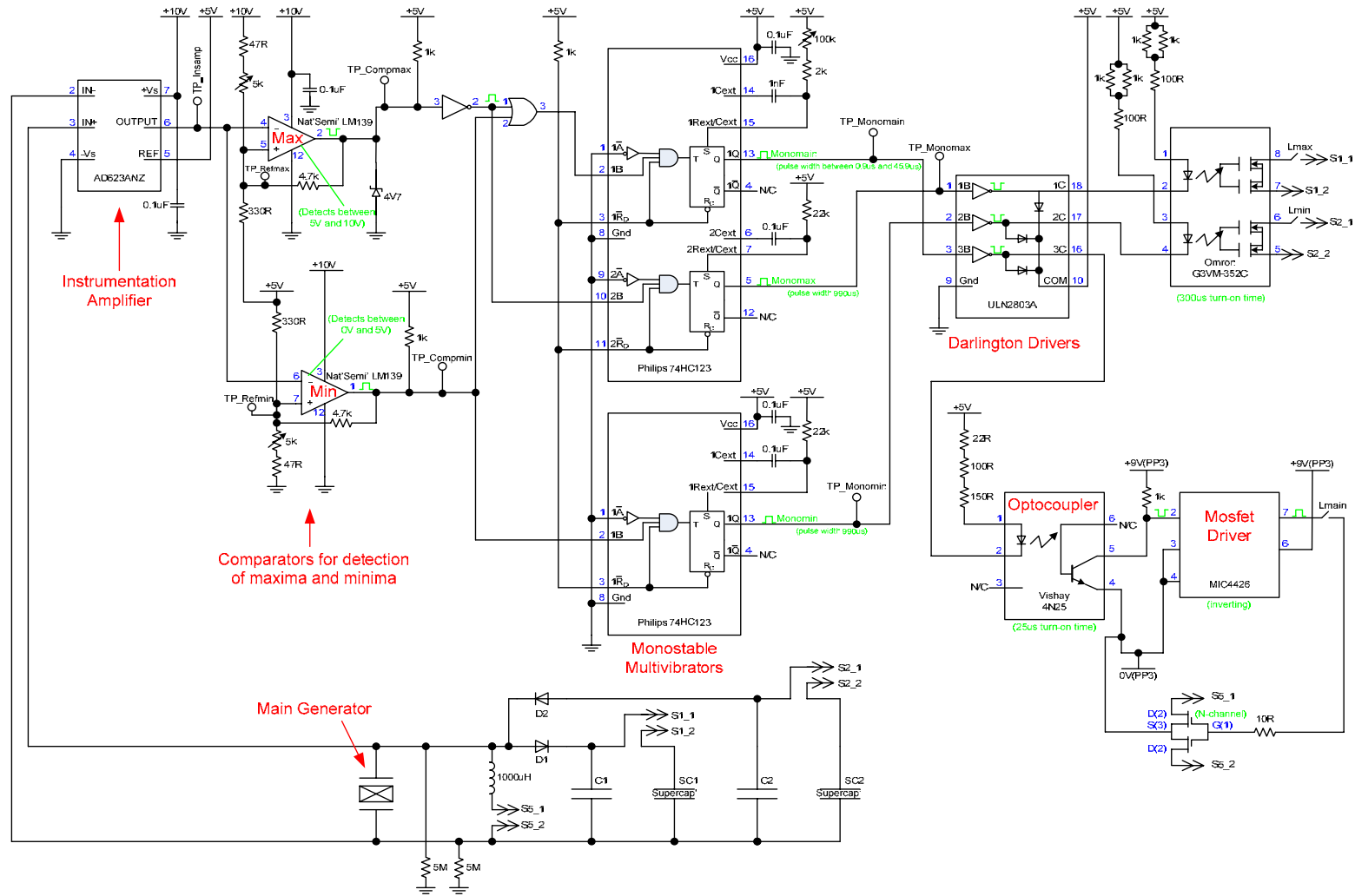


Figure 4-26 Circuit schematic of the electronic circuit designed to implement the proposed new harvesting circuit concept.

4.4.1 Design of the Main Generator Block

The main generator is simply the optimised piezoelectric vibration energy harvesting device developed in Chapter 3 of this thesis. The measured characteristics of this device, when subjected to a simple harmonic motion-type of vibration with acceleration amplitude $\pm 0.23g$ and a frequency matching the natural frequency of the device, were as follows:

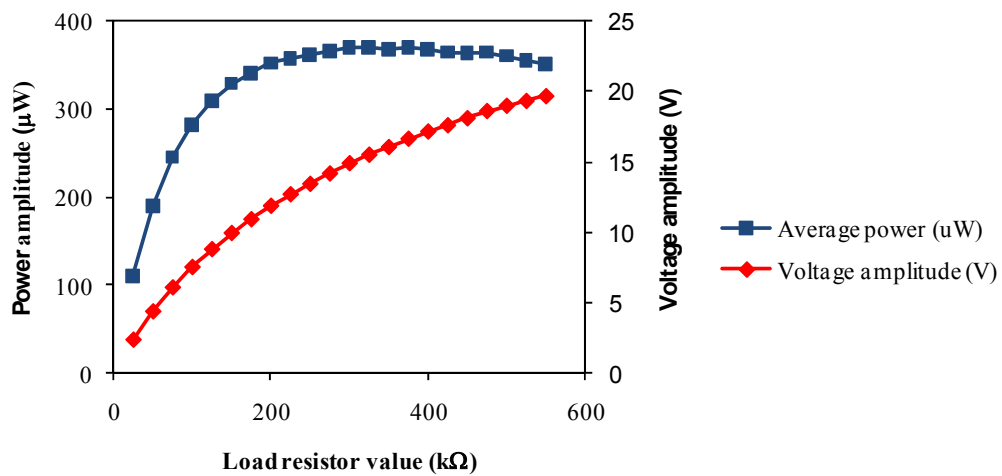


Figure 3-36 (from Chapter 3, page 205): measured output voltage and power of the optimised device versus load resistor value.

Maximum power output: $370.37\mu W$

Optimum load resistor value: $325k\Omega$

Voltage amplitude at maximum power output: $15.52V_{pk}$

Resonant frequency of the device with a $325k\Omega$ load: $87Hz$

4.4.2 Design of the SSHI Block

Figure 2-34, shown in the literature review on page 108, shows the fundamental components required for implementation of the SSHI technique. In actual implementation, the circuit developed to perform the SSHI function is shown on the following page in Figure 4-27 (where the greyed-out parts are irrelevant, i.e. not required for SSHI).

The calculation of a suitable inductor value was carried out simply by using equation (6) on page 109 for the resonant frequency of an oscillating parallel LC circuit, which is repeated here for convenience:

$$\frac{1}{2 \cdot \pi \cdot \sqrt{L \cdot C}} \quad (6)$$

Where L is the inductor value and C is the capacitance of the piezoelectric energy harvesting device.

The capacitance of the piezoelectric energy harvester was measured using an impedance analyser, and was found to be 3.49nF. The capacitance can also be calculated from theory by using equation (52) given in Chapter 3 (page 171):

$$C_1 = C_2 = \frac{\epsilon_r \cdot \epsilon_0 \cdot A}{h_p} \quad (52)$$

Where, remembering that the piezoelectric generator consists of two piezoelectric layers connected electrically in parallel, C_1 and C_2 are the capacitance values of each layer, A is the area of one electrode, and h_p is the thickness of one piezoceramic layer. The calculated theoretical capacitance for the piezoelectric generator (since $A = 19.3\text{mm}^2$, $\epsilon_r = 3800$ and $h_p = 0.278\text{mm}$) is 4.67nF. This means that there is a discrepancy between the measured and calculated value of 1.18nF. It is feasible that this could be due to

manufacturing tolerances; the device was fabricated by hand and it is very difficult to achieve more than a 0.5mm (see Table 3-5 on page 183 for the device dimensions that resulted from the optimisation process). It is possible that when removing some of the electrode material by application of Ferric Chloride solution, FeCl_3 , the resulting surface area did not exactly match the required 19.3mm^2 . From equation (52), an error in the length of the electrode by 1mm would give a capacitance of 3.9nF, which is closer to the measured value. For the purposes of circuit calculations, the measured value of the capacitance of the beam was used.

Given the measured value then, a suitable inductor value can be chosen that gives an *LC* oscillation frequency somewhere in the kHz region; the actual frequency value is not so important, as the only requirement is that it has to be much faster than the frequency that the piezoelectric generator is vibrating at. A value of $1000\mu\text{H}$ was chosen; this results in an LC oscillation frequency of 85kHz.

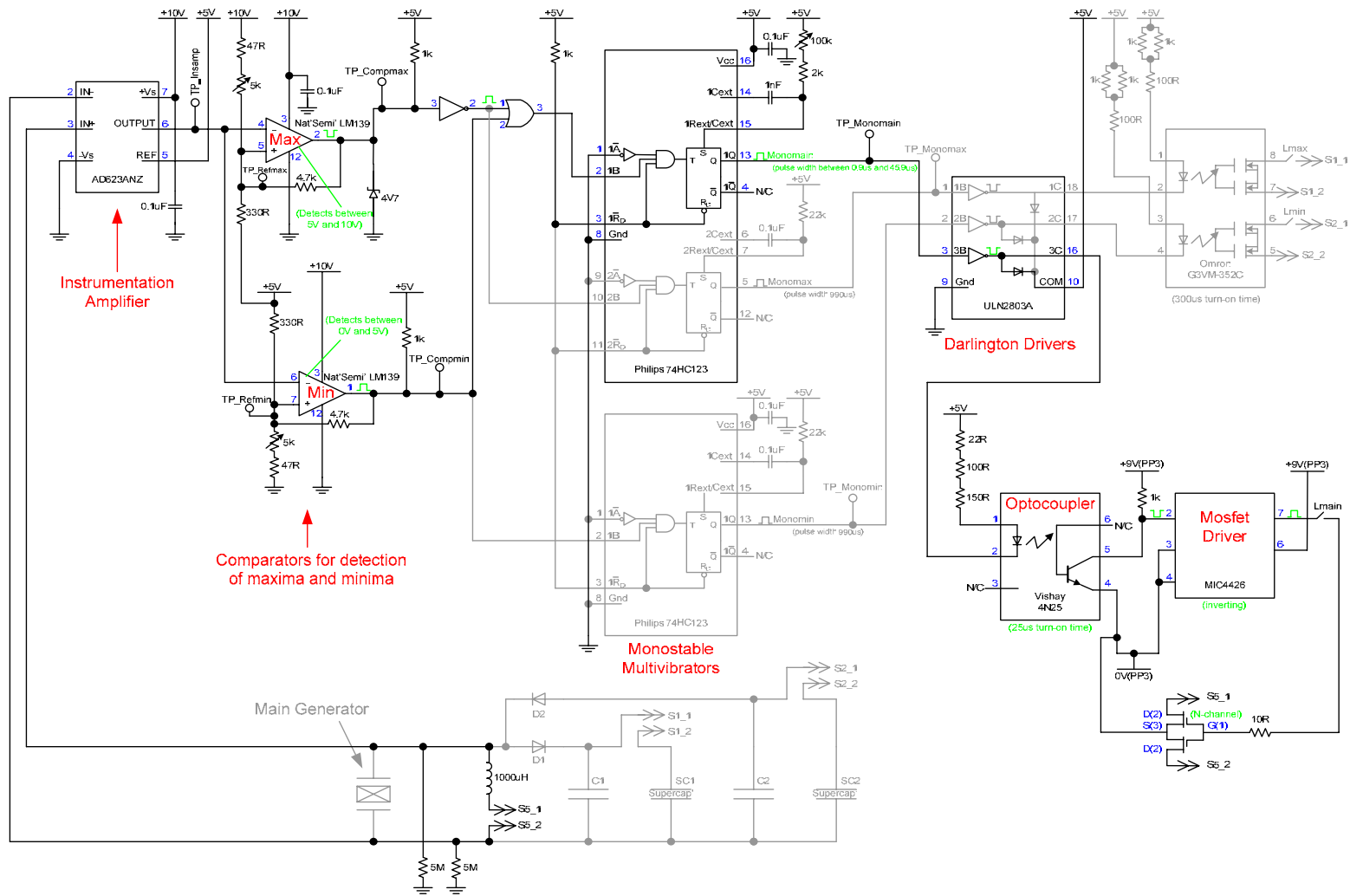


Figure 4-27 Circuit diagram designed to implement the SSHI technique (greyed-out parts are irrelevant).

The purpose of the instrumentation amplifier is twofold: first and foremost it presents a high impedance to the output of the generator so as not to load it too heavily. If an interface with a low input impedance is connected to the output of the piezoelectric generator the load current would be too great, meaning that in the act of measuring the output voltage, the output voltage would change. Also, due to the increased current consumption of the device with a low input impedance, power would be lost from the generator. Secondly, using an instrumentation amplifier when measuring the piezoelectric generator waveform for the purpose of detecting the peak and trough (or maxima and minima) results in good accuracy, since the instrumentation amplifier is fundamentally a *differential* amplifier, meaning that there is a degree of common mode rejection (i.e. noise voltages common to both inputs will not be amplified – only the difference between the two inputs are passed through to the output). The amplifier in this case was configured to have a gain of one, and the reference terminal of the amplifier was connected to +5V.

The two comparator circuits are each inverting with hysteresis. Design of these was non-trivial. Since the input waveform to both is AC, care needs to be taken in the design of the comparator that detects the voltage when it is decreasing; in this case it is easy to inadvertently design a comparator that gives multiple transitions on its output due to the hysteresis ‘pulling’ the comparator reference in the same direction as the input signal. In Figure 4-27 the top comparator (labelled “Max”), through the use of a 5k Ω potentiometer on the reference terminal, can detect a voltage between +5.25V and +9.34V with 250mV hysteresis at the lower voltage and 36mV hysteresis at the higher voltage, while the bottom one (labelled “Min”), again through the use of a 5k Ω potentiometer on the reference terminal, can detect a voltage between +620mV and

+4.42V with 35mV hysteresis at the lower voltage and 289mV hysteresis at the higher voltage. The comparators, therefore, are capable of detecting the peak and trough (or maxima and minima) of any AC voltage waveform from the harvesting device that has a pk-pk voltage that falls within the range of $1.16V_{pk-pk}$ to $9.34V_{pk-pk}$.

The use of a monostable multivibrator with an external potentiometer provides a very easy method of obtaining a controllable-width pulse with which to operate switch S5. Some flexibility in the pulse width value is necessary since, although the half-period of the LC resonant circuit can be predicted with accuracy, the switch-driving elements of the circuit (the Darlington drivers, optocoupler and MOSFET driver plus the MOSFETS themselves) all have a 'switch-on' time that has to be taken into account, and in some cases tolerances on those values, which are specified in the data sheets, also have to be considered. In practice, it was found that only the switch-on time of the optocoupler was significant (being 25 μ s, compared to a total of 236ns for all the other devices combined). The monostable multivibrator was configured to provide a pulse width that varies between 0.9 μ s and 45.9 μ s depending on the position of the 100k Ω potentiometer. Full details of the calculations made for component selection can be found in appendix F.

The Darlington drivers are required to provide the current drive to the optocoupler device, enabling a faster switching time than would be possible if the output of the monostable multivibrator were used directly.

The optocoupler provides isolation, to maintain separation of the ground-referenced detection and switch driving functions of the circuitry, and the floating-source piezoelectric generator. An optocoupler was chosen over other types of isolation device

because it has a relatively fast switch-on time, $25\mu\text{s}$, compared to other types of isolation device. The MOSFET Driver IC drives two N-channel low power MOSFETs (2 x 2N7000s), configured such as to constitute a bidirectional switch so that SSHI charge inversion in both directions (peak-positive-to-peak-negative, and peak-negative-to-peak-positive) can be achieved.

4.4.3 Design of the Storage Block

Section 4.3 (Figure 4-21) shows the fundamental components and describes the operation of the storage block. Actual implementation was achieved using the circuit shown on the following page in Figure 4-28, where the greyed-out parts are for the SSHI technique, and therefore are not relevant to the charge storage function. The commonality between the circuit that implements the SSHI function (Figure 4-27) and the circuit that implements the charge storage function (Figure 4-28) can now clearly be seen. This illustrates one of the salient advantages of the new charge storage concept developed in this thesis, which is that regardless of how the maxima and minima waveform detection circuits are implemented (in this case it has been in prototype form through a mixture of discrete and integrated components), they need be implemented only once.

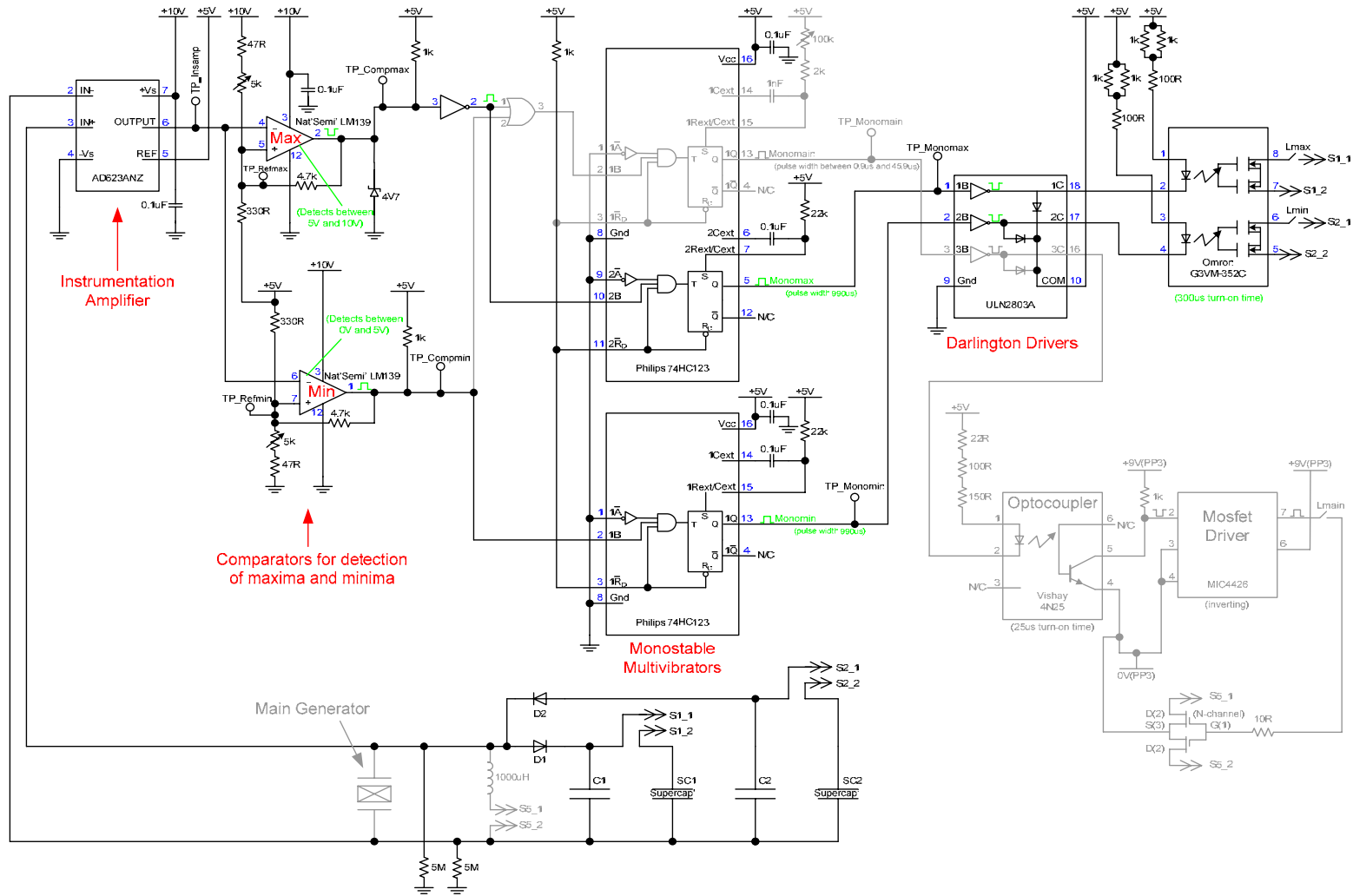


Figure 4-28 Circuit diagram designed to implement the charge transfer function (greyed-out parts are irrelevant).

In regard to selection of suitable component values for components C1, SC1, C2, SC2, D1 and D2, it was mentioned before that it would be beneficial if SC1 and SC2 were supercapacitors: the actual chosen component was a Powerstor (Cooper Bussmann, Ellisville, MO, USA) Aerogel Series A 2.5V 0.47F supercapacitor. For C1 and C2, as mentioned before, for maximum power transfer it is desirable that the capacitance of these capacitors match the capacitance of the piezoelectric generator; however, since 3.49nF is not a preferred component value, the nearest that is was practical to achieve was a pair of Kemet (Simpsonville, SC, USA) ceramic C315C332K1R5TA X7R 3.3nF 100V radial leaded capacitors. D1 and D2 were simply 1N4001 silicon rectifier diodes.

Since the instrumentation amplifier and comparator circuits are also used for the SSHI technique, their purpose and operation has already been described in the previous section (section 4.4.2), and no duplication of explanation will be provided here.

As can be seen from Figure 4-28, two other monostable functions are required for correct functioning of the storage block. This is because there are some differences between the requirements that switch S5, for the SSHI technique, must fulfil and those that switches S1 and S2, for the charge transfer concept, must fulfil. These differences are discussed here:

- 1) Switch S5 must be bidirectional because it is an AC application, whereas switches S1 and S2 need only be unidirectional.
- 2) Switch S5 must have fast operation, because a half-period of the oscillating LC network, which has a resonant frequency of 85kHz, is 5.9 μ s. The switch-on time requirements for switches S1 and S2 are less stringent, since the only

requirement is that charge transfer to either SC1 or SC2 is complete within a half-period of the driving vibration frequency.

In addition to the above listed points, the relative timings of switches S1 and S2 with S5 also have to be carefully considered. Switch S1 or S2 (whichever is in operation, depending on whether positive or negative charge is being evacuated into the supercapacitors) should not close at *exactly* the same time as S5. This is because there would be a risk that the charge available on the piezoelectric element at a displacement extremum could be prematurely evacuated into a supercapacitor, which would reduce the voltage on the piezoelectric element to 0V, thus leaving no voltage to invert when switch S5 is closed. For this reason, there should be a short delay (in the order of 100 μ s or so) between the closing of switch S5 and the closing of switch S1 or S2 (whichever is in operation).

The circuit presented in the schematic of Figure 4-28 makes allowance for the above discussed points through the following design choices:

- 1) Since the operation time of switches S1 and S2 do not need to be tightly controlled, no potentiometer has been included in the monostable multivibrator external components, unlike the case for the SSHI circuit, where tight control is required in order to exactly achieve a pulse width that is equal to a half-period of the *LC* oscillator. The pulse widths that control switches S1 and S2 are simply programmed to both be fixed at 0.99ms. Appendix G details the calculations for the component choices made.

- 2) Solid-state optocoupler MOSFET relays have been used to isolate the ground-referenced detection and switch driving functions of the circuitry, and the floating-

source piezoelectric generator. These devices were chosen because they have a turn-on time of $300\mu\text{s}$, which means there will always be a delay between switch S5 closing and S1 or S2 closing, since S5 is driven from a much faster ($25\mu\text{s}$ turn-on time) optocoupler device with a transistor output. The $300\mu\text{s}$ turn-on time is also appropriate for charge transfer from C1 to SC1 (or C2 to SC2), since it fits well within the half-period of any driving vibration frequency that lies below 200Hz.

3) Considering the bidirectional/unidirectional issue in regard to the switches, all three are in fact bidirectional in this implementation. However, this is just ‘design coincidence’ since the solid-state relays are inherently bidirectional.

4.5 Construction of the Circuit

Figure 4-29 shows a photo of the built circuit. The circuit was constructed on square pad prototyping board. One side of the board has a ground plane in order to minimise noise effects and provide a low inductance path to ground. Connections are made to the board via sprung terminals (arrowed in Figure 4-29) and the location of each of the potentiometers is indicated. In the circuit, several ‘links’ were designed-in, which can be broken as required so that the SSHI function and the charge storage function can operate independently. These are shown as *Lmain* (for the SSHI technique) and *Lmin* and *Lmax* (for the charge storage function) in Figure 4-28, and are arrowed in Figure 4-29.

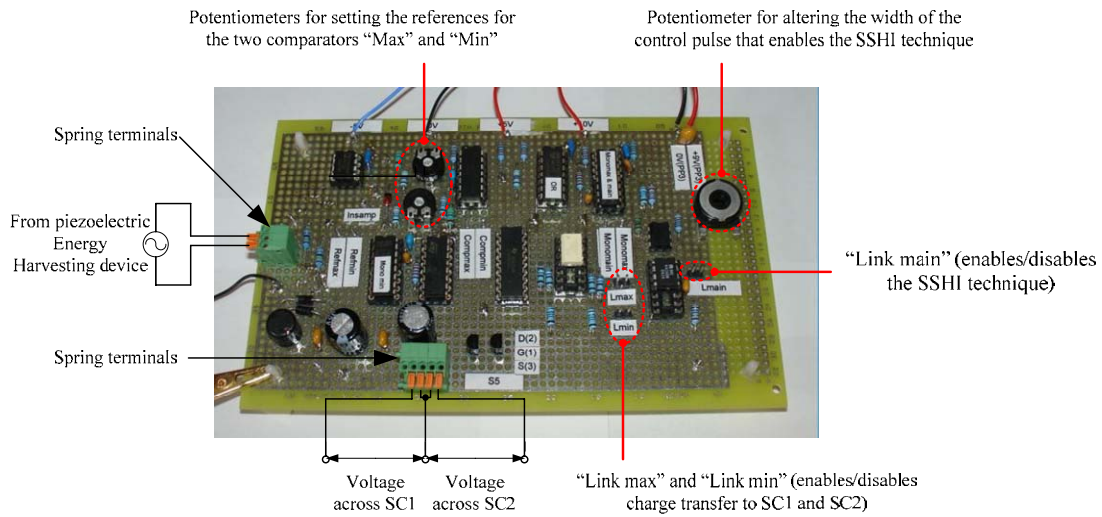


Figure 4-29 Photo of the built prototype harvesting circuit.

4.6 Testing of the Circuit

Section 4.1 of this chapter described some initial experimental investigations that were conducted with a bridge rectifier and the prototype harvesting device, and Section 4.2 discussed the conclusions drawn from these initial investigations. A description of the evolution behind the proposed new harvesting circuit concept was then given in section 4.3, and section 4.3.3 described the advantages of the new concept. Section 4.4 described the prototype circuit that was designed to implement the new concept and section 4.5 gave information on the construction of the circuit. The purpose of this section is to detail the test setup and equipment, and to describe the procedure used for testing the new harvesting circuit concept.

4.6.1 Test-setup and Equipment

The tests carried out were split into two types. First, tests were set up to verify that the SSHI technique does result in the expected benefits; i.e. to verify that a voltage increase and related power increase is observed when the technique is used with the optimised

harvesting device developed in this thesis. Secondly, tests were set up to verify the complete new harvesting circuit concept; i.e. with both the SSHI technique and charge pump-type circuit operational. In the second set of tests the performance of the proposed concept was compared against the performance of a bridge rectifier circuit, in order to ascertain whether or not the new concept results in an increased level of energy harvested into a storage capacitor.

4.6.1.1 Test Setup for the SSHI Tests

Figure 4-30 shows a schematic of the test equipment setup. This setup enables the connection of different resistive loads to the piezoelectric vibration energy harvesting device both when the SSHI technique is applied, and when it is not applied. The National Instruments hardware and software that was used to test the optimised vibration energy harvesting device and which is described in Chapter 3 (see section 3.7.1, page 188, for details), is used again in the SSHI tests:

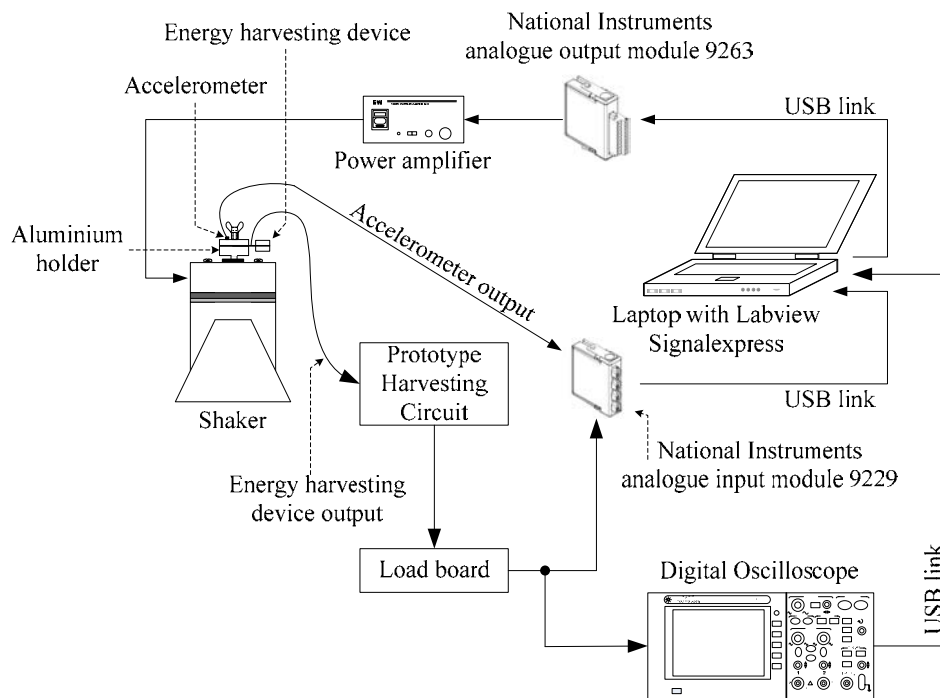


Figure 4-30 Test equipment setup for SSHI tests.

As before, the optimised piezoelectric generator is mounted onto the armature of the electrodynamic shaker via the aluminium holder. The energy harvesting device output is this time connected to the custom-built load board via the harvesting circuit board. The load board used is the same as that used in the testing of the optimised harvester; see section 3.7.1 and appendix D for details. Links L_{max} and L_{min} in the harvesting circuit (see Figure 4-27 and the photo of Figure 4-29) are removed in order to disable the charge storage function of the harvesting circuit, leaving only the SSHI function operative. The output of the load board is connected to an oscilloscope (Agilent Technologies model no. DSO3062A), in order that the voltage waveform of the piezoelectric generator with the SSHI technique applied can be viewed, and also to the NI analogue input module, for automatic recording of voltage amplitude levels using LabVIEW SignalExpress. As before, the vibration applied to the harvesting device is controlled from the Laptop using LabVIEW SignalExpress, and the accelerometer output is connected to the NI 9229 analogue input module for this purpose.

4.6.1.2 Testing Procedure for the SSHI Tests

The purpose of the SSHI tests is to verify that the SSHI technique does result in an increase in the voltage output, and hence an increase in the power output, of the optimised piezoelectric vibration energy harvesting device. One way to do this is to subject the generator to a frequency sweep at constant vibration acceleration amplitude, and apply different resistive loads both with and without the SSHI technique applied. Indeed, this was the approach adopted in characterising the power output of the optimised generator in Chapter 3 (see section 3.7.2, page 201). However, the active integrated components that comprise the harvesting circuitry are run from either 5V or 10V DC supplies, and from the results given in Chapter 3 (section 3.8, page 203) the

output of the piezoelectric generator reached a maximum AC voltage of $\pm 19.68\text{V}$. Therefore, the same approach with the same vibration acceleration amplitude value cannot be implemented. The ‘front end’ of the circuit design, i.e. the instrumentation amplifier, is powered from $+10\text{V}$ while its reference terminal is connected to $+5\text{V}$. This provides a maximum swing of only $\pm 5\text{V}$ ‘headroom’ for the input signal (slightly less in practice, according to the output swing range specified in the data sheet). Therefore, in order to carry out these tests, there was a choice of two possible methods:

- 1) Decrease the acceleration amplitude of the driving vibrations so that the maximum expected AC voltage output (also taking into consideration the voltage boosting effects of the SSHI technique) always falls below $\pm 5\text{V}$.
- 2) Choose a vibration frequency that is off-resonance in order to lower the voltage output amplitude, and maintain this frequency while sweeping the load resistor value both with and without the SSHI technique.

The second option was chosen here since it was easier to ascertain what the maximum output voltage was likely to be using this method, making it more convenient when performing the experimental work. The test procedure was then as follows:

The frequency of vibration was set at 60Hz , and the amplitude of vibration was set, as before, to $\pm 0.23\text{g}$ using LabVIEW SignalExpress software. These values were chosen because even with the highest load resistance value, $550\text{k}\Omega$, and taking into account the typical gain of 0.8 in voltage output expected from the SSHI technique, the maximum expected voltage should not exceed $4.5V_{\text{pk}}$, which is a value within the capability of the harvesting circuitry.

With the harvesting circuitry board initially removed from the test system, so that no SSHI is applied, (i.e. the output of the piezoelectric generator is connected directly to the load board in Figure 4-30) a sweep of resistive load value from 25k Ω to 550k Ω in 25k Ω steps was performed using the load board. The voltage output amplitude from the energy harvesting device was recorded for each value of load resistance applied.

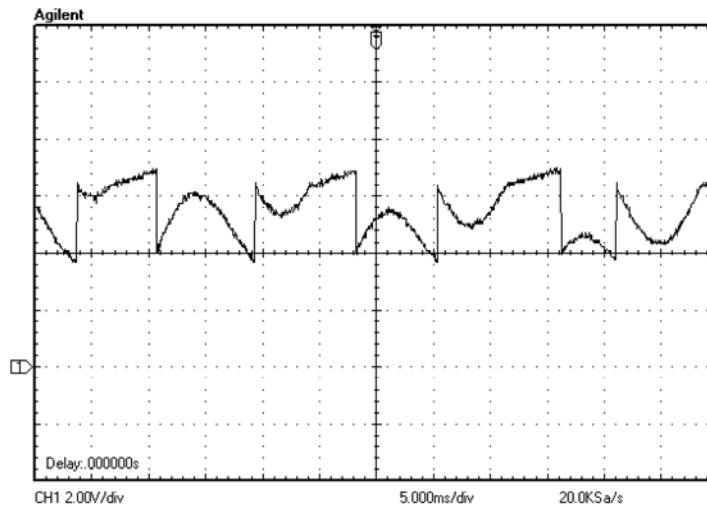
The harvesting circuitry board, and hence SSHI technique, was then introduced into the test system as per Figure 4-30 and the resistive load sweep repeated. In order to do this test however, some manual adjustment of the potentiometers on the reference terminals of the level detection comparators (i.e. the comparators labelled 'min' and 'max' in Figure 4-26 through Figure 4-28; pages 254-262) was required for each resistive value applied. The procedure adopted was as follows:

- 1) Turn both potentiometers until they hit the end stops; i.e. so that the comparators are set to their maximum amplitude detection levels, which is +9.34V for the comparator detecting the maxima of the piezoelectric generator output waveform (labelled 'max'), and +620mV for the one detecting the minima of the waveform, (labelled 'min'). Note: remember that the output of the instrumentation amplifier, and hence the piezoelectric generator output waveform, is referenced to +5V, which is roughly central between +620mV and +9.34V.
- 2) Set labview running, so that vibration excitation of $\pm 0.23g$ at 60Hz is applied to the harvesting device.
- 3) Adjust either one of the potentiometers until SSHI begins to work on either the maxima or minima (depending on which potentiometer is adjusted) of the

piezoelectric generator output voltage waveform. This could be achieved because the waveform could be viewed using the oscilloscope.

- 4) Adjust the other potentiometer until it begins to work on the opposite (maxima or minima).

Typically, after following these steps, some further ‘fine tuning’ adjustment was required on both potentiometers to ‘reverse’ the initial adjustment somewhat until SSHI was properly achieved, otherwise the waveform did not actually increase much in amplitude. Figure 4-31 attempts to show this:



(a)



(b)

Figure 4-31 (a) Waveform after initial adjustment; i.e. after following steps 1-4 outlined above
 (b) Photo of the SSHI waveform achieved after further ‘fine tuning’ adjustments (channel 1 shows the SSHI waveform. Channel 2 shows the pulse that controls the length of time the inductor is switched into the circuit for).

The procedure just described had to be reiterated for every different value of resistive load, since changes in the load resistor value result in changes in the amplitude of the piezoelectric generator output voltage, necessitating different potentiometer settings. In practice, it was found that this situation was less than ideal. The comparators are level detectors, and not peak and trough or maxima and minima detectors. Therefore, as the waveform changed shape as it transitioned from a sinusoid to a SSHI-shape waveform, the values of the extrema were altered, and the original settings for the potentiometers became invalid, hence the necessary further ‘fine tuning’ adjustment mentioned. Also

practically, it was found that it was sometimes difficult to obtain the SSHI waveform without losing it several times first; i.e. when completing the adjustments, if either potentiometer was moved too far, the waveform would quickly revert back to its sinusoidal form, necessitating a repeat of the whole procedure. This author would like to suggest that actual peak and trough detectors, while more difficult to achieve than level detectors, may well be worth the effort in this case.

Given a working SSHI waveform for each resistive load value, the voltage output amplitude from the energy harvesting device was recorded for each value of load resistance applied. The average power output of the device for each case (i.e. with and without SSHI) was then calculated using equation (48):

$$P_{ave_in_R}(f) = \frac{V_R(f)^2}{2 \cdot R} \quad (48)$$

Where $P_{ave_in_R}$ is the average power dissipated in the load resistor, R is the load resistor value, and V_R is the output voltage amplitude (peak voltage) of the energy harvesting device measured across the load resistor.

4.6.1.3 Test Setup for the Complete Harvesting Circuit Concept Tests

In order to analyse the effectiveness (in terms of enhancing the power output) of the charge storage concept proposed in this thesis, its performance was compared with that of the bridge rectifier circuit. Figure 4-32 shows a schematic of the test equipment setup:

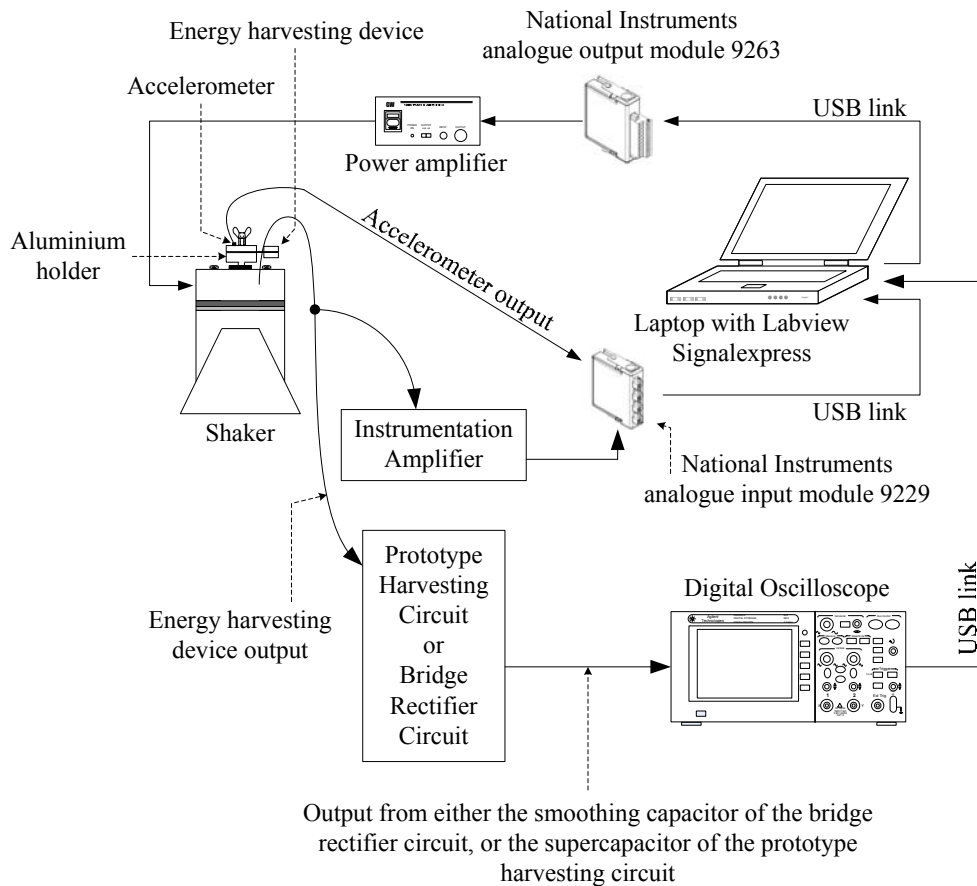


Figure 4-32 Test equipment setup for charge storage tests.

As for all previous tests, the optimised piezoelectric generator was mounted onto the armature of the electrodynamic shaker via the aluminium holder. The energy harvesting device output was this time connected to either the bridge rectifier circuit or the prototype harvesting circuit. The voltage output of the piezoelectric generator was recorded via an instrumentation amplifier and using LabVIEW SignalExpress regardless of which circuit was in place. However, the voltage across either the smoothing capacitor of the bridge rectifier circuit or the supercapacitor of the proposed harvesting circuit had to be manually recorded once every minute by using a differential measurement on the oscilloscope (Agilent Technologies model no. DSO3062A); i.e. by using both channels, channel 1 and channel 2, and using the math function “A-B”. The

reason for this is, in the new harvesting circuit concept case, that the parts of the circuit that comprise the new concept; i.e. the inductor through to SC2 (essentially the bottom half of the circuit shown in Figure 4-26 through Figure 4-28; pages 254-262) are floating with respect to the control functions of the circuit (also see Figure 4-48 on page 299 for an explanation), therefore neither terminal of the reservoir capacitor could be connected to ground through the earth lead of an oscilloscope probe. In addition, the voltage across the capacitor in either the bridge rectifier circuit or new concept circuit could not be recorded by directly using a differential input on the NI analogue input module, due to the $1\text{M}\Omega$ input impedance; nor could it be recorded via the use of an instrumentation amplifier (as per the output of the piezoelectric generator): in this case it was found that the input bias current of the instrumentation amplifier charged the capacitor, thus affecting the measurement. The measuring procedure chosen, although labour-intensive, ensured that the correct measurement could be made, while also ensuring that the impedance presented to both the generator output and capacitors during measurement for all cases was $10\text{M}\Omega$, thereby ensuring a fair test.

As for all previous tests, the vibration applied to the harvesting device was controlled from the Laptop using LabVIEW SignalExpress, and the accelerometer output was connected to the NI 9229 analogue input module for this purpose.

4.6.1.4 Testing Procedure for the Complete Harvesting Circuit Concept Tests

The purpose of these tests was to verify first of all that the proposed charge storage concept is feasible (i.e. that it works), and to analyse its effectiveness in comparison with a standard bridge rectifier circuit. The standard bridge rectifier circuit was tested first. The diodes used in construction of the rectifier circuit were the same diodes used for D1 and D2 in the proposed harvesting circuit: 1N4001 silicon rectifier diodes, and

the smoothing capacitor used was a 220 μ F 10V electrolytic. This value was chosen because it is large enough to constitute a substantial storage reservoir when fully charged (from the equation for energy stored in a capacitor: $\frac{1}{2} \cdot C \cdot V^2$, 2.75mJ would be available in the event that the voltage across it reaches 5V, giving 2.75mW for 1 second, or 45.8 μ W for 1 minute), and the charging time was judged to be not unreasonable for measurement purposes. As per the SSHI tests, the optimised energy harvesting device of Chapter 3 was used as the generator and the frequency of vibration was set at 60Hz. The acceleration amplitude was this time set to $\pm 0.125g$ using LabVIEW SignalExpress. The voltage output of the energy harvesting device and the voltage across the smoothing capacitor of the bridge rectifier were recorded using the test setup of Figure 4-32.

Following this test, the bridge rectifier circuit was removed from the system and the prototype harvesting circuit installed in its place. Initially, only links L_{main} and L_{max} in the prototype harvesting circuit (see Figure 4-28 and the photo of Figure 4-29) were connected in order to enable the SSHI technique and the charge storage function that collects positive charge only from the piezoelectric harvester. In addition, supercapacitor SCI (see Figure 4-28) was replaced by a 220 μ F 10V electrolytic capacitor in order to achieve fair comparison with the performance of the bridge rectifier circuit. The test that was performed for the bridge rectifier circuit was then repeated with the same conditions (vibration at 60Hz and $\pm 0.125g$ acceleration amplitude), and both the voltage output of the energy harvesting device and the voltage across the 220 μ F capacitor were recorded using the test setup of Figure 4-32.

In order to obtain results for different vibration acceleration amplitudes, the tests performed with the bridge rectifier circuit and proposed harvesting circuit, initially done at an acceleration amplitude of $\pm 0.125g$ for both cases, were then repeated at $\pm 0.095g$.

Finally, link L_{min} was connected in the prototype harvesting circuit in order that negative charge as well as positive charge could be collected from the piezoelectric generator, and the test was again repeated with the acceleration amplitude again set at $\pm 0.125g$.

4.7 Test Results

In this section, the SSHI tests results are presented and discussed first, and the complete concept test results are presented and discussed second.

4.7.1 SSHI Test Results and Discussion

Figure 4-33 shows the voltage amplitude measured across different resistive load values both with and without the SSHI technique for a vibration frequency of 60Hz and a vibration acceleration value of $\pm 0.23g$:

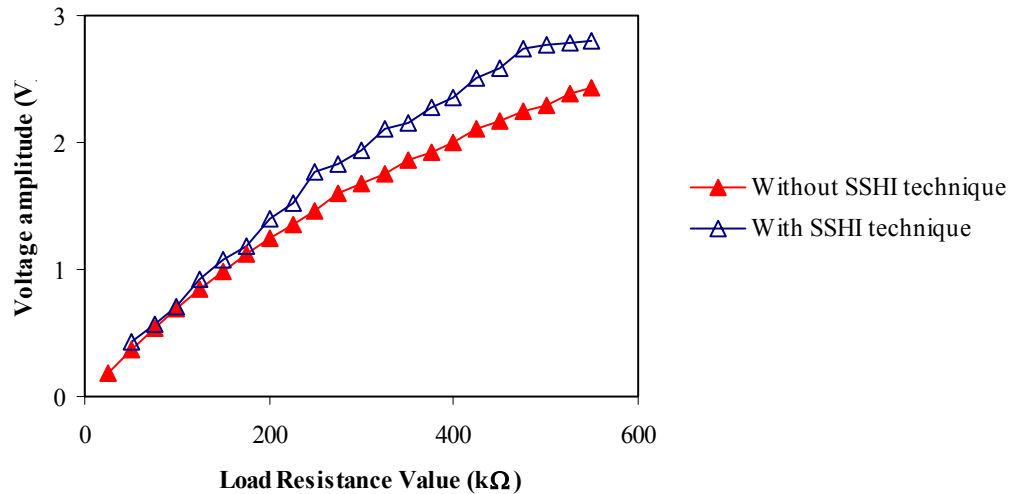
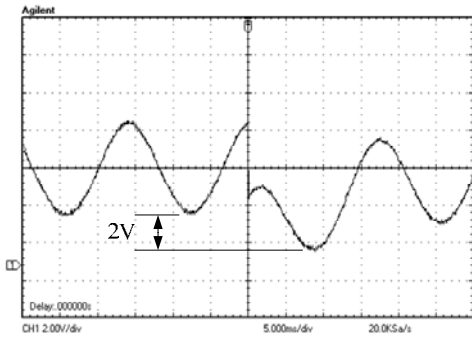
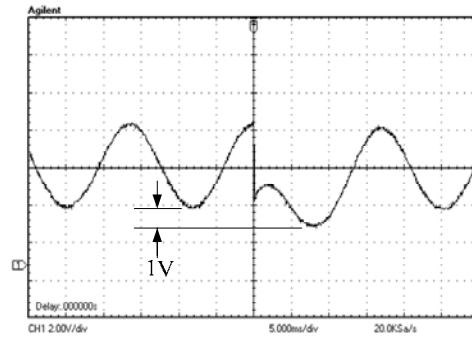


Figure 4-33 Measured output voltage of the piezoelectric vibration energy harvesting device with and without the SSHI technique (frequency = 60Hz; acceleration = $\pm 0.23g$).

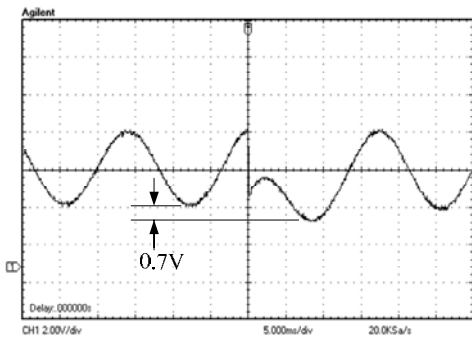
The highest output voltage measured with the SSHI technique applied was 2.80V, compared with 2.43V without the SSHI technique. This result is not as expected since, from the literature, a voltage boost of around 80% is expected. The reason why the voltage amplitude achieved using SSHI in these experiments is so low becomes apparent when the waveforms that were captured on the oscilloscope are analysed. Figure 4-34 shows oscilloscope traces that show the voltage output of the optimised harvesting device when it is connected to a range of different value load resistors and subjected to SSHI. Each waveform shows one charge inversion event only (this could be arranged by adjusting the potentiometers in the circuit), in order to give a visual effect of how much the voltage amplitude has increased by in each case.



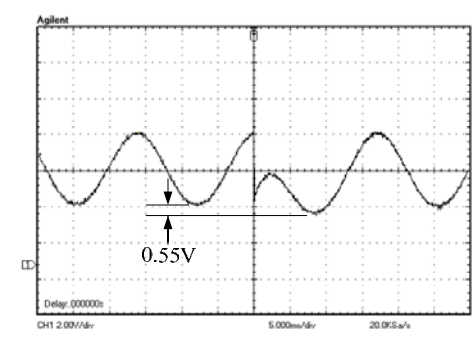
(a) Load resistor = $5\text{M}\Omega$



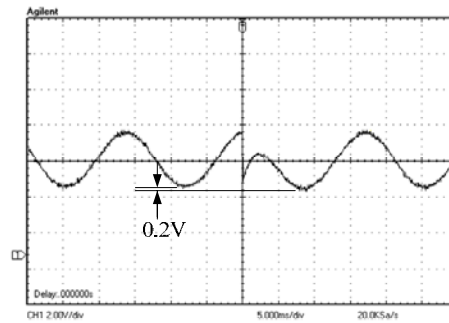
(b) Load resistor = $4\text{M}\Omega$



(c) Load resistor = $3\text{M}\Omega$



(d) Load resistor = $2\text{M}\Omega$



(e) Load resistor = $1\text{M}\Omega$

Figure 4-34 Oscilloscope traces showing the voltage output of the optimised harvesting device when connected to a series of different load resistor values.

From a visual inspection of the waveforms presented in Figure 4-34, it is obvious that the effectiveness of the SSHI technique is decreased as the value of load resistor is decreased, since the gain in voltage amplitude achieved using the technique becomes less as the value of load resistance decreases.

This effect has not been reported in the literature to date. In an effort to understand it, a model of the energy harvesting device and implementation of the SSHI technique was constructed in the circuit simulation tool Switchercad (Linear Technology, Milpitas, CA, USA). This is shown in Figure 4-35:

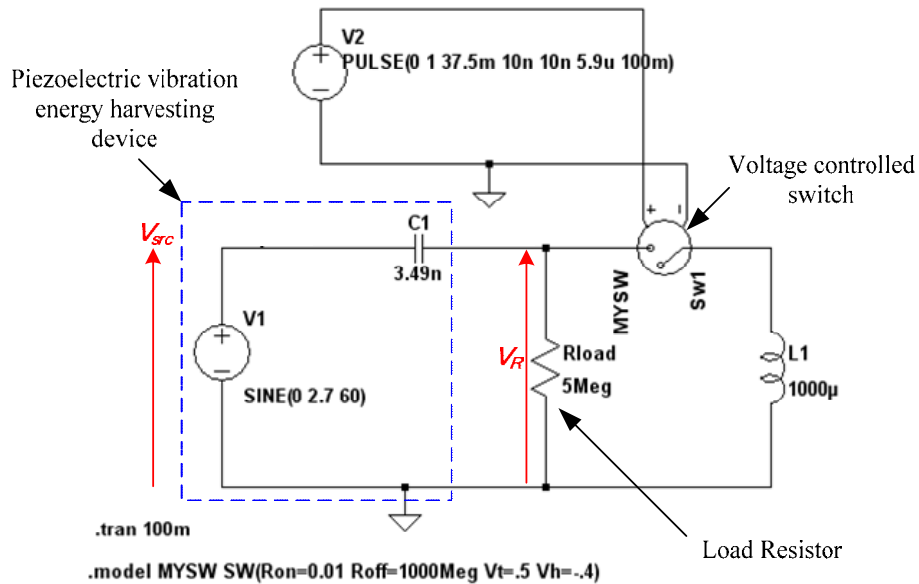


Figure 4-35 SSHI circuit with resistive load, built in Switchercad.

The voltage controlled switch of the simulated circuit operates once only, at one maxima of the piezoelectric generator voltage output waveform. The resulting waveforms from the simulations are shown in Figure 4-36 overleaf.

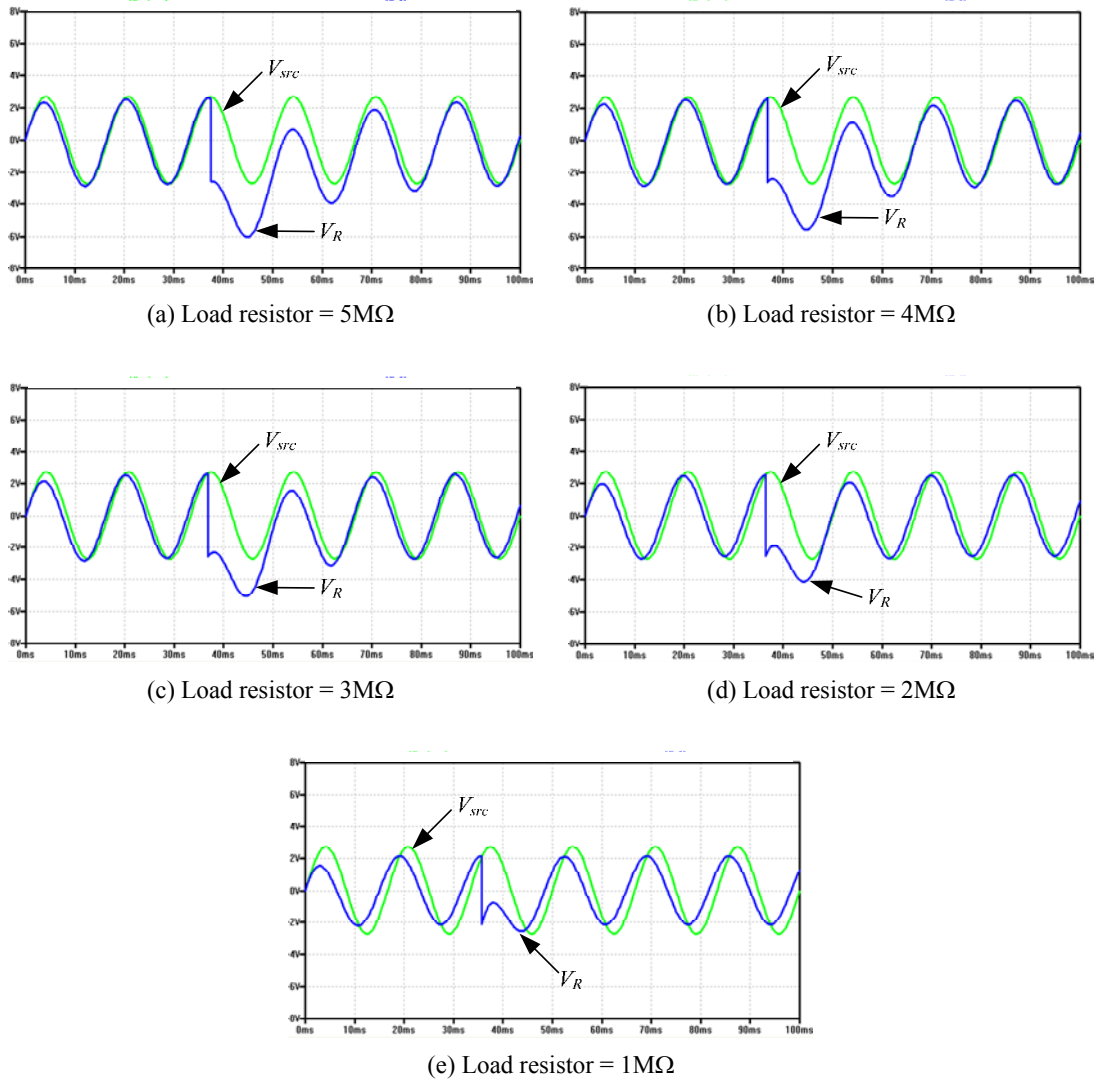


Figure 4-36 Simulated waveforms showing the voltage output of the optimised harvesting device when connected to a series of different load resistor values.

The circuit simulations show the same effect that the experimental results of Figure 4-34 show; that is, the effectiveness of the SSHI technique is decreased as the value of load resistor is decreased. However, in the circuit simulations, the advantage is that V_{src} (see Figure 4-35 for identification of V_{src}) can be examined (obviously, this cannot be done by experiment since it is internal to the piezoelectric generator), and this shows that as the value of resistive load is decreased, the phase difference between V_{src} and V_R

increases. On close examination of the simulated voltage waveforms, the same pattern can be seen for each load resistor case: although initially (at the left-hand-side of each waveform) the two voltage waveforms start off in phase, they quickly become out-of-phase. This is expected from electrical theory as follows: for most of the time the circuit of Figure 4-35 consists of only the capacitance of the piezoelectric generator connected in series with the load resistor, since the inductor is only switched in periodically for a very short time. In such a circuit the following conditions occur: the same current flows through the capacitor and resistor; the current through the capacitor leads the voltage developed across it, V_C , by 90° ; the voltage developed across the resistor, V_R , is in phase with the current. This means that the voltage developed across the capacitor lags the voltage developed across the resistor by 90° , and V_{src} , which is the source voltage, is the phasor sum of the V_C and V_R . V_{src} therefore lags the current flowing in the circuit by an angle lying somewhere between 90° and 0° , and the greater the ratio of capacitive reactance, X_C , to load resistance, R , the greater the angle (phase difference). The phasor diagrams and calculations used to perform a theoretical analysis are shown in Figure 4-37 and equations (64) and (65):

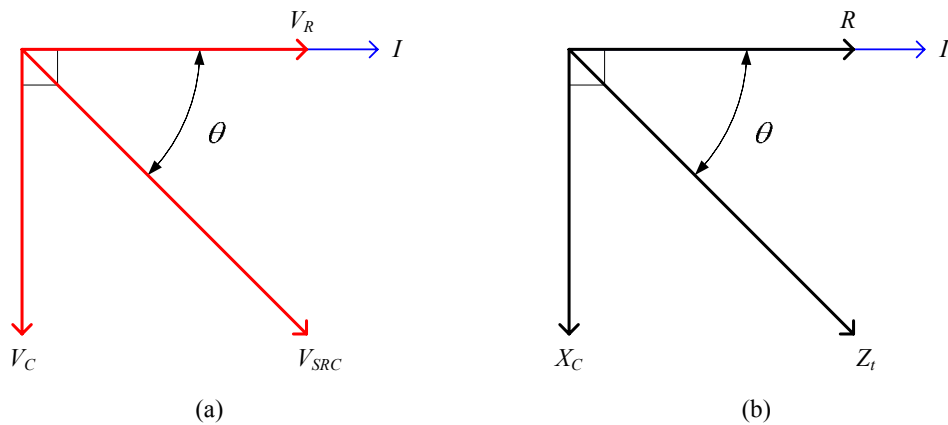


Figure 4-37 Phasor diagrams for a CR series circuit (a) the voltage phasor diagram (b) the impedance phasor diagram.

$$\theta = \tan^{-1} \frac{V_C}{V_R} \quad (64)$$

$$\theta = \tan^{-1} \frac{X_C}{R} \quad (65)$$

Where: I is the current flowing through the circuit, Z_t is the total impedance of the circuit and θ is an angle lying somewhere between 90° and 0° . For the case considered here, where the capacitance of the optimised harvesting device, 3.49nF (as found through measurement in section 4.5.2, page 256) is in series with the load resistor, the relationship between the ratio X_C/R and the phase angle is as follows for load resistor values varying between $1\text{M}\Omega$ and $5\text{M}\Omega$:

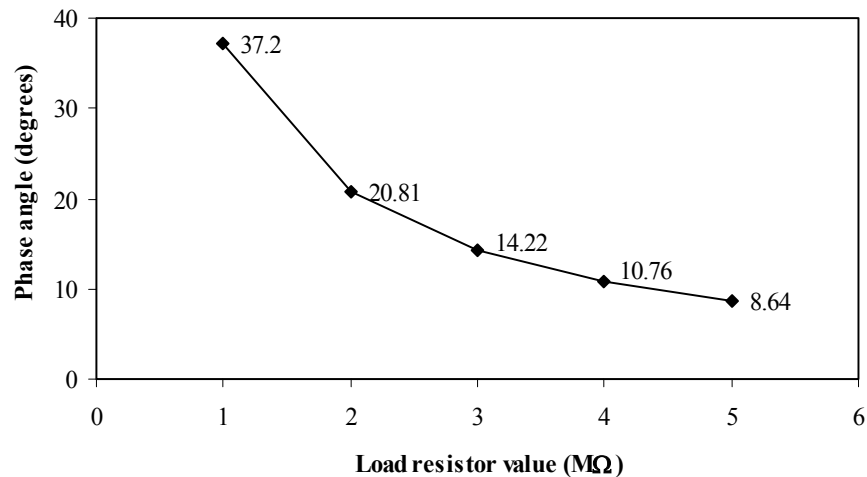


Figure 4-38 Relationship between the ratio X_C/R and the phase angle between V_{src} and V_R .

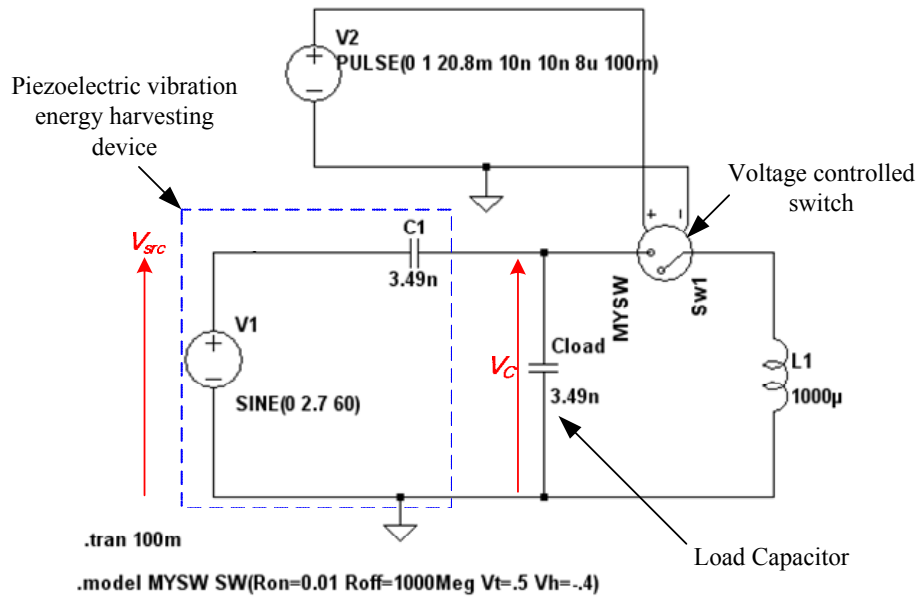
It can be seen that as the value of load resistor is decreased, the phase angle by which V_{src} lags V_R (and hence I) increases. The values calculated from theory appear to support the results obtained from both simulation and experiment. It is clear that this increasing phase difference between V_{src} and I at the lower load resistance values forms part of the story of why the SSHI technique has not been fully effective: the SSHI technique

requires that the voltage on which the inversion is desired be in phase with the displacement of the generator, so that when both are simultaneously at a maxima or minima, reversing the polarity of the voltage means that the generator can have maximum travel on its next stroke, thus doubling the voltage. However, the voltage in question, in this case, is that across the load resistor: V_R . If V_R is out of phase with the harvesting device displacement, the resulting voltage increase can only be a fraction of the full doubling effect.

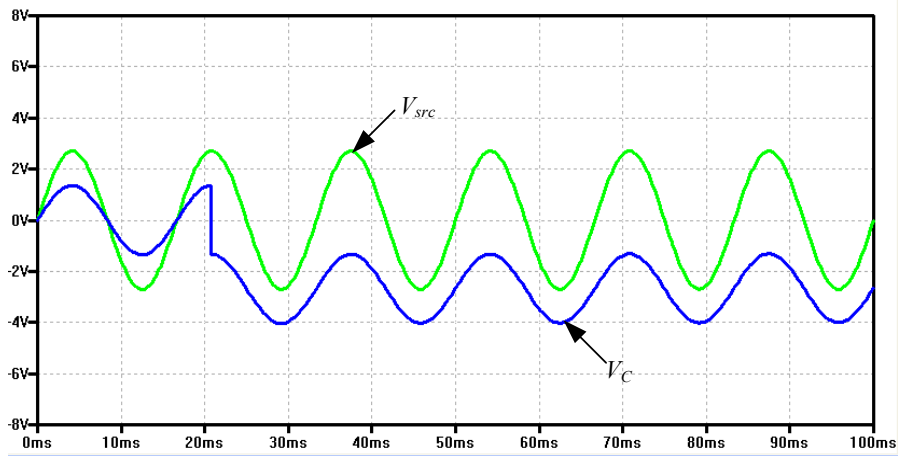
In the case considered here, the load connected to the harvesting device output is a resistive load, R , and in the simulation of Figure 4-36, V_{src} is assumed to be in phase with the harvesting device displacement. Because of the reactive capacitive load internal to the piezoelectric generator, it has been shown in this case that the smaller the value of R , the larger the phase shift between V_{src} and V_R . However, the addition of any load (resistive or otherwise) that results in a phase shift between generator displacement and the voltage on which the inversion is desired will result in a sub optimal voltage inversion, regardless of whether extrema on the displacement or voltage is used to initiate charge inversion. It is the case that for SSHI to be fully effective, the harvesting device displacement and the voltage on which inversion is desired must be in phase, otherwise a full charge inversion cannot be achieved.

Although these findings may pose a problem for some harvesting circuits employing the SSHI technique (and this problem has not been reported in the literature to date), it is possible that the SSHI technique can still be used with the harvesting circuit concept proposed in this thesis, since a resistive load is not employed. Instead, a charge pump-type of circuit is employed as described in section 4.3 and shown in Figure 4-21 (and Figure 4-22), where the load capacitor has a value that is matched to the capacitance of

the generator. This means that for all vibration conditions, the source impedance of the piezoelectric generator matches the load impedance, and also, since everything in the circuit (aside from the inductance, which is switched in only periodically and for a very short period of time) has a capacitive reactance there can be no voltage phase shift to be concerned with. As verification, a simulation of this type of circuit was performed using Switchercad, and the results show that the SSHI technique can work with a matched capacitive load, as shown in Figure 4-39:



(a)



(b)

Figure 4-39 (a) SSHI circuit with capacitive load, built in Switchercad (b) Simulated waveform showing the voltage output of the optimised harvesting device with a matched capacitive load.

Note that in Figure 4-39, V_{src} and V_C are in phase, and this remains true regardless of the value of load capacitance. The next set of tests: testing of the new charge storage

concept, can therefore go ahead. The test setup for these is given in section 4.6.1.3 (page 273) and the test procedure is described in section 4.6.1.4 (page 275).

4.7.2 Complete Harvesting Circuit Concept Test Results and Discussion

Figure 4-40 shows a comparison of voltages obtained using the bridge rectifier circuit and the proposed harvesting circuit for a vibration frequency of 60Hz and vibration acceleration amplitude of $\pm 0.125g$:

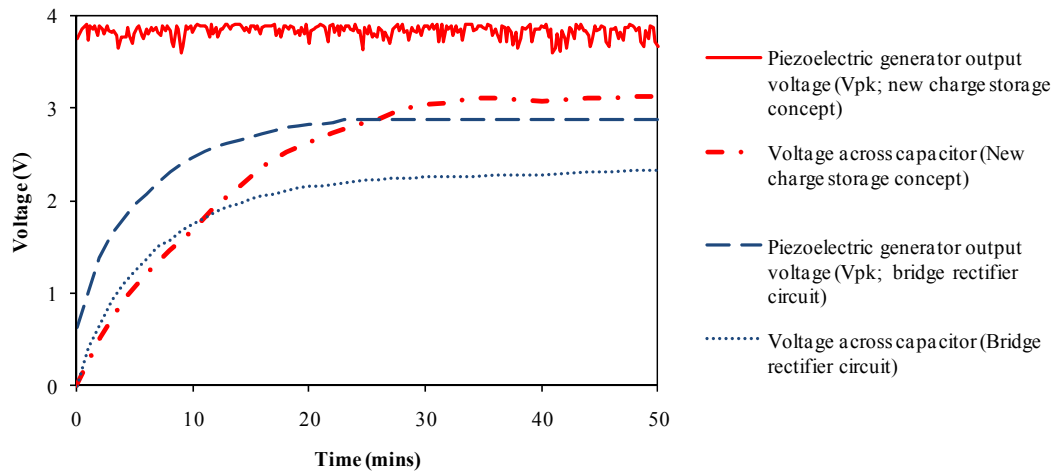


Figure 4-40 Voltage amplitude of piezoelectric generator and voltage obtained on the $220\mu F$ capacitor for both the bridge rectifier circuit and the proposed harvesting circuit (vibration of $\pm 0.125g$ at 60Hz).

The first thing of note in Figure 4-40 is that the voltage amplitude of the piezoelectric harvesting device is much higher when using the proposed new harvesting circuit: an average of 3.83V, than it is when using the bridge rectifier circuit, where it reaches 2.53V. It could be that this 51.4% increase is partly due to the impedance-matched load in the proposed harvesting circuit and partly due to the voltage-increasing effects of the SSHI technique. It can also be seen that the voltage output of the generator when using the proposed harvesting circuit remains at the same level throughout the time when the

storage capacitor is being charged, whereas when the bridge rectifier circuit is used, the voltage output of the generator increases steadily from 0.64V to its final value. This is because of the way that the proposed harvesting circuit functions: by collecting charge from each AC cycle of the generator in a matched-capacitance (3.3nF) capacitor, and then dumping it into a larger storage capacitor, the piezoelectric generator is offered a degree of isolation from the large capacitance (220 μ F) of the storage capacitor. This does not occur in a bridge rectifier circuit, since the voltage across the 220 μ F capacitor (which is initially zero at the start of charging) is linked to the voltage output of the piezoelectric generator by the forward bias voltage of a diode, as seen in the analysis performed in section 4.1.3 (page 217); hence the voltage output of the piezoelectric generator for the bridge rectifier case increases as the voltage on the capacitor increases, until it reaches its final value.

It appears from Figure 4-40 that the increase in generator output voltage achieved using the proposed harvesting circuit translates directly into an increase in the amount of energy harvested in the 220 μ F storage capacitor, because the voltage achieved on the capacitor using the proposed circuit: 3.10V, is more than that achieved using the bridge rectifier circuit: 2.29V. However, it should be borne in mind that the proposed harvesting circuit is also capable of collecting charge during the negative half-cycle of the generator AC output as well as the positive, and in the test performed thus far, only positive charge has been collected. This implies that an equal amount of charge can be simultaneously harvested in the other storage capacitor of the proposed harvesting circuit; i.e. in the capacitor labelled SC2 in Figure 4-28 (page 262). The proposed harvesting circuit may therefore be capable of harvesting more than twice the amount of energy than the bridge rectifier circuit; this prospect is explored later.

In the meantime, in order to examine the effects of a change in acceleration amplitude of the driving vibrations, the tests were repeated for an acceleration amplitude of $\pm 0.095g$. The acceleration could only be decreased from the initial $\pm 0.125g$ value in any further tests, because increasing the acceleration amplitude would result in a higher output voltage from the piezoelectric generator, which would then be outside the $\pm 5V$ limits imposed by the instrumentation amplifier interface to the generator output. Figure 4-41 shows the results for the lower acceleration value of $\pm 0.095g$:

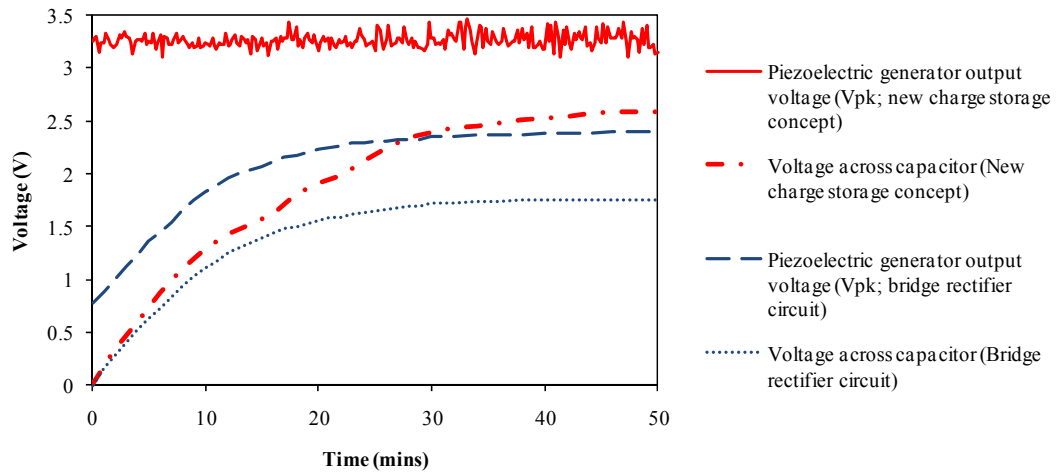


Figure 4-41 Voltage amplitude of piezoelectric generator and voltage obtained on the $220\mu F$ capacitor for both the bridge rectifier circuit and the proposed harvesting circuit (vibration of $\pm 0.095g$ at 60Hz).

Again, Figure 4-41 shows that use of the harvesting circuit proposed in this thesis allows a higher voltage output from the piezoelectric generator (3.26V, as opposed to 2.38V when using the bridge rectifier circuit) and a higher amount of energy harvested in the $220\mu F$ storage capacitor: the voltage across it reaches 2.55V as opposed to 1.75V when the bridge rectifier is used.

Initial indications are that the change in the acceleration amplitude of the vibration corresponds linearly with the change in the piezoelectric generator output voltage amplitude, and thus with the change in the amount of energy harvested in the capacitor. In order to attempt to show this, two more graphs were plotted: Figure 4-42 shows the voltages achieved for the different acceleration levels using the bridge rectifier circuit only, and Figure 4-43 shows the voltages achieved for different acceleration levels using the proposed harvesting circuit only.

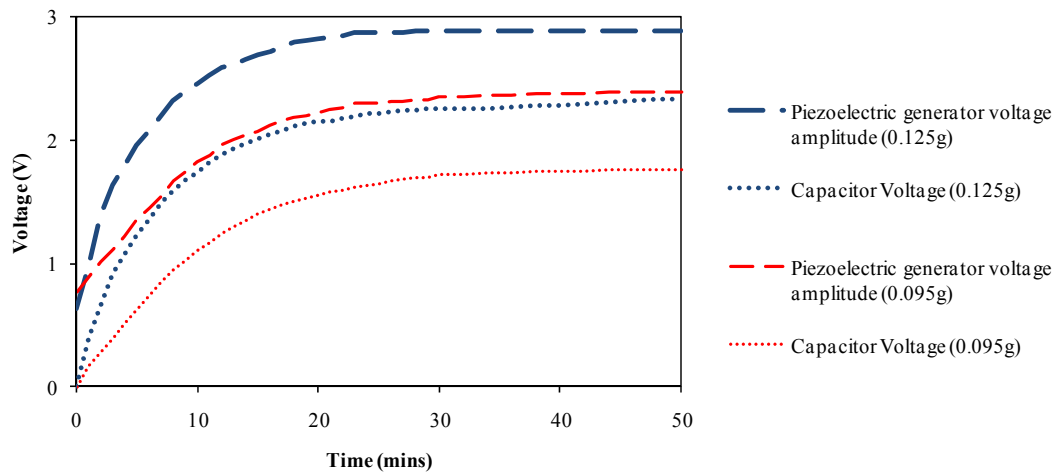


Figure 4-42 Voltage amplitude of piezoelectric generator and voltage obtained on the $220\mu\text{F}$ capacitor for the bridge rectifier circuit under different acceleration conditions (frequency of vibration = 60Hz).

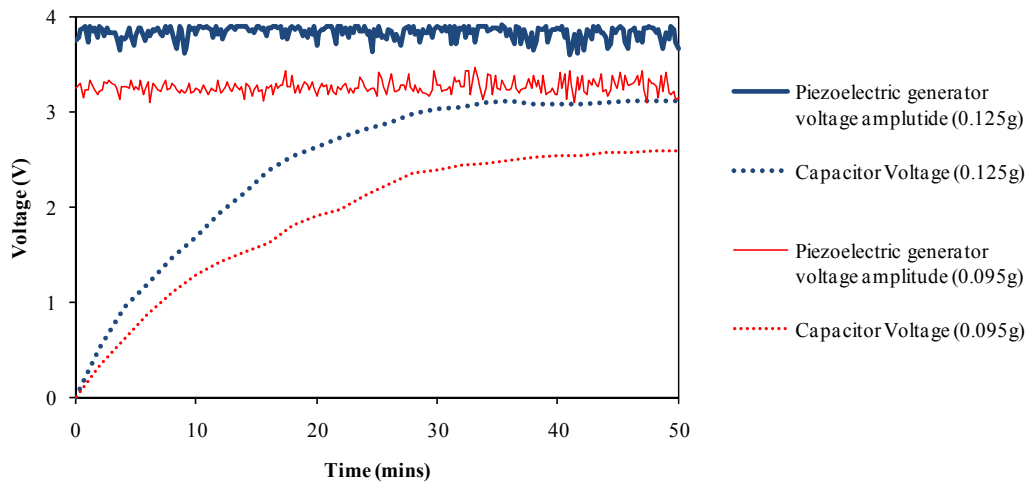


Figure 4-43 Voltage amplitude of piezoelectric generator and voltage obtained on the $220\mu\text{F}$ capacitor for the proposed harvesting circuit under different acceleration conditions (frequency of vibration = 60Hz).

For the final test, the driving vibration was again set to 60Hz and $\pm 0.125\text{g}$ acceleration amplitude, and all of the links in the proposed harvesting circuit; that is: L_{main} , L_{max} , and L_{min} (see Figure 4-28 and the photo of Figure 4-29) were connected such that

negative charge could be harvested as well as positive. The results for this test are shown in Figure 4-44:

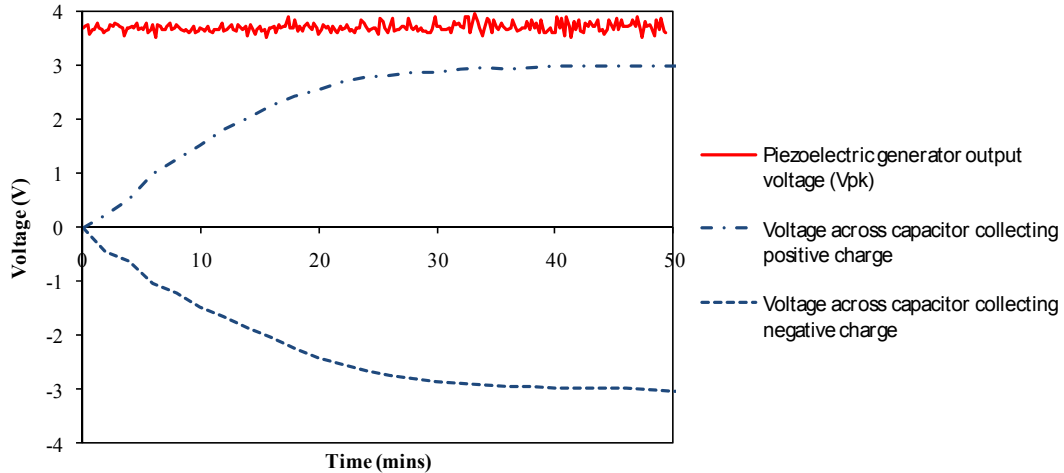


Figure 4-44 Voltage amplitude of piezoelectric generator, voltage obtained on the 220 μ F capacitor collecting positive charge, and voltage on the 220 μ F capacitor collecting negative charge for the proposed harvesting circuit (vibration of $\pm 0.125g$ at 60Hz).

Figure 4-44 shows that nearly equivalent amounts of energy are harvested in the 220 μ F capacitor collecting positive charge and in the 220 μ F capacitor collecting negative charge. The voltage across the former capacitor reaches 3.00V, while the voltage across the latter reaches -3.03V. Therefore, if these two capacitors were connected in series, as described in section 4.3 (Figure 4-24, page 248), a total of 6.03V (equating to 2.00mJ of energy, which is 2.00mW for 1 second, or 33 μ W for 1 minute) would be available for powering a buck-boost DC-DC converter. Given that such converters can be capable of efficiencies of up to around 85%, an application circuit drawing 10 μ W, such as the RFID tag shown in Figure 2-1 (page 28), could be powered for 2.8 minutes. Alternatively, an application circuit drawing 1.75mW such as the Sunflower miniature computing system could be powered for 971ms. If the bridge rectifier circuit were used,

Figure 4-40 shows that a total of 0.577mJ of energy would be available for the same vibration conditions, which, via the same DC-DC converter, could power the RFID tag for 49 seconds, or the Sunflower system for 277ms. Therefore, the new charge storage concept proposed in this thesis can provide approximately 247% more regulated DC power than the bridge rectifier circuit for the same vibration conditions.

4.8 Simulation of the Concept: Analysing Average Power Output for the Purpose of Comparison with Other Circuit Techniques

4.8.1 Introduction

The previous set of tests showed that the amount of energy that can be harvested into storage capacitance using the new harvesting circuit concept is a factor of 3.47 higher than that which can be harvested when the bridge rectifier is used, for the same value storage capacitor and the same input vibration conditions. As discussed in the background section of this chapter (section 4.3.1 on page 237) the main philosophy underlying the new concept, because the energy output of meso-scale harvesting devices is generally very small, is to collect charge over time in a storage reservoir, and then when the reservoir is full to disconnect it from the harvesting circuitry and connect it instead to the end application or, more likely, to a DC-DC converter which then powers the end application. Because of this, the findings presented thus far have been from results that are based on measuring the voltage achieved on the storage reservoir (i.e. the 220 μ F capacitor), and from these voltage readings the energy content of the storage capacitor in each case has been calculated, by using the expression $\frac{1}{2}CV^2$ (where C is the value of the storage capacitor and V is the voltage across the capacitor). However, this author understands that it is perhaps unusual to characterise the energy output of an energy harvesting system in this way. Most of the literature chooses to analyse average

power output over time rather than energy accumulated in a storage reservoir, and this might make it difficult to compare the new concept proposed herein with other existing techniques in the literature.

With this in mind, the purpose of this section is to provide, through simulation, a means of comparing the technique presented herein with other existing circuit techniques. In order to do this, the maximum average power output that can be obtained using the concept needs to be measured, which means that a method of obtaining the average power output needs to be devised. As mentioned in the previous paragraph, the system is designed to store (i.e. build up) charge in a reservoir capacitor over time, and then power an application from the stored charge. So far, the practical experimental work done proves the concept as far as charging the large reservoir capacitor is concerned, however it has not been taken further whereby the harvested energy is actually used to power an end application or load. One means by which the average power output can be measured then, is to take the concept one stage further; i.e. when the capacitive reservoir is full, disconnect it from the charging circuit and connect it instead to a load. Given several repetitive charge/discharge cycles of the reservoir capacitor, the average power output can be easily calculated. This can then be compared with the average power output of other techniques given in the literature.

4.8.2 Description of the Simulations

In this section, three simulations will be undertaken, as follows:

- 1)** A simulation to determine the maximum average power output of a piezoelectric harvesting device; done by measuring the power dissipation of an optimal load resistance connected directly across the output terminals of the harvesting device; i.e.:

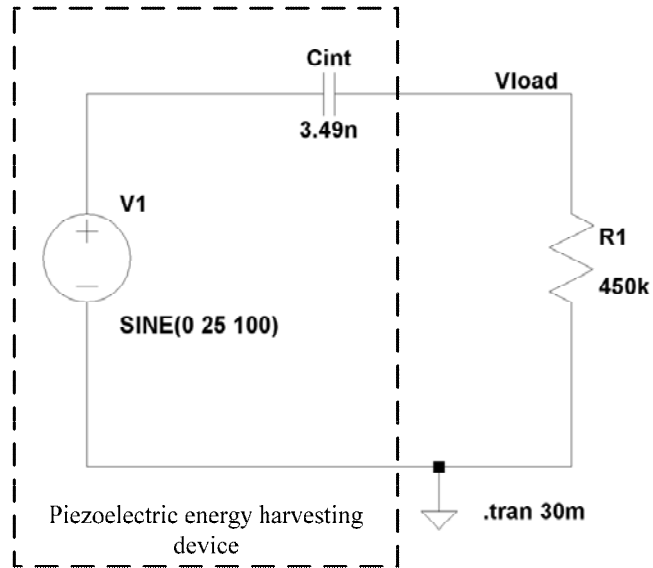


Figure 4-45 Simulation circuit, built in Switchercad for the purpose of ascertaining the theoretical maximum average power output of a piezoelectric harvesting device.

2) As an example of something to compare with (i.e. another technique given in the literature), a simulation to ascertain the maximum power output when the technique proposed by Ottman et al [93] [133] is used will be carried out. The work of Ottman et al is already mentioned in the literature review (page 107). Their target application is the charging of an electrochemical battery, and so they begin by suggesting that the first stage needed in an energy harvesting circuit is an AC-DC rectifier, since electrochemical batteries require a DC charging supply. Taking the case of a bridge rectifier with a smoothing capacitor and constant current load, they show through analytical analysis that the peak output power occurs when the voltage across the smoothing capacitor (V_{rect} in their circuit) is equal to one-half the peak open-circuit voltage of the harvesting device. Their strategy is then to always maintain this optimal rectifier output voltage regardless of any changes in the characteristics of the vibration exciting the harvesting device. Their method of achieving this is to use a DC-DC converter as an automatic adaptive impedance interface, so that for a given battery load

(with a given battery voltage that is essentially constant) maximum current flow from the harvesting device is always achieved, which corresponds to the output voltage of the rectifier, V_{rect} , being maintained at its optimal value. The DC-DC converter is controlled as part of a closed loop control system, in which the current flowing into the battery is sensed (using a current sense resistor) and the sign of the slope of the battery current curve is used to adjust the duty cycle of the converter. See Figure 4-46:

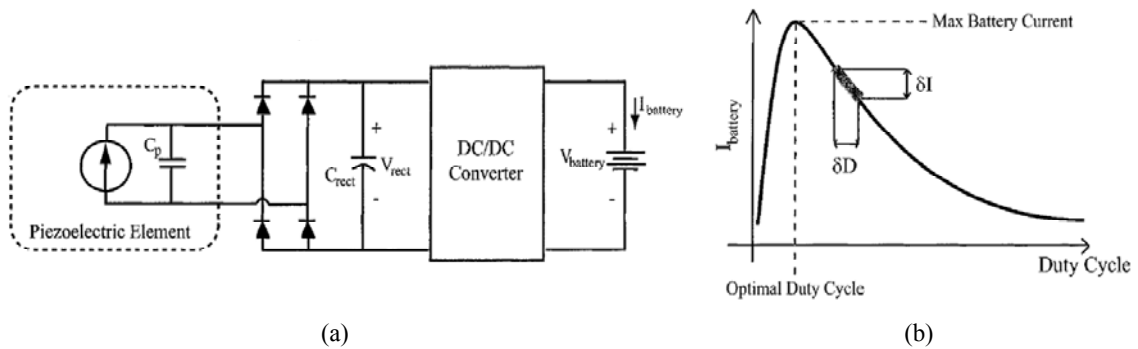


Figure 4-46 (a) Adaptive energy harvesting circuit given in [93] (b) Steady-state battery current as a function of DC-DC converter duty cycle [93].

Since maximum power output corresponds to V_{rect} being maintained at half the peak open-circuit voltage of the harvesting device, which corresponds to a certain impedance being interfaced to the rectifier output, a simulation of the technique does not necessarily need to include the full control system and DC-DC converter. It can be done simply with a bridge rectifier, smoothing capacitor and variable resistive load. As a self-check, at the load value at which maximum power is transferred, the rectifier voltage, V_{rect} , should be equal to one-half the peak open-circuit voltage of the harvesting device. The circuits used in simulation therefore, are shown in Figure 4-47:

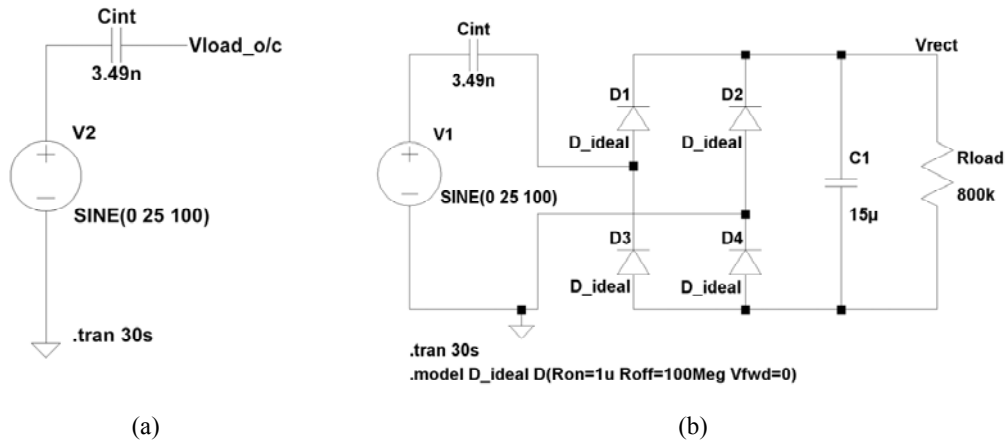


Figure 4-47 Circuit simulation for the technique proposed by Ottman et al: (a) Circuit used to obtain the peak open-circuit voltage output of the generator (b) Circuit used to ascertain the load resistor value which results in maximum power output, the power dissipation in the load, and the power extracted from the harvesting device.

In both circuits, the piezoelectric generator is represented as a voltage source in series with its own internal capacitance, C_{int} . The value chosen for the internal capacitance, 3.49nF, is the measured capacitance of the optimised device developed in this thesis. Since Ottman et al [93], state the assumption of the use of ideal diodes in their analytical analysis, the diode model used in the simulation was modified to become ideal: the on resistance was set to $1\mu\Omega$, the off resistance to $100M\Omega$ and the forward bias to 0V, therefore the diodes in Figure 4-47 (b), labelled D_{ideal} , essentially behave as switches.

3) The last simulation performed will be that of the harvesting circuit concept developed in this thesis, with the addition of a variable resistive load that can be connected when the reservoir capacitors are full, and then disconnected when the capacitors have reached some pre-defined near-empty point. In order to obtain the average power, a repetitive charge/discharge operation will be performed on the

reservoir capacitors; that is, the capacitors will be charged and discharged a number of times, to enable the calculation of an average power output.

Thus far in the thesis, a circuit has been designed and built (this work is detailed in sections 4.3 through 4.5) that can implement the new concept proposed. By discussing the modifications to the circuit that are needed in order to achieve the connection of a variable load resistor at the required times (and to achieve measurement of the voltage across that load resistor), such that the charge/discharge operation mentioned above can be realised, the reasons for choosing a simulation methodology rather than an experimental methodology for this section of the thesis will become evident.

The physical circuit available up to this point (shown in Figure 4-29 on page 266), as mentioned before, is capable of charging reservoir capacitors SC1 (collecting positive charge) and SC2 (collecting negative charge) using the new concept. However, that is where its functionality ends. In order to add a load periodically to achieve the discharge part of the above described repetitive charge/discharge operation, the circuit would have to be further designed to include the following additional functions:

- 1) A level detector to detect a ‘high’ voltage level on one of the reservoir capacitors,
- 2) A method of disconnecting the reservoir capacitors from the charging circuit, when the ‘high’ voltage level is reached, and connecting them instead to the load resistor; (the reverse operation is obviously also needed, for when the reservoir capacitors are empty).
- 3) A level detector to detect a ‘low’ voltage level on one of the reservoir capacitors,
- 4) A method of measuring the voltage across the load resistor in order to calculate average power dissipation.

While these functions may at first seem trivial, incorporating these into the design of the circuit shown in Figure 4-29 would not be a straightforward task. This is largely because, as mentioned in section 4.6.1.3 (page 273), the sections of the circuit that comprise the new concept (of which the reservoir capacitors are two components) are floating; that is: they are not referenced to the main circuit 0V, to which all the control functions are referenced, but are instead referenced to a net (a signal or physical track) that acts as a 'virtual' 0V. Figure 4-48 attempts to show this:

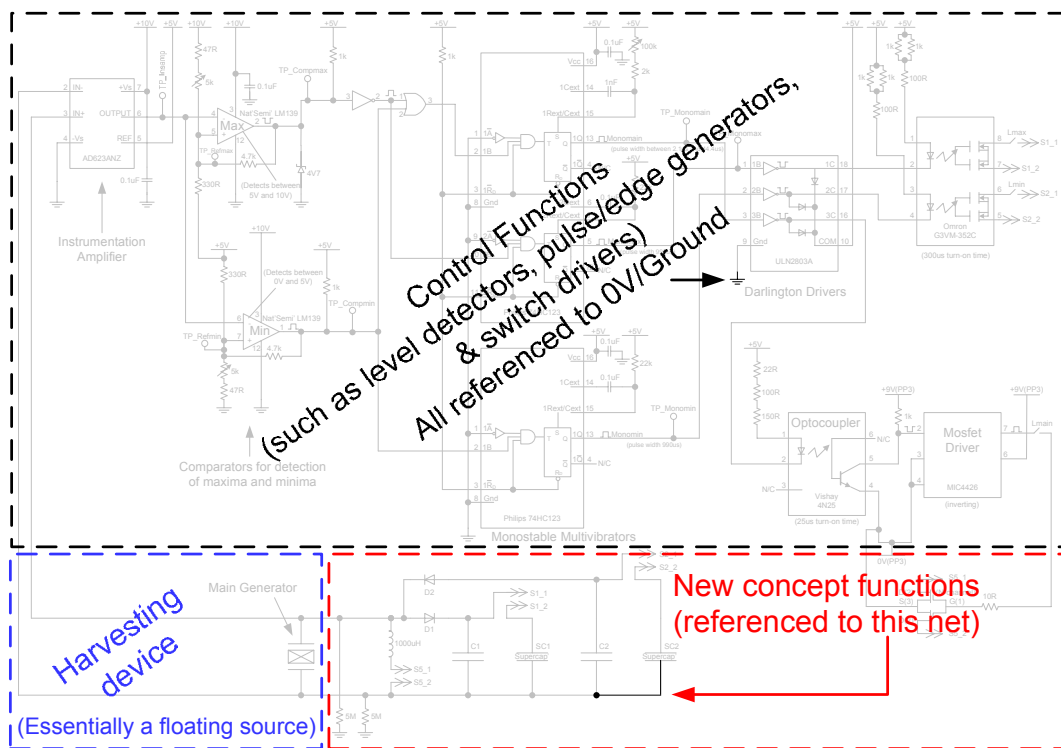


Figure 4-48 Circuit diagram of Figure 4-26 through Figure 4-28, showing those parts of the circuit which are referenced to the main circuit 0V (which in turn is connected to ground), and those parts of the circuit that are floating.

The difficulties this causes in measuring the voltage across the reservoir capacitor have already been discussed briefly in section 4.6.1.3 (page 273), where voltage measurements had to be taken manually using a differential measurement on the

oscilloscope because the input impedance of the differential input to the National Instruments data acquisition device was too low, and use of an instrumentation amplifier affected the measurement. Therefore, this author believes that designing, testing and building a practical circuit to incorporate these new extra functions may also be non-trivial, hence the reason for choosing simulation for this part of the thesis. Put simply, it was perceived that the extra complexity needed (and component lead times etc) in adding the further required functions to the physical circuit shown in Figure 4-29 on page 266, was too great to attempt in the remaining project time. Also, in the ideal environment of the simulation, measurements can be made without affecting the quantity being measured.

The circuit used for simulation of the concept developed in this thesis is shown in Figure 4-49 on the following page:

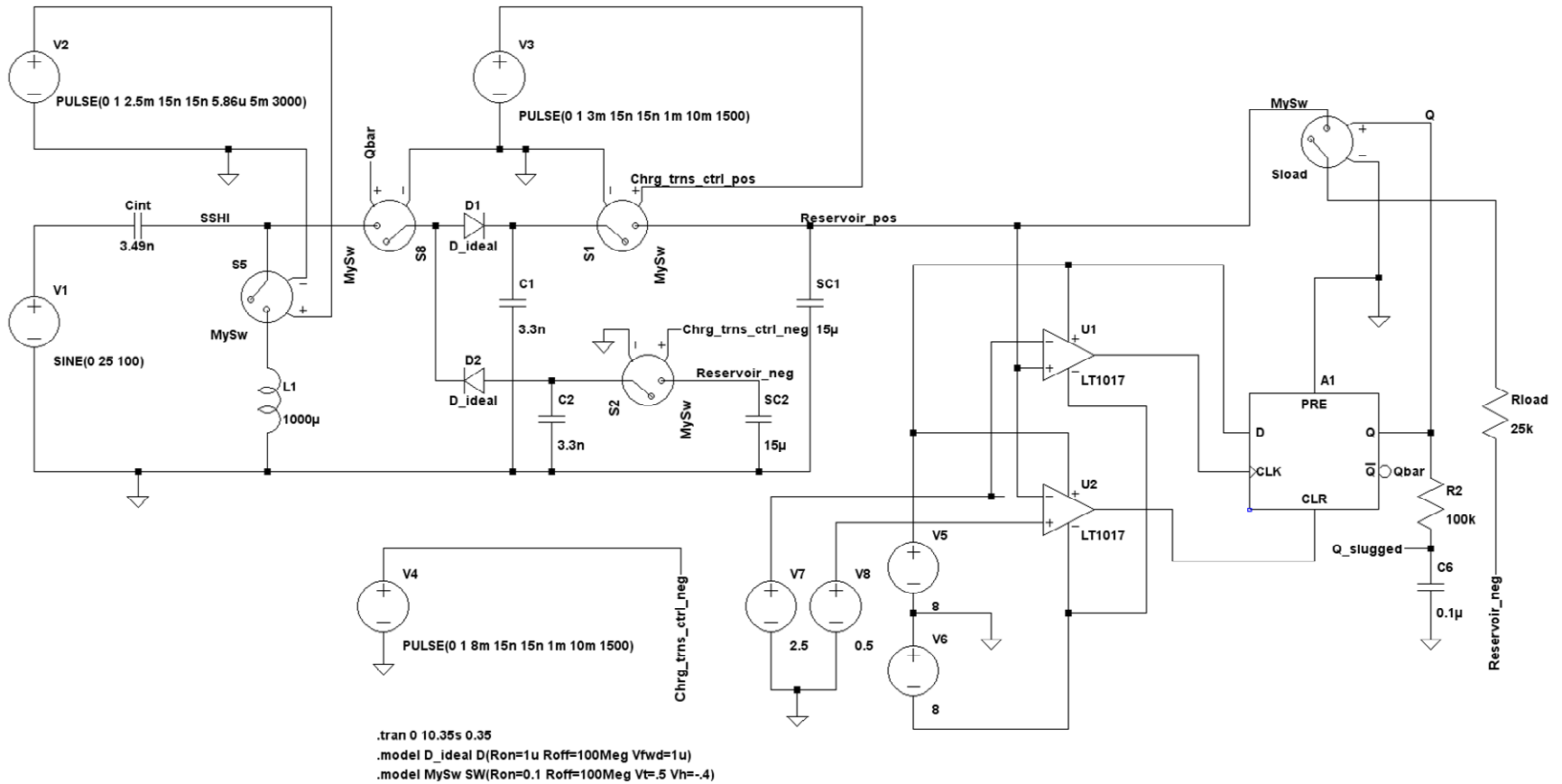


Figure 4-49 Circuit schematic of the proposed harvesting concept, built in SwitcherCAD for simulation purposes.

In Figure 4-49, the piezoelectric generator is again represented by a voltage source in series with its own internal capacitance, C_{int} , and again the value of that internal capacitance is 3.49nF, which is the measured capacitance of the optimised device developed in this thesis. The component identifiers, e.g. “ $C1$ ”, “ $S2$ ” and so on have been made the same as those shown in Figure 4-26 through Figure 4-28, as far as is practicable, so that the reader can cross reference the circuits if need be. Switch $S5$ and inductor $L1$ implement the SSHI technique; $C1$ and $C2$ are the two ‘bucket’ capacitors ($C1$ transferring positive charge and $C2$ transferring negative charge respectively); $SC1$ is the reservoir capacitor collecting positive charge and $SC2$ is the reservoir capacitor collecting negative charge. The level detection of the voltage on one of the reservoir capacitors, carried out to indicate a full charge in both capacitors, is performed on $SC1$, and is achieved through the use of two comparators: $U1$ and $U2$, both of which are without hysteresis, since noise effects are neglected in the simulation. The D-type flip flop, $A1$, provides the drive for the switch $Sload$, which switches the resistive load into the circuit by connecting it in parallel with $SC1$ and $SC2$ (which are themselves connected in series at the times when $Rload$ is connected, e.g. as per Figure 4-24 on page 248). The purpose of switch $S8$ is to disconnect the reservoir capacitors from the rest of the harvesting circuit while the resistive load is connected. Switches $S5$, $S1$, and $S2$, which implement respectively: SSHI, charge transfer from bucket capacitor $C1$ to reservoir capacitor $SC1$, and charge transfer from bucket capacitor $C2$ to $SC2$, are each controlled by pulsed voltage sources: $V2$, $V3$ and $V4$ (again respectively). The parameters for the pulsed voltage sources are given in the brackets nearby and correspond, in sequence, to: initial voltage, on voltage, delay time, risetime, falltime, on time and time period. The timings of the switch operation in each case are therefore

‘manually programmed’ rather than triggered by a circuit event such as a voltage level detector. For example: $V2$, which controls $S5$ for implementation of the SSHI technique, is set to give a first pulse whose rising edge begins at 2.5ms in the simulation, since this is exactly $\frac{1}{4}$ of the time period of the 100Hz cycle of $V1$ (which is the source simulating the piezoelectric harvesting device), and hence switch $S5$ will operate exactly at the first extrema of the harvesting device voltage output waveform. It is then set with a duty cycle of 5ms, to ensure that it will operate at every extrema of the output waveform. Also, the length of time of the specified for the pulse, $5.86\mu\text{s}$, is exactly half the time period of the resonant network formed by the internal capacitance of the piezoelectric generator, C_{int} , and inductor LI , thereby enabling full charge inversion on the piezoelectric element through SSHI.

In terms of simulation of this circuit, there is one further issue to be resolved, and that is what to do with the output of the piezoelectric generator at the times when the resistive load is attached to the reservoir capacitors, since the concept given thus far has been described such that the reservoir capacitors are disconnected from the charging circuit while they are being utilised in powering a load or application. In real life, given a constant vibration source, the SSHI waveform would simply run open-circuit until it settles at some steady-state amplitude that is dependant on the losses within the SSHI circuit itself, which might include: core losses in the inductor, losses caused by capacitance between windings of the inductor, losses through radiation caused by the fast SSHI edges, resistance of the switch, and some equivalent series resistance and inductance in the components and wires. However, in this simulation, the components are ideal, which results in a perfect doubling of the amplitude of the SSHI waveform on

every occurrence of a charge inversion. The SSHI waveform, therefore, quickly reaches kV proportions! See Figure 4-50:

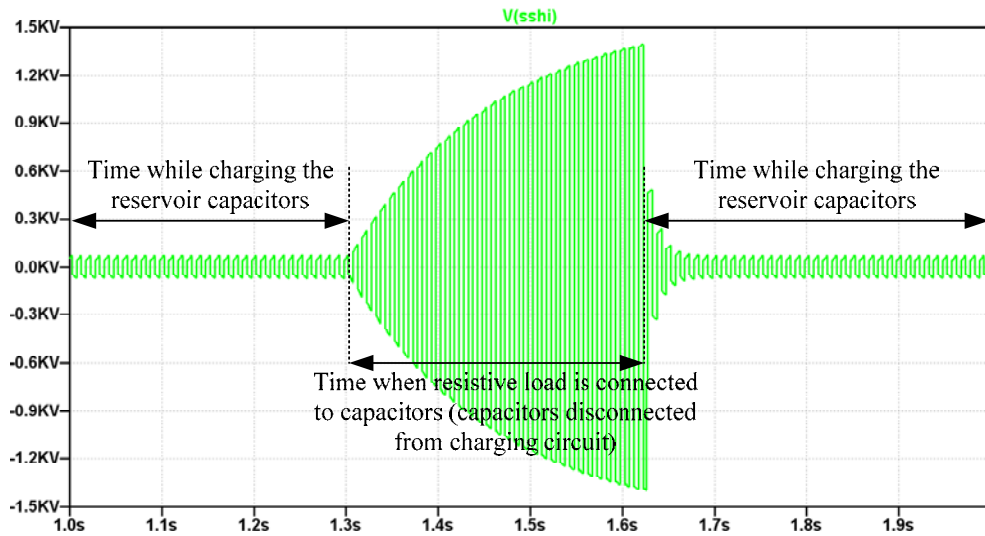


Figure 4-50 Simulation of the proposed harvesting circuit concept, showing the SSHI waveform only.

Note that the amplitude reaches 1.39kV during the time when the resistive load is being powered from the reservoir capacitors and the reservoir capacitors are disconnected from the charging circuit. This will have implications when calculating the average power output from the harvesting device, in that the average power output will be much higher than is possible in practice due to the perfect voltage doubling. In order to obtain some realistic values for the average power output of the harvesting device, the effect has to be somehow nulled, therefore the question is: what is to be done with the output of the harvesting device at the times when the load resistor is being powered from the reservoir capacitors? One answer to this question is that since, in reality, a vibration source is unlikely to halt exactly when the reservoir capacitors are full, and then start again when they are empty, another pair of capacitors could be charged during the times in question. For example, when the resistive load (akin to an application system or DC-

DC converter in a real life situation) is being powered from one pair of reservoir capacitors, another identical pair could be being charged. This idea is also described in the future work section: section 5.4.2.2 on page 351 (no. 1) and was actually present in this author's mind at the time of conception of the proposed harvesting circuit concept, but it has not been mentioned until now for two reasons: concern over the complexity of adding it into the explanation of the concept, and that it was perceived as a further step to be tackled once the basic principle has been proved with one pair of harvesting capacitors. Incorporating this idea into the simulation though, would have the advantage that the average power output from the harvesting device would remain in a steady-state condition, ensuring that the output of the harvesting device is never in an open-circuit condition, therefore eliminating the perfect voltage doubling effect shown in Figure 4-50. To this end, the circuit of Figure 4-49 has been modified slightly, to include another switch, S_6 , and another set of bucket plus reservoir capacitors (C_3 & C_4 , and SC_3 & SC_4). See Figure 4-51 on the following page:

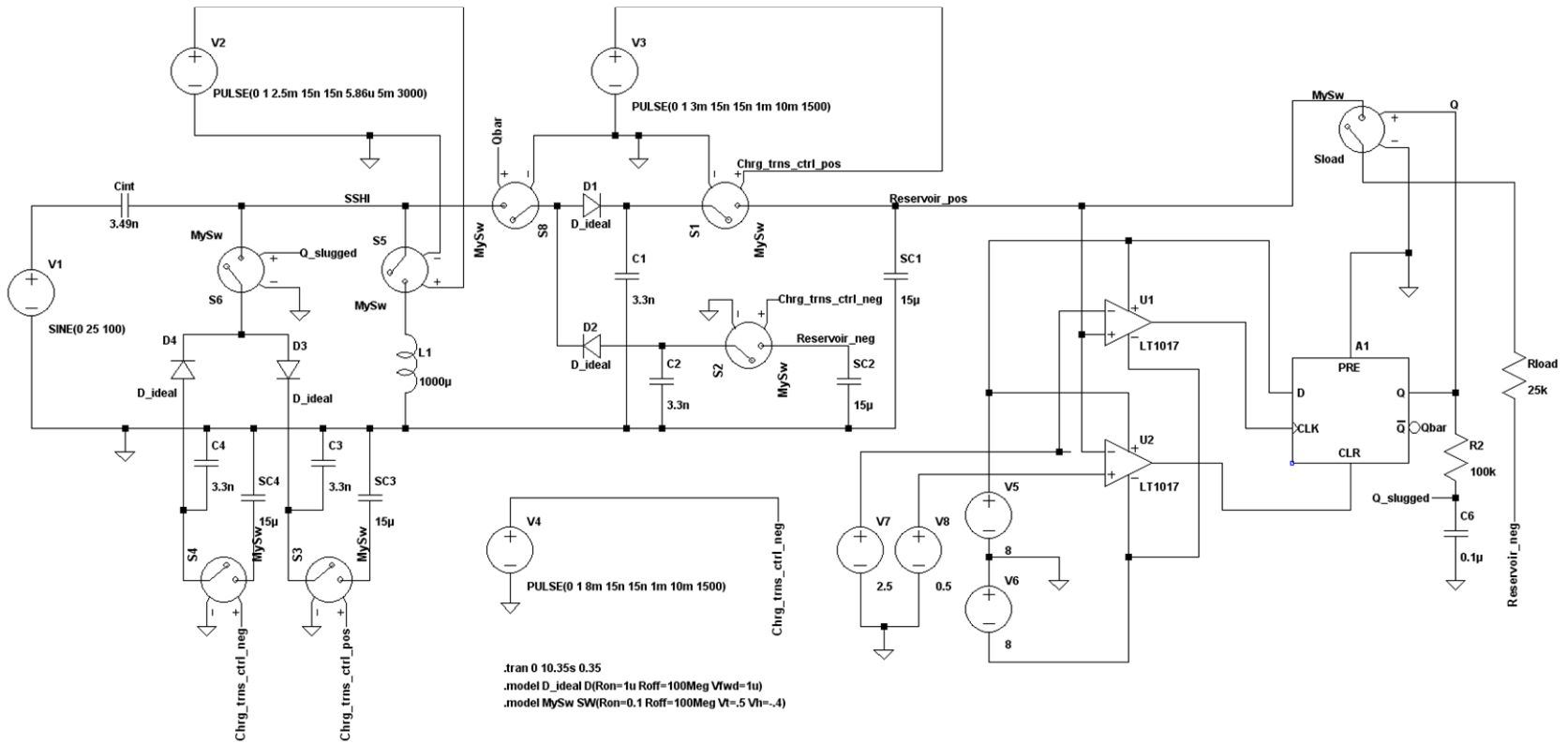


Figure 4-51 Circuit schematic of the proposed harvesting concept including an additional set of reservoir capacitors, built in SwitcherCAD for simulation purposes.

Returning our focus now to the description of all three simulation circuits, for all three circuits; i.e. that shown in Figure 4-45 for the determination of the ‘theoretical maximum’ average power output of the device, that shown in Figure 4-47 for the technique proposed by Ottman et al, and that shown in Figure 4-51 for the concept proposed in this thesis, several conditions are made common:

- 1) The piezoelectric generator is represented by a voltage source in series with its own internal capacitance,
- 2) The value of the internal capacitance is that measured for the optimised device developed in this thesis, which was 3.49nF.,
- 3) The voltage source representing the piezoelectric generator is set as an AC source with amplitude 25V and frequency 100Hz. These values were chosen because the results obtained using simulation no. 1 (see page 294), which was performed to find the maximum theoretical average power output of a piezoelectric harvesting device, were not too dissimilar to those obtained with the optimised device under real-life vibration conditions of $\pm 0.23g$ acceleration at 120Hz (see Figure 3-36, page 205).
- 4) All simulation results are collected under steady-state circuit conditions; i.e. not during initial start-up transient circuit states.

In addition, the component values specified for the simulations are the same as those used in the real-life tests of section 4.6 as far as possible. The exception is the value of the smoothing capacitor of the bridge rectifier circuit used to emulate the technique proposed by Ottman et al (Figure 4-47), and the value of the reservoir capacitors in the concept proposed in this thesis (Figure 4-51), which were all given the value 15 μ F, whereas in real life they were 220 μ F. This is because in the real-life tests, each test

using the proposed concept took approximately 1 hour to complete, and with twenty two load resistor values, and taking into account that simulation time is slower than real time (not to mention the amount of data that would be accumulated and written to the hard drive of the PC), it was unfeasible to specify a 220uF capacitor value for *SC1* or *SC2* in the simulation.

4.8.3 Simulation Results

4.8.3.1 Simulation to determine the theoretical maximum average power output of the piezoelectric harvesting device

The results for this simulation are given in Figure 4-52:

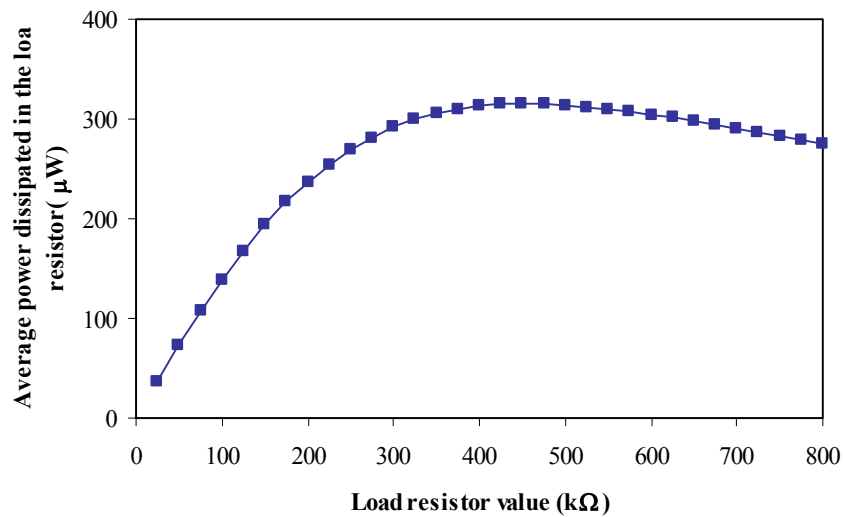


Figure 4-52 Simulated average power dissipated by the load resistor for the circuit of Figure 4-45 (page 295).

The maximum average power dissipated by the load resistor, based on the simulation results of Figure 4-52, is 315.25µW. Given that the simulation circuit consists of only the harvesting device and load resistor (see Figure 4-45 on page 295), the average power dissipated by the resistor is the same as the average power output of the harvesting device. The latter can be measured by plotting the current through *Cint*

multiplied by the voltage V_{load} (which gives a plot of the instantaneous power output of the harvesting device) and then performing an integral calculation on the waveform, which is a function available in the simulation tool, such that an average value is obtained. When done in practice, this gave $315.26\mu\text{W}$ as the result, which is extremely close to $315.25\mu\text{W}$.

The maximum theoretical power output of the harvesting device then, based on the simulation results of Figure 4-52, is $315.26\mu\text{W}$, which occurs with a load resistor value of $450\text{k}\Omega$.

4.8.3.2 Simulation to determine the maximum average power output of the harvesting device when the technique proposed by Ottman et al.

The results for this simulation are given in Figure 4-53:

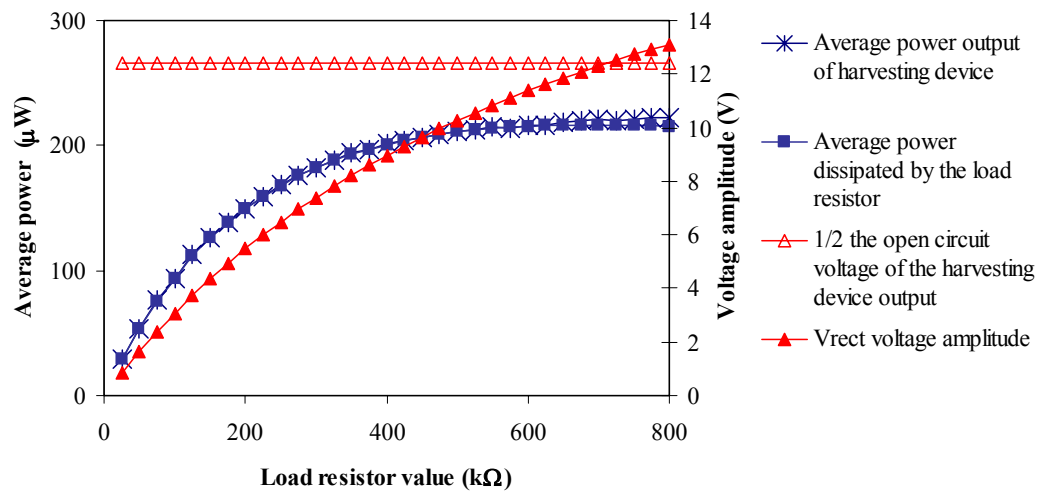


Figure 4-53 Simulated curves for the average power dissipated by the load resistor, average power output of the harvesting device, voltage amplitude of V_{rect} , and $\frac{1}{2}$ the open-circuit voltage of the harvesting device for the technique proposed by Ottman et al.

According to Ottman et al [93], the maximum average power harvested should occur when the voltage at the output of the rectifier, V_{rect} in Figure 4-47 (page 297), is equal

to half the open-circuit voltage of the piezoelectric generator. From the simulation results given in Figure 4-53, this does appear to be the case: maximum power dissipated by the load resistor is $216.7\mu\text{W}$, which occurs when V_{rect} is 12.31V , and half the open-circuit voltage of the harvesting device is 12.4V . In all the voltage results that make up Figure 4-53, the difference between V_{rect} and $\frac{1}{2}$ the open-circuit voltage of the harvesting device is smallest at the load resistor value when power dissipated by the load is maximum.

It can also be seen that the average power dissipated by the load resistance is very close in value at all times to the average power output of the harvesting device; the two curves on the graph appear to track each other. This makes sense given that the diodes used in the simulation are very close to ideal, with no forward bias, and given that the smoothing capacitor, CI , is also ideal, so that all the energy put into the capacitor is returned to the circuit. Essentially there are no losses in the circuit, so that all of the power output from the harvesting device is dissipated in the load resistor.

4.8.3.3 Simulation to determine the maximum average power output of the harvesting device when using the concept proposed in this thesis.

Because the simulation circuit for the concept proposed in this thesis is more complicated than the previous two simulation circuits, it is interesting to examine the different waveforms that occur in the circuit as the repetitive charge/discharge process of the reservoir capacitors takes place. The figures that follow show, for an arbitrary simulation time of 5 seconds with a $25\text{k}\Omega$ resistive load, traces for the voltage across the reservoir capacitors $SC1$ and $SC2$, the power dissipation in the load resistor, and the SSHI waveform.

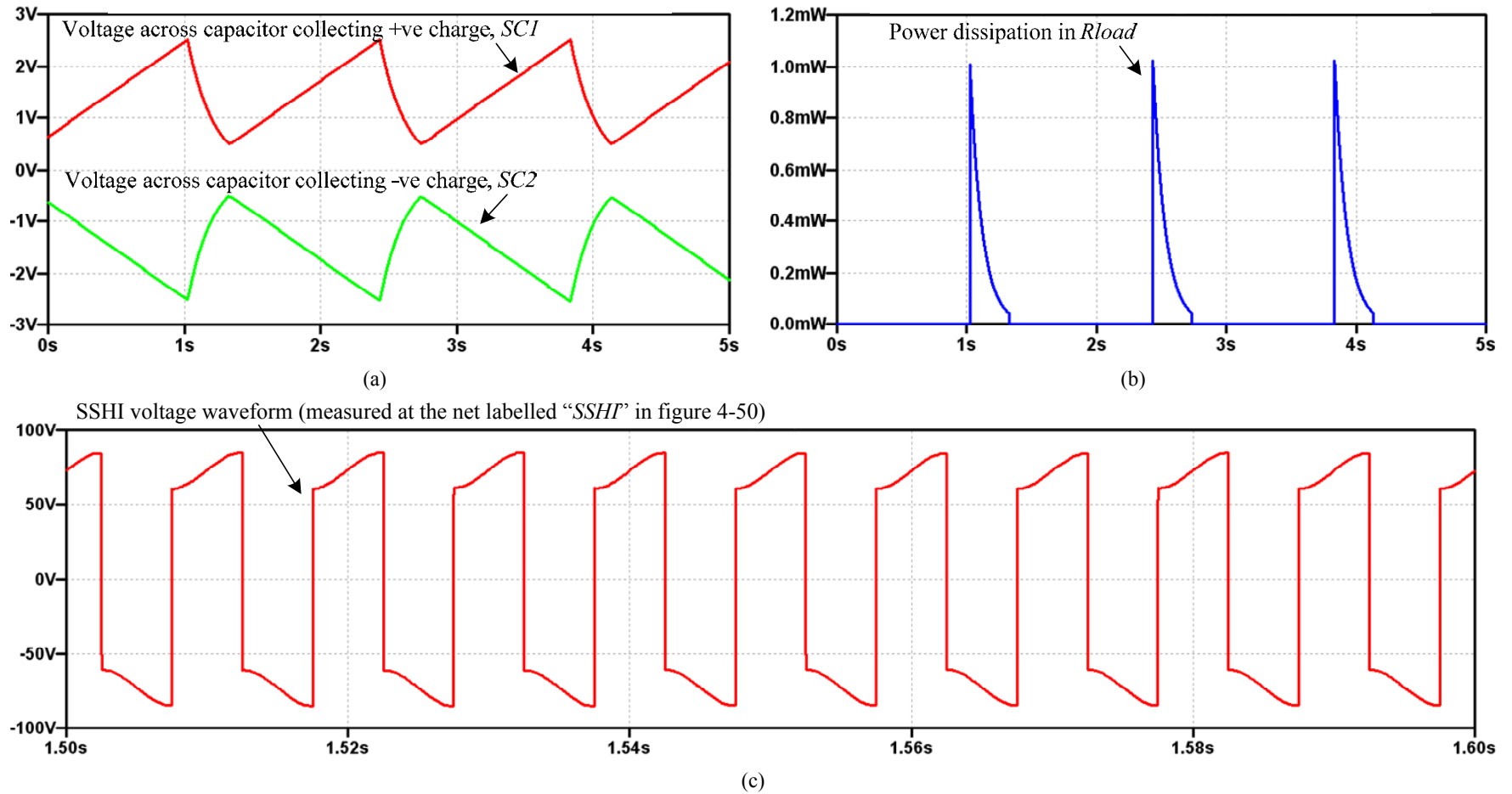


Figure 4-54 (a) Simulated voltages across the reservoir capacitors $SC1$ and $SC2$ (b) Simulated instantaneous power dissipated by the load resistor (c)

Simulated SSHI waveform; all for the circuit concept proposed in this thesis.

The capacitor charging/discharging curves can clearly be seen, and these coincide with the trace that shows the power dissipation in the load resistor, in that during the times when the resistor is dissipating power, the capacitors are in their discharge portions of the curves. The SSHI trace remains steady-state throughout the simulation. Figure 4-55 on the next page shows the voltages across $C1$ and $C2$, which are the 'bucket' capacitors that transfer charge to $SC1$ and $SC2$ respectively. As expected, these follow the SSHI waveform. It can be seen that there is a slight gap in the timing between the charge inversion events on the SSHI waveform, and charge evacuation out of $C1$ and $C2$. This was done on purpose. Switches $S1$ and $S2$, which control charge transfer from $C1$ to $SC1$ and charge transfer from $C2$ to $SC2$ respectively, have been set to wait for 0.5ms after a charge inversion event before operating. The reason for this is that otherwise there would be a risk of the charge in $C1$ and $C2$ being evacuated before the charge inversion event occurs, which would lead to a condition where there is no voltage on the piezoelectric element to invert!

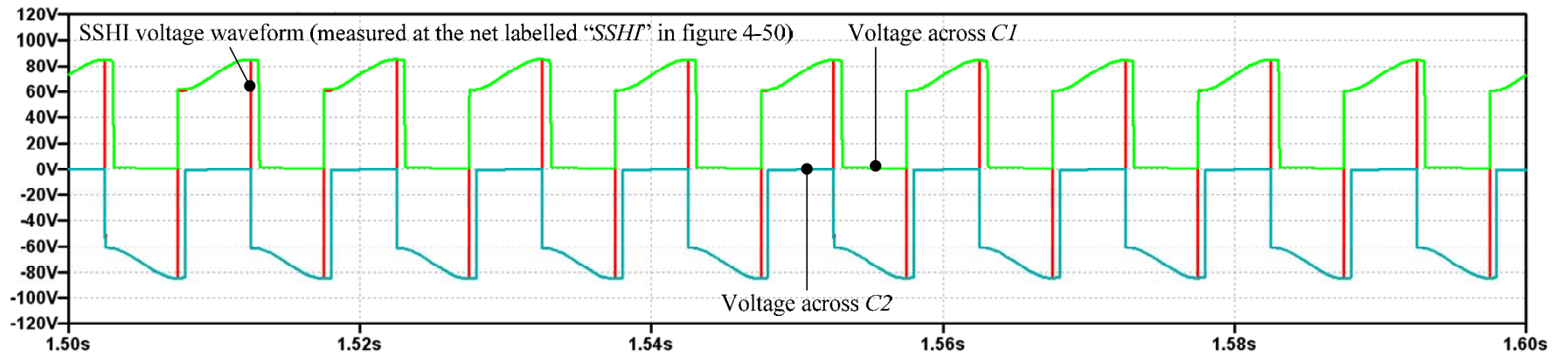


Figure 4-55 Simulated voltages across the bucket capacitors $C1$ and $C2$, and simulated SSHI waveform, for the circuit concept proposed in this thesis.

The results for the simulation, in terms of power outputs, are given in Figure 4-56:

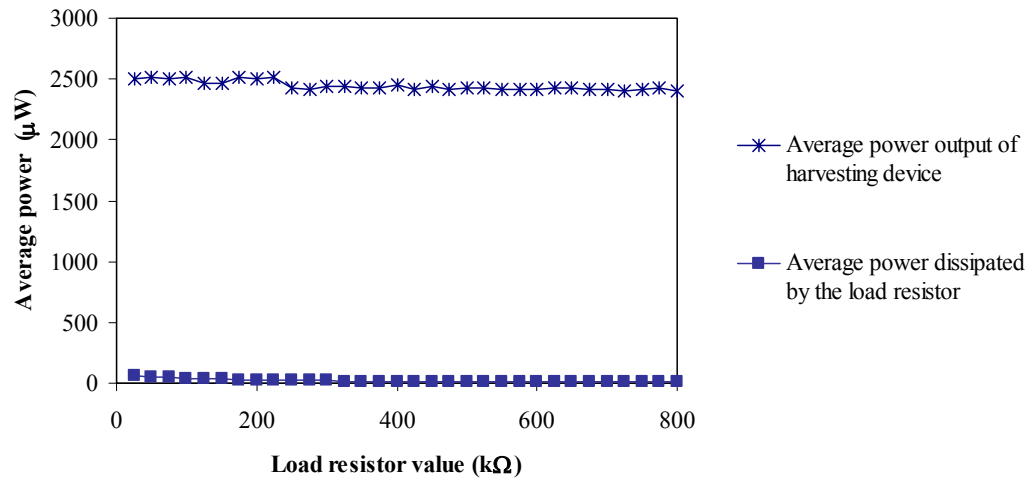


Figure 4-56 Simulated curves for the average power dissipated by the load resistor and average power output of the harvesting device, for the harvesting circuit concept proposed in this thesis.

In order to determine the values for the average powers shown in Figure 4-56, each time the simulation was run (i.e. for each load resistor value), one or more exact charge/discharge time periods were selected in the waveform viewer and the average calculated using the integral function provided in the software. It can clearly be seen that for all load resistor values there is a big difference between the average power output of the harvesting device and the average power dissipated by the load resistor.

When the power dissipated by the load resistor is plotted alone, it appears as follows:

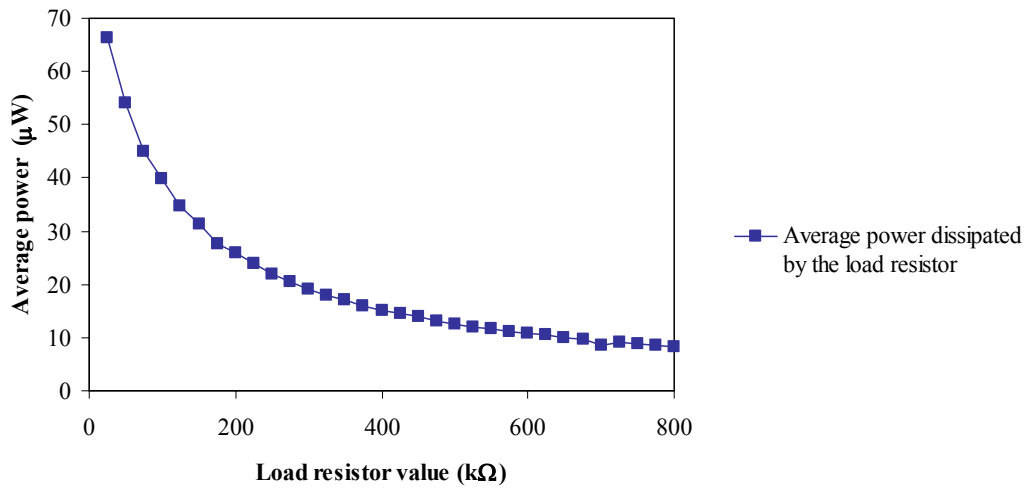


Figure 4-57 Simulated curves for the average power dissipated by the load resistor for the harvesting circuit concept proposed in this thesis.

The shape of this curve is consistent with theory, in that if a circuit is considered where a capacitor with an initial charge is connected to a series of increasing resistor values, as per Figure 4-58, then the power dissipated by the load resistor follows this shape.

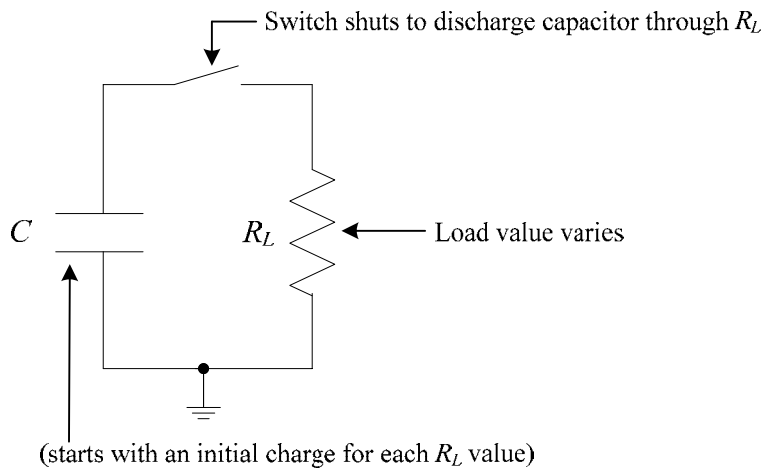


Figure 4-58 A theory representation of a charged capacitor being discharged through a load resistor, which is a situation akin to the charge/discharge simulation of the concept proposed in this thesis.

From Figure 4-56, it is evident that there is a large difference between the average power output of the harvesting device and the average power dissipated by the load resistor: the average power output of the harvesting device is consistently around 2.44mW, whereas the power dissipated by the load resistor is only 66 μ W at its highest value. This is partly because of the charge/discharge operation itself: the portion of the time period of the power dissipation cycle (shown in the *Rload* curve of Figure 4-54 (b)) where there is no power dissipation; i.e. the portion that is ‘dead’ time, which occurs when the reservoir capacitors are recharging, is significant, bringing the average value down, but in addition, through examining the circuit, it is evident that some power dissipation is also occurring in the circuit components. Table 4-2 on the following page sums the total power dissipation in the circuit components:

Table 4-2 Simulated power dissipation of the various circuit components of Figure 4-51 with different load resistor values

(all power values quoted are in μW).

Load resistor value (Ω)/ Component	25k	75k	125k	175k	225k	275k	325k	375k	425k	475k	525k	575k	625k	675k	725k	775k
S5	66	66	65	65	67	67	68	69	70	72	74	75	78	80	82	85
L1	69	71	73	76	80	79	79	79	79	79	79	79	80	82	48	88
S8	13	27	31	36	38	40	41	43	44	45	45	46	47	47	48	48
S1	847	570	450	367	306	265	234	198	186	163	143	148	124	113	107	101
S2	907	627	483	391	328	283	246	217	197	177	160	160	137	127	116	110
S6	51	33	24	23	16	14	12	10	9	9	7	6	5	6	4	4
S4	247	541	677	761	819	848	878	894	902	908	912	912	910	905	903	897
S3	234	501	621	708	747	796	810	813	834	843	858	843	851	844	844	836
Total:	2434	2436	2424	2427	2401	2392	2368	2323	2321	2296	2278	2250	2232	2201	2188	2169

Note that in Table 4-2 only the power dissipation of the switches and inductor LI has been recorded; this is because the losses in the diodes are negligible, given that they are close to ideal. This simulation differs from the previous two in that essentially there was no power dissipation in the circuit components of the previous two, whereas there is a total of between 2.44mW and 2.19mW average power dissipation, depending on the value of load resistance, in the circuit components in this simulation. If the total values of average power dissipation in the circuit components were added to the average power dissipated by the load resistor, giving the overall total power dissipation in the complete circuit (i.e. components plus load resistor), the values are close to the average power output of the harvesting device, as shown in Figure 4-59:

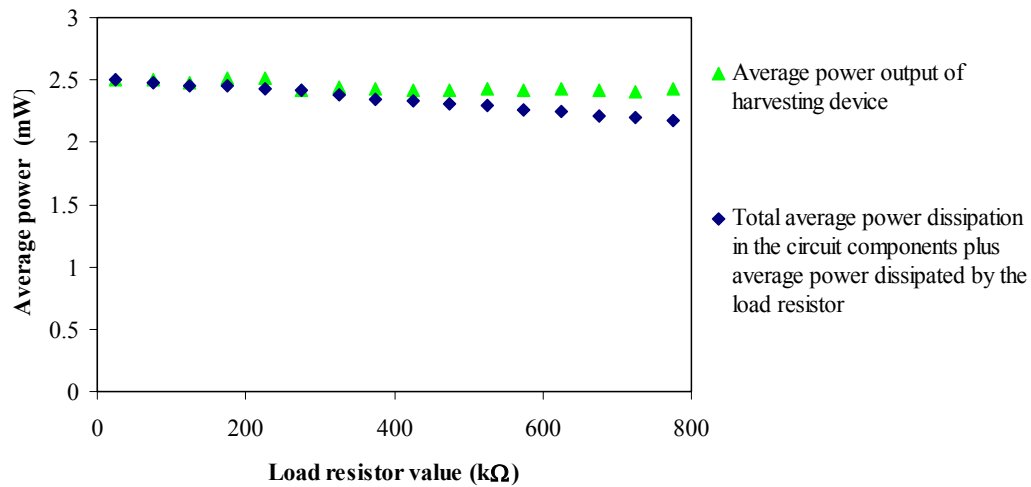


Figure 4-59 Simulated average power output of the harvesting device, and simulated total power dissipation in the complete circuit (components plus load) for the harvesting circuit concept proposed in this thesis.

One possible further reason for the low power dissipation in the load resistor, given the high power output of the harvesting device, is that during any complete time period of the power dissipation cycle (shown in the $Rload$ curve of Figure 4-54 (b)) the harvesting

device charges two sets of reservoir capacitors: $SC1$ & $SC2$, and then $SC3$ & $SC4$, but only one set: $SC1$ and $SC2$, is used to provide power to the load resistor. No advantage is taken of the energy accumulated in $SC3$ & $SC4$. If $SC3$ & $SC4$ were used to power the load resistor also, then the average power dissipated by it would be increased, though it could only be doubled as a best case.

For comparison purposes, it is useful to plot the simulated power dissipations of all three simulation circuits on one chart, as shown in Figure 4-60:

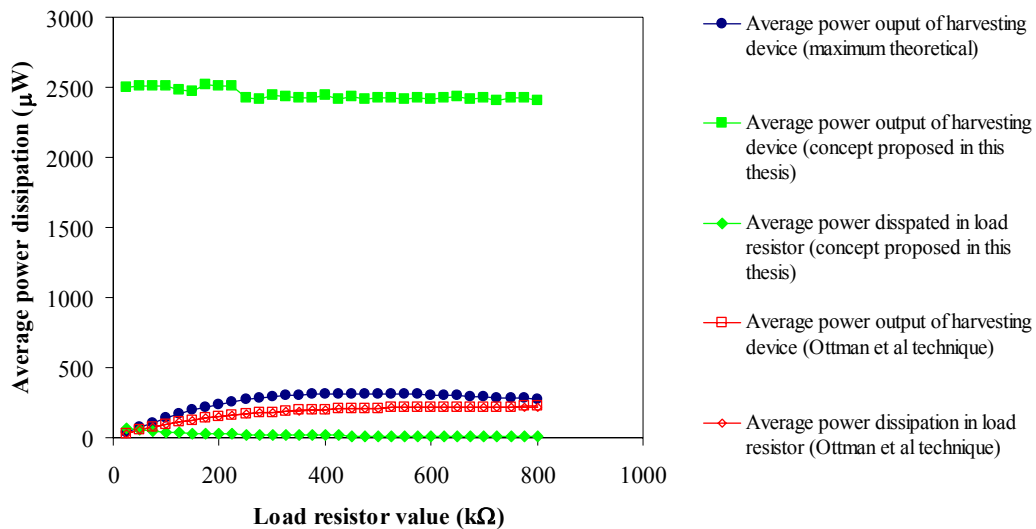


Figure 4-60 A comparison of average power dissipated in the load resistor, and average power output of the harvesting device, for all three simulation circuits.

From the results shown in Figure 4-60, it can clearly be seen that the average power extracted from the energy harvesting device when using the concept proposed in this thesis is much greater than the average power extracted when the technique proposed by Ottman et al is used, and even outweighs the “maximum theoretical” average power output. Given that the concept proposed in this thesis uses the SSHI technique, which has the effect of boosting the voltage from the piezoelectric generator, and given that in

the simulation environment the voltage inversion of the SSHI waveform is near perfect (because the components that make up the SSHI function part of the circuit are ideal), then perhaps this result is not surprising. The “maximum theoretical” power output was simply ascertained with a load resistor connected directly across the terminals of the piezoelectric generator; i.e. with no voltage-boosting techniques used.

In the simulation however, the increase in average power output of the harvesting device gained by using the proposed concept, does not translate directly into power dissipation in the load resistor. It appears from Table 4-2 that there are significant power losses in the switches within the circuit, particularly in the switches that transfer charge between the ‘bucket’ capacitors and reservoir capacitors, $S1$ & $S2$, and $S3$ & $S4$. This could be because the switches are near to ideal, with an ‘on’ resistance that is set to 0.1Ω , and an ‘off’ resistance that is set to $100M\Omega$. Even though each switch has been set to transition smoothly between these two states, the switching time is fast enough such that a large current is produced when the switch in question is closed and charge is suddenly evacuated from the bucket capacitor to the reservoir capacitor. This author is at present unsure of how to lessen this effect without introducing further impedance to the flow of current, which might therefore result in a situation where one power dissipation problem is solved by introducing another!

In regard to the technique proposed by Ottman et al, in the simulation nearly all of the power output of the harvesting device translates into power dissipation in the load resistor. The automatic impedance matching technique used to achieve this condition in practice though, can only ever result in a maximum which is dependant on the vibration characteristics of the vibration environment (i.e. amplitude and frequency), and the size of, configuration of, and materials used in the construction of, the harvesting device. It

cannot be increased without altering one of these listed items. However, in the concept proposed in this thesis, the value of the reservoir storage capacitors can be changed, so that for a trade-off of time (i.e. the extra time required to charge a larger capacitor), the user can have more energy available to power a more power hungry application. Although he was referring to the case of a battery when he said it, Lesieutre [149] said: “*One can store a lot of energy in a battery, even at low charging rates, if one can wait long enough*”. The same is true here. The important point to note is that this is an option; an option that is not available if an application system is to be powered immediately from a harvesting device (albeit with some power conditioning), and the advantage that the option brings is flexibility. In the concept proposed in this thesis, the user may select the optimum reservoir capacitor value for his/her particular application system. Since, in energy harvesting: “*there is no one solution that will fit all, or even a majority, of applications*” [25], this is a very useful option to have, because it provides a means by which a wider range of applications can be powered. Similarly, the user could potentially connect any one of a range DC-DC converters to the charged reservoir capacitors, leaving them the choice of choosing one that is best suited to their particular application. This is possible because the proposed concept demonstrated collects charge over time such that an energy reservoir is built up. In a harvesting circuit that does not incorporate an energy storage medium, akin to that proposed by Ottman et al, the maximum power output cannot exceed the continuously available mean value. Therefore, while average power output over time is useful as a means of comparison between harvesting devices and circuits, and that is the purpose of conducting these simulations in this section of the thesis; i.e. to understand how the proposed concept fits in with other circuit techniques in this regard, there are other attributes to be considered

when choosing an energy harvesting system, that is: transducer plus circuitry, for a given application. The harvesting circuit concept proposed in this thesis was developed for the purpose of enhancing the power output of a piezoelectric energy harvesting device but, as mentioned in the objectives section (page 18) and at the end of the motivation section (section 1.1; beginning page 3), the aim was also to condition and manage the power, because the power is simply not useful for many applications unless it is in the form of a regulated DC supply.

As a further note in regard to the technique proposed by Ottman et al, the output of the DC-DC converter used to implement the adaptive impedance interface, in terms of voltage, is held at 3V in [93] by a battery. By maximising the current flow into the battery, they maximise the power output of the harvesting device. If the load to be powered is not a battery however, it might be the case that, since current flow to the application is the metric that is used to alter the duty cycle of the DC-DC converter, the voltage at the output of the converter might fluctuate somewhat, potentially causing problems for the application system. In regard to the concept proposed in this thesis, since an energy reservoir is collected, a DC-DC converter can be powered simply to provide a regulated DC supply to the application system.

4.9 Conclusions

This chapter began with some initial experimental investigations, which were performed using the prototype harvesting device of Chapter 3 (the optimised device was not available at the time) and two bridge rectifier circuits: one constructed of silicon rectifier diodes and the other constructed of schottky diodes. Two sets of tests were performed: one where no load resistor was applied so that the amount of energy

harvested into the smoothing capacitor was measured (the output of the bridge rectifier circuit was, in effect, open-circuit), and one where a set of load resistors of different values were applied, such that average power output over time could be ascertained. The expected outcome in the first set of tests was that, for the same input vibration conditions, the energy harvested into the smoothing capacitor when the schottky diodes were used would be greater than the energy harvesting into the same capacitor when the silicon rectifier diodes were used. The expected output in the second set of tests was that, again for the same input vibration conditions, the power dissipated by the load resistors (representing ‘useful’ power output; i.e. that which can be used to power a load) would be more when the schottky diodes were used than when the silicon rectifier diodes were used. The reasoning for these expectations came from the fact that the forward bias of the silicon rectifier diodes was around 0.6V, whereas the forward bias of the schottky diodes was below 1.8V (extrapolating from the curves given in the data sheets). However, the experimental results proved the opposite proved to be true. In the first set of tests, 7.6 μ J was harvested into the capacitor when the schottky diodes were used, whereas 13.5 μ J was harvested when the silicon diodes were used. In the second set of tests, the maximum average power dissipated by a load resistor when using the rectifier with schottky diodes was 0.22 μ W, whereas the maximum average power dissipated by a load resistor when using the rectifier with silicon diodes was 0.87 μ W. This unexpected result was attributed to the higher reverse leakage current of the schottky diodes.

The purpose of the initial experiments was to ascertain whether or not the synchronous rectifier route was worth pursuing, since the use of MOSFETs in place of the diodes of a bridge rectifier would mean that potentially, no forward bias voltage drop would be

present, thus leading to a higher efficiency rectifier circuit and more power harvested. Although this assertion was not proved by the experiments performed with the two types of bridge rectifier, the experiments did lead to an in-depth analysis of the operation of a bridge rectifier circuit, as a result of which, the decision was taken to concentrate on the development of a new kind of harvesting circuit concept: one that combined the voltage-boosting effect of the SSHI technique with a charge pump-type circuit, and which was capable of both harvesting charge throughout the whole of the AC voltage output cycle of the piezoelectric generator (i.e. so that the generator output is never in an open-circuit condition), and inherently converting from AC to DC. The philosophy behind the new concept was to collect charge over time in a set of storage reservoir capacitors, such that when the reservoirs became full, they could be disconnected from the charging circuit and connected instead to an end application system. The main reason for adopting this philosophy was that in an energy harvesting system where the end application is powered continually from the harvester whenever vibration is present, the power output is usually small. Indeed, there generally exists a mismatch in power requirements versus power availability. Therefore it was considered that it perhaps makes more sense instead to build up an energy reserve over time, such that a large energy reservoir is eventually obtained, from which higher power application devices can then be powered.

In experimental tests, the new circuit concept proposed in this thesis proved to be capable of harvesting more than three times the amount of energy into storage capacitance than the bridge rectifier circuit for the same input vibration conditions. The new concept was also compared with two other circuits, through simulation, for the purpose of comparing average power output over time (instead of energy harvested into

storage capacitance). The two other circuits were: 1) one in which a variable value load resistor was directly connected across the output terminals of the harvesting device, used as a method of determining the ‘theoretical maximum’ average power output, and 2) one that implements the technique proposed by Ottman et al [93]. It was shown that for the same input conditions, the average power output of the piezoelectric harvesting device when the new concept was used was nearly eleven times more than when the technique proposed by Ottman et al [93] was used (i.e. an increase from $222.01\mu\text{W}$ to 2.44mW), and was nearly eight times more than the theoretical maximum average; i.e. from $315.26\mu\text{W}$ (theoretical maximum), to 2.44mW . The concept proposed in this thesis is capable of obtaining more power from the harvesting device than the ‘theoretical maximum’, which was obtained by the circuit in which a load resistor was directly connected across the output terminals of the device, because the new concept takes advantage of the SSHI technique, which boosts the output voltage of the device.

Although in the simulation the proposed harvesting circuit concept enabled a much greater power output from the harvesting device, this increase in power did not translate into greater power dissipation in the load resistor. The power dissipated by the load resistor when using the new concept was low when compared with use of the other circuits. It was found that in the simulation, because the proposed circuit was more complex than the other two circuits (involving the use of switches) the power dissipation in the circuit components was high in comparison with the other two circuits. This ‘overhead’ of conversion losses will translate by some degree in a real implementation of a physical circuit. Indeed, the proposed harvesting circuit concept does not come for free. For the circuit designed and built in this project, shown in the photograph of Figure 4-29 (page 266), three separate supplies were required: a $\pm 5\text{V}$

supply, a +10V supply, and a +9V supply from a PP3 type battery. A power budget calculated for this circuit (see appendix H) shows that expected total power dissipation of the circuit is between 29.6mW and 46mW. In practice, the current consumption values recorded on the bench power supplies were 0A for the -5V supply, 13mA for the +5V supply, and 4mA for the 10V supply, giving a total power dissipation of 105mW. However, it needs to be reiterated here, that because proving the new harvesting circuit concept, with its perceived improvements over other techniques, was deemed to be of more importance in this thesis than implementing the detection, switch driving and management functions of the circuit by elegant engineering design, this author believes that it is entirely possible that alternative low power methods of implementing the required functions could be achieved.

It is also worth noting that, although in the case of the simulation of the technique proposed by Ottman et al, nearly all of the power output of the harvesting device was translated into power dissipation in the load resistor, in practice their technique also required external bench laboratory equipment [93], including an external power supply (to power the high-side MOSFET driver), a controller card, and some external voltage amplification circuitry, as per Figure 4-61:

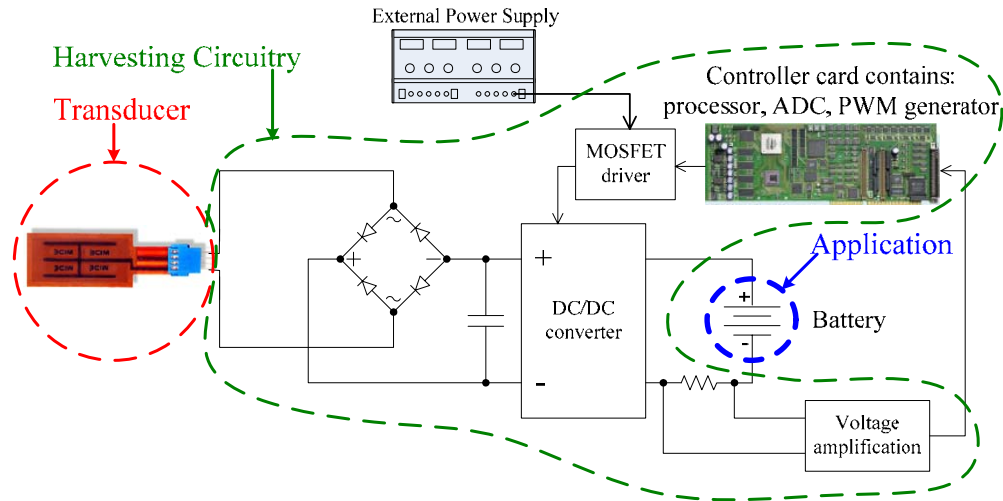


Figure 4-61 A schematic of the experimental system used by Ottman et al [93] (this author's interpretation).

It is probable that the controller card represents the highest power consumption overhead of this system, because it is most likely mounted inside a PC. In a second paper [150] Ottman et al reduce the power consumption of their system somewhat by implementing a dual method within their control circuit: they found that at high vibration excitation levels, the optimal duty cycle for their DC-DC converter was nearly constant, and so under these conditions they ran the converter at a set optimal duty cycle [150] and the energy harvested was worth the circuit overhead energy expenditure. At low vibration excitation levels, they found that the optimal duty cycle varied considerably, with the result that the energy harvested would not be worth the expenditure of continuously adapting the duty cycle. Under these conditions then, they adopted a pulse-charging circuit for the battery application, with the DC-DC converter bypassed. They estimated that their overall power consumption for the control circuitry of this new dual method system was 5.74mW [150].

Therefore, while the circuit concept proposed in this thesis at present requires power from external sources: approx 105mW was measured with the circuit implementation given in this thesis, it is not alone in this regard. Indeed, in comparing physical implementations of the two techniques, it is possible that the ratio of average power output from the harvesting device to power consumption of the control circuitry may actually be higher for the concept proposed in this thesis than it is for the technique proposed by Ottman et al. However, this cannot be asserted on the strength of the simulations performed here, since in the case of the concept proposed in this thesis, most of the power output of the harvesting device is lost in dissipation in the circuit switches (this is likely an idiosyncrasy of working in an ideal simulation environment), and in the case of the technique proposed by Ottman et al, the power dissipation of the DC-DC converter, controller card or PC is not taken into account in the simulation. A comparison based on the simulations performed therefore, would not be fair. Nor can the comparison immediately be done based on experimental grounds, since although data does exist in terms of power output values and power consumption levels for the two techniques (it can be found in [150] and within this thesis) the piezoelectric harvesting device used was different for each case, as were the input vibration conditions applied.

In summary, the following conclusions can be surmised:

- 1) A new harvesting circuit concept has been developed which combines the voltage-boosting effects of the SSHI technique with a method of collecting charge during the whole of each AC cycle of the piezoelectric generator output. This is an advantage over the bridge rectifier circuit, which is the circuit normally used as an interface to energy harvesting devices, in two respects: firstly there is the voltage

increase obtained through the inclusion of the SSHI technique, and secondly the bridge rectifier circuit, when in steady-state operation, is only able to harvest charge from the piezoelectric generator for part of its AC output cycle, unlike the new harvesting circuit concept. Following the evolution of the concept and assessment of its perceived advantages, two different approaches were taken to assess the performance of the new concept: (1) an experimental approach was adopted to compare it with a bridge rectifier circuit in terms of the amount of energy that could be harvested into storage capacitance (2) a simulation approach was adopted in order to compare it with another technique reported in the literature in terms of average power output over time.

- 2) In terms of enhancing the power output of a piezoelectric vibration energy harvesting device, the new harvesting circuit concept performed well. Compared with the performance of the standard bridge rectifier circuit in the experimental tests, the new concept harvested 247% more energy into storage capacitance in a similar length of time and for the same input vibration conditions. It was determined that with the addition of a buck-boost DC-DC converter, an application circuit drawing $10\mu\text{W}$, such as the RFID tag of Figure 2-1 (page 28), could be powered for 2.8 minutes. Alternatively, an application circuit drawing 1.75mW , such as the Sunflower miniature computing system could be powered for 971ms. If the bridge rectifier circuit were used with the same DC-DC converter, the RFID tag could be powered for only 49s, and the Sunflower system could be powered for just 277ms. Therefore, the new harvesting circuit concept can provide approximately 247% more regulated DC power than the bridge rectifier circuit for the same vibration conditions.

When compared through simulation with the performance of another technique reported in the literature: that proposed by Ottman et al [93] [150], the new concept proved capable of enhancing the output of the energy harvesting device by as much as a factor of eleven; i.e. from $222.01\mu\text{W}$ (achieved by using the technique proposed in [93]) to 2.44mW (achieved using the new concept). However, the enhanced output gained from the harvesting device by using the new concept did not translate into greater power dissipation in the load resistor. The maximum average power dissipated by the load resistor when the new concept was used was low when compared with the technique proposed in [93], being $66\mu\text{W}$ in comparison with $217\mu\text{W}$. It was found that in the simulation, losses in the switches within the control circuit greatly accounted for the disparity between harvesting device power output, and power dissipated by the load.

- 3) The philosophy behind the new concept is to collect charge over time in capacitive storage reservoirs, and then when the reservoirs are full, to use the stored charge to power an application. The process can be repeated with the reservoir being alternately connected to the charging circuit and application system so that it is repeatedly charged and discharged. The reasoning behind this choice of circuit operation method was that the power output of meso-scale harvesters is generally very small. By adopting this method, higher power applications can be powered than would otherwise be possible with a circuit technique that uses a continuous powered approach; i.e. one that makes more immediate use of the power output from the harvester and does not store it.
- 4) The main advantages that the new concept developed in this thesis offers over the standard bridge rectifier circuit are:

- a. Because of the philosophy adopted, i.e. collecting charge over time such that a reservoir is built up, higher power applications can be powered than would otherwise be possible with a continuous powered approach; i.e. one where the application is powered immediately from the harvesting device (albeit with some power conditioning), such as the bridge rectifier.
- b. Because, in the concept, the application system is powered from a capacitive reservoir rather than immediately from the harvesting device, the application system is offered a degree of ‘buffering’ or protection from the uncertainties of the vibration environment, e.g. in terms of variations in amplitude and intermittent periods.
- c. The concept takes advantage of the increase in the voltage output of the harvesting device that results from using the SSHI technique.
- d. Power is harvested from the piezoelectric energy harvesting device during the whole of its AC output voltage cycle, rather than for just part of it.
- e. The concept inherently converts from AC to DC, by the accumulation of charge in two storage capacitors (one collecting the positive charge generated by the harvesting device, and one collecting the negative generated charge) which are then connected together in series to form an energy reservoir with a positive terminal and a negative terminal. This negates the need for four rectifier diodes and allows for the connection of a buck-boost DC-DC converter.
- f. The concept uses pre-existing maxima and minima detection circuitry (since it is already required for the SSHI technique) therefore a minimum of extra components need be added.

- g. The concept is simple, i.e. if built into a full system as per Figure 4-25 (page 251), the microprocessor only needs to fulfil a few functions and can operate with a very low clock rate, and therefore it can be very low power and a small size.
 - h. The concept allows the SSHI technique to be fully integrated into a circuit that fulfils the traditional requirements of electronic devices and systems; i.e. it provides a regulated DC supply. Although the SSHI technique, when operating alone, results in an improvement in the power output of the device it cannot convert from AC to DC or provide a regulated DC output.
 - i. The impedance match of the load capacitor (i.e. C1 or C2 of Figure 4-21 on page 246) with the source (i.e. the piezoelectric generator) in theory results in maximum power transfer at all times, since if the frequency of the driving vibration sources changes, resulting in a change in frequency of the harvesting device voltage output, the impedance remains matched because the load attached to the generator is always purely capacitive.
- 5) In order to implement the new concept for the experimental tests, a circuit was designed and built which required power from external bench power supplies. The total measured power consumption of the circuit was 105mW. The circuit is a prototype only however, and was built using a mixture of discrete and integrated components solely for the purpose of proving the new harvesting circuit concept. This author believes that it is entirely possible that alternative low power methods of implementing the required functions could be achieved.

CHAPTER 5: CONCLUSIONS, DISCUSSION & RECOMMENDATIONS FOR FUTURE WORK

This subject of this thesis is energy harvesting; that is: deriving energy from environmental sources such as vibrations, air flow or electromagnetic fields. In this case, the focus was on vibrations. The term “meso-scale” in this thesis is used to indicate a focus on energy harvesting devices with volumes of no more than a few cm^3 (or areas of no more than a few cm^2), that have dimensions in the mm-cm range, and that can be built largely without resorting to MEMS processing techniques. The motivation for using these small devices for harvesting environmental energy is, in many cases, to enable another class of device that has wide application potential: the autonomous wireless sensor node. In this way, it is considered that ‘free’ energy can be used to power devices that could, for example, form part of a control system that monitors the glucose level and administers insulin to a diabetic patient, or monitor the temperature of the seas in order to collect climate change data. The focus of this thesis is on the amount of power that can be achieved using meso-scale harvesting devices, and more specifically the problem tackled is: how can the power output of a vibration powered energy harvesting device be enhanced?

The thesis started with a literature survey of the power requirements of a range of electronic devices and systems. Following this, a review of the various energy harvesting technologies available for harvesting from the different types of energy source was conducted. Energy sources covered included: solar, air flow, thermal, pressure variations, radio frequency radiation and mechanical. For each energy source, the most commonly employed mechanism for energy conversion was detailed, relative advantages and disadvantages were outlined, and power output levels that have been

achieved through experiment have been reported. From this, it was deduced that piezoelectric conversion of vibrations tends to result in higher power outputs: generally in the hundreds of μW to a few mW region (e.g. $335\mu\text{W}$, $462\mu\text{W}$, $900\mu\text{W}$, 1.3mW), and voltages reach from high single figures to tens of volts DC or peak (e.g. $8.3V_{\text{pk}}$, $13V_{\text{pk}}$, $9.8V_{\text{RMS}}$, $20.57V_{\text{DC}}$). The powers achieved are large enough to be useful, and the voltages achieved at the reported power levels are practicable; that is, they are large enough such that the power can be conditioned with relative ease. For these reasons piezoelectric conversion of vibration energy was chosen as the technology basis for this thesis. The subject choice of power enhancement was selected after a brief review of the other potential avenues of exploration, which included: geometric variations of the harvesters (for different purposes), wearable or implantable harvesters, tuned or wideband harvesters and durability of the harvesters. Power enhancement was chosen on the basis that it fundamentally dictates system feasibility, and that despite recent advances, the low power output of harvesting devices remains a limitation for the adoption of energy harvesting technology.

Following this, the concept of piezoelectricity was introduced, both in historical and technological contexts, and a review of the history and state-of-the-art in power enhancement of piezoelectric generators was given, including both power enhancement through advances in the design of the generator (e.g. tapered cantilever shapes and different mass shapes) and power enhancement through use of the harvesting circuitry (focussing on impedance adaptation and synchronised techniques).

The remainder of the thesis reported on research efforts to enhance the power output of a piezoelectric vibration energy harvesting device. Two methods were investigated: the first involved constructing a model of the harvesting device that can be used with a

computer-based optimisation algorithm to provide an optimised device design; i.e. a design which, in terms of its dimensions, is optimised for maximum power output for the volume the device may utilise in an application. The second method involved both experimental and simulation implementations of a new harvesting circuit concept that is proposed in the thesis. The new concept is based on a combination of the SSHI technique and a charge pump-type circuit, and holds advantages over the standard bridge rectifier circuit in that energy is harvested during the whole of the AC output voltage waveform of the piezoelectric generator, and that it inherently converts from AC to DC without the need for four rectifier diodes. In addition, because it makes use of an energy storage medium and collects charge over time so that an energy reservoir is built up, (from which the application system can then be powered), more power hungry applications can be powered than would otherwise be possible with a circuit technique that is based on a continuous powered approach; i.e. one that makes more immediate use of the harvesting device power output such as the bridge rectifier circuit.

5.1 Review of Aims and Objectives

Aims

The aim of this thesis was to enhance the power output of a piezoelectric-based vibration energy harvesting device. Two areas were investigated for this purpose: the energy harvesting device itself, and the ‘harvesting circuitry’, i.e. the circuitry that is usually connected to the beam to condition and/or manage the electrical power output.

Objectives: Harvesting device

- 1) To develop an analytical model for the harvesting device that considers all of the dimensional parameters of the device,

- 2) To use the model with a computer-based optimisation algorithm to optimise the geometric parameters of the generator such that the best use is made of the volume the device may utilise in an application, resulting in an increase in the power density (W/cm^3) of the device.
- 3) To design and build a suitable test setup.
- 4) To build and then test the optimised device with a series of load resistors in order to ascertain its power output.

Objectives: Harvesting circuitry

- 1) To analyse in detail the operation of the standard bridge rectifier circuit in order to find an area in which it can be improved,
- 2) To develop an improved concept for the harvesting circuitry based on the findings from objective (1) above,
- 3) To perform the electronic design for a circuit that will implement the concept developed in objective (2) above,
- 4) To build and test the circuit and compare the performance of the new concept with that of the standard bridge rectifier circuit.

5.2 Conclusions of the Harvesting Device Optimisation

Work on the optimisation of the harvesting device began with an experimental approach, where a prototype cantilever beam-type harvesting device was constructed from a commonly-available piezoelectric ‘buzzer’ sourced from Maplin Electronics (Rotherham, South Yorkshire, UK). A first test setup was also built using a self-built

'linear ramp generator' circuit and commonly available electronics laboratory equipment: a function generator, power amplifier and oscilloscope. The power output of the prototype device, using this test setup, was found to be just $8.18\mu\text{W}$, which occurred with a load resistor value of $500\text{k}\Omega$. The voltage across the resistor at the maximum power point was 2.86V_{pk} . In regard to other fabricated piezoelectric energy harvesting devices reported in the literature, this output power was very low, being amongst the bottom few.

This first prototype device was built without any guidance on how the geometric dimensions of it might affect its power output. It was considered that the power output might be significantly improved if, for example, the thickness of the piezoceramic material was increased, or the ratio of brass layer to piezoceramic layer thicknesses was changed, but with no knowledge of how the dimensions affect the power output, such ideas could at most only be conjecture. Without guidance, it was clear that the only option was to rely on a trial-and-error approach, which is usually both costly and very time consuming.

Therefore, in an effort to achieve a higher power output, it was considered that a modelling approach would be useful. However, it was considered that the model should not simply predict outputs of the device (e.g. power or voltage) when provided with dimensions and material characteristics, since this still would not provide guidance on how to design a harvester for an increased power output; i.e. the designer still has to rely on a trial-and-error approach (albeit this time with the aid of a model). Instead, the model should be used with an optimisation algorithm to provide the device design itself; i.e. the model should be designed for use with a computer-based optimisation algorithm,

such that the output of the optimisation process is a list of values for the device dimensions that together constitute a design that has been optimised for maximum power output. To this aim, an analytical model was developed. The model resulted in an expression for the power output of the device that, because it has within its arguments all of the dimensional parameters of the device, can be used with a computer-based optimisation algorithm to optimise the geometrical parameters of the device. An example of how the model can be used was given in the thesis using the complex conjugate optimisation algorithm provided by Mathcad 2000 Professional software, and a design for a device that was optimised for maximum power output given a volume constraint of 1cm^3 was obtained. The optimised device was then fabricated and tested using an improved, purpose built, test setup and a series of different values of load resistor. The maximum power achieved from the optimised harvesting device was $370.37\mu\text{W}$, which occurred with a $325\text{k}\Omega$ resistive load. A voltage amplitude of 15.52V was measured at this maximum power level, and the resonant frequency of the device with a $325\text{k}\Omega$ load was 87Hz .

The results from the optimised harvesting device compared very favourably with those obtained from the initial prototype harvesting device, which was fabricated without any guidance on how the geometric dimensions of it might affect its power output, giving an increase in power of a factor of 45. In addition, the results from the optimised harvesting device compare very well with reports of other fabricated piezoelectric harvesting devices detailed in the literature. The power density achieved, $370.37\mu\text{W}/\text{cm}^3$, is one of the highest and the voltage achieved at the maximum power output, 15.52V , is very suitable for the purposes of power conditioning; i.e. converting from AC to a regulated DC supply. This implies that the model developed is useful for

the purpose of optimising, through the use of a computer-based optimisation algorithm, the dimensions of a cantilever-based piezoelectric vibration energy harvesting device in order to obtain maximum power output such that the best use is made of the volume the device may utilise in an application. This, effectively, is a method of increasing the power density (W/cm^3) of the device. Through use of the analytical model developed in this thesis, the power output of a piezoelectric vibration energy harvesting device has been enhanced.

5.3 Conclusions of the Proposed New Harvesting Circuit Concept

As well as focussing on an optimisation of the piezoelectric vibration energy harvesting device, this thesis has also explored the use of the harvesting circuitry (i.e. the circuitry that is usually connected to the harvesting device to condition and/or manage the electrical power output), in order to find a method of enhancing the power output. This aspect of the work began with some simple experiments involving the prototype harvesting device (the optimised device was not available at the time) and a traditional bridge rectifier circuit. In tests with no load applied, in which the voltage across the smoothing capacitor (or ‘DC link’) was simply measured in order to determine the amount of energy harvested into the capacitor, it was found that the energy that could be harvested into the capacitor was very small: only $13.5\mu\text{J}$, which translates into $13.5\mu\text{W}$ of power for 1 second or 225nW for 1 minute. In tests with a load resistor attached; i.e. connected across the capacitor, which enabled average power output to be plotted through calculating the power dissipation in the load resistor, the maximum average power output achieved was $0.87\mu\text{W}$, which occurred with a load resistor value of $450\text{k}\Omega$.

It was initially thought that perhaps a more efficient method of converting AC to DC could be found and that using a synchronous rectifier, where MOSFETs are employed in place of diodes, might be a suitable starting point. However, following the simple experiment described and a subsequent analysis of the bridge rectifier circuit carried out with the aid of a circuit simulation tool, it became this author's opinion that the bridge rectifier circuit, regardless of whether it is implemented in its traditional form or in a synchronous form, is not the most efficient method of converting from AC to DC for an energy harvesting application. This opinion was primarily based on the fact that under steady-state conditions the output of the piezoelectric generator spends much of its time in the open-circuit condition, where there is no power transfer from generator to load. It was considered therefore that it would be more beneficial if a circuit could be developed where energy is harvested during the whole of each AC voltage cycle of the piezoelectric generator output, rather than for just part of it. In addition, it is this author's belief that the power obtained from an energy harvesting device is of little use unless it is converted into a regulated DC format and that therefore the circuit should also provide for this. To this aim, a novel harvesting circuit concept was developed. The concept is based on a combination of the SSHI technique and a charge pump-type circuit, taking advantage of the voltage boosting effect of the SSHI technique while implementing a bucket-type method (where a small 'bucket' capacitor harvests charge during each AC cycle of the generator output and then 'dumps' it into a larger storage capacitor) to provide a method of enhancing the power output of the piezoelectric generator. The concept enables a large charge reservoir to be built up over time, such that higher power application systems can be powered.

In the work presented, a circuit was designed and built to implement the new concept, and the performance of the concept was assessed in two ways: (1) it was compared, through experiment, to the performance of the standard bridge rectifier circuit in regard to how much energy could be stored in a large reservoir capacitance (i.e. with no electrical load using the power). In this case, the most notable result was that, for a vibration acceleration amplitude of $\pm 0.125g$, a total of 2mJ of energy was harvested into two 220 μ F storage capacitors, in comparison with 0.577mJ of energy harvested into one 220 μ F storage capacitor using the bridge rectifier circuit. It was determined that if a buck-boost DC-DC converter with an efficiency of 85% was connected to the storage capacitors, an application circuit drawing 10 μ W, such as the RFID tag of Figure 2-1 (on page 28), could be powered for 2.8 minutes using the new harvesting circuit concept. Alternatively, an application circuit drawing 1.75mW such as the Sunflower miniature computing system (also shown in Figure 2-1) could be powered for 971ms. If the bridge rectifier circuit were used with the same DC-DC converter and the same input vibration conditions, the RFID tag could be powered for only 49s, whereas the Sunflower system could be powered for 277ms. Therefore, in this respect the new harvesting circuit concept proposed in this thesis can provide 247% more regulated DC power than the bridge rectifier circuit for the same vibration conditions.

The second method of assessing the performance of the concept was: (2) it was compared, through simulation, with two other circuits for the purpose of comparing average power output over time (instead of energy harvested into storage capacitance). The two other circuits were: (a) one in which a variable value load resistor was directly connected across the output terminals of the harvesting device, used as a method of determining the ‘theoretical maximum’ average power output (see Figure 4-45 on page

295), and (b) one that implemented the circuit technique proposed by Ottman et al [93] (see Figure 4-46 on page 296). It was shown that for the same input conditions, the average power output of the harvesting device when the new concept was used was nearly eleven times more than when the technique proposed by Ottman et al [93] was used (i.e. an increase from $222.01\mu\text{W}$ to 2.44mW), and was nearly eight times more than the theoretical maximum average; i.e. from $315.26\mu\text{W}$ (theoretical maximum), to 2.44mW . The new concept is capable of obtaining more power from the harvesting device than the ‘theoretical maximum’, which was ascertained by the circuit in which a load resistor was directly connected across the output terminals of the device, because the new concept takes advantage of the SSHI technique, which boosts the output voltage of the device.

Although in the simulation comparison the proposed harvesting circuit concept enabled a much greater average power output from the harvesting device, the increase in power did not translate into greater average power dissipation in the load resistor in the circuit. The maximum average power dissipated by the load resistor when using the new concept was low when compared with use of the other two circuits, being $66\mu\text{W}$ in comparison with $217\mu\text{W}$ (technique proposed by Ottman et al) and $315\mu\text{W}$ (maximum theoretical). It was found that in the simulation, because the proposed circuit was more complex than the other two circuits (involving the use of switches) the power dissipation in the circuit components was high in comparison with the other two circuits. This overhead of conversion losses observed in the simulation will translate by some degree in a real implementation of a physical circuit. Indeed, the circuit designed and built for implementing the new concept, used in the experimental tests (see Figure 4-29 on page 266), required power from external bench power supplies and had a total

measured power consumption of 105mW. The circuit is a prototype only however, and was built using a mixture of discrete and integrated components solely for the purpose of proving the new harvesting circuit concept, not as an example of low power elegant engineering design. This author believes that it is entirely possible that alternative low power methods of implementing the required functions could be achieved.

In regard to the simulation of the circuit technique proposed by Ottman et al [93], it was found that nearly all of the power output of the harvesting device translated into power dissipation in the load resistor. The automatic impedance matching technique used to achieve this condition in practice though, also used external laboratory equipment, including an external power supply, a controller card mounted within a PC, and some external voltage amplification circuitry; none of which was accounted for in the simulation. Therefore, it initially appears that in comparison with the technique proposed by Ottman et al in [93], the circuit concept proposed in this circuit might consume less power, since the measured power consumption of the circuit developed in this thesis 105mW whereas the technique used in [93] used a controller card mounted within a PC. However, in a later work Ottman et al [150] developed their control circuitry further to implement a dual method, whereby at high vibration excitation levels they ran their DC-DC converter at a set optimal duty cycle, and at low vibration excitation levels they adopted a pulse-charging circuit and bypassed the DC-DC converter. They estimated that their overall power consumption for the control circuitry of this new dual method system was 5.74mW [150], which is ≈ 99 mW less than the consumption of the particular implementation of circuit designed to implement the concept proposed in this thesis. Table 5-1 makes an attempt to show a comparison between the new concept and technique proposed in [93]:

Table 5-1 A comparison of maximum average output powers achieved, and power consumptions of circuits, for the circuit concept proposed in this thesis and the circuit technique proposed by Ottman et al [93] [150].

	Maximum average power output of harvesting device (mW)	Maximum average power dissipated in the load resistor (mW)	Power consumption of control circuitry (mW)
New concept	2.44 (simulated)	0.066 (simulated)	105 (measured)
Technique proposed in [93]	0.222 (simulated)	0.217 (simulated)	In the order of watts for the implementation in [93] (this author's estimate) 5.74 for the implementation in [150] (value calculated in [150])

In summary, it is difficult to make a fair comparison between the concept proposed in this thesis and the technique proposed in [93], because in regard to the simulation performed to implement the technique given in [93], not all the control circuit power consumptions are accounted for, e.g. the controller card, and in regard to the simulation performed to implement the new concept, there is a question over how much of the power dissipated by the switches in the circuit would be valid for a real implementation of the circuit. However, in terms of the maximum average power output obtained from the piezoelectric harvesting device (disregarding the power consumption of the control circuitry, which impacts on the power available to the load application), it does appear that the concept proposed in this thesis is capable of producing an enhanced power output from the harvesting device for the same input conditions.

Through developing the new harvesting circuit concept proposed in this thesis, this author understands that there are several possible reasons for why the concept is capable of enhancing the power output of the piezoelectric generator. However, at the present time it is unclear of what proportion of the increased output power is attributable to which reason, or indeed, how it could be measured in order to find out. Nevertheless,

the increase in transferred energy attained is a strong argument for using the concept.

The possible reasons are:

- 1) The concept takes advantage of the increase in the voltage output of the harvesting device that results from using the SSHI technique.
- 2) Power is harvested from the generator during the whole of every cycle of the AC output voltage, rather than just for part of it, as occurs with the bridge rectifier circuit when it operating in the steady-state condition.
- 3) The concept ensures, through the use of a matched-capacitance load (i.e. the load attached to the generator output is always a capacitor that has a capacitance which is the same value as that of the piezoelectric generator) that there is an impedance match between source and load. Therefore, maximum power transfer can take place at all times, even if the frequency of the vibration source changes, resulting in a change in the impedance of the piezoelectric generator. In this event the impedance of the load changes also, since it is capacitive, thus it remains matched.
- 4) By collecting the charge harvested in two supercapacitors (one collecting the positive charge generated by the harvesting device, and one collecting the negative generated charge) which are then connected together in series to form an energy reservoir with a positive terminal and a negative terminal, the need for four rectifier diodes is negated. Instead, only two diodes are required, thus reducing the power dissipated by the harvesting circuitry AC-DC conversion function.

In addition to an enhanced level of power output, the new concept offers other advantages over both the standard bridge rectifier circuit and the SSHI circuit, which can be summarised as follows:

- 1) Because of the philosophy adopted, i.e. collecting charge over time such that a reservoir is built up, higher power applications can be powered than would otherwise be possible with a continuous powered approach; i.e. one where the application is powered immediately from the harvesting device (albeit with some power conditioning), such as the bridge rectifier or the technique proposed by Ottman et al [93] [150].
- 2) Because, in the concept, the application system is powered from a capacitive reservoir rather than immediately from the harvesting device, the application system is offered a degree of 'buffering' or protection from the uncertainties of the vibration environment, e.g. in terms of variations in amplitude and intermittent periods.
- 3) Due to its simplicity, the concept allows for easy implementation of power management. If built into a full system as per Figure 4-25 (shown on page 251 but repeated here for clarity), the microcontroller only needs to fulfil a few functions and can operate with a very low clock rate, and therefore it can be very low power and a small size. In addition to controlling the switching functions of the system, the microcontroller could provide the application system (e.g. a wireless sensor node) with a low power warning signal, thereby enabling safe shutdown in the event that the charge in the reservoir capacitors runs low.

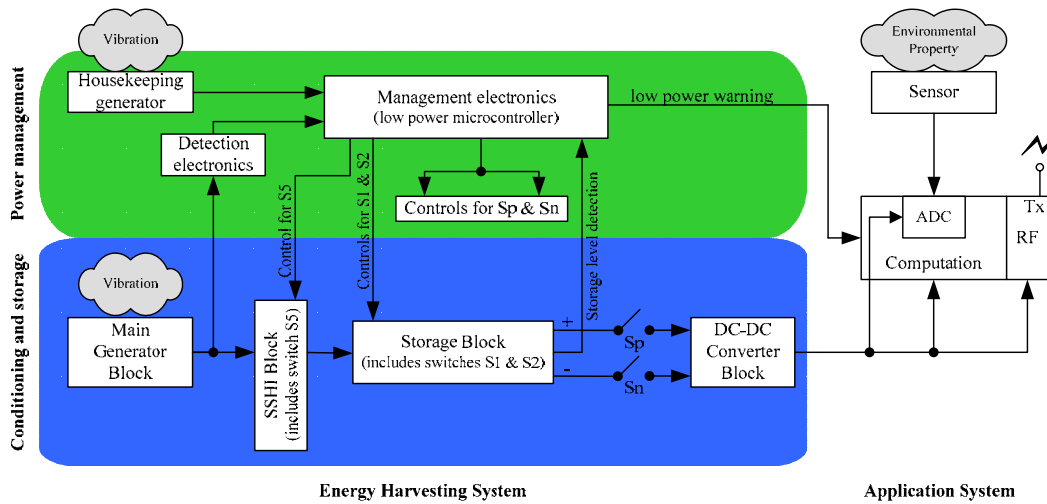


Figure 4-25 Block diagram of the proposed harvesting circuit and envisaged power management circuitry.

- 4) Although the SSHI technique is capable of enhancing the power output of the piezoelectric generator by up to 900% [1], if operating alone, it cannot convert from AC to DC. The use of the concept developed here integrates the SSHI technique with a method of providing the AC-DC conversion function that is required if the power is to be used to supply electronic devices and systems.
- 5) The concept uses pre-existing maxima and minima detection circuitry (since it is already required for the SSHI technique) therefore a minimum of extra components need be added to include the charge storage concept.

5.4 Discussions

5.4.1 Implications of the work

An increased level of output power from a meso-scale vibration energy harvesting device is always a useful prospect. By enhancing the power output while keeping the device size the same, which is in effect the same as increasing the power density of the

device, a greater number of potential applications can be realised. Through the two methods of power enhancement suggested in this thesis, this study has gone some way towards closing the gap that exists between the power requirements of electronic devices and systems, and the amount of power that can be harvested by piezoelectric conversion of vibration energy.

5.4.2 Recommendations for Future Work

The prospect of being able to power wireless sensor nodes or portable electronic devices through the use of energy harvesting techniques and technologies is growing quickly in the present era. By discovering new ways to enhance the power output of meso-scale devices, this possibility is brought one step closer: the greater the amount of energy that can be harvested, the wider the application potential. The research presented in this thesis results in two suggested methods for enhancing the power output of a piezoelectric vibration energy harvesting device. The first is based on a geometric optimisation of the energy harvesting device itself, while the second uses the harvesting circuitry to enhance the power. Following these efforts, this author feels there may be several areas in which the work might be extended or improved.

5.4.2.1 Regarding the Optimisation of the Harvesting Device Performed in this Thesis

In regard to the optimisation of the harvesting device, further ideas are outlined below:

(1) An investigation into how each geometric parameter affects the power output

The model developed in this thesis, though built for the purpose of developing an expression for power that can be used as an objective function in conjunction with a computer-based optimisation algorithm, could be useful for another purpose:

performing an investigation into how each parameter affects the power output. The expression obtained through the modelling for the power output of the device in this thesis is equation (53) on page 363, which is repeated here:

$$P_{ave_in_R}(f) = \frac{E_p^2 \cdot d_{31} \cdot Y^2 \cdot \omega(f)^5 \cdot h_{av}^2 \cdot m^2 \cdot (4L_b^2 + 6L_b L_m + 3L_m^2)^2 \cdot b \cdot h_p}{256 \cdot (EI)^2 \cdot \left[\left[1 - \left(\frac{\omega(f)}{\omega_n} \right)^2 \right]^2 + \left(2\zeta \frac{\omega(f)}{\omega_n} \right)^2 \right] \cdot \varepsilon_r \cdot \varepsilon_0 \cdot L_b}$$

The advantage of an expression in this format is that it lends itself easily to experimentation in terms of manually varying one or other geometric parameter and examining the effect. This would give an opportunity, in a quick and easy visual way, to build up physical intuition regarding this type of generator in terms of which parameters have the most effect, and consequently which design spaces might provide the amount of power required for a proposed application. As an example, in the above expression it would be an easy matter to vary the value of the length of the beam, L_b , and analyse its effect on the power output. If done for other geometric parameters as well, such experimentation would result in a series of graphs that resemble the following two examples:

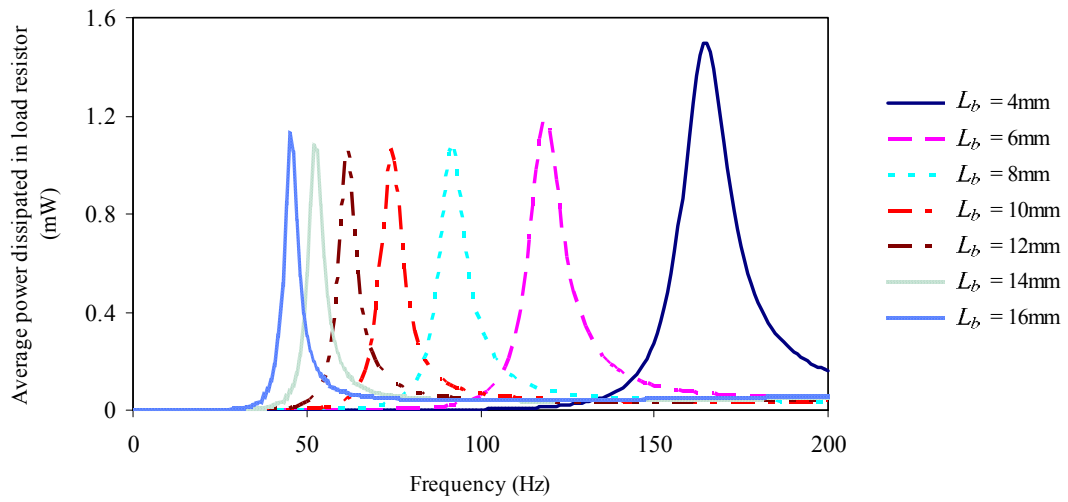


Figure 5-1 Simulated effect of different beam lengths on the power output of the optimised harvesting device.

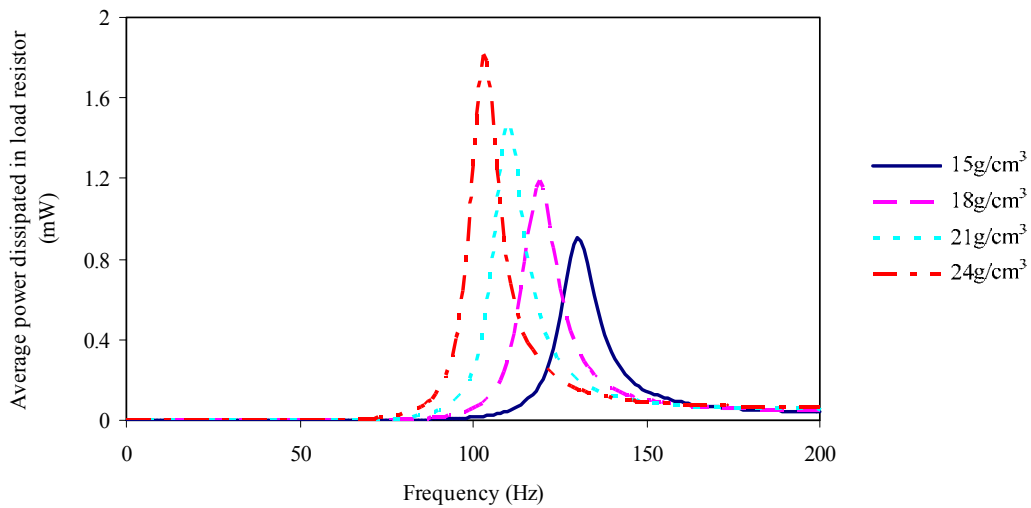


Figure 5-2 Simulated effect of different mass densities on the power output of the optimised harvesting device.

The reasons behind the relationships observed could be investigated, leading to greater knowledge in how to make the best use of a space envelope that the device may utilise in a proposed application scenario.

(2) Including the piezoelectric backward coupling effect in order to improve the accuracy of the analytical model

A way in which the model can be improved was highlighted in section 3.4.1.3 (page 147), where the discussion focuses on the non-inclusion of the piezoelectric backward coupling effect in the model, for reasons of simplicity. Due to the electromechanical coupling dictated by the piezoelectric constitutive equation, which is given in equation (9) in this thesis (page 155), stress applied to the piezoelectric material results in a change in charge density displacement across the piezoelectric layers, which in turn results in the generation of an electrical field. However, the electrical field generated affects to an extent the motion of the cantilever through the piezoelectric converse effect; i.e. as in the case for an actuator; therefore dampening the response of the generator to some degree and lessening its voltage output. This effect is not accounted for in the model, and finding a way to include it would almost certainly help towards improving accuracy.

5.4.2.2 Regarding the Harvesting Circuit Concept Developed in this Thesis

In regard to the use of the harvesting circuitry, further ideas are outlined below:

(1) Increasing the energy harvesting capacity of the harvesting circuit concept developed in this thesis:

Currently, the harvesting circuit concept that has been proposed in this thesis charges two storage capacitors from a piezoelectric vibration energy harvesting device. When

they are fully charged the capacitors are disconnected from the harvesting device and connected instead to a buck-boost DC-DC converter in order to provide a regulated DC supply to an end application electronic system. However, during the time when the capacitors are providing energy (via the DC-DC converter) to the application system no charge is being harvested from the harvesting device. This lost opportunity for collecting charge could be remedied by the inclusion of another pair of capacitors, such that while one pair is being used to power the application, the ‘free’ pair are being recharged. This leads to the possibility of continuously powering the application system. In the case of a wireless sensor node this might be a significant advantage, since the node could transmit a message whenever required, rather than first having to wait for adequate charge to be built up in the storage capacitors. In addition, during quiet times when the node is not required to transmit any data for a long period of time, both sets (i.e. both pairs) of capacitors could be fully recharged, leading to a significant energy reserve available for use when needed. According to the results presented in this thesis (with the components used in the circuit developed in this thesis) a potential energy reserve of 4mJ, which equates to 4mW for 1 second or 66.7 μ W for 1 minute, could be built up over a time period of approximately 1 hour from 60Hz vibrations that are just ± 0.125 g in acceleration amplitude.

(2) A study of the use of the harvesting circuit concept developed in this thesis for harvesting from variable frequency, variable amplitude, and intermittent vibration environments:

Another potential avenue to explore in the future might be the use of the harvesting circuit concept developed in this thesis for overcoming some of the problems associated with harvesting from intermittent, variable frequency and variable amplitude vibration

environments. The vibration source considered in this thesis is a simple harmonic motion type of vibration, of a single frequency only. However, it is known that vibrations are often composed of a number of frequencies, which can vary in amplitude and may also suffer from intermittency. In terms of coping with variations in frequency the circuit concept developed in this thesis has the advantage that, because it operates on the maxima and minima of the harvesting device displacement, it will function regardless of the frequency of vibration in the case of a simple harmonic type of vibration source. In the case of non-harmonic vibrations, made up of more than one frequency, or in the case of random vibrations with no cyclic basis the expected performance of the new concept may be difficult to analyse, though this could form a basis for a future study. In terms of coping with variable amplitude vibrations, the concept should function well: the charge pump-type circuit, which employs a small ‘bucket’ capacitor to harvest energy during each AC cycle of the generator output before ‘dumping it’ into a larger storage capacitance, means that the system can be arranged (by careful choice of capacitor values) such that an energy reservoir can be built up in the storage capacitor with even very small vibration displacement amplitudes. This author considers that it might also be possible to explore other charge pump circuit configurations; perhaps there is one that allows the voltage across the bucket capacitor to be always higher than the voltage across the storage capacitor, thus leading to a reliable incremental increase of the energy stored in the storage capacitor with each AC cycle regardless of the displacement amplitude of the driving vibrations. The last unpredictable element that needs to be considered in the case of some vibration environments is intermittency in the vibration source. In this event, it could be argued that the best that can be done under such circumstances is to mitigate the effects of the

interrupted supply by providing a low power warning signal to the application system, thus enabling safe shutdown of the application system. The harvesting circuit concept developed in this thesis, if built into a full system with a micro-power microcontroller controlling the power management aspects, as shown in Figure 4-25 on page 251 (repeated on page 347), could easily provide a ‘low power warning signal’ to the application system. Overcoming the problems that variable frequency, variable amplitude and intermittent vibration environments pose to the development of harvesting devices and circuitry is, in this author’s opinion, one of the next major hurdles to be overcome if vibration is going to be used successfully for powering wireless sensor nodes or portable electronic devices.

(3) Optimal component selection for the harvesting circuit concept:

The purpose of developing the harvesting circuit concept that has been proposed in this thesis was to provide a new method of enhancing the power output of a piezoelectric vibration energy harvesting device. As such, it was the feasibility of the concept that has been proven here, and the implementation of it is not an optimal one. This author considers therefore that it may be possible to implement a more efficient version of the proposed energy harvesting circuit concept by considering an optimal choice of component values. For example, considerations such as the equivalent series resistance (ESR) of the bucket capacitors, the quality (Q) factor of the inductor and the choice of reservoir capacitor technology (electrolytic versus supercapacitor) might benefit from further attention.

In addition to an optimal component selection of the fundamental components required for the proposed harvesting circuit concept, the detection, control and management functions could also be implemented by more elegant circuit design, using low power

discrete and integrated components in order to achieve a self-powered system. The last obstacle to overcome may well be the important issue of self-starting the system; i.e. in the case of a self-powered system, there is initially no energy with which to provide any active (powered) components, the operation of which might be required to achieve energy storage. In the block diagram of Figure 4-25 on page 251, this author proposed the use of a ‘housekeeping transducer’; i.e. another piezoelectric generator, present for the purpose of initially supplying the microcontroller with power. However, this is a far from ideal situation, leading to a greater system size and weight and potentially decreasing the reliability of the system. With careful consideration, this author believes that it may be possible to develop a system with self-starting capability.

5.4.2.3 Further Work regarding areas other than Power Enhancement

From the literature review conducted in this thesis, it is clear that the fundamental and most pressing limitation of energy harvesting devices remains their low power outputs. Figure 2-14 on page 70, which shows a range of power requirements of electronic devices and systems, indicates that the power consumptions of many of the most useful applications, including some of the most recently developed wireless sensor node platforms, remains above the power generation capability of most meso-scale energy harvesting devices. However, the literature review also highlighted several others areas that will require attention, including tuned or wideband harvesters and the durability/longevity of harvesting devices.

Concerning tuned or wideband piezoelectric harvesters, it is clear that much work has been carried out. However, most current methods of altering the resonant frequency of a harvesting device seem to involve some kind of human intervention in order to actively alter some physical aspect of the vibration harvester (see Figure 2-17 on page 80). This

somewhat negates the objective of using energy harvesting devices in remote environments or embedded in structures. It is clear that there is still work to be done in this area, as environments do exist where the frequencies of the vibration source can be guaranteed, such as on rotating machinery, other environments, such as by the roadside or on structures subjected to wind, may have varying frequencies of vibration, and for these broadband or self-tuning harvesting devices would definitely be an asset.

On the durability of piezoelectric harvesters, little work has been done. As mentioned before, it may be that there are more important considerations to be overcome in the short-term, but since one of the advantages often cited for the use of energy harvesting is the long-term longevity of the application, this author feels that it will be important in the future to consider and characterise the fatigue, failure modes and temperature dependence of energy harvesting devices.

5.4.3 The Future and Toward MEMS Harvesting Devices

Although energy harvesting technology has not yet become mainstream, it is on its way. Large semiconductor manufacturing companies such as Linear Technology and Texas Instruments are currently investing in the development of products that can be powered from energy scavenging devices operating from a range of energy-environments: e.g. solar, vibration or thermal. Linear Technologies at present supply four devices that can be powered from energy harvesting devices, one of which can be powered using piezoelectric conversion of vibration energy: an IC that features a low-loss bridge rectifier and DC-DC buck converter (Figure 5-3).

Home > Products > Energy Harvesting > LTC3588-1

Products

- > Data Conversion
- > Signal Conditioning
- > Power Management
- > Interface
- > High Frequency and Optical
- > Special Functions

LTC3588-1 - Piezoelectric Energy Harvesting Power Supply

FEATURES	DESCRIPTION	PACKAGING	ORDER INFO	SIMULATE	
----------	-------------	-----------	------------	----------	--

FEATURES

- 950nA Input Quiescent Current (Output in Regulation – No Load)
- 450nA Input Quiescent Current in UVLO
- 2.7V to 20V Input Operating Range
- Integrated Low-Loss Full-Wave Bridge Rectifier
- Up to 100mA of Output Current
- Selectable Output Voltages of 1.8V, 2.5V, 3.3V, 3.6V
- High Efficiency Integrated Hysteretic Buck DC/DC
- Input Protective Shunt – Up to 25mA Pull-Down at $V_{IN} \geq 20V$
- Wide Input Undervoltage Lockout (UVLO) Range
- Available in 10-Lead MSE and 3mm x 3mm DFN Packages

TYPICAL APPLICATION

100mA Piezoelectric Energy Harvesting Power Supply

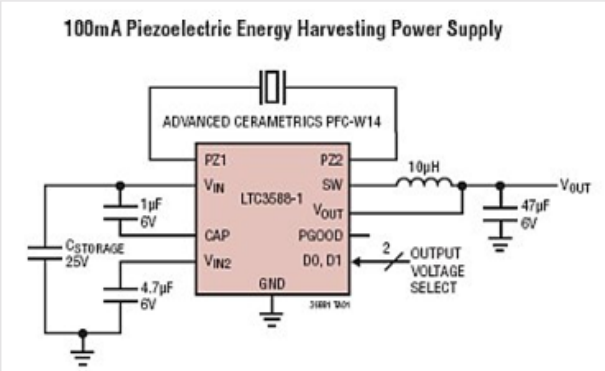


Figure 5-3 A DC-DC buck converter developed by linear technologies for providing power from a vibrating piezoelectric bimorph [151].

It seems clear that the future trend in both industry and research will be to continue to try to increase the power density of energy harvesting devices, while at the same time to continue to decrease the power consumptions of electronic devices and systems. As the two meet, a greater number of practical applications can be achieved. It seems likely that this trend will lead to the development of the next generation of harvesting devices: micro-scale harvesters, fabricated using MEMS processing techniques. Indeed, the

possibility of such harvesting devices is already being considered, with a few research groups exploring into the idea, as shown in Table 5-2:

Table 5-2 Micro-power vibration energy harvesting device power outputs when connected directly to a resistive load.

Power Generated (μW)	Voltage (pk) at max' power point (mV)	Resonant Frequency (Hz)	Applied Acceleration (g)	Volume (mm^3)	Optimal Load Resistance ($\text{k}\Omega$)	Bimorph or Unimorph	Thickness of one PZT layer (μm)	Reference
0.8	853	1496.3	2	0.509	450	Unimorph	1	[152]
2.15	160	461.25	2	2.22	6	Unimorph	1	[153]
2.16	304	609	1	0.616	21.4	Unimorph	1.64	[154]

{Note that in Table 5-2, the volume was calculated from using the longest dimensions of the overall device (beam with mass), i.e. overall length x overall width x overall height}. The power outputs of these tiny devices may at present be too small to provide power to electronic devices or systems, but eventually they might be capable of doing so, and then the possibility of providing power to millions of tiny wireless sensor nodes or an ever expanding range of implantable medical devices will become even more a realisable prospect.

REFERENCES

- [1] Guyomar, D.; Badel, A.; Lefeuvre, E. and Richard, C. Toward energy harvesting using active materials and conversion improvement by nonlinear processing. *IEEE Trans. Ultrason. Ferroelectr. Freq. Control*, 52(4), 2005, pp.584-595.
- [2] Satyanarayanan, M. Avoiding dead batteries. *IEEE Pervasive Comput*, 4(1), 2005, pp. 2-3.
- [3] Gates, B. The disappearing computer. *The world in 2003 (The Economist)*, 2002. Cited in: Roundy, S. Energy scavenging for wireless sensor nodes with a focus on vibration-to-electricity conversion. *University of California, Berkeley*, 2003 (Powerpoint presentation).
- [4] Wright, M. Harvesters gather energy from the ether, power lightweight systems. *Electronic Design News*, Dec 2006, pp. 57-62.
- [5] Brown, C. Endless energy is Harvesting's Promise. *EE Times*, Feb 2006, (3 pp.).
- [6] Zhang, P.; Sadler, C. M.; Lyon, S. A. and Martonosi, M. Hardware design experiences in zebanet. In: 2nd *ACM conference on embedded networked sensor systems (SenSys '04)*, Baltimore, MD, USA, Nov 3-4 2004.
- [7] Inversen, W. Scavenging energy for wireless sensor networks. *Automation world*, March 2005, p. 24.
- [8] IET electronic systems & software sector news (19th December 2006) *UK Government puts money into energy scavengers*. <http://www2.theiet.org/oncomms/sector/electronics/news.cfm/> (accessed 15th August 2007).
- [9] Randall, Julian F. Designing indoor solar products: photovoltaic technologies for AES, Chichester: John Wiley, 2005.
- [10] Harrop, P. and Das, R. *Energy harvesting and storage for electronic devices 2009-2019*. 1st ed. (IDTechEx report), 2009.
- [11] Raju, M. (Texas Instruments). ULP meets energy harvesting: a game-changing combination for design engineers. *Texas Instruments White Paper*, November 2008.
- [12] OSRAM Opto Semiconductors. SFH 7741 Proximity sensor data sheet. 4th February 2010, (14 pp.).
- [13] OSRAM Opto Semiconductors. SFH 5711 Ambient light sensor data sheet. 3rd April 2007, (9pp.).

- [14] Stanley-Marbell, P. and Marculescu, D. An 0.9 x 1.2", low power, energy-harvesting system with custom multi-channel communication interface. In: *Design, automation & test in Europe conference & exhibition (DATE '07)*, Nice, France, April 16-20 2007, pp. 1-6.
- [15] Ryckaert, J.; Desset, C.; Fort, A.; Badaroglu, M.; De Heyn, V.; Wambacq, P.; Van der Plas, G.; Donnay, S.; Van Poucke, B. and Gyselinckx, B. Ultra-wide-band transmitter for low-power wireless body area networks: design and evaluation. *IEEE Trans. Circuits Syst. I-Regular Papers*, 52(12), 2005, pp. 2515-2525.
- [16] Analog Devices. ADXL103/ADXL203 $\pm 1.7g$ Single-/Dual-Axis iMEMS[®] Accelerometer data sheet. Rev. A 2006, (12pp.).
- [17] Paradiso, J. A. and Feldmeier, M. A compact, wireless, self-powered pushbutton controller. In: *3rd international conference on ubiquitous computing (UBICOMP '01)*, Atlanta, GA, USA, Sept 30-Oct 2 2001, pp. 299-304.
- [18] Chao, B. (Advanced Linear Devices Inc). *Zero-power modules point the way for energy harvesting*.
<http://www.powermanagementdesignline.com/showArticle.jhtml?articleID=196900812> (posted 14th January 2007, accessed 23rd February 2010).
- [19] Roundy, S. and Wright, P. K. A piezoelectric vibration based generator for wireless electronics. *Smart Mater. Struct.*, 13(5), 2004, pp. 1131-1142.
- [20] Flatscher, M.; Dielacher, M.; Herndl, T.; Lentsch, T.; Maticsek, R.; Prainsack, J.; Pribyl, W.; Theuss, H. and Weber, W. A bulk acoustic wave (BAW) based transceiver for an in-tire-pressure monitoring sensor node. *IEEE J. Solid-State Circuit*, 45(1), 2010, pp. 167-177.
- [21] Ferrari, M.; Ferrari, V.; Guizzetti, M. and Marioli, D. An autonomous battery-less sensor module powered by piezoelectric energy harvesting with RF transmission of multiple measurement signals. *Smart Mater. Struct.*, 18(8), 2009, 085023 (9 pp.).
- [22] Jiang, X.; Polastre, J. and Culler, D. Perpetual environmentally powered sensor networks. In: *4th international symposium on information processing in sensor networks (IPSN '05)*, UCLA, CA, USA, Apr 25-27 2005, pp. 463-468.
- [23] Rahimi, M.; Shah, H.; Sukhatme, G.S.; Heideman, J. and Estrin, D. Studying the feasibility of energy harvesting in a mobile sensor network. In: *IEEE international conference on robotics and automation (ICRA '03)*, Taipei, Taiwan, Sept 14-19 2003, Vol 1. pp. 19-24.
- [24] Sangani, K. The sun in your pocket. *IET Engineering and Technology magazine*, August 2007, pp. 36-38.

- [25] Roundy, S.; Wright, P. K. and Rabaey, J. M. *Energy scavenging for wireless sensor networks with special focus on vibrations*, 1st ed. London: Kluwer Academic Publishers, 2004.
- [26] Mathúna, C. Ó.; O'Donnell, T.; Martinez-Catala, V.; Rohan, J. and O'Flynn, B. Energy scavenging for long-term deployable wireless sensor networks. *Talanta*, 75(3), 2008, pp. 613-623.
- [27] Woodall, J. M. and Hovel, H. J. High-efficiency Ga_{1-x}Al_xAs-GaAs solar cells. *Appl. Phys. Lett.* 21(8), 1972, p. 379 (3 pp.).
- [28] Archer, M. D. and Hill, R. *Clean electricity from photovoltaics*. 1st ed. London: Imperial College Press, 2001.
- [29] Lee, J. B.; Zizhang, C.; Allen, M. G.; Rohatgi, A. and Ayra, R. A high voltage solar cell array as an electrostatic MEMS power supply. In: *IEEE workshop on Micro electro mechanical systems - 1994 (MEMS '94)*, Oiso, Japan, Jan 25-28 1994, pp.331-336.
- [30] Guilar, N.; Chen, A.; Kleeburg, T. and Amirtharajah, R. Integrated solar energy harvesting and storage. In: *International symposium on low power electronics and design – 2006 (ISLPED '06)*, Tegernsee, Germany, Oct 4-6 2006, pp. 20-24.
- [31] Guilar, N. J.; Kleeburg, T. J.; Chen, A.; Yankelevich, D. R. and Amirtharajah, R. Integrated solar energy harvesting and storage. *IEEE Trans. Very Large Scale Integr. (VLSI) Syst.* 17(5), 2009, pp. 627-637.
- [32] Chen, C-T.; Islam, R. A. and Priya, S. Electric energy generator. *IEEE Trans. Ultrason. Ferroelectr. Freq. Control.* 53(3) 2006, pp. 656-661.
- [33] Rancourt, D.; Tabesh, A. and Fréchette, L. G. Evaluation of centimeter-scale micro wind mills: aerodynamics and electromagnetic power generation. In: *7th international workshop on micro and nanotechnology for power generation and energy conversion applications (PowerMEMS 2007)*, Freiburg, Germany, Nov 28-29 2007.
- [34] Pobering, S. and Schwesinger, N. Power supply for wireless sensor systems. In: *IEEE sensors 2008*, Lecce, Italy, Oct 26-29 2008, pp. 685-688.
- [35] Federspiel, C. C. and Chen, J. Air-powered sensor. In: *2nd IEEE international conference on sensors (Sensors 2003)*, Toronto, Canada, Oct 22-24 2003, Vol. 1, pp. 22-25.
- [36] Bonus Energy A/S (now Siemens Wind Power A/S). The wind turbine components and operation. *Bonus Info Special Issue*, Denmark, Autumn 1999 (company literature).

- [37] Holmes, A.S.; Hong, G.; Pullen, K.R. and Buffard, K.R. Axial-flow microturbine with electromagnetic generator: design, CFD simulation, and prototype demonstration. In: *17th IEEE international conference on micro electro mechanical systems (MEMS)*, Maastricht, Netherlands, Jan 25-29 2004, pp. 568-571.
- [38] Priya, S. Modeling of electric energy harvesting using piezoelectric windmill. *Appl. Phys. Lett.*, 87 184101, 2005, (3 pp.).
- [39] Priya, S.; Chen, C-T.; Fye, D. and Zahnd, J. Piezoelectric windmill: a novel solution to remote sensing. *Jpn. J. Appl. Phys.*, 44(3), 2005, pp. 104-L 107.
- [40] Myers, R.; Vickers, M. and Kim, H. Small scale windmill. *Appl. Phys. Lett.*, 90 054106, 2007, (3 pp.).
- [41] Leonov, V.; Fiorini, P.; Sedky, S.; Torfs, T. and Hoof, C. V. Thermoelectric MEMS generators as a power supply for a body area network. In: *13th international conference on solid-state sensors, actuators and Microsystems*, Seoul, Korea, Jun 5-9 2005, Vol. 1, pp. 291-294.
- [42] Lay-Ekuakille, A.; Vendramin, G.; Trotta, A. and Mazzotta, G. Thermoelectric generator design based on power from body heat for biomedical autonomous devices. In: *IEEE international workshop on medical measurements and applications (MeMeA 2009)*, Cetraro, Italy, May 29-30 2009, pp.1-4.
- [43] International thermoelectric society. Thermoelectric power for automobiles arrives in Europe. <http://www.its.org/node/5670> (accessed 11th February 2010).
- [44] Sanz-Bobi, M. A. and Palacios, R. Potential use of small waste heat sources based on thermoelectricity: application to an overhead projector and a battery charger. In: *15th European workshop on thermoelectrics*, Pardubice, Czech Republic, Sept 20-21 1999, pp.58-65.
- [45] Wu, C. Analysis of waste-heat thermoelectric power generators. *Applied Thermal Engineering*, 16(1), 1996, pp. 63-69.
- [46] Stordeur, M. and Stark, I. Low power thermoelectric generator - self-sufficient energy supply for micro systems. In: *16th international conference on thermoelectrics (ICT '97)*, Dresden Germany, Aug 26-29 1997, pp. 575-577.
- [47] Leonov, V.; Torfs, T.; Fiorini, P. and Van Hoof, C. Thermoelectric converters of human warmth for self-powered wireless sensor nodes. *Sensors Journal*, 7(5), 2007, pp.650-657.

- [48] Kishi, M.; Nemoto, H.; Hamao, T.; Yamamoto, M.; Sudou, S.; Mandai, M. and Yamamoto, S. Micro-thermoelectric modules and their application to wristwatches as an energy source. In: *18th international conference on thermoelectrics (ICT '99)*, Baltimore, MD, USA, Aug 29-Sept 2 1999, pp.301-307.
- [49] Seiko Instruments Inc. *Seiko thermic wristwatch*.
<http://www.seikowatches.com/technology/index.html> (accessed 20th November 2006).
- [50] Strasser, M.; Aigner, R.; Franosch, M. and Wachutka, G. Miniaturized thermoelectric generators based on poly-Si and poly-SiGe surface micromachining. *Sens. Actuator A-Phys.*, Vols 97-98, 2002, pp. 535-542.
- [51] Yang, S. M. and Lee, T. Development of a thermoelectric energy harvester with thermal isolation cavity by standard CMOS process. *Sens. Actuator A-Phys.*, 153(2) 2009, pp.244-250.
- [52] Ferrari, M.; Ferrari, V.; Guizzetti, M.; Marioli, D. and Taroni, A. Characterization of thermoelectric modules for powering autonomous sensors. In: *Instrumentation and measurement technology conference (IMTC '07)*, Warsaw, Poland, May 1-3 2007, pp.1-6.
- [53] Jung, S.; Lauterbach, C.; Strasser, M. and Weber, W. Enabling technologies for disappearing electronics in smart textiles. In: *IEEE international solid-state circuits conference (ISSCC '03)*, San Francisco, CA, USA, Feb 9-13 2003, pp. 386-387.
- [54] Krähenbühl, D.; Zwyssig, C.; Weser, H. and Kolar, J. W. Theoretical and experimental results of a mesoscale electric power generation system from pressurized gas flow. *J. Micromech. Microeng.*, 19(9), 2009, 094009 (6 pp.).
- [55] Hagerty, J.A.; Helmbrecht, F.B.; McCalpin, W.H.; Zane, R. and Popovic, Z.B. Recycling ambient microwave energy with broad-band rectenna arrays. *IEEE Trans. Microw. Theory Tech.*, 52(3), 2004, pp. 1014-1024.
- [56] Araiza, J. U. M. Wireless transmission of power for sensors in context aware spaces. *Massachusetts institute of technology*, Jun 2002, (MSc Thesis)
- [57] D'Souza, M.; Bialkowski, K.; Postula, A. and Ros, M. A wireless sensor node architecture using remote power charging, for interaction applications. In: *10th Euromicro conference on digital system design architectures (DSD '07)*, Lübeck, Germany, Aug 29-31, pp. 485-494.
- [58] Le, T.; Mayaram, K. and Fiez, T. Efficient far-field radio frequency energy harvesting for passively powered sensor networks. *IEEE J. Solid-State Circuit*, 43(5), 2008, pp. 1287-1302.

- [59] Sample, A.P.; Yeager, D.J.; Powledge, P.S.; Mamishev, A.V. and Smith, J.R. Design of an RFID-based battery-free programmable sensing platform. *IEEE Trans. on Instr. And Meas.*, 57(11), 2008, pp. 2608-2615.
- [60] Tang, L. and Guy, C. Radio frequency energy harvesting in wireless sensor networks. In: *International conference on wireless communications and mobile computing (IWCMC '09)*, Leipzig, Germany, Jun 21-24 2009, pp.644-648.
- [61] Starner, T. Human-powered wearable computing. *IBM systems journal*, 35(3&4), 1996, 618-629.
- [62] Torah, R. N.; Beeby, S. P.; Tudor, M. J.; O'Donnell, T. and Roy, S. Development of a cantilever beam generator employing vibration energy harvesting. In: *6th international workshop on micro and nanotechnology for power generation and energy conversion applications (PowerMEMS 2006)*, Berkeley, CA, USA, Nov 29-Dec 1 2006.
- [63] Mizuno, M and Chetwynd, D. G. Investigation of a resonance microgenerator. *J. Micromech. Microeng.*, 13, 2003, pp. 209-216.
- [64] Shearwood, C. and Yates, R. B. Development of an electromagnetic micro-generator. *Electron. Lett.*, 33(22), 1997, pp. 1883-1884.
- [65] Scherrer, S.; Plumlee, D.G. and Moll, A.J. Energy scavenging device in LTCC materials. In: *IEEE workshop on microelectronics and electron devices (WMED '05)*, Boise, ID, USA, Apr 15-15 2005, pp. 77-78.
- [66] Roundy, S.; Wright, P. K. and Rabaey, J. M. A study of low level vibrations as a power source for wireless sensor nodes. *Comput. Commun.*, 26(11), 2003, pp. 1131-1144.
- [67] duToit, N. E.; Wardle, B. L. and Kim, S. G. Design considerations for MEMS-scale piezoelectric mechanical vibration energy harvesters. *Integr. Ferroelectr.*, 71(1), 2005, pp. 121-160.
- [68] Miyazaki, M.; Tanaka, H.; Ono, G.; Nagano, T.; Ohkubo, N.; Kawahara, T. and Yano, K. Electric-energy generation using variable-capacitive resonator for power-free LSI: Efficiency analysis and fundamental experiment. In: *International symposium on low power electronics and design (ISLPED '03)*, Seoul, Korea, Aug 25-27 2003, pp. 193-198.
- [69] Despesse, G.; Jager, T.; Chaillout, J.-J.; Leger, J.-M. and Basrour, S. Design and fabrication of a new system for vibration energy harvesting. In: *PhD research in microelectronics and electronics*, Lausanne, Switzerland, Jul 25-28 2005, Vol. 1 pp. 225-228.

- [70] Kulah, H. and Najafi, K. An electromagnetic micro power generator for low-frequency environmental vibrations. In: *17th IEEE international conference on micro electro mechanical systems (MEMS '04)*, Maastricht, Netherlands, Jan 25-29 2004, pp. 237-240.
- [71] Amirtharajah, R. and Chandrakasan, A. P. Self-powered signal processing using vibration-based power generation. *IEEE J. Solid-State Circuit*, 33(5), 1998, pp. 687-695.
- [72] Li, W. J.; Ho, T. C. H.; Chan, G. M. H.; Leong, P. H. W. and Hiu Yung Wong. Infrared signal transmission by a laser-micromachined, vibration-induced power generator. In: *43rd IEEE Midwest symposium on circuits and systems*, Lansing, MI, USA, Aug 8-11 2000, Vol. 1 pp. 236-239.
- [73] El-hami, M.; Glynne-Jones, P.; White, N. M.; Hill, M.; Beeby, S.; James, E.; Brown, A. D. and Ross, J. N. Design and fabrication of a new vibration-based electromechanical power generator. *Sens. Actuator A-Phys.*, 92(1-3), 2001, pp. 335-342.
- [74] Ching, Neil N. H.; Wong, H. Y.; Li, Wen J.; Leong, Philip. H. W. and Wen, Zhiyu. A laser-micromachined multi-modal resonating power transducer for wireless sensing systems. *Sens. Actuator A-Phys.*, 97-98, 2002, pp. 685-690.
- [75] James, E. P.; Tudor, M. J.; Beeby, S. P.; Harris, N. R.; Glynne-Jones, P.; Ross, J. N. and White, N. M. An investigation of self-powered systems for condition monitoring applications. *Sens. Actuator A-Phys.*, 110(1-3), 2004, pp. 171-176.
- [76] Kulkarni, S.; Koukharenko, E.; Tudor, J.; Beeby, S.; O'Donnell, T. and Roy, S. Fabrication and test of integrated micro-scale vibration based electromagnetic generator. In: *14th international conference on solid-state sensors, actuators and microsystems (Transducers '07)*, Lyon, France, Jun 10-14 2007, pp. 879-882.
- [77] Torah, R.N.; Tudor, M.J.; Patel, K.; Garcia, I.N. and Beeby, S.P. Autonomous low power microsystem powered by vibration energy harvesting. In: *IEEE Sensors 2007*, Atlanta, GA, USA, Oct 28-31 2007, pp. 264-267.
- [78] Koukharenko, E.; Beeby, S. P.; Tudor, M. J.; White, N. M.; O'Donnell, T.; Saha, C.; Kulkarni, S. and Roy, S. Microelectromechanical systems vibration powered electromagnetic generator for wireless sensor applications. *Microsyst. Technol.*, 12(10-11), 2006, pp. 1071-1077.
- [79] Glynne-Jones, P.; Tudor, M. J.; Beeby, S. P. and White, N. M. An electromagnetic, vibration-powered generator for intelligent sensor systems. *Sens. Actuator A-Phys.*, 110(1-3), 2004, pp. 344-349.
- [80] Beeby, S. P.; Tudor, M. J. and White, N. M. Energy harvesting vibration sources for microsystems applications. *Meas. Sci. Technol.*, 17(12), 2006, R175-R195.

- [81] Chiu, Y. and Tseng, V. F. G. A capacitive vibration-to-electricity energy converter with integrated mechanical switches. *J. Micromech. Microeng.*, 18(10), 2008, 104004 (8 pp.).
- [82] Hoffmann, D.; Folkmer, B and Manoli, Y. Fabrication, characterization and modelling of electrostatic micro-generators. *J. Micromech. Microeng.*, 19(9), 2009, 094001 (11 pp.).
- [83] Naruse, Y.; Matsubara, N.; Mabuchi, K.; Izumi, M. and Suzuki, S. Electrostatic micro power generation from low-frequency vibration such as human motion. *J. Micromech. Microeng.*, 19(9), 2009, 094002 (5 pp.).
- [84] Tashiro, R.; Kabe1, N.; Katayama, K; Tsuboi, E. and Tsuchiya, K. Development of an electrostatic generator for a cardiac pacemaker that harnesses the venricular wall motion. *J. Artif. Organs*, 5(4), 2002, pp. 0239-0245.
- [85] Sterken, T.; Fiorini, P.; Altena, G.; Van Hoof, C. and Puers, R. Harvesting energy from vibrations by a micromachined electret generator. In: *14th international conference on solid-state sensors, actuators and microsystems (Transducers '07)*, Lyon, France, Jun 10-14 2007, pp. 129-132.
- [86] Miao, P.; Mitcheson, P. D.; Holmes, A. S.; Yeatman, E. M.; Green, T. C. and Stark, B. H. MEMS inertial power generators for biomedical applications. *Microsyst. Technol.*, 12(10-11), 2006, pp. 1079-1083.
- [87] Arakawa, Y.; Suzuki, Y. and Kasagi, N. Micro seismic power generator using electret polymer film. In: *4th international workshop on micro & nanotechnology for power generation and energy conversion applications (Power MEMS '04)*, Kyoto, Japan, Nov 28-30 2004, pp. 187-190.
- [88] Tsutsumino, T.; Suzuki, Y.; Kasagi, N. and Sakane, Y. Seismic power generator using high-performance polymer electret. In: *19th IEEE international conference on Micro electro mechanical systems – 2006 (MEMSYS '06)*, Istanbul, Turkey, Jan 22-26 2006, pp. 98-101.
- [89] Tsutsumino, T.; Suzuki, Y. and Kasagi, N. Electromechanical modeling of micro electret generator for energy harvesting. In: *14th international conference on solid-state sensors, actuators and microsystems (Transducers '07)*, Lyon, France, Jun 10-14 2007, Vol. 2 pp. 863-866.
- [90] Moulson, A. J. and Herbert, J. M. *Electroceramics: materials, properties, applications*, 2nd ed. Chichester: John Wiley and Sons, 2003.
- [91] Kim, H. W.; Batra, A.; Priya, S.; Uchino, K.; Markley, D.; Newnham, R. E. and Hofmann, H. F. Energy harvesting using a piezoelectric “cymbal” transducer in dynamic environment. *Jpn. J. Appl. Phys.*, 43(9A), 2004, pp. 6178-6183.

- [92] Glynn-Jones, P.; Beeby, S. P. and White, N. M. Towards a piezoelectric vibration-powered microgenerator. *Proc. IEEE*, 148(2), 2001, pp. 68-72.
- [93] Ottman, G. K.; Hofmann, H. F.; Bhatt, A. C. and Lesieutre, G. A. Adaptive piezoelectric energy harvesting circuit for wireless remote power supply. *IEEE Trans. Power Electron.*, 17(5), 2002, pp.669-676.
- [94] Midé. *Vibration energy harvesting products – online catalog*.
http://www.mide.com/products/vulture/vulture_catalog.php#peh (accessed 12th February 2010).
- [95] Sodano, H. A.; Park, G. and Inman, D. J. Estimation of electric charge output for piezoelectric energy harvesting. *Strain*, 40(2), 2004, pp. 49-58.
- [96] Kymissis, J.; Kendall, C.; Paradiso, J. and Gershenfeld, N. Parasitic power harvesting in shoes. In: *2nd IEEE international conference on wearable computing (ISWC '98)*, Pittsburgh, PA, USA, Oct 19-20 1998, pp. 132-139.
- [97] Shenck, N. S. and Paradiso, J. A. Energy scavenging with shoe-mounted piezoelectrics. *IEEE Micro*, 21(3), 2001, pp. 30-42.
- [98] Mossi, K.; Green, C.; Ounaies, Z. and Hughes, E. Harvesting energy using a thin unimorph prestressed bender: geometrical effects. *J. Intell. Mater. Syst. Struct.*, 16(3), 2005, pp. 249-261.
- [99] Baker, J.; Roundy, S. and Wright, P. Alternative geometries for increasing power density in vibration energy scavenging for wireless. In: *3rd AIAA international energy conversion engineering conference*, San Francisco, CA, USA, Aug 15-18 2005, (paper number AIAA 2005-5617).
- [100] Kim, S.; Clark, W. W. and Wang, Q-M. Piezoelectric energy harvesting with a clamped circular plate: analysis. *J. Intell. Mater. Syst. Struct.*, 16(10), 2005, pp. 847-854.
- [101] Kim, S.; Clark, W. W. and Wang, Q-M. Piezoelectric energy harvesting with a clamped circular plate: experimental study. *J. Intell. Mater. Syst. Struct.*, 16(10), 2005, pp. 855-863.
- [102] Choi, W. J.; Jeon, Y.; Jeong, J-H.; Sood, R. and Kim, S. G. Energy harvesting MEMS device based on thin film piezoelectric cantilevers. *J. Electroceram.*, 17(2-4), 2006, pp. 543-548.
- [103] Mateu, L. and Moll, F. Optimum piezoelectric bending beam structures for energy harvesting using shoe inserts. *J. Intell. Mater. Syst. Struct.*, 16(10), 2005, pp.835-845.
- [104] Mossi, K.; Ounaies, Z. and Oakley, S. Optimizing energy harvesting of a composite unimorph pre-stressed bender. In: *16th technical conference of the*

American society for composites, Blacksburg, VA, USA, Sept 9-12 2001.

- [105] Mossi, K.; Ounaies, Z.; Smith, R. and Ball, B. Prestressed curved actuators: characterization and modeling of their piezoelectric behaviour. In: *Proc. SPIE: smart structures and materials 2003: active materials: behaviour and mechanics*, San Diego, CA, USA, March 2-6 2003, Vol. 5053, pp. 423-435.
- [106] Yoon, H-S.; Washington, G. and Danak, A. Modeling, optimization, and design of efficient initially curved piezoceramic unimorphs for energy harvesting applications. *J. Intell. Mater. Syst. Struct.*, 16(10), 2005, pp. 877-888.
- [107] Yuantai, H. U.; Hongping, H. U. and Jiashi, Y. A low frequency piezoelectric power harvester using a spiral-shaped bimorph. *Science in China Series G: Physics Mechanics and Astronomy*, 49(6), 2006, pp. 649-659.
- [108] Myers, G. H.; Parsonnet, V.; Zucker, I. R.; Lotman, H. A. and Asa, M. M. Biologically-energized cardiac pacemaker. *IRE transactions on bio-medical electronics*, 10(2), 1963, p. 83.
- [109] Sohn, J. W.; Choi, S. B. and Lee, D. Y. An investigation on piezoelectric energy harvesting for MEMS power sources. *Proc. Inst. Mech. Eng. Part C-J. Eng. Mech. Eng. Sci.*, 219(4), 2005, pp. 429-436.
- [110] Platt, S.R.; Farritor, S.; Garvin, K. and Haider, H. The use of piezoelectric ceramics for electric power generation within orthopaedic implants. *IEEE-ASME Trans. Mechatron.*, 10(4), 2005, pp. 455-461.
- [111] Platt, S. R.; Farritor, S. and Haider, H. On low-frequency electric power generation with PZT ceramics. *IEEE-ASME Trans. Mechatron.*, 10(2), 2005, pp. 240-252.
- [112] Antaki, J. F.; Bertocci, G. E.; Green, E. C.; Nadeem, A.; Rintoul, T.; Kormos, R. L. and Griffith, B. P. A gait-powered autologous battery charging system for artificial organs. *ASAIO Journal*, 41(3), 1995, pp. M588-M595.
- [113] Klimiec E.; Zaraska, W.; Zaraska, K.; Gąsiorowski, K. P.; Sadowski, T and Pajda, M. Piezoelectric polymer films as power converters for human powered electronics. *Microelectronics Reliability*, 48(6), 2008, pp. 897-901.
- [114] Rocha, J. G.; Goncalves, L. M.; Rocha, P. F.; Silva, M. P. and Lanceros-Méndez, S. Energy harvesting from piezoelectric materials fully integrated in footwear. *IEEE Trans. Ind. Electron.*, 57(3), 2010, pp. 813-819.

- [115] Renaud, M.; Sterken, T.; Fiorini, P.; Puers, R.; Baert, K. and van Hoof, C. Scavenging energy from human body: design of a piezoelectric transducer. In: *13th international conference on solid-state sensors, actuators and Microsystems (Transducers '05)*, Seoul, Korea, Jun 5-9 2005, Vol. 1, pp. 784-787.
- [116] Challa, V. R.; Prasad, M. G.; Shi, Y. and Fisher, F. T. A vibration energy harvesting device with bidirectional resonance frequency tunability. *Smart Mater. Struct.*, 17(1), 2008, 015035 (10 pp.).
- [117] Wu, X.; Lin, J.; Kato, S.; Zhang, K.; Ren, T. and Liu, L. A frequency adjustable vibration energy harvester. In: *8th international workshop on micro and nanotechnology for power generation and energy conversion applications (PowerMEMS '08)*, Sendai, Japan, Nov 9-12 2008, pp. 245-248.
- [118] Leland, E. S. and Wright, P. K. Resonance tuning of piezoelectric vibration energy scavenging generators using compressive axial preload. *Smart Mater. Struct.*, 15(5), 2006, pp. 1413-1420.
- [119] Eichhorn, C.; Goldschmidtboeing, F. and Woias, P. A frequency tunable piezoelectric energy converter based on a cantilever beam. In: *8th international workshop on micro and nanotechnology for power generation and energy conversion applications (PowerMEMS '08)*, Sendai, Japan, Nov 9-12 2008, pp. 309-312.
- [120] Ferrari, M.; Ferrari, V.; Guizzetti, M.; Marioli, D. and Taroni, A. Piezoelectric multifrequency energy converter for power harvesting in autonomous microsystems. *Sens. Actuator A-Phys.*, 142(1), 2008, pp. 329-335.
- [121] du Plessis, A. J.; Huigsloot, M. J. and Discenzo, F. D. Resonant packaged piezoelectric power harvester for machinery health monitoring. In: *Proc. SPIE: smart structures and materials 2005: active materials: behaviour and mechanics*, San Diego, CA, USA, March 6-10 2005, Vol. 5762, pp. 224-235.
- [122] Ballato, A. Piezoelectricity: history and new thrusts. In: *IEEE ultrasonics symposium*, San Antonio, TX, USA, Nov 3-6 1996, Vol. 1 pp. 575-583.
- [123] Katzir, S. *The beginnings of piezoelectricity*, Dordrecht [London]: Springer, 2006.
- [124] Piezo Systems, Inc. *History of Piezoelectricity*.
<http://www.piezo.com/tech4history.html> (accessed 12th February 2010).
- [125] Taylor, G. W. *Piezoelectricity (Ferroelectricity and related phenomena; vol 4)*, Gordon and Breach (Now Taylor & Francis Group), 1985.
- [126] Haertling, G. H. Ferroelectric ceramics: history and technology. *J. Am. Ceram. Soc.*, 82(4), 1999, pp. 797-818.

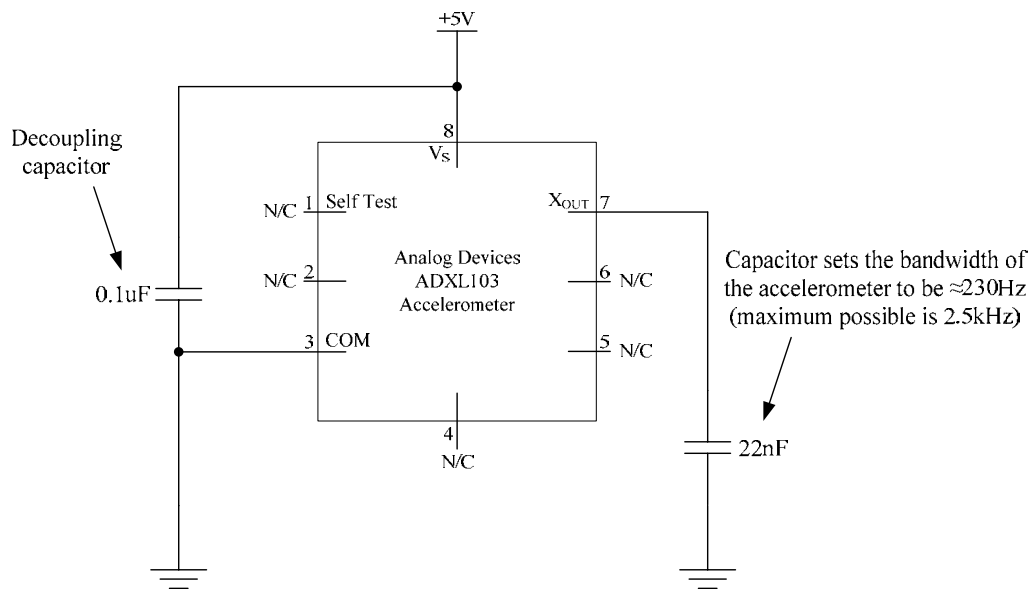
- [127] Physik Instrumente. *Fundamentals of piezoelectricity*.
<http://www.physikinstrumente.com/en/products/prdetail.php?sortnr=400600.00>
 (accessed 12th February 2010).
- [128] Roundy, S. J. Energy scavenging for wireless sensor nodes with a focus on vibration to electricity conversion. *The university of California, Berkeley*, Spring 2003, (PhD Thesis).
- [129] Li, W. G.; He, S. and Yu, S. D. Improving power density of a cantilever piezoelectric power harvester through a curved L-shaped proof mass. *IEEE Trans. Ind. Electron.*, 57(3), 2010, pp.868-876.
- [130] Goldschmidtboeing, F. and Woias, P. Characterisation of different beam shapes for piezoelectric energy harvesting. *J. Micromech. Microeng.*, 18(10), 2008, 104013 (7 pp.).
- [131] Kauffman, J. K. and Lesieutre, G. A. A low order model for the design of piezoelectric energy harvesting devices. *J. Intell. Mater. Syst. Struct.*, 20(5), 2009, pp. 495-504.
- [132] Lu, F.; Lee, H. P. and Lim, S. P. Modeling and analysis of micro piezoelectric power generators for micro-electromechanical-systems applications. *Smart Mater. Struct.*, 13(1), 2004, pp. 57-63.
- [133] Ottman, G. K.; Hofmann, H. F. and Lesieutre, G. A. Optimized piezoelectric energy harvesting circuit using step-down converter in discontinuous conduction mode. *IEEE Trans. Power Electron.*, 18(2), 2003, pp.696-703.
- [134] Lefeuvre, E.; Badel, A.; Richard, C. and Guyomar, D. Piezoelectric energy harvesting device optimization by synchronous electric charge extraction. *J. Intell. Mater. Syst. Struct.*, 16(10), 2005, pp. 865-876.
- [135] Zhu, M.; Worthington, E. and Njuguna, J. Analyses of power output of piezoelectric energy harvesting devices directly connected to a load resistor using a coupled piezoelectric-circuit finite element method. *IEEE Trans. Ultrason. Ferroelectr. Freq. Control*, 56(7), 2009, pp. 1309-1317.
- [136] Steinberg, D. S. *Vibration analysis for electronic equipment*. 3rd ed. New York: John Wiley & Sons, 2000.
- [137] Priya, S. and Inman, D. J. *Energy harvesting technologies*. 1st ed. London: Springer, 2008.
- [138] Liao, Y and Sodano, H. A. Model of a single mode energy harvester and properties for optimal power generation. *Smart Mater. Struct.*, 17(6), 2008, 065026 (14 pp.).

- [139] Liao, Y and Sodano, H. A. Structural effects and energy conversion efficiency of power harvesting. *J. Intell. Mater. Syst. Struct.*, 20(5), 2009, pp. 505-514.
- [140] Ertuk, A. and Inman, D. J. Issues in mathematical modelling of piezoelectric energy harvesters. *Smart Mater. Struct.*, 17(6), 2008, 065016 (14 pp.).
- [141] Ertuk, A. and Inman, D. J. An experimentally validated bimorph cantilever model for piezoelectric energy harvesting from base excitations. *Smart Mater. Struct.*, 18(2), 2009, 025009 (18 pp.).
- [142] Zhu, M.; Worthington, E. and Tiwari, A. Design study of piezoelectric energy-harvesting devices for generation of higher electrical power using a coupled piezoelectric-circuit finite element method. *IEEE Trans. Ultrason. Ferroelectr. Freq. Control*, 57(2), 2010, pp. 427-437.
- [143] Shigley, J. E. *Applied mechanics of materials*. 1st ed. London: McGraw-Hill, 1976.
- [144] Kaye, G. W. C. and Laby, T. H.; *Tables of physical and chemical constants*, 16th ed. Harlow: Longman, 1995.
- [145] Dallago, E.; Miatton, D.; Venchi, G.; Frattini, G. and Ricotti, G. Self-supplied integrable active high-efficiency AC-DC converter for piezoelectric energy scavenging. In: *IEEE international symposium on circuits and systems, 2007 (ISCAS '07)*, New Orleans, LA, USA, May 27-30 2007, pp. 1633-1636.
- [146] Salivahanan, S.; Suresh Kumar, N. and Vallavaraj, A. *Electronic devices and circuits*. (24th reprint 2007), New Delhi: Tata McGraw-Hill, 2007.
- [147] Seeman, M.D.; Sanders, S.R. and Rabaey, J.M. An ultra-low-power management IC for energy-scavenged wireless sensor nodes. In: *39th IEEE power electronics specialists conference, 2008 (PESC '08)*, Rhodes, Greece, Jun 15-19 2008, pp. 925-931.
- [148] Shukla, A. K.; Sampath, S. and Vijayamohanan, K. Electrochemical supercapacitors: energy storage beyond batteries. *Current Science*, 79(12), 2000, pp. 1656-1661.
- [149] Patch, K. Circuit gets more power from shakes. *Technology Research News*, Nov 2002.
http://www.trnmag.com/Stories/2002/111302/Circuit_gets_more_power_from_shakes_111302.html (accessed 2nd August 2010).
- [150] Ottman, G. K.; Hofmann, H. F. and Lesieutre, G. A. Optimized piezoelectric energy harvesting circuit using step-down converter in discontinuous conduction mode. *IEEE Trans. Power Electron.*, 18(2), 2003, pp.696-703.

- [151] Linear Technologies Website: *LTC3588-1 – Piezoelectric energy harvesting power supply*.
<http://www.linear.com/pc/productDetail.jsp?navId=H0,C1,C1003,C1799,P90393>
(accessed 23rd February 2010).
- [152] Marzencki M.; Ammar Y. and Basrou S. Integrated power harvesting system including a MEMS generator and a power management circuit. *Sens. Actuator A-Phys*, 145-146(special issue: actuator section), 2008, pp. 363-970.
- [153] Shen D.; Park J.H.; Ajitsaria J.; Choe S.Y.; Wikle III H.C. and Kim D.J. The design, fabrication and evaluation of a MEMS PZT cantilever with an integrated Si proof mass for vibration energy harvesting. *J. Micromech. Microeng.* 18(5), 2008, 055017 (7 pp.).
- [154] Fang H.B.; Liu J.Q.; Xu Z.Y.; Dong L.; Wang L.; Chen D.; Cai B.C. and Liu Y. Fabrication and performance of MEMS-based piezoelectric power generator for vibration energy harvesting. *Microelectronics Journal*, 37(11), 2006, pp. 1280-1284.

APPENDICES

Appendix A: Circuit Schematic for the Accelerometer



Appendix B: Properties of the materials used in construction of the optimised piezoelectric vibration energy harvesting device of Chapter 3

Substrate material: brass

Young's modulus (GPa)	100
Density (kg/m ³)	8780

Piezoelectric material: PSI-5H4E (Piezo Systems Inc, MA, USA)

Young's modulus E_{11} (GPa)	62
Density (kg/m ³)	7800
Piezoelectric charge constant d_{31} ($\times 10^{-12}$ m/V)	-320
Coupling coefficients k_{31}	0.44
Relative dielectric constant ϵ_{33}	3800
Mechanical quality factor Q	32

Seismic mass material: Tungsten alloy

(M&I Materials Ltd/Wolfmet, Manchester, UK)

Density (kg/m ³)	18100
------------------------------	-------

Appendix C: Mathcad file used for optimisation of the piezoelectric vibration energy

harvesting device

Beam properties:

$h_s := 0.102 \cdot 10^{-3}$ Height of substrate material
 $h_{lp} := 0.278 \cdot 10^{-3}$ Height of lower layer of piezoceramic material
 $h_{up} := 0.278 \cdot 10^{-3}$ Height of upper layer of piezoceramic material
 $b := 3.2 \cdot 10^{-3}$ Width of beam

Material properties:

$E_s := 100 \cdot 10^9$ Young's modulus of substrate material (brass)
 $E_p := 62 \cdot 10^9$ Young's modulus of piezoceramic material (not known for present beam, so is an arbitrary value)
 $d_{31} := 320 \cdot 10^{-12}$ Charge constant

$h_n := \frac{(h_{lp} + h_s + h_{up})}{2}$ This expression finds the distance h_n (from bottom of beam to neutral axis): $h_n = 3.29 \times 10^{-4}$

Properties of the driving vibrations:

$Y := 3.95 \cdot 10^{-6}$ Amplitude
 $f := 0, 0.01, 200$ Frequency in Hz $f := 120$
 $\omega(f) := 2 \cdot \pi \cdot f$ Angular frequency in rad/s

Beam properties

$L_b := 6.5 \cdot 10^{-3}$ Length of beam
 $h_{np} := \frac{h_s}{2} + \frac{h_{up}}{2}$ Distance between neutral axis and top of beam
 $\zeta := 0.05$ Damping ratio
 $L_m := 8.5 \cdot 10^{-3}$ Length of mass
 $h_m := 7.7 \cdot 10^{-3}$ Height of mass
 $b_m := 6.7 \cdot 10^{-3}$ Width of mass
 $\rho_m := 18100$ Density of mass material (tungsten alloy)
 $\rho_p := 7800$ Density of piezoceramic material
 $\rho_s := 8780$ Density of centre shim material (brass)

Material property

$\sigma_c := 3800$

$h_p := h_{lp}$

Permittivity of a vacuum

$\epsilon_0 := 8.854 \cdot 10^{-12}$

$$P_{ave_in_R}(f, L_b, L_m, h_m, b_m, Y) := \frac{256 \cdot \left[E_p \cdot \left(\int_{-h_n}^{-h_n+h_{lp}} y^2 \cdot b \, dy \right) + E_s \cdot \left(\int_{-h_n+h_{lp}}^0 y^2 \cdot b \, dy \right) + E_s \cdot \left(\int_0^{h_s+h_{lp}-h_n} y^2 \cdot b \, dy \right) + E_p \cdot \left(\int_{h_s+h_{lp}-h_n}^{h_s+h_{lp}+h_{up}-h_n} y^2 \cdot b \, dy \right) \right]}{L_b \cdot L_m \cdot h_m \cdot b_m \cdot Y^2}$$

Given

$$f \geq 60 \quad L_b > 0 \quad L_m > 0 \quad h_m > 0 \quad b_m > 0$$

$$f \leq 140$$

$$\sqrt{\frac{12 \left[E_p \cdot \left(\int_{-h_n}^{-h_n+h_p} y^2 \cdot b \, dy \right) + E_s \cdot \left(\int_{-h_n+h_p}^0 y^2 \cdot b \, dy \right) + E_s \cdot \left(\int_0^{h_s+h_p-h_n} y^2 \cdot b \, dy \right) + E_p \cdot \left(\int_{h_s+h_p-h_n}^{h_s+h_p+h_p-h_n} y^2 \cdot b \, dy \right) \right]}{(4 \cdot L_b^3 + 6 \cdot L_b^2 \cdot L_m + 3 \cdot L_m^2 \cdot L_b) \left[(L_m \cdot h_m \cdot b_m \cdot \rho_m) + (L_m \cdot h_s \cdot b \cdot \rho_s) + [L_m \cdot (h_p + h_p) \cdot b \cdot \rho_p] \right]}} = 2 \cdot \pi \cdot 120$$

$$\left[(h_s + h_p + h_p + h_m) \cdot L_m \cdot b_m \right] + [(h_s + h_p + h_p) \cdot L_b \cdot b] - 1 \cdot 10^6 \leq 1$$

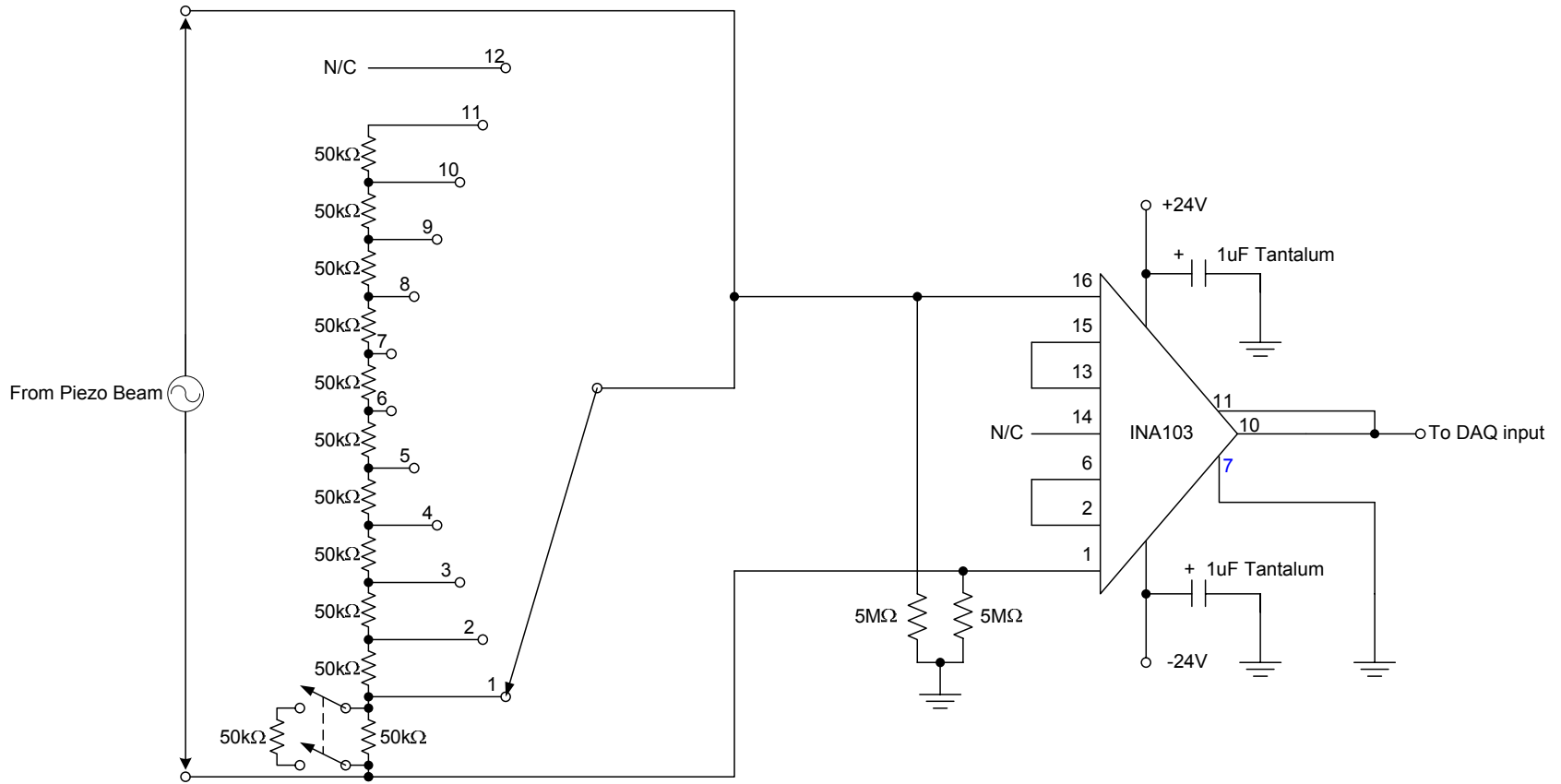
$$L_b \geq \frac{1}{2} \cdot L_m$$

$$Y = \left[\frac{2.25}{\sqrt{\frac{12 \left[E_p \cdot \left(\int_{-h_n}^{-h_n+h_p} y^2 \cdot b \, dy \right) + E_s \cdot \left(\int_{-h_n+h_p}^0 y^2 \cdot b \, dy \right) + E_s \cdot \left(\int_0^{h_s+h_p-h_n} y^2 \cdot b \, dy \right) + E_p \cdot \left(\int_{h_s+h_p-h_n}^{h_s+h_p+h_p-h_n} y^2 \cdot b \, dy \right) \right]}{(4 \cdot L_b^3 + 6 \cdot L_b^2 \cdot L_m + 3 \cdot L_m^2 \cdot L_b) \left[(L_m \cdot h_m \cdot b_m \cdot \rho_m) + (L_m \cdot h_s \cdot b \cdot \rho_s) + [L_m \cdot (h_p + h_p) \cdot b \cdot \rho_p] \right]}}}} \right]^2$$

$$\text{Maximiz} \left(P_{\text{ave_in_R}}, f, L_b, L_m, h_m, b_m, Y \right) = \begin{pmatrix} 120.457 \\ 6.033 \times 10^{-3} \\ 0.012 \\ 9.374 \times 10^{-3} \\ 8.159 \times 10^{-3} \\ 3.958 \times 10^{-6} \end{pmatrix}$$

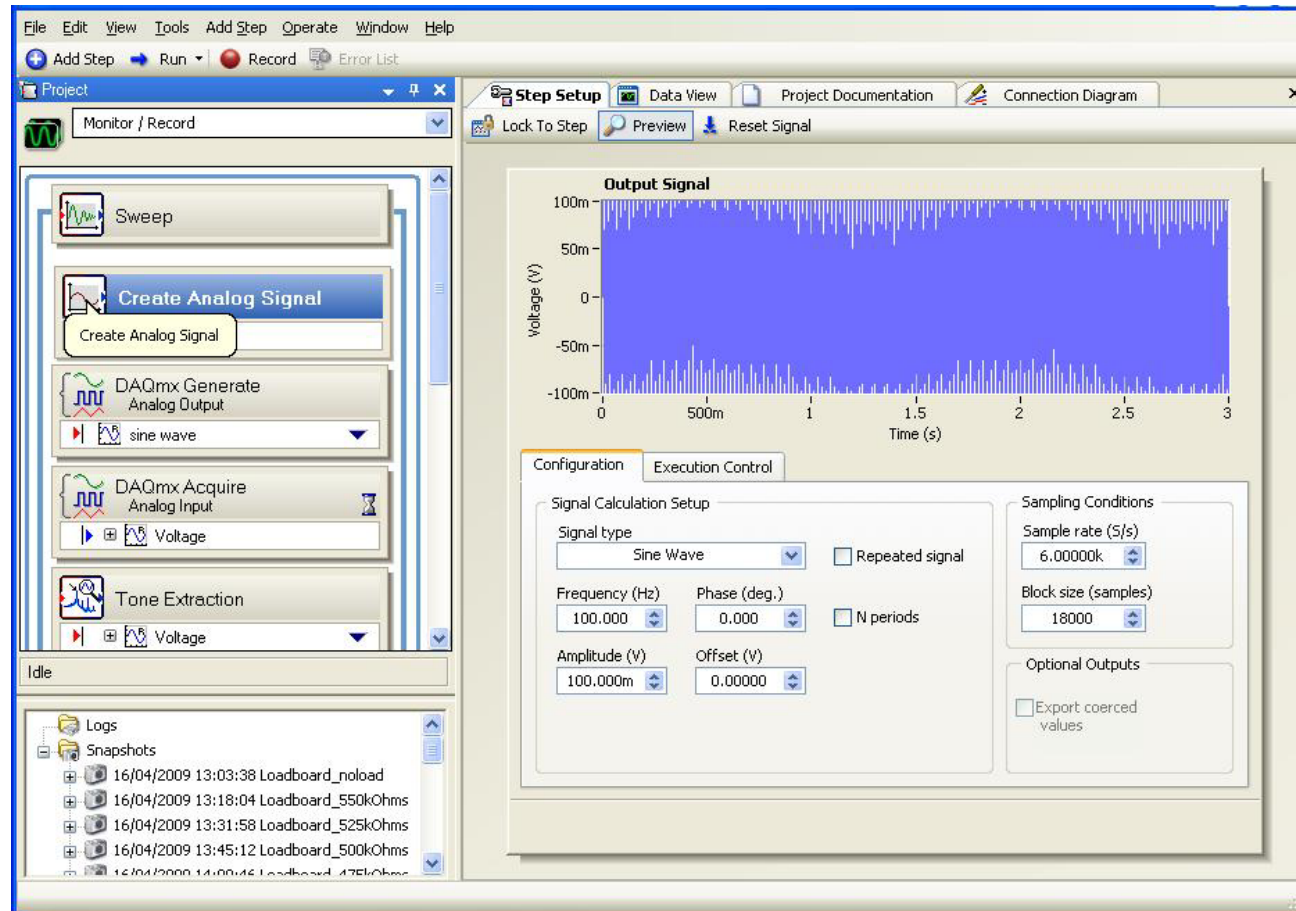
Appendix D: Circuit schematic for the custom-built load board

377



Appendix E: User Interface of LabVIEW SignalExpress, showing the configuration of each step used in the program developed in this thesis

378



File Edit View Tools Add Step Operate Window Help

+ Add Step Run Record Error List

Project Monitor / Record

Sweep

Create Analog Signal

sine wave

DAQmx Generate Analog Output

DAQmx Generate Analog Output

DAQmx Acquire Analog Input

Voltage

Tone Extraction

Voltage

Idle

Logs

Snapshots

- 16/04/2009 13:03:38 Loadboard_noload
- 16/04/2009 13:18:04 Loadboard_550kOhms
- 16/04/2009 13:31:58 Loadboard_525kOhms
- 16/04/2009 13:45:12 Loadboard_500kOhms
- 16/04/2009 14:00:46 Loadboard_475kOhms

Step Setup Data View Project Documentation Connection Diagram

Lock To Step Preview Connection Diagram

1

Configuration Triggering Advanced Timing Execution Control

Channel Settings

+ X Details >>

cDAQ1Mod3_ao0

Voltage Output Setup

Settings

Signal Output Range

Max 10

Min -10

Scaled Units

Volts

Terminal Configuration

<Let NI-DAQ Choose>

Custom Scaling

<No Scale>

Timing Settings

Generation Mode

N Samples

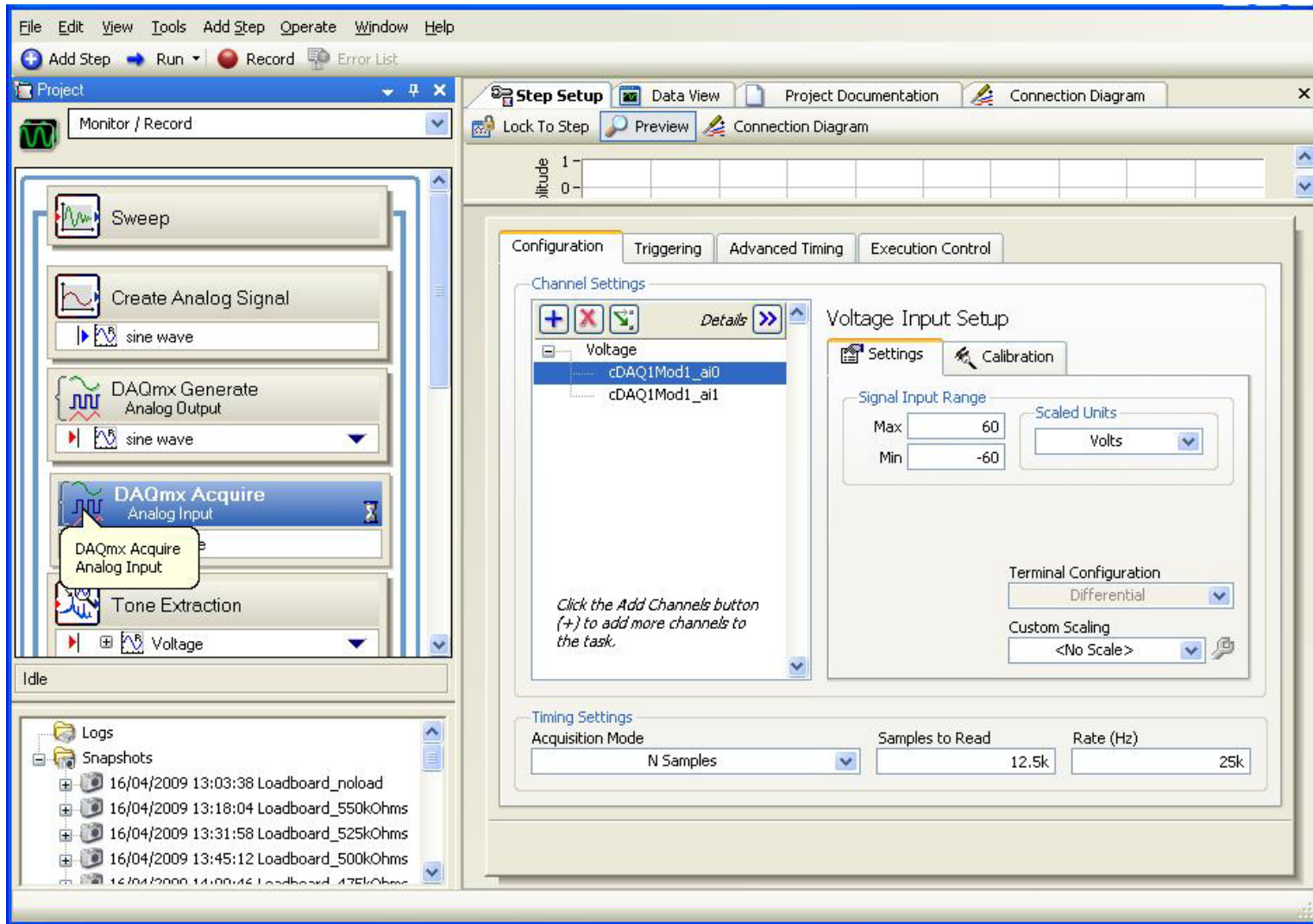
Samples to Write

100

Rate (Hz)

1k

Click the Add Channels button (+) to add more channels to the task.



The screenshot shows a software interface with a menu bar (File, Edit, View, Tools, Add Step, Operate, Window, Help) and a toolbar with buttons for Add Step, Run, Record, and Error List. The main window is titled "Step Setup" and contains several tabs: "Step Setup", "Data View", "Project Documentation", and "Connection Diagram".

On the left side, there is a "Project" pane showing "Monitor / Record". Below it is a task list with the following steps:

- Create Analog Signal
 - sine wave
- DAQmx Generate Analog Output
 - sine wave
- DAQmx Acquire Analog Input
 - Voltage
- Tone Extraction
 - detected frequency
 - detected amplitude
 - detected phase

The main area contains two empty plots:

- Exported Time Signal:** The y-axis is labeled "Amplitude" with values 0, 250m, 500m, 750m, and 1. The x-axis is labeled "Time" with values from 0 to 100m in 10m increments. A dropdown menu shows "cDAQ_ai0_Accel" and "Displayed signal".
- Exported Power Spectrum:** The y-axis is labeled "Magnitude (dB)" with values -100, -75, -50, -25, 0, and 20. The x-axis is labeled "Frequency (Hz)" with values from 0 to 100m in 10m increments. A checkbox for "Autoscale magnitude" is checked.

At the bottom, there are tabs for "Input/Output", "Configuration", and "Advanced". The "Input/Output" tab is active, showing an "Input signal:" dropdown set to "Voltage". A context menu is open over the "Voltage" dropdown, listing options: "sine wave", "Voltage" (highlighted), and "From Snapshot...". A secondary menu is open over "Voltage", listing: "All Elements", "Define Subgroup...", "cDAQ_ai0_Accel", and "cDAQ_ai1_Beam".

File Edit View Tools Add Step Operate Window Help

+ Add Step Run Record Error List

Project

Monitor / Record

Sweep

Create Analog Signal

sine wave

DAQmx Generate Analog Output

sine wave

DAQmx Acquire Analog Input

Voltage

Tone Extraction

Voltage

Idle

Logs

Snapshots

- 16/04/2009 13:03:38 Loadboard_noload
- 16/04/2009 13:18:04 Loadboard_550kOhms
- 16/04/2009 13:31:58 Loadboard_525kOhms
- 16/04/2009 13:45:12 Loadboard_500kOhms
- 16/04/2009 14:00:46 Loadboard_475kOhms

Step Setup Data View Project Documentation Connection Diagram

Lock To Step Preview

Sweep Configuration Sweep Output

Sweepable parameters:

Parameter Name	Step Name	Affected Output	Alias
Frequency (Hz)	Create Analog Signal	sine wave	

Configuration

Type: Linear

Start: Frequency (Hz): 30

Stop: Frequency (Hz): 150

Number of points: 241

Sweep Points

Values

Iteration

Appendix F: Monostable Multivibrator Calculations for the Circuit that Implements the SSHI Function (calculated using Mathcad)

Values for Monostable "Monomain" for the Optimised Piezoelectric Vibration Energy Harvester:

$L := 1000 \cdot 10^{-6}$ L is the chosen inductor value
 $C := 3.49 \cdot 10^{-9}$ C is the measured capacitance of the beam
 $LCfreq := \frac{1}{2 \cdot \pi \cdot \sqrt{L \cdot C}}$ LCfreq = 85.194×10^3
 $Halftimeperiod := \frac{1}{2 \cdot LCfreq}$ Halftimeperiod = 5.869×10^{-6} Time taken for energy to transfer from C to L and back again so as to achieve charge inversion on the piezoelectric element
 $Opto_{on} := 25 \cdot 10^{-6}$ Vishay 4N25 Optocoupler turn-on time
 $tw := (Halftimeperiod + Opto_{on})$ Total required pulse width in seconds: $tw = 30.869 \times 10^{-6}$
 $tw_n := tw \cdot 10^9$ Total required pulse width in nanoseconds (required units for the expression given in monostable data sheet): $tw_n = 30.869 \times 10^3$
 $C_{ext} := 1 \cdot 10^{-9}$ Chosen external capacitor value
 $C_{ext_in_pf} := C_{ext} \cdot 10^{12}$ Chosen external capacitor value in picofarads: (required units for expression given in monostable data sheet): $C_{ext_in_pf} = 1 \times 10^3$
 $R_{val_in_kOhms} := \frac{tw_n}{0.45 \cdot C_{ext_in_pf}}$ Required resistor value in kOhms (expression is from datasheet): $R_{val_in_kOhms} = 68.598$

The following section is to check the values:

$R_{val_f} := 2$ Chosen value of fixed resistor in kOhms
 $R_{val_pot} := 100$ Chosen value of potentiometer in kOhms
 $tw_{ns} := 0.45 \cdot C_{ext_in_pf} \cdot (R_{val_f} + R_{val_pot})$ Equation from data sheet
 $tw_{ns} = 4.59 \times 10^4$ Pulse width in nanoseconds
 $tw := tw_{ns} \cdot 10^{-9}$ $tw = 45.9 \times 10^{-6}$ Pulse width in seconds

Appendix G: Monostable Multivibrator Calculations for the Circuit that Implements the New Charge Storage Concept

Values for Monostables "Monomin and Monomax":

$\text{time_period} := \frac{1}{87}$ Time period of AC source from piezo device $\text{time_period} = 11.494 \times 10^{-3}$

$\text{pulse_width} := 0.99 \cdot 10^{-3}$ Required pulse width in seconds

$\text{tw_monomin} := (\text{pulse_width}) \cdot 10^9$ Pulse width in nanoseconds: $\text{tw_monomin} = 990 \times 10^3$

$C_{\text{extmonomin}} := 0.1 \cdot 10^{-6}$ External capacitor value

$C_{\text{extmonomin_in_pf}} := C_{\text{extmonomin}} \cdot 10^{12}$ External capacitor value in picofarads: $C_{\text{extmonomin_in_pf}} = 100 \times 10^3$

$R_{\text{valmonomin_in_kOhms}} := \frac{\text{tw_monomin}}{0.45 \cdot C_{\text{extmonomin_in_pf}}}$ Resistor value in kOhms (expression is from datasheet) $R_{\text{valmonomin_in_kOhms}} = 22$

$R_{\text{valmonomin}} := R_{\text{valmonomin_in_kOhms}} \cdot 10^3$ Resistor value in Ohms $R_{\text{valmonomin}} = 22 \times 10^3$

The following section is to check the values:

$R_{\text{calvalmonomin}} := 22$ Value of fixed resistor in kOhms

$\text{twmonomin}_{\text{ns}} := 0.45 \cdot C_{\text{extmonomin_in_pf}} \cdot R_{\text{calvalmonomin}}$ Equation from data sheet

$\text{twmonomin}_{\text{ns}} = 9.9 \times 10^5$ Pulse width in nanoseconds

$\text{twmonomin} := \text{twmonomin}_{\text{ns}} \cdot 10^{-9}$ Pulse width in seconds $\text{twmonomin} = 990 \times 10^{-6}$

Appendix H: Power budget for the circuit built to implements the proposed harvesting concept

Device	Current consumption			Supply voltage			Power consumption			Notes
	Quiescent	Maximum	Units	Dual/single?	Value	Units	Quiescent	Maximum	Units	
Instrumentation amplifier IC: AD623	305	550	μA	Single	+10	V	3050	5500	μW	
Comparator IC: LM339	800	2000	μA	Single	+10	V	8000	20000	μW	
Hex Inverter IC: HCF4049	0.02	1	μA	Single	+5	V	0.1	5	μW	
Quadruple OR gate IC: HEF4071	0.01	0.25	μA	Single	+5	V	0.05	1.25	μW	
Monostable multivibrator IC: 74HC123	Not given	8	μA	Single	+5	V	Not given	40	μW	DC characteristics
	Not given	Not given	N/A				15	Not given	μW	AC Characteristics (power figure calculated using formula on page 2 of data sheet)
Darlington Driver output (ULN2803) plus Optocoupler MOSFET relay IC: G3VM-352C	----	----	N/A	----	----	N/A	3744	----	μW	Power figure obtained through simulation of the circuit given in appendix I There are two of these in the circuit
Darlington Driver output (ULN2803) plus Optocoupler phototransistor output (4N25)	----	----	N/A	----	----	N/A	87	----	μW	Power figure obtained through simulation of the circuit given in appendix J
MOSFET driver MIC4426	180	0.4	μA	Single	+9	V	1620	3600	μW	
Resistor network for comparator input	930	No figure	μA	Single	+5	V	4649	No figure	μW	When output of comparator is high (it spends most of its time in this state) There are two of these networks in the circuit

Sum Quiescent total: 29.59815 mW

Sum Maximum total: 46.03425 mW

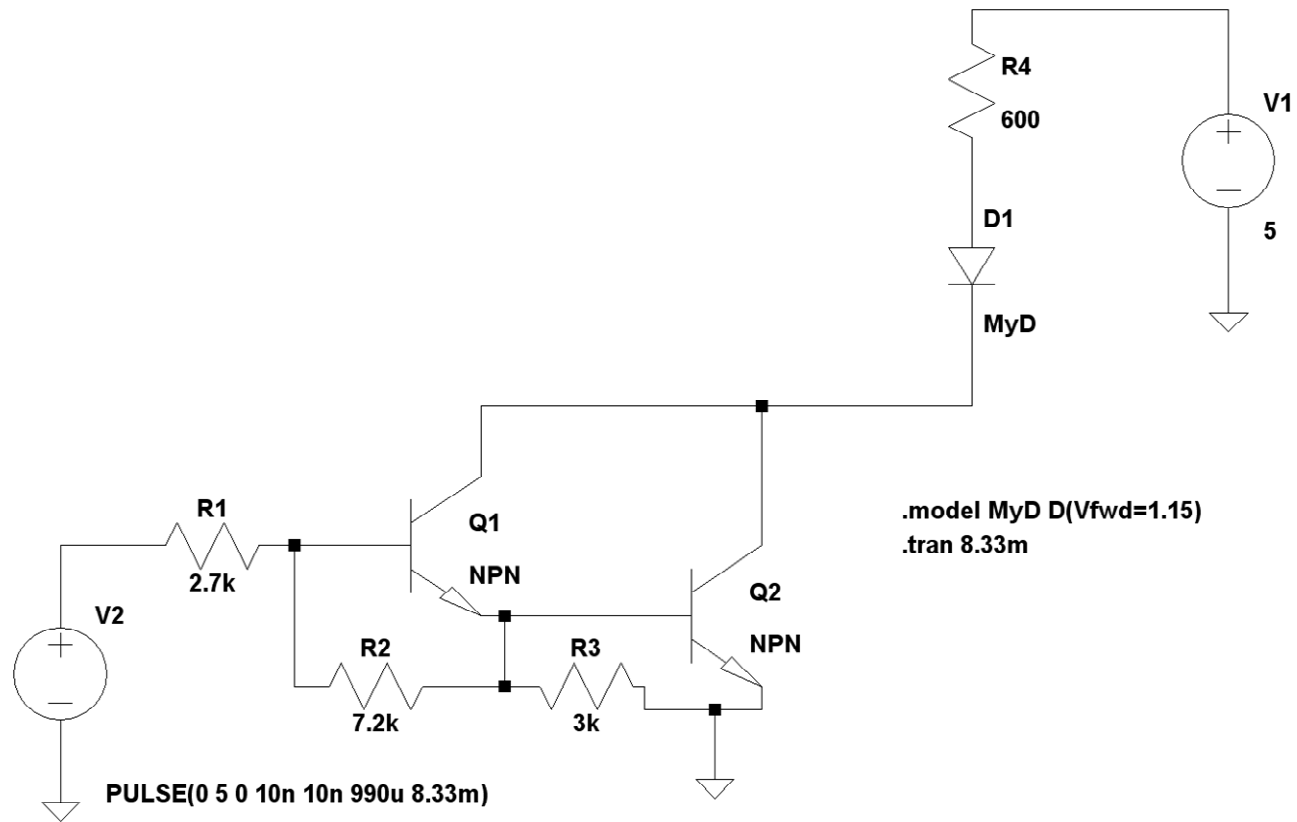
Notes:

*This estimate is for the detection and switch-driving circuitry only and does not include losses in the actual SSHI circuit or any power used by an application circuit.

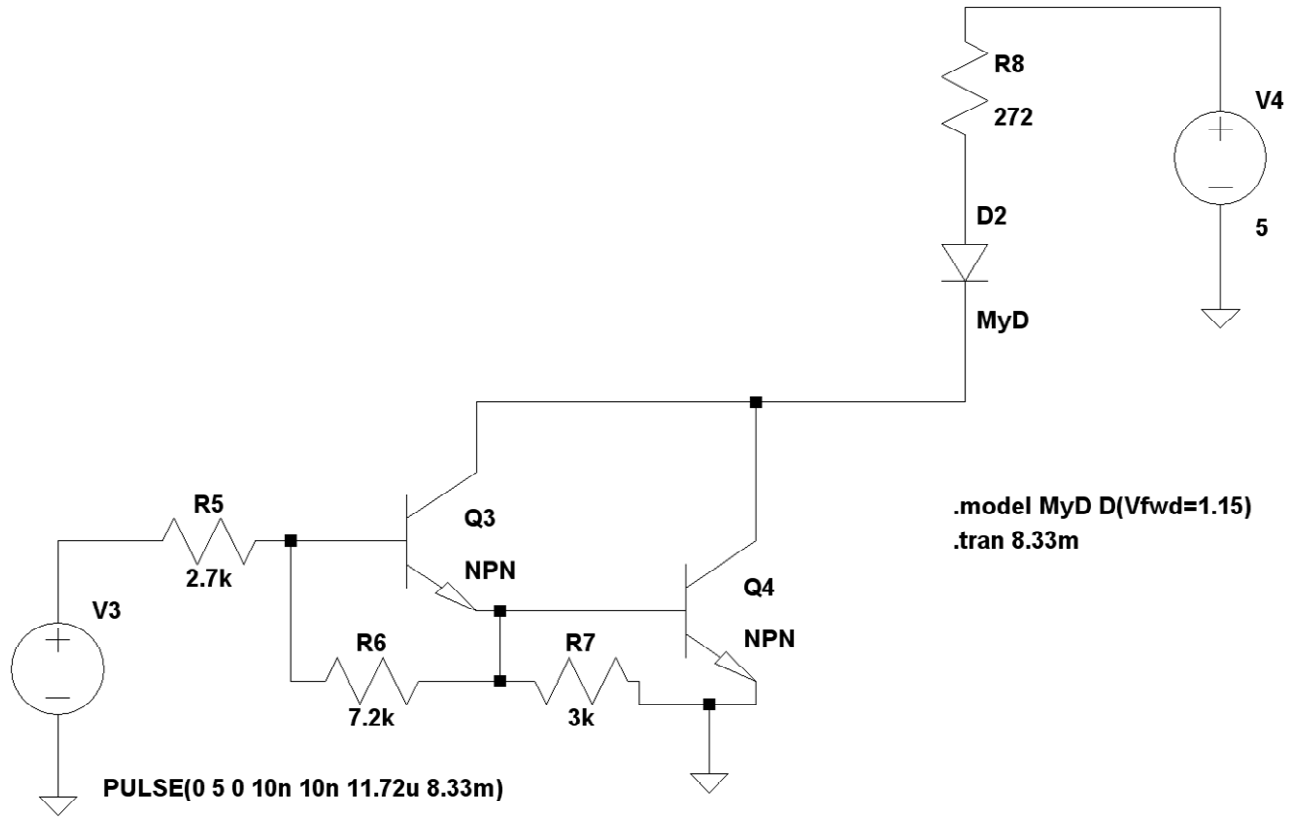
**dynamic power dissipation for the CMOS buffers is not accounted for (because the frequency is so low based on 120Hz vibration excitation)

Appendix I: Simulation circuit used to obtain power consumption of darlington driver output plus optocoupler MOSFET relay

386



Appendix J: Simulation circuit used to obtain power consumption of darlington driver output plus optocoupler phototransistor output



RELATED PUBLICATIONS AND POSTS

1) Journal Paper (1st author):

E. Worthington and M. Zhu, Geometrical optimisation of a piezoelectric energy harvesting device using a simplified analytical model for the generation of higher levels of electrical power, *Smart Mater. Struct.*, In review.

2) Journal Paper (1st author):

E. Worthington and M. Zhu, Experimental study on the electric output performance of a piezoelectric energy harvesting device directly connected to a resistive load. *IEEE Trans. Ultrason. Ferroelectr. Freq. Control*, In review.

3) Journal Paper (2nd author):

M. Zhu, E. Worthington and J. Njuguna, Analyses of power output of piezoelectric energy harvesting devices directly connected to a load resistor using a coupled piezoelectric-circuit finite element method, *IEEE Trans. Ultrason. Ferroelectr. Freq. Control*, 56(7), 2009, pp. 1309-1317.

4) Journal Paper (2nd author):

M. Zhu, E. Worthington and A. Tiwari, Design study of piezoelectric energy harvesting devices for generation of higher electrical power output using a coupled piezoelectric-circuit finite element method, *IEEE Trans. Ultrason. Ferroelectr. Freq. Control*, 57(2), 2010, 427-437.

5) Conference Paper (2nd author):

M. Zhu, E. Worthington and J. Njuguna, Coupled piezoelectric-circuit FEA to study influence of a resistive load on power output of piezoelectric energy devices, In: SPIE

Europe microtechnologies for the new millennium, Dresden, Germany, May 4-6 2009, Vol. 7362 pp. 736202-736202-12.

6) Conference Paper (2nd author):

M. Zhu and E. Worthington, Design and testing of piezoelectric energy harvesting devices for generation of higher electric power for wireless sensor networks, In: *8th IEEE annual conference on sensors (IEEE Sensors 2009)*, Canterbury, New Zealand, Oct 25-28 2009, pp. 699-702.

7) Conference Poster:

E. Worthington, M. Zhu and P. Kirby, Piezoelectric energy harvesting device with optimised charge transfer to storage. In: Knowledge Transfer Network Energy Harvesting Technologies Event “*Enabling Remote and Wireless Sensing*”, London, Nov. 26th, 2008.

8) Conference Poster:

M. Zhu, E. Worthington and J. Njunguna, Coupled piezoelectric-circuit FEA to study influence of a resistive load on piezoelectric energy devices, Knowledge Transfer Network Energy Harvesting Technologies Event “*Enabling Remote and Wireless Sensing*”, London, Nov. 26th, 2008.

CV

Emma Louise Worthington was born in Bury, Greater Manchester, England in the 1970s. Growing up in a post-industrial mill town, Emma became interested in industrial history, and mechanical and electrical engineering. Her engineering career began when she trained as a motor vehicle mechanic via City & Guilds at Bury College in 1995. After struggling to find an apprenticeship, she decided to stay in full-time education and undertook a BTEC OND in electrical and electronic engineering at Bolton Community College in Greater Manchester, and a subsequent BTEC HND in the same subject at Liverpool John Moores University in Liverpool, UK, in 1998. In 2001 she received a 1st Class Hons degree in applied electronics from Liverpool John Moores University, and until 2006 worked as an electronic design engineer in the aerospace industry in the South East of England. In 2006, she left the aerospace industry to undertake a PhD in the field of energy harvesting. Her interest is mainly in the development of circuitry for conditioning the power output of energy harvesting devices. Following her PhD, Emma is returning to the north west of England and hopes to obtain employment either as a researcher in the field of energy harvesting, as an engineer or researcher working in the renewable energies sector, or as an engineer working on the development of the next generation of electric road vehicles.

